Physics Library
QC
1
.U5C

Volume 65A
Number 3
May–June 1961

UNIVERSITY OF MICHIGAN
JUN 20 1961
PHYSICS LIBRARY

Physics and Chemistry

SECTION A

JOURNAL OF RESEARCH

NATIONAL BUREAU OF STANDARDS

Journal of Research
of the
National Bureau of Standards

A. Physics and Chemistry

MAY–JUNE • 1961

VOLUME • 65A

NUMBER • 3

Editor: U. Fano

Associate Editors: L. M. Kushner
I. M. Richardson

Publication dates:
Feb. 1, Apr. 1, June 1, Aug. 1, Oct. 1, Dec. 1, 1961.

JOURNAL OF RESEARCH

The National Bureau of Standards Journal of Research reports research and development in the fields of activity shown at right. Also included from time to time are survey articles on topics closely related to the Bureau's scientific and technical program.

The Journal is published in four separate sections as follows:

A. Physics and Chemistry

Contains papers of interest primarily to scientists working in these fields. Issued six times a year. Annual subscription: domestic, $4.00; foreign, $4.75.

B. Mathematics and Mathematical Physics

Presents studies and compilations designed mainly for the mathematician and the theoretical physicist. Issued quarterly. Annual subscription: domestic, $2.25; foreign, $2.75.

C. Engineering and Instrumentation

Reports research and development results of interest chiefly to the engineer and the applied scientist. Issued quarterly. Annual subscription: domestic, $2.25; foreign, $2.75.

D. Radio Propagation

Reports work in radio propagation, upper atmospheric physics and communications. Issued six times a year. Annual subscription: domestic, $4.00; foreign, $4.75.

U.S. DEPARTMENT OF COMMERCE
Luther H. Hodges, Secretary

NATIONAL BUREAU OF STANDARDS
A. V. Astin, Director

Functions and Activities

The functions of the National Bureau of Standards are set forth in the Act of Congress, March 3, 1901, as amended. These include the development and maintenance of the national standards of measurement and the provision of means and methods for making measurements consistent with these standards; the determination of physical constants and properties of materials; the development of methods and instruments for testing materials, devices, and structures; advisory services to government agencies on scientific and technical problems; invention and development of devices to serve special needs of the Government; and the development of standard practices, codes, and specifications. The work includes basic and applied research, development, engineering, instrumentation, testing, evaluation, calibration services, and various consultation and information services. The Bureau also serves as the Federal technical research center in a number of specialized fields. The scope of activities of the National Bureau of Standards is suggested in the following listing of the divisions and sections engaged in technical work.

Washington, D.C.

Electricity. Resistance and Reactance. Electrochemistry. Electrical Instruments. Magnetic Measurements. Dielectrics.

Metrology. Photometry and Colorimetry. Refractometry. Photographic Research. Length. Engineering Metrology. Mass and Scale. Volumetry and Densimetry.

Heat. Temperature Physics. Heat Measurement. Cryogenic Physics. Equation of State. Statistical Physics.

Radiation Physics. X-ray. Radioactivity. Radiation Theory. High Energy Radiation. Radiological Equipment. Nucleonic Instrumentation. Neutron Physics.

Analytical and Inorganic Chemistry. Pure Substances. Spectrochemistry. Solution Chemistry. Standard Reference Material. Applied Analytical Research.

Mechanics. Sound. Pressure and Vacuum. Fluid Mechanics. Engineering Mechanics. Rheology. Combustion Controls.

Organic and Fibrous Materials. Rubber. Textiles. Paper. Leather. Testing and Specifications. Polymer Structure. Plastics. Dental Research.

Metallurgy. Thermal Metallurgy. Chemical Metallurgy. Mechanical Metallurgy. Corrosion. Metal Physics. Electrodeposition.

Mineral Products. Engineering Ceramics. Glass. Refractories. Enameled Metals. Crystal Growth. Physical Properties. Constitution and Microstructure.

Building Research. Structural Engineering. Fire Research. Mechanical Systems. Organic Building Materials. Codes and Safety Standards. Heat Transfer. Inorganic Building Materials.

Applied Mathematics. Numerical Analysis. Computation. Statistical Engineering. Mathematical Physics.

Data Processing Systems. SEAC Engineering Group. Components and Techniques. Digital Circuitry. Digital Systems. Analog Systems. Applications Engineering.

Atomic Physics. Spectroscopy. Infrared Spectroscopy. Solid State Physics. Electron Physics. Atomic Physics.

Instrumentation. Engineering Electronics. Electron Devices. Electronic Instrumentation. Mechanical Instruments. Basic Instrumentation.

Physical Chemistry. Thermochemistry. Surface Chemistry. Organic Chemistry. Molecular Spectroscopy. Molecular Kinetics. Mass Spectrometry. Molecular Structure and Radiation Chemistry.

• Office of Weights and Measures.

Boulder, Colo.

Cryogenic Engineering. Cryogenic Equipment. Cryogenic Processes. Properties of Materials. Gas Liquefaction.

Ionosphere Research and Propagation. Low Frequency and Very Low Frequency Research. Ionosphere Research. Prediction Services. Sun-Earth Relationships. [illegible] Engineering. Radio Warning Services.

Radio Propagation Engineering. Data Reduction Instrumentation. Radio Noise. Tropospheric Measurements. Tropospheric Analysis. Propagation-Terrain Effects. Radio-Meteorology. Lower Atmosphere Physics.

Radio Standards. High Frequency Electrical Standards. Radio Broadcast Service. Radio and Microwave Materials. Atomic Frequency and Time Interval Standards. Electronic Calibration Center. Millimeter-Wave Research. Microwave Circuit Standards.

Radio Systems. High Frequency and Very High Frequency Research. Modulation Research. Antenna Research. Navigation Systems. Space Telecommunications.

Upper Atmosphere and Space Physics. Upper Atmosphere and Plasma Physics. Ionosphere and Exosphere Scatter. Airglow and Aurora. Ionospheric Radio Astronomy.

Order all publications from the Superintendent of Documents
U.S. Government Printing Office, Washington 25, D.C.

Use of funds for printing this publication approved by the Director of the Bureau of the Budget (June 24, 1958).

JOURNAL OF RESEARCH of the National Bureau of Standards—A. Physics and Chemistry
Vol. 65A, No. 3, May–June 1961

International Practical Temperature Scale of 1948

Text Revision of 1960

H. F. Stimson

(February 1, 1961)

The International Practical Temperature Scale of 1948 is a text revision of the International Temperature Scale of 1948, the numerical values of temperatures remaining the same. The adjective "Practical" was added to the name by the International Committee on Weights and Measures. The scale continues to be based upon six fixed and reproducible equilibrium temperatures to which values have been assigned, and upon the same interpolation formulas relating temperatures to the indications of specified measuring instruments. Some changes have been made in the text to make the scale more reproducible than its predecessor. The triple point of water, with the value 0.01 °C replaces the former ice point as a defining fixed point of the scale. It is also recommended that the zinc point, with the value 419.505 °C, be used instead of the sulfur point. The recommendations include new information that has become available since 1948.

An internationally accepted scale on which temperatures can be measured conveniently and accurately is necessary for science and industry. As early as 1911 the directors of the national laboratories of Germany, Great Britain, and the United States agreed to undertake the unification of the temperature scales in use in their respective countries. A practical scale, named the International Temperature Scale, was finally agreed upon, was recommended to the Seventh General Conference on Weights and Measures by its International Committee on Weights and Measures, and was adopted in 1927.[1]

The General Conference on Weights and Measures is the official international body now representing 36 nations that subscribe to the Treaty of the Meter. The General Conference normally meets every six years, and at those times may adopt recommendations submitted by the International Committee. The International Committee is the executive body elected by the General Conference. It consists of 18 scientists, only one from any one nation, and it normally meets every two years. The International Committee now has six advisory committees of specialists most of whom represent large national laboratories. The Advisory Committee on Thermometry was authorized in 1933 and first met in 1939.

In 1948 a revision of the International Temperature Scale was prepared by the Advisory Committee and proposed to the International Committee. The International Committee recommended this revision to the Ninth General Conference which adopted it.[2] At this time the General Conference also adopted the designation of degree Celsius in place of degree Centigrade or Centesimal.[3] The revised scale was designed to conform as nearly as practicable to the thermodynamic scale as then known, while incorporating certain refinements, based on experience, to make the scale more uniform and reproducible than its predecessor. In the revision there were only three changes which affected values of temperatures on the scale. One was to increase the value assigned to the silver point by 0.3 degree, merely to make the scale more uniform. Another was to specify Planck's radiation formula instead of Wien's formula so the scale would be consistent with the thermodynamic scale above the gold point. The third was to increase the value for the second radiation constant to bring it nearer to the value derived from atomic constants.

In 1954 the Advisory Committee proposed a resolution redefining the Kelvin thermodynamic scale by assigning a value to the triple point of water. This kind of definition was what Kelvin, in 1854, had said "must be adopted ultimately." This resolution was recommended by the International Committee and adopted by the Tenth General Conference.[4] As soon as this resolution had been adopted it was pointed out that it would be necessary to revise the introduction of the text of the International Temperature Scale of 1948 to conform with the action just taken.

In preparing a tentative proposal for a new text of the introduction it soon became evident that the other three parts of the text would also profit by a revision. For example, the triple point of water could now be made one of the defining fixed points of the scale and thus become the one defining fixed point common to both the international and the Kelvin scales. The Recommendations could include new information that had become available since 1948. At the higher temperatures some new determinations of differences between the international and thermodynamic scales could be included.

[1] Comptes Rendus de la Septième Conférence Générale des Poids et Mesures, p. 94 (1927).
[2] Comptes Rendus de la Neuvième Conférence Générale des Poids et Mesures, p. 89 (1948).
[3] Comptes Rendus de la Neuvième Conférence Générale des Poids et Mesures, p. 64 (1948).
[4] Comptes Rendus de la Dixième Conférence Générale des Poids et Measures, p. 79 (1954).

The values reported for these differences, however, were still not certain enough to warrant a change of the scale itself. The new text, therefore, does not change the value of any temperature on the 1948 scale by as much as the experimental error of measurement.

In 1958 the tenative proposal was discussed in detail at sessions of the Advisory Committee in June, and many suggested changes were agreed upon. It was proposed to the International Committee in October. Minor corrections were made during the next two years, and in 1960 the International Committee gave the scale its new name. The International Committee recommended this text revision to the Eleventh General Conference and it was adopted in October 1960.

A translation of the official text [5] follows.

1. Introduction

The Kelvin thermodynamic scale, on which temperatures are designated as °K and denoted by the symbol T, is recognized as the fundamental scale to which all temperature measurements should ultimately be referable. The magnitude of the degree Kelvin is now defined by the decision (Tenth General Conference on Weights and Measures, 1954, Resolution 3) fixing the thermodynamic temperature of the triple point of water at exactly 273.16 °K.

The experimental difficulties inherent in the measurement of temperature on the thermodynamic scale led to the adoption in 1927, by the Seventh General Conference on Weights and Measures, of a practical scale called the "International Temperature Scale". This scale was intended to be conveniently and accurately reproducible and to agree as closely as practicable with the thermodynamic scale.

The International Temperature Scale was revised in 1948 to make it conform with the state of the knowledge then available.

In May 1960 the International Committee on Weights and Measures approved the new name, "International Practical Temperature Scale of 1948", for the scale presented in this document. Inasmuch as the numerical values of temperature on this scale are the same as in 1948, this scale is not a revision of the scale of 1948 but merely a revision of its text.

2. Definition of the International Practical Temperature Scale of 1948

Temperatures on the International Practical Temperature Scale of 1948 are expressed in degrees Celsius, designated by °C or °C (Int. 1948), and are denoted here by the symbol t or t_{int}.

The International Practical Temperature Scale is based on six reproducible temperatures (defining fixed points), to which numerical values are assigned, and on formulas establishing the relation between temperature and the indications of instruments calibrated by means of values assigned to the six defining fixed points. These fixed points are defined by specified equilibrium states, each of which, except for the triple point of water, is under a pressure of 101 325 newtons/meter^2 (1 standard atmosphere).

The fixed points of the scale and the exact numerical values assigned to them are given in table 1.

TABLE 1. *Defining fixed points*

Exact values assigned. The pressure is 1 standard atmosphere, except for the triple point of water.

	Temperature °C (Int. 1948)
Temperature of equilibrium between liquid oxygen and its vapor (oxygen point)	−182. 97
Temperature of equilibrium between ice, liquid water, and water vapor (triple point of water)	+0. 01
Temperature of equilibrium between liquid water and its vapor (steam point)	100
Temperature of equilibrium between liquid sulfur and its vapor (sulfur point)	444. 6*
Temperature of equilibrium between solid silver and liquid silver (silver point)	960. 8
Temperature of equilibrium between solid gold and liquid gold (gold point)	1063

*In place of the sulfur point, it is recommended to use the temperature of equilibrium between solid zinc and liquid zinc (zinc point) with the value 419.505 °C (Int. 1948). The zinc point is more reproducible than the sulfur point and the value which is assigned to it has been so chosen that it use leads to the same values of temperature on the International Practical Temperature Scale as does the use of the sulfur point.

The procedures for interpolation lead to a division of the scale into four parts.

a. From 0 °C to 630.5 °C (antimony point) the temperature t is defined by the formula

$$R_t = R_0(1 + At + Bt^2),$$

where R_t is the resistance at temperature t of the platinum wire resistor of a standard resistance thermometer, and R_0 is the resistance at 0 °C. The constants R_0, A, and B are to be determined from the values of R_t at the triple point of water, at the steam point, and at the sulfur point (or the zinc point). The platinum wire of a standard resistance thermometer shall be annealed and its purity shall be such that R_{100}/R_0 is not less than 1.3920.

b. From the oxygen point to 0 °C, the temperature t is defined by the formula

$$R_t = R_0\,[1 + At + Bt^2 + C(t - t_{100})t^3],$$

where R_0, A, and B are determined in the same manner as in *a* above, the constant C is to be determined from the value of R_t at the oxygen point, and $t_{100} = 100$ °C.

c. From 630.5 °C to the gold point the temperature t is defined by the formula

$$E = a + bt + ct^2,$$

where E is the electromotive force of a standard thermocouple of platinum and platinum-rhodium alloy, when one of the junctions is at 0 °C and the other at the temperature t. The constants a, b, and c are to be determined from the values of E at 630.5 °C, at the silver point, and at the gold point. The value of the electromotive force at 630.5 °C is to be determined by measuring this temperature with a standard resistance thermometer.

[5] Comptes Rendus de la Onzième Conférence Générale des Poids et Mesures (1960).

The wires of the standard thermocouple shall be annealed and the purity of the platinum wire shall be such that the ratio R_{100}/R_0 is not less than 1.3920. The platinum-rhodium wire shall consist nominally of 90 percent platinum and 10 percent rhodium by weight. When one junction of the thermocouple is at 0 °C and the other is successively at 630.5 °C, the silver point, and the gold point, the completed thermocouple shall have electromotive forces such that

$$E_{Au}=10\,300\ \mu v \pm 50\ \mu v$$

$$E_{Au}-E_{Ag}=1183\ \mu v+0.158\ (E_{Au}-10300\ \mu v)\pm 4\ \mu v$$

$$E_{Au}-E_{630.5}=4766\ \mu v+0.631\ (E_{Au}-10300\ \mu v)\pm 8\ \mu v.$$

d. Above the gold point the temperature t is defined by the formula

$$\frac{J_t}{J_{Au}}=\frac{\exp\left[\frac{C_2}{\lambda(t_{Au}+T_0)}\right]-1}{\exp\left[\frac{C_2}{\lambda(t+T_0)}\right]-1},$$

where J_t and J_{Au} are the radiant energies per unit wavelength interval at wavelength λ, emitted per unit time per unit solid angle per unit area of a blackbody at the temperature t and the gold point respectively, C_2 is the second radiation constant with the value $C_2=0.014\ 38$ meter-degrees, λ is in meters, and $T_0=273.15$ degrees.

3. Recommendations

The following recommendations are advisory rather than mandatory. The recommended apparatus, methods, and procedures represent good practice at the present time, but there is no intention of retarding the development and use of improvements and refinements. Experience has shown these recommendations to be in the interest of uniformity and reproducibility in the realization of the International Practical Temperature Scale defined in Section 2.

3.1. Standard Resistance Thermometer

A standard resistance thermometer should be so designed and constructed that the wire of the platinum resistor is as nearly strainfree as practicable and will remain so during continued use. The platinum wire should be drawn from a fused ingot, not from forged sponge.

Standard resistance thermometers have been made of wire with diameters between 0.05 and 0.5 mm, at least a short portion of each lead adjacent to the resistor also being of platinum. The completed resistor of the thermometer should be annealed in air at a temperature higher than the highest temperature at which it is to be used, but in no case below 450 °C. There is reason to believe, furthermore, that better stability is obtained when the tube protecting the completed resistor is filled with gas containing some oxygen.

Useful criteria which serve as safeguards against inferior construction of the completed thermometer and against errors in the calibrations at the fixed points are that the value of the constant B is $(-0.5857\pm0.0010)\times10^{-6}/\text{deg}^2$ and that the value of the constant C is $(-4.35\pm0.05)\times10^{-12}/\text{deg}^4$. Another useful criterion of the adequacy of the annealing and of the reliability of the thermometer is the constancy of its resistance at some reference temperature. For example the resistance of a thermometer at the triple point of water should not change by as much as the equivalent of 0.001 deg when the thermometer is subjected to temperature cycles such as are necessary for its calibration.

3.2. Standard Thermocouple

Standard thermocouples have been made of wires having a diameter between 0.35 and 0.65 mm.

Before calibration the wires of the thermocouple should be carefully annealed to ensure the constancy of the electromotive forces during use. For this it is necessary to heat the platinum wire to a temperature of at least 1100 °C and the platinum-rhodium wire to 1450 °C. If the annealing is done before the wires are mounted in their insulators, the completed thermocouple should be heated again to a temperature of at least 1100 °C, until the electromotive force is stable and local inhomogeneities caused by strains have disappeared. When the thermocouple has been annealed sufficiently, its indications should not vary with a change in the temperature gradient along the wire; they should not vary, for example, with the depth of immersion in an enclosure at uniform temperature.

The electromotive force of the thermocouple at 630.5 °C should be determined from measurements at some uniform and constant temperature between 630.3 and 630.7 °C.

3.3. Pressure

In practice, pressures are determined with a mercury column. Pure mercury may be taken as having a mean density at 20 °C of 13 545.87 kg/m³ in a mercury column balancing one atmosphere. In the practical determination of the standard atmosphere the International Committee on Weights and Measures recommends that the value of local gravity be expressed in the Potsdam system until it sanctions the use of another system.

In the following sections on the oxygen point, the steam point, and the sulfur point the formulas for the equilibrium temperatures t_p are given as polynomials in powers of (p/p_0-1), where p is the equilibrium pressure and p_0 is one standard atmosphere. The limits of accuracy are also given for stated ranges of pressure. In practice, the errors caused by using these formulas are less than the errors caused by the instability of systems open to the atmosphere. Greater stability and increased accuracy can be realized in closed systems held at a constant pressure which is maintained within a few parts in a thousand of one atmosphere. Only the first power terms of (p/p_0-1) in the polynomials are then needed.

3.4. Zero Point of the Scale and Triple Point of Water

a. Zero Point of the Scale

The zero point of the International Practical Temperature Scale is defined as being the temperature exactly 0.01 deg below the triple point of water. Calculations show that the temperature of the former "ice point", defined as the temperature of equilibrium between ice and air-saturated water under a pressure of one standard atmosphere, is 0 °C within 0.0001 deg.

It is difficult, however, to obtain the ice point directly with an accuracy better than ± 0.001 deg; but when this accuracy suffices, the temperature 0 °C may be be realized by the use of a mixture of finely divided ice and water saturated with air at 0 °C in a well insulated container such as a Dewar flask. The equilibrium temperature t corresponding to an ambient atmosphere pressure p and at a depth h below the surface of the water, may be calculated by the formula

$$t = 0.01\ (1 - p/p_o)\ ^\circ\mathrm{C} - (0.7 \times 10^{-6}\ \mathrm{deg/mm})h.$$

b. Triple Point of Water

The temperature of the triple point of water has been realized in sealed glass cells which contain only water of high purity; these cells have axial re-entrant wells for thermometers. In such cells the triple-point temperature is realized wherever ice is in equilibrium with a liquid-vapor surface. At a depth of h below the liquid-vapor surface the equilibrium temperature between ice and liquid water is given by the formula

$$t = 0.01\ ^\circ\mathrm{C} - (0.7 \times 10^{-6}\ \mathrm{deg/mm})h.$$

The recommended method of preparing a triple-point cell for use is first to freeze a thick mantle of ice around the well by cooling from within, and then to melt enough of this mantle, also from within, to produce a new water-ice interface close to the well. After these cells have been prepared for use, the temperatures measured in the wells have been found to rise by amounts ranging from 0.0001 to 0.0005 deg before becoming stable after from 1 to 3 days. This initial change can probably be explained either by the increase in the dimensions of the crystals of ice or by the slow release of strains in the crystals. A cell prepared in this manner and kept in an ice bath is capable of maintaining a temperature which is constant within about 0.0001 deg for several months. When cells from different sources have been compared under these conditions, no differences greater than 0.0002 deg have been reported.

Water from most natural sources (normal water) contains about 0.0148 mole percent deuterium, 0.20 mole percent O^{18}, and 0.04 mole percent O^{17}. Variations from this norm as large as 0.0015 mole percent have been found in the deuterium content of natural waters. An increase of 0.001 mole percent in the deuterium content of water corresponds to an increase of 0.000 04 deg in the triple-point temperature. Waters from rivers that rise to the leeward of mountain ranges or at the base of permanent glaciers may contain less than the normal amount of deuterium, whereas waters from the surface of large lakes may contain more than the normal amount.

The isotopic composition at the water-ice interfaces in the triple-point cells depends also on the natural differences in the proportions of the oxygen isotopes, on the process of distilling water, and on the procedure of freezing. The effects of these different isotopic compositions on the temperatures realized in triple-point cells are probably sufficiently small to be neglected.

3.5. Oxygen Point

The temperature of equilibrium between liquid oxygen and its vapor is usually realized by the static method. The platinum resistor of a standard thermometer and the liquid oxygen in its container are brought to the same temperature in a metal block placed in a suitable cryostat. The metal block is usually immersed in a well-stirred bath of liquid oxygen open to the atmosphere, but greater stability has been obtained by enclosing the metal block inside an evacuated envelope maintained at a uniform temperature near the oxygen point. The oxygen vapor pressure is transmitted through a tube leading out to a manometer. The entire length of this tube should be at temperatures above the saturation temperature of the oxygen.

Criteria that the equilibrium temperature has been realized are that the observed temperature, corrected to constant pressure at the free surface of the oxygen, is independent of: Small variations in the depth of immersion of the thermometer in the metal block, the ratio of the volume of the liquid oxygen to the volume of the vapor, and small variations in the temperature of the envelope.

The equilibrium temperature t_p corresponding to a pressure p at the surface of the liquid oxygen may be found to an accuracy of a few thousandths of a degree over the range from $p = 660$ mm to $p = 860$ mm of mercury by means of the formula

$$t_p = [-182.97 + 9.530(p/p_o - 1) - 3.72(p/p_o - 1)^2 + 2.2(p/p_o - 1)^3]^\circ\mathrm{C}.$$

3.6. Steam Point

The temperature of equilibrium between liquid water and its vapor is usually realized by the dynamic method with the thermometer placed within the saturated vapor. Open systems were formerly used for the realization of the steam point but for precise calibration it is preferable to use a closed system in which a boiler and a manometer are connected to a manostat filled with air or, preferably, helium.

The boiler should be constructed so as to avoid all contamination of the vapor. The thermometer should be shielded against radiation from bodies that are at temperatures different from the saturation temperature.

The criteria that the equilibrium temperature has been realized are that the observed temperature, corrected to a constant pressure, is independent of: The water used, the elapsed time, the variations in the heat input to the liquid water, and the depth of immersion of the thermometer.

The equilibrium temperature t_p, corresponding to a pressure p, may be found to within 0.001 deg over the range between $p=660$ mm and $p=860$ mm of mercury by means of the formula

$$t_p=[100+28.012(p/p_o-1) -11.64(p/p_o-1)^2+7.1(p/p_o-1)^3]°C.$$

A change in the proportion of deuterium in water produces about one third as much change at the boiling-point temperature as that produced at the triple point, and in the same direction.

3.7. Sulfur Point

The temperature of equilibrium between liquid sulfur and its vapor is usually realized by the dynamic method in an aluminum boiler similar in shape to that used for the steam point except that extra shielding against radiation and larger spaces for free circulation of the vapor are needed.

The addition of 0.1 percent of arsenic and then of 0.1 percent of selenium to sulfur has been reported to raise the normal boiling point by 0.02 deg and then by 0.07 deg. These elements are common in sulfur from volcanic sources. Commercial sulfur contains organic impurities which slowly decompose and leave carbon when the sulfur is boiled. Carbon itself probably has no observable effect on the boiling point of sulfur, but it is preferable to remove the organic matter and carbon.

The criteria that the sulfur point has been realized are similar to those for the realization of the steam point, except that it may take many hours to reach a constant temperature.

The equilibrium temperature t_p, corresponding to a pressure p, may be found to an accuracy of about 0.001 deg in the range between $p=660$ mm and $p=800$ mm of mercury by means of the formula

$$t_p=[444.6+69.010(p/p_o-1)-27.48(p/p_o-1)^2 +19.14(p/p_o-1)^3]°C.$$

3.8. Zinc Point

Highly reproducible temperatures, closely related to those which give the temperature of the liquidus curve of an alloy, have been realized as plateau temperatures on slow-rate freezing curves of high purity (99.999 weight percent) zinc.

The zinc is usually melted and frozen in high purity artificial graphite (99.999 weight percent) crucibles with axial thermometer wells, in simple block furnaces. The crucibles should be about 5 cm in diameter and deep enough to eliminate the effects of heat conduction along the thermometer leads.

When cooling has been started and solid has begun to form on the crucible wall, the thermometer should be removed, cooled to the room temperature, and then reinserted in its well to induce a thin mantle of solid zinc on the outside of the well. Another technique, which has been used, is to remove the thermometer when the temperature indicated by it is 0.01 deg below the freezing point, and to insert a silica rod for about 30 sec; the thermometer is then replaced in its well. The plateau temperature is that of equilibrium between the liquid zinc and the solid zinc of the mantle while freezing is progressing slowly inward from the outside of the crucible. The melts are best made in an inert atmosphere to inhibit oxidation of the graphite and zinc, yet there has been no evidence of the plateau temperatures being affected by zinc oxide in the melt even after prolonged heating in air. The plateau temperatures have been found to increase 0.0043 deg per atmosphere.

A criterion of adequate purity of a sample is that its melting range is not greater than about 0.001 deg. Samples of zinc of this high purity, originating in different countries, have given plateau temperatures which were practically identical (within 0.0002 deg). Samples with melting ranges of about 0.01 deg yielded plateau temperatures that were low by from 0.0004 deg to 0.0016 deg.

3.9. Silver and Gold Points

The temperature of equilibrium between solid and liquid silver or between solid and liquid gold has been realized in covered crucibles either of high purity artificial graphite, or ceramic, or vitreous silica. The dimensions of the crucibles should be such as to allow for the considerable expansion of these metals on melting and the crucibles should be deep enough to eliminate the effects of heat conduction along the thermocouple wires. Silver must be protected from oxygen while molten.

The crucible and its contents should be brought to a uniform temperature a few degrees above the melting point of the metal and then allowed to cool slowly. A thermocouple, mounted in a protecting tube of porcelain or other suitable material, with insulators separating the two wires, is immersed in the molten metal which is then allowed to freeze.

Criteria that the equilibrium temperature has been realized are: That the electromotive force of the thermocouple is independent of small changes in the depth of immersion during successive freezings, and that the electromotive force remains essentially constant for a period of at least 5 min during a single freezing.

For the range of the scale above 1063 °C, where the Planck radiation formula is used, the gold-point crucible should be modified to have a blackbody cavity at the temperature of the freezing gold.

4. Supplementary Information

4.1. Resistance—Temperature Formulas

The interpolation formula for the range 0 to 630.5 °C as given in the definition of the scale (sec. 2, *a*),

$$R_t=R_0(1+At+Bt^2),$$

may be written in the Callendar form

$$t=\frac{1}{\alpha}\left(\frac{R_t}{R_0}-1\right)+\delta\left(\frac{t}{t_{100}}-1\right)\frac{t}{t_{100}}$$

where

$$\alpha=\frac{1}{t_{100}}\left(\frac{R_{100}}{R_0}-1\right), \text{ and } t_{100}=100\,°C.$$

The relations between the coefficients are

$$A=\alpha\left(1+\frac{\delta}{t_{100}}\right), \qquad \alpha=A+Bt_{100},$$

$$B=-\frac{\alpha\delta}{t_{100}^2}, \qquad \delta=-\frac{Bt_{100}^2}{A+Bt_{100}}.$$

The interpolation formula for the range 0°C to the oxygen point as given in the definition of the scale (sec. 2b),

$$R_t=R_0[1+At+Bt^2+C(t-t_{100})t^3],$$

may be written in the Callendar-Van Dusen form

$$t=\left[\frac{1}{\alpha}\left(\frac{R_t}{R_0}-1\right)+\delta\left(\frac{t}{t_{100}}-1\right)\frac{t}{t_{100}}+\beta\left(\frac{t}{t_{100}}-1\right)\left(\frac{t}{t_{100}}\right)^3\right]°C.$$

The relations connecting A, B and α, δ are the same as those given above and the other relations are

$$C=-\frac{\alpha\beta}{t_{100}^4}, \qquad \beta=-\frac{Ct_{100}^4}{A+Bt_{100}}.$$

4.2. Secondary Reference Points

In addition to the defining fixed points of the scale, given in table 1, certain other points may be useful for reference purposes. Some of these and their corresponding reported temperatures on the International Practical Temperature Scale of 1948 are given in table 2. Except for the triple points, each temperature is for a system in equilibrium under a pressure of 1 standard atmosphere. The formulas for the variation of temperature with pressure are intended for use over the range of pressures from $p=680$ mm to $p=780$ mm of mercury.

4.3. Relation Between the International Practical Temperature Scale and the Thermodynamic Scale

When the International Temperature Scale was adopted in 1927 it was in as close accord with the thermodynamic scale as was practicable with the knowledge then available. It was recognized, however, that further research would increase our knowledge of the actual differences between values of temperature on the two scales. When it is desired to know the value of a temperature on the thermodynamic scale, the usual procedure is to obtain the value on the International Practical Temperature Scale and then to convert it to the thermodynamic scale by adding the appropriate difference between the scales. These differences, however, have to be determined by experiment. They are difficult to determine accurately because they are small compared with their Kelvin temperature. Some of these differences obtained in various parts of the scale are given below in order to how the present state of our information about the agreement of the two scales.

TABLE 2. *Secondary reference points*

Under a pressure of 1 standard atmosphere, except for the triple points.

	Temperature °C (*Int. 1948*)
Temperature of equilibrium between solid carbon dioxide and its vapor	−78.5
$t_p=[-78.5 \text{ to } +12.12(p/p_o-1)-6.4(p/p_o-1)^2]$°C	
Temperature of equilibrium between solid mercury and liquid mercury	−38.87
Temperature of equilibrium between ice and air-saturated water	0.000
Temperature of triple point of phenoxybenzene (diphenyl-ether)	26.88
Temperature of transition of sodium sulphate decahydrate	32.38
Temperature of triple point of benzoic acid	122.36
Temperature of equilibrium between solid indium and liquid indium	156.61
Temperature of equilibrium between liquid naphthalene and its vapor	218.0
$t_p=[218.0+44.4(p/p_o-1)-19(p/p_o-1)^2]$°C	
Temperature of equilibrium between solid tin and liquid tin	231.91
Temperature of equilibrium between liquid benzophenone and its vapor	305.9
$t_p=[305.9+48.8(p/p_o-1)-21(p/p_o-1)^2]$°C	
Temperature of equilibrium between solid cadmium and liquid cadmium	321.03
Temperature of equilibrium between solid lead and liquid lead	327.3
Temperature of equilibrium between liquid mercury and its vapor	356.58
$t_p=[356.58+55.552(p/p_o-1)-23.03(p/p_o-1)^2+14.0(p/p_o-1)^3]$°C	
Temperature of equilibrium between solid aluminum and liquid aluminum	660.1
Temperature of equilibrium between solid copper and liquid copper (in a reducing atmosphere)	1083
Temperature of equilibrium between solid nickel and liquid nickel	1453
Temperature of equilibrium between solid cobalt and liquid cobalt	1492
Temperature of equilibrium between solid palladium and liquid palladium	1552
Temperature of equilibrium between solid platinum and liquid platinum	1769
Temperature of equilibrium between solid rhodium and liquid rhodium	1960
Temperature of equilibrium between solid iridium and liquid iridium	2443
Temperature of melting tungsten	3380

On account of the uncertainties in these differences it seems preferable not to modify the values of temperature on the International Practical Temperature Scale now but to further improve our knowledge of the differences between the scales. When it is desired, it will be possible to improve the means of determining temperatures on the International Practical Temperature Scale without changing significantly the values of temperature. This procedure will avoid the confusion which would result from too frequent changes in values of temperature.

In the range from 0 °C to the sulfur point, intercomparisons of two nitrogen gas thermometers with standard resistance thermometers were reported in 1939 from The Massachusetts Institute of Technology. The differences found between the thermodynamic Celsius temperature t_{th} (definition of 1954) and the temperature t_{int} (1948 scale) have been formulated as follows:

$$t_{th}-t_{int}=\frac{t}{t_{100}}\left[-0.0060+\left(\frac{t}{t_{100}}-1\right)(0.041\,06-7.363\times10^{-5}\,\text{deg}^{-1}t)\right]\text{deg}.$$

This relation gives 99.994 °C (therm.) for the steam point and 444.70 °C (therm.) for the sulfur point. The results obtained with the two gas thermometers differed by 0.005 deg at the steam point and 0.05 deg at the sulfur point. In 1958 the Physikalisch-Technische Bundesanstalt reported the value 444.66 °C (therm.) for the sulfur point.

In the range from the oxygen point to 0 °C, investigations at the Physikalisch-Technische Reichsanstalt, reported in 1932, and at the University of Leiden, reported in 1935, give a set of values which indicate that the differences $t_{th}-t_{int}$ have a maximum of about +0.04 deg at about −80 °C. Below −100 °C some of the reported differences have opposite signs. These differences are of the order of magnitude of the possible uncertainties in the gas thermometer measurements. For the oxygen point, the results published since 1927 by four laboratories have been recalculated on the basis of the value $T_0=273.15$°K (adopted in 1954). These values are 90.191 °K from the Physikalisch-Technische Reichsanstalt (1932), 90.17 °K from the Tohoku University, Sendai, Japan (1935), 90.160 °K from the University of Leiden (1940), and 90.150 °K from the Pennsylvania State University (1953). The average of these four results is 90.168 °K or −182.982 °C (therm.).

The International Practical Temperature Scale is not defined below the oxygen point.

In the neighborhood of 1000 °C new determinations of the thermodynamic temperature of the silver point and gold point have been made in recent years in Germany and Japan. At the Physikalisch-Technische Bundesanstalt (1958) 962.16 °C (therm.) was obtained for the silver point and 1064.76 °C (therm.) for the gold point. At the Tokyo Institute of Technology (1958), the values 961.20 °C (therm.) and 1063.73 °C (therm.) were obtained for these points; these last two values being little different from those reported by the same laboratory in 1956, namely 961.28 °C (therm.) and 1063.69 °C (therm.)

In the range above the gold point the Planck radiation formula is used. The Planck formula is consistent with the thermodynamic scale and hence it would give true values of Kelvin temperature if the correct values were known for the Kelvin temperature of the gold point and for the second radiation constant C_2.

An analysis of variance of data on atomic constants by The California Institute of Technology, published in 1955, gave the value 0.014 388 8 meter-degree for C_2. A similar analysis from The Johns Hopkins University, published in 1957, gave the value 0.014 388 6 meter-degree for C_2.

The international practical Kelvin temperatures are obtained by adding the value of $T_0=273.15$ deg to the international practical Celsius temperatures, defined above. Values of the thermodynamic Celsius temperatures are obtained by subtracting T_0 from the thermodynamic Kelvin temperatures. Table 3 gives the recommended designations; the arrows point from the defined temperatures to the temperatures derived by changing the origin.

TABLE 3.

International Practical Scales		
Celsius		Absolute
	Names	
International Practical Temperature	→	International Practical Kelvin Temperature
	Symbols	
t_{int}		$T_{int}=t_{int}+T_0$
	Designations	
°C (Int. 1948) degrees Celsius international practical 1948		°K (Int. 1948) degrees Kelvin international practical 1948
Thermodynamic Scales		
Celsius		Absolute
	Names	
Thermodynamic Celsius Temperature	←	Thermodynamic Kelvin Temperature
	Symbols	
$t=T-T_0$		T
	Designations	
°C (therm.) degrees Celsius thermodynamic		°K degrees Kelvin

($T_0=273.15$ deg)

NOTE. For the international practical temperature, the subscript "int" after t may be omitted if there is no possibility of confusion.

(Paper 65A3–96)

JOURNAL OF RESEARCH of the National Bureau of Standards—A. Physics and Chemistry
Vol. 65A, No. 3, May–June 1961

Evaluation of the NBS Unit of Resistance Based on a Computable Capacitor

Robert D. Cutkosky

(January 16, 1961)

An evaluation of the unit of resistance maintained at the National Bureau of Standards, based on the prototype standards of length and time, is described. The evaluation is based on a nominally one-picofarad capacitor whose value may be calculated from its mechanical dimensions to high accuracy. This capacitor is used to calibrate an 0.01-microfarad capacitor. A frequency-dependent bridge involving this capacitor establishes the value of a 10^4-ohm resistor. Comparison of that resistor with the bank of one-ohm resistors maintaining the NBS unit of resistance establishes that this unit is

$$\Omega_{BU} = \mathbf{1.000002_3\ ohms \pm 2.1\ ppm.}$$

The indicated uncertainty is an estimated 50 percent error of the reported value based on the statistical uncertainty of the measurements and allowing for known sources of possible systematic errors other than in the speed of light, assuming that the speed of light $c = 2.997925 \times 10^{10}$cm/sec.

1. Introduction

The United States national standard of resistance is maintained at the National Bureau of Standards by a group of 1-ohm manganin resistors. Values of resistance are assigned to the 1-ohm reference standards by techniques based ultimately upon the national prototype standards of length and time.

The most accurate methods which have been used for this purpose in the past made use of either self-inductors or mutual inductors whose inductances were computable from their mechanical dimensions. In principle, it is then straightforward to compare the impedance of the computable inductor at a known frequency with that of the 1-ohm reference standard resistors. In practice, this comparison is likely to involve several steps, and may not even make use of sinusoidal currents through the inductor.

An alternative method for assigning values to the reference resistors involves constructing a capacitor whose capacitance may be calculated from its mechanical dimensions. By comparing the impedance of the capacitor at a known frequency with that of the reference standard resistors one may establish the values of the reference resistors in terms of the prototype standards.

Within recent years the development of an improved computable capacitor [1, 2, 3, 4] [1] and improved methods for the precise comparison of capacitances [5, 6] have made the latter process appear to be the more fruitful.

The method involves stepping up from a 1-pf three-terminal computable capacitor to two 0.01-μf three-terminal capacitors. The step-up is made in four steps, using a transformer whose nominally 10:1 ratio may be accurately measured. The average admittance of the two 0.01-μf capacitors at an angular frequency of 10^4 radians per second is compared with the average admittance of two 10^4-ohm shielded a-c resistors using a bridge network to be described. These measurements serve to assign values to the 10^4-ohm a-c resistors in terms of the prototype standards.

A conventional d-c step-down from these 10^4-ohm a-c resistors to the 1-ohm NBS reference resistors provides an absolute calibration of the 1-ohm resistors. A small correction must be applied to the results so obtained because of the a-c–d-c differences of the 10^4-ohm resistors. This correction is determined by comparison with a special transfer resistor.

2. Computable Cross Capacitor

Computable capacitors of the traditional guard-ring or guard-cylinder design require, in general, the measurement of several dimensions. For example, with the guard-ring type, area, plate separation, flatness of electrodes, parallelism, and proper location of the guarded island are of major concern. Most of these dimensions have to be measured to a higher accuracy than the required overall accuracy of the computed capacitance.

The development by A. M. Thompson and D. G. Lampard of a device called by them a computable cross capacitor [1] has made possible the construction of a capacitor whose value may be computed from dimensional measurements with an accuracy considerably higher than that attainable with any previous design.

[1] Figures in brackets indicate the literature references at the end of this paper.

A cross capacitor consists of a cylindrical arrangement of four electrodes, with cross section as shown in figure 1. Electrodes 1, 2, 3, and 4 are separated from each other by very small insulating gaps. Let C_1/L be the direct capacitance per unit length (perpendicular to the plane of the drawing) between electrodes 1 and 3 with electrodes 2 and 4 grounded, and let C_2/L be the direct capacitance per unit length between electrodes 2 and 4 with electrodes 1 and 3 grounded. It may be shown that in *cgs*, esu,

$$e^{-4\pi^2 C_1/L}+e^{-4\pi^2 C_2/L}=1, \text{ or in MKS units,}$$

$$\overline{C}=\frac{1}{2}(C_1+C_2)=\epsilon_0 L(\ln 2/\pi)[1+0.087(\Delta C/\overline{C})^2]$$

$$+\mathcal{O}\{(\Delta C/\overline{C})^4\}] \text{ farads} \qquad (1)$$

where $\epsilon_0=1/\mu_0 c^2$, c is the speed of light, and $\Delta C=C_2-C_1$. The notation "$\mathcal{O}$" means that all remaining terms in eq (1) are fourth order or higher in $\Delta C/\overline{C}$, and their sum approaches zero as $K(\Delta C/\overline{C})^4$ as $\Delta C/\overline{C}$ tends to zero. This relationship allows $\overline{C}$ to be calaculated from a single measured length L. One finds that if $C_1 \approx C_2$, then $\overline{C}/L \approx 2$ pf/meter $\approx$ 0.05 pf/in.

The requirements that both $\overline{C}$ and L be easily measurable have led to the use at NBS of two cross capacitors in parallel, each about 10 in. long, to produce a capacitance of about 1pf [6]. Figure 2 shows the cross section of the NBS 1-pf computable cross capacitor, which is housed in an evacuated chamber. Electrodes 1, 2, 5, and 6; and electrodes 2, 3, 6, and 7 of the two cross capacitors are steel bars ⅞ in. in diameter supported with accurately ground glass slips and disks, shown dotted in the figure, resting on a precision granite surface plate. The bottom row of bars is held together with a phosphor-bronze coil spring between bars 4 and 8 at each end of the assembly. The glass spacers are all located within guard sections at the ends of the capacitor, so that no solid dielectric appears between the bars within the active length of the capacitor. Figure 3 shows a side view of electrode 6, which is similar to electrode 2. The assembly is constructed of precision gage blocks having circular cross sections, with wrung joints between the 10-in. bar and its adjacent 2-in. bars, and insulated with firmly cemented 0.002-in. mica spacers between each pair of 2-in. bars. The outer 2-in. bars constitute the guard sections, and are grounded. The composite 14-in. central section defines the length of the cross capacitor, and extends roughly between the centers of each insulated gap. Electrodes 1, 3, 5, and 7 are approximately 18 in. long, and so extend well beyond the active sections of bars 2 and 6.

Additional shields not shown in figure 2 eliminate capacitive coupling between electrodes around the outside of the grounded electrodes. This is essential, since (1) deals only with the capacitance associated with the region in the interior of the electrode system.

One capacitance measurement is made, with electrodes 1, 3, and 6 grounded, of the direct capacitance between electrodes 5 and 7 in parallel and the central section of electrode 2. Another measurement is made, with electrodes 5, 7, and 2 grounded, of the capacitance between electrodes 1 and 3 in parallel and the central section of electrode 6. If we neglect, for the moment, the small second order correction $0.087(\Delta C/\overline{C})^2$ in eq 1, the average of these two capacitances is equal to $2\times\epsilon_0 L'\ln 2/\pi$; where L' is the average length of the two central sections of electrodes 2 and 6, or approximately 14 in. If the 10-in. gage blocks are removed from electrodes 2 and 6 and the 2-in. bars on either end are wrung directly together, a new cross capacitor is formed with a length differing

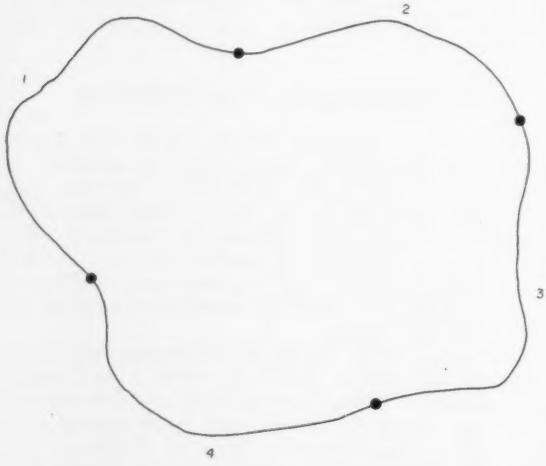

FIGURE 1. *Cross section of a general cross capacitor.*

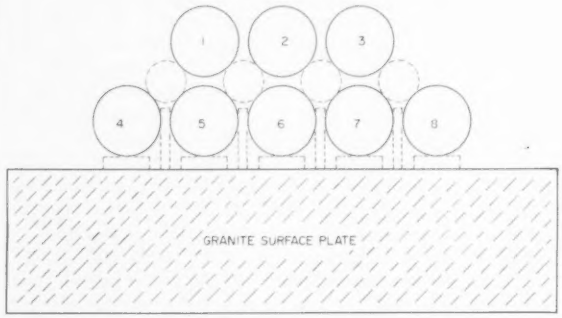

FIGURE 2. *Cross section of the NBS cross capacitor.*

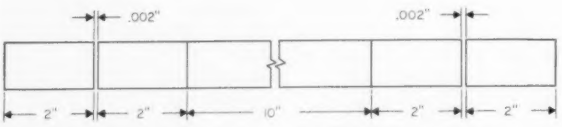

FIGURE 3. *Side view of the NBS cross capacitor detector electrodes.*

from the first by twice the average length of the 10-in. bars, or about 20 in. The difference between the two cross capacitances so measured is not affected by irregularities or lack of perfect centering of the bars near the insulated gap, provided that the end sections are not rotated or otherwise disturbed when the 10-in. bars are removed or replaced.

The small discontinuities caused by the slightly-rounded ends of the gage blocks produce only second-order errors in the capacitance computed from eq (1). These errors have been investigated experimentally by introducing additional discontinuities on the bars.

Between May 12 and May 18, 1960, and again between July 21 and July 27, 1960, two series of measurements with the NBS computable cross capacitors were made to establish the value of a fixed, 1-pf, air-dielectric, three-terminal, reference capacitor; NBS 89790–B. This capacitor was maintained in an oil bath at a constant temperature near 25 °C.

A transformer ratio-arm bridge was used for this purpose with the circuit shown in figure 4. The cross capacitor with the 10-in. bars in place has a capacitance slightly under 1.4 pf so that the bridge may be balanced with a small adjustable capacitance p as shown, and a small adjustable conductance not shown, which may be placed on either side of the bridge. The bridge components have been described in detail elsewhere [6] and will not be elaborated upon here.

The bridge circuit for the measurement with the 10-in. bars removed is similar to figure 4 except that the cross capacitance is now about 0.4 pf, so the 1-pf capacitor in the lower portion of the circuit must be removed. The 4-pf capacitor consists of 4 one-pf capacitors which may each be compared directly with the 1-pf standard, and then connected in parallel. Since the adjustable capacitor has a relatively high reading, it is also necessary to calibrate it for each measurement.

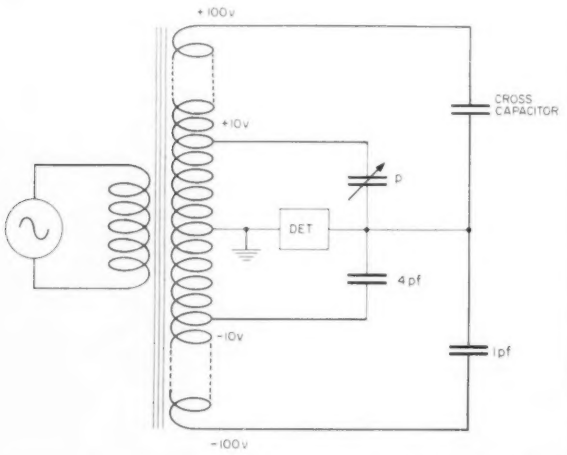

FIGURE 4. *Inductively coupled ratio arm bridge used with the NBS cross capacitor.*

All of the above steps are straightforward and can be done in a symmetrical fashion (calibration, cross-capacitor measurement, and recalibration) in less than 30 min by an experienced operator.

Before and after the determination, the 1-pf capacitor used is compared with the 1-pf reference capacitor in the oil bath.

Although small direct (three-terminal) capacitances are much easier to measure than small two-terminal capacitances because of the virtual elimination of connection problems, a particularly troublesome source of error arises when capacitance to ground is very high, as is the case with the NBS cross capacitor. Figure 5 shows a three-terminal capacitor with direct capacitance C_1 connected to a bridge with leads of inductance L_1, L_2, and L_3. It may be shown that the effective capacitance seen by the bridge is given by

$$C_{eff} \approx C_1[1-\frac{\omega^2(C_2C_3)}{C_1}L_1+\omega^2C_3L_2+\omega^2C_2L_3+ \omega^2C_1(L_2+L_3)].$$

For C_1, C_2, and C_3 all less than 1000 pf, the important error, expressed as an additive term, is $-\omega^2L_1C_2C_3$; which is independent of C_1 and hence relatively more important for a very small C_1. Thompson [5] has shown that if the capacitor is treated as a four-terminal network as in figure 5 with a high perme-

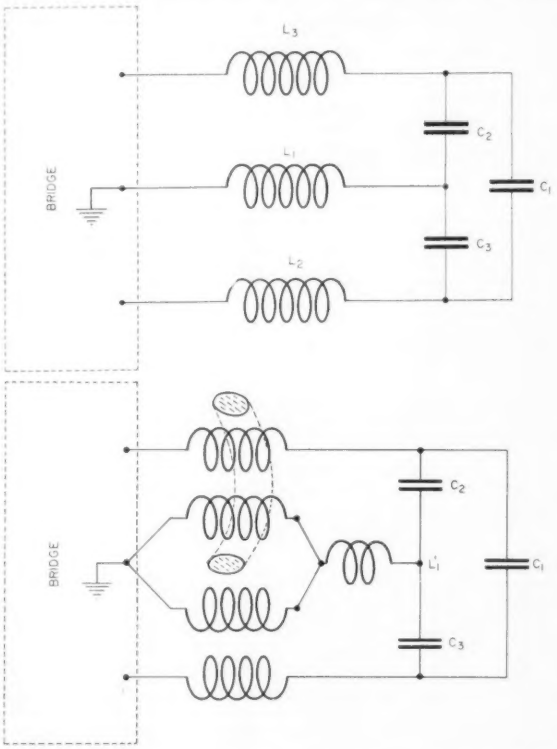

FIGURE 5. *Three-terminal capacitor C_1 connected to a bridge with three leads, with four leads and using a high permeability core (See text).*

ability core linking one ground lead with one active electrode lead, the troublesome error term is eliminated. This technique has been used throughout the measurements reported here. It is impossible with the NBS cross capacitor to completely eliminate all common ground lead inductance in this way, and a small inductance L_1' remains in the cross capacitor circuit. We have found it necessary to measure C_{eff} as a function of frequency and extrapolate to zero frequency under the assumption that the error is proportional to ω^2. With most of L_1 eliminated by the use of high permeability cores, the factor $\omega^2 L_1' C_2 C_3$ is very small, and the d-c value may be determined to high accuracy.

Table 1 shows the results of two complete series of measurements on the NBS computable cross capacitor, based on the assumption that the reference capacitor in the oil bath was exactly 1 pf.

The correction term in the measured capacitance $0.087(\Delta C/\overline{C})^2$ is less than two parts in 10^7 and has been neglected. The calculated cross capacitance also appears in table 1, based on the measured lengths of the 10-in. gage blocks, and taking the speed of light $c=2.997925\times10^{10}$ cm/sec as adopted recently by the IGGU and the URSI. Combining these figures we obtain true values for the reference capacitor at the time of measurement. The difference between the May and July figures reflects a shift in the temperature of the oil bath which occurred some time in June, and has no effect on the final results quoted in this paper. The stability of the reference capacitor and the closeness of temperature regulation during each of the determinations was sufficient to reduce any error arising from the variability of the reference capacitor considerably below 1 ppm.

TABLE 1. *Capacitance of cross capacitor*

Based on 1-pf reference capacitor #NBS 89790–B.

Time and date (1960)	Nominal length	Frequency	Measured capacitance	D-c capacitance
	in.	*c/s*	*pf*	*pf*
11:00 a.m. May 12	14	1592	1.3898231	1.3898241
8:55 a.m. May 13	14	1592	1.3898224	1.3898234
9:40 a.m. May 13	14	1592	1.3898222	1.3898231
2:05 p.m. May 13	14	1000	1.3898229	1.3898233
2:50 p.m. May 13	14	1592	1.3898220	1.3898229
1:20 p.m. May 16	4	1592	0.3973528	0.3973532
2:00 p.m. May 16	4	1592	.3973531	.3973535
2:55 p.m. May 16	4	1000	.3973536	.3973538
10:45 a.m. May 18	14	1592	1.3898201	1.3898210
11:35 a.m. May 18	14	1000	1.3898211	1.3898215
12:20 p.m. May 18	14	1592	1.3898198	1.3898208

Measured cross capacitance difference=0.9924687 pf.
Computed cross capacitance difference=0.9924151 pf.
True value of reference capacitor=1-pf −54.0 ppm (May 1960).

Based on 1-pf reference capacitor #NBS 89790–B.

Time and date (1960)	Nominal length	Frequency	Measured capacitance	D-c capacitance
	in.	*c/s*	*pf*	*pf*
9:22 a.m. July 21	14	1592	1.3898177	1.3898187
10:15 a.m. July 21	14	1000	1.3898177	1.3898180
12:45 p.m. July 21	14	1000	1.3898171	1.3898175
1:15 p.m. July 21	14	1592	1.3898164	1.3898174
9:45 a.m. July 25	4	1592	0.3973511	0.3973515
11:20 a.m. July 25	4	1000	.3973511	.3973513
1:00 p.m. July 25	4	1000	.3973512	.3973514
1:43 p.m. July 25	4	1592	.3973507	.3973511
9:15 a.m. July 27	14	1592	1.3898154	1.3898164
10:05 a.m. July 27	14	1000	1.3898165	1.3898168
12:52 p.m. July 27	14	1000	1.3898155	1.3898169
1:15 p.m. July 27	14	1592	1.3898165	1.3898175

Measured cross capacitance difference=0.9924661.
Computed cross capacitance difference=0.9924151.
True value of reference capacitor=1-pf −51.4 ppm (July 1960).

3. Capacitance Step-Up

The bridge for comparing capacitive reactance with resistance, to be described in a later section, requires the use of two 0.01-μf capacitors. These capacitors must be calibrated in terms of the 1-pf reference capacitor. A transformer ratio-arm bridge with a nominally 10:1 ratio is used for this calibration in the circuit of figure 6.

The balance conditions are, to a sufficiently close approximation,

$$C_2=10\ C_1(1+\alpha)-p, \text{ and } g_2=10\ g_1-10\omega C_1\beta-q,$$

where p and q are small adjustable admittances for balancing the bridge. One may connect p and q to point "B" instead of "A" to change their apparent signs if this is needed to obtain a balance.

Shielding completely surrounds each of the capacitors in the circuit in such a way that the measurement compares the direct capacitances C_1 and C_2. This technique allows the direct capacitance of the 10-pf capacitor to be determined relative to the 1-pf reference capacitor. The 10-pf capacitor is in turn compared with a 100-pf capacitor, to reach after four such steps the 0.01-μf mica capacitors used in the resistance bridge. All of the step-up capacitors are located in a regulated oil bath. The 0.01-μf capacitors as well as the 1000-pf capacitor are sufficiently large to require correction for the equivalent series inductances of the transformer. The total inductance correction was found to be two parts in 10^7 for each 0.01-μf capacitor [6].

It was desired that the total uncertainty in the step-up be less than one part in 10^7, which requires that the transformer ratio $10(1+\alpha+j\beta)$ be known to

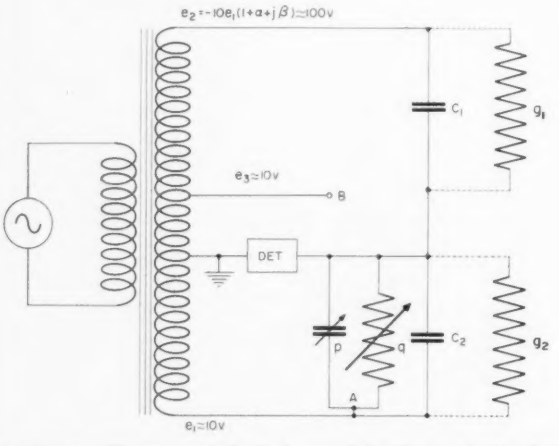

FIGURE 6. *Ten-to-one inductively-coupled ratio arm bridge for stepping up from 1 pf to 0.01 μf in four steps.*

an accuracy of about two parts in 10^8. A procedure for calibrating such a transformer to the required accuracy has been described [7] which involves the use of 11 nominally equal three-terminal capacitors having their detector electrodes connected together. Provision is made for switching any one of the capacitors to the high voltage side of the transformer while the other 10 are in parallel on the low voltage side. The bridge was balanced with a small admittance on one side or the other of the bridge with each of the 11 capacitors in turn on the high voltage transformer winding. After applying small corrections for lead impedances one obtains from this series of measurements values for α and β in the expression for the transformer ratio.

4. Resistance-Capacitance Bridge

Several bridges capable of being used for the comparison of resistance with capacitive reactance have been used in the past, one of the most popular being the Wien bridge. The Wien bridge, like many frequency dependent bridges, is difficult to shield against stray pickup. The difficulty comes from the fact that one arm of the bridge contains a resistor and a capacitor in series. If this arm is shielded, leakage currents from their common point to the shield produce errors which are difficult to evaluate with high accuracy.

4.1. Bridge Equations

In theory it is simple to compare resistance with capacitive reactance provided that one may obtain two a-c voltage sources exactly 90° out of phase and exactly equal in magnitude. Figure 7 shows two such sources used to compare a capacitance C with a conductance G. The balance condition is $G=\omega C$. The components may be readily shielded as shown with dotted lines; leakage paths to ground are either across the detector, which at balance has no voltage on it; or across one of the generators, which is assumed to have a very low impedance. Although it has not been possible to construct voltage sources with the required phase and magnitude relationships, accurate low impedance voltage sources equal in magnitude and 180° apart in phase are readily procurable from a center-tapped transformer.

A double bridge using the principles of figure 7 may be constructed with the circuit of figure 8, which shows all voltages referred to one generator as reference.[2] The voltages $+1$ and $-1(1+\alpha+j\beta)$ are approximately equal and 180° out of phase, with α and β representing magnitude and phase angle errors respectively. The voltage $j(1+z)$ is approximately 90° out of phase with each of the other generators. The small complex number z represents the departure of the generator from its nominal value.

Figure 8 also shows the residual leakage conductances g_1 and g_2 of the main capacitors C_1 and C_2, and the stray capacitances c_1 and c_2 of the main conductance standards G_1 and G_2.

[2] Bridge networks of this type were investigated at the National Standards Laboratory in Sidney, Australia, in 1952 but the findings were not published. The network described in this paper was subsequently developed independently.

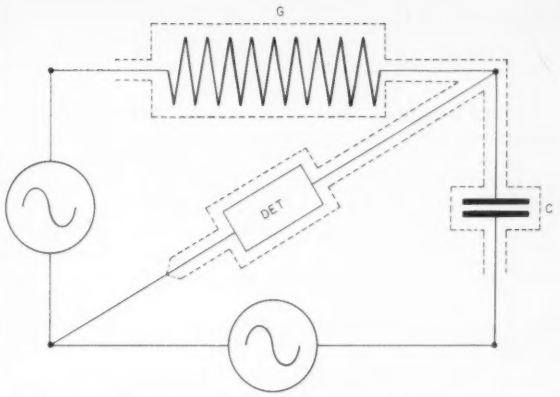

FIGURE 7. *Basic bridge for comparing conductance with capacitive susceptance.*

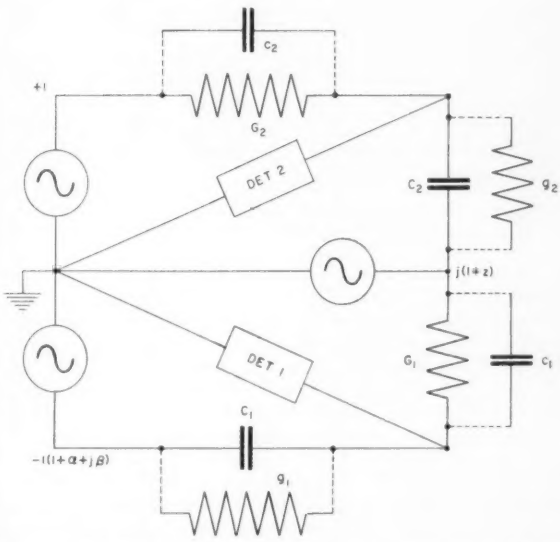

FIGURE 8. *Double bridge for comparing conductance with capacitive susceptance.*

This circuit is used with $C_1 \approx C_2 \approx 0.01$ μf, $G_1 \approx G_2 \approx 10^{-4}$ mhos, and $\omega \approx 10^4$ radians per second (about 1592 c/s).

With both bridges balanced we have the conditions

$$j\omega c_2 + G_2 = -j(1+z)(j\omega C_2 + g_2)$$

and

$$(1+\alpha+j\beta)(j\omega C_1 + g_1) = j(1+z)(j\omega c_1 + G_1).$$

Eliminating z from these equations we have

$$(j\omega c_2 + G_2)(j\omega c_1 + G_1) = -(1+\alpha+j\beta)(j\omega C_2 + g_2)(j\omega C_1 + g_1).$$

Separating real and imaginary parts we find

$$G_1 G_2 = (1+\alpha)\omega^2 C_1 C_2 + \beta(\omega C_1 g_2 + \omega C_2 g_1) - (1+\alpha) g_1 g_2 + \omega^2 c_1 c_2,$$

and

$$\omega[c_1G_2+c_2G_1]+(1+\alpha)\omega[C_1g_2+C_2g_1]=\beta\omega^2C_1C_2-\beta g_1g_2.$$

It may be shown that if all residual parameters are small, we may write approximately

$$\overline{G}=(1+\tfrac{1}{2}\alpha)\omega\overline{C} \tag{2}$$

and

$$\omega\overline{cG}+\omega\overline{Cg}=\tfrac{1}{2}\beta\omega^2\overline{C}^2 \tag{3}$$

where bars over letters signify the average of the two values involved.

The voltage appearing at the terminals of detector 1 may be reduced to zero by making either C_1 or G_1 and either c_1 or g_1 adjustable, and similarly for detector 2. One finds that even if z is zero, either c_1 or g_1 and either c_2 or g_2 must be negative. As shown in figure 9, this is accomplished by connecting an adjustable conductance q_1 from point A to D_1 and an adjustable capacitance p_1 from point B to D_2. The main capacitors C_1 and C_2 consist of the 0.01-μf mica capacitors in parallel with adjustable capacitors having ranges of 1 pf. With these provisions eq (3) is replaced by

$$\omega\overline{cG}+\omega\overline{Cg}-\tfrac{1}{2}(\omega p_1\overline{G}+\omega\overline{c}q_1)=\tfrac{1}{2}\beta\omega^2\overline{C}^2. \tag{4}$$

It is apparent from figure 9 and the above equations that C_2 is the effective capacitance including the correction resulting from self inductance between junctions C and D_2, and G_1 must include the series resistance correction between junctions C and D_1. If the open circuit transformer-ratio parameters α and β are used, C_1 and G_2 must include the effects of impedances ζ_1 and ζ_2, measured from junctions D_1 and D_2 respectively, through the transformer to the ground point G. To avoid the problems of accurately measuring the transformer impedances, we have found it profitable to measure the loaded rather than the open circuit transformer ratio between A and B to G while the bridge is balanced. Using the values so obtained for α' and β', the required values of G_2 and C_1 include impedances only to junctions A and B.

The loaded transformer ratio is easily measured with a third bridge involving C_3, C_4, and detector 3 on the left of figure 9. This bridge is balanced with the circuit as shown and rebalanced after interchanging C_3 and C_4. The readings of p_2 and q_2 are called p_2' and q_2' before interchanging, and p_2'' and q_2'' after interchanging. The transformer parameters α' and β' are calculated from the formulas

$$\alpha'=-\frac{p_2'+p_2''}{C_3+C_4} \text{ and } \beta'=\frac{q_2'+q_2''}{\omega(C_3+C_4)}.$$

The signs of p_2 and q_2 are positive if connected to B as shown, and negative if connected to A. It is found that for this bridge, with the loading shown in figure 9, $\alpha'\approx+17\times10^{-6}$ and $\beta'\approx-16\times10^{-6}$.

4.2. Physical Bridge Arrangement

In order to minimize current loops and localize the junction points A, D_2, C, D_1, B, and D_3, a hexagonal bridge center was constructed of copper as shown in figure 10. Each segment consists of five coaxial connectors with their shields bolted to a ¼-in. copper top plate and their inner conductors connected by means of a copper plate. These six connecting plates shown dotted in the figure, are shielded from each other so that capacitance and conductance between segments arises only from external elements that are connected between pairs of coaxial connectors in the various segments. The intersections of the arms of the copper connecting plates define the junction points referred to in the discussion of figure 9. The bridge center is located just above the liquid level in the middle of a large temperature-regulated oil bath.

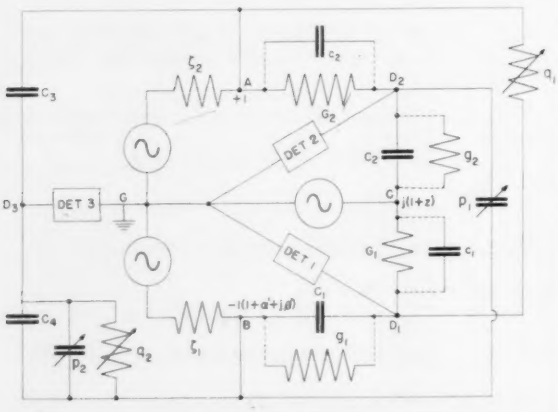

FIGURE 9. *Complete bridge with auxiliary components.*

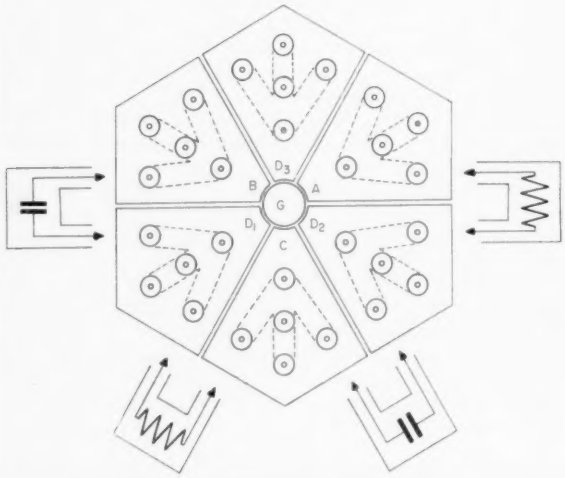

FIGURE 10. *Diagram of bridge center.*

The voltage sources are connected to the bridge center points A, B, and C, by heavy wires passing through a tube that is welded to the bottom of the oil bath tank and extends above the liquid level beneath the center. The 10^4-ohm resistors and the 0.01-μf capacitors, hermetically sealed and immersed in the oil to maintain them at a constant temperature, are connected to the center with rigid coaxial leads positioned as in figure 10.

Coaxial detector leads run from the connectors at D_1, D_2, and D_3, upwards through an eye-level shelf to filters, amplifiers, and visual detectors.

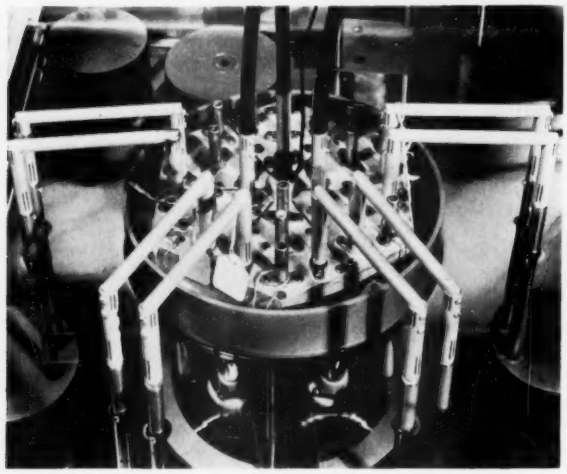

FIGURE 11. *Photograph of components shown in figure 10.*

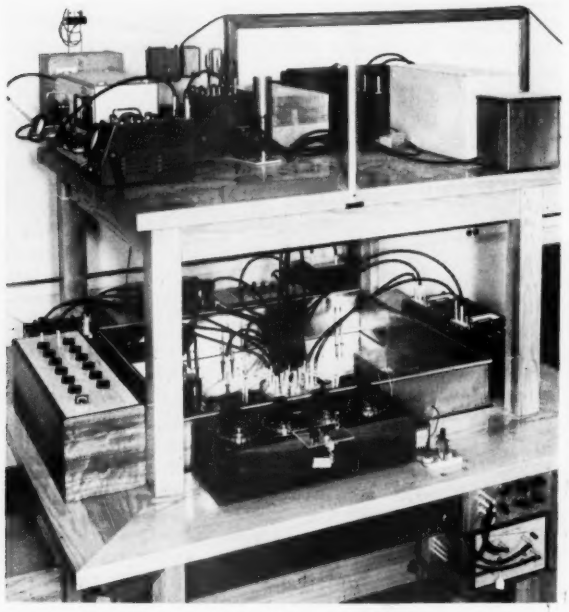

FIGURE 12. *Photograph of bridge assembly for comparing conductance with capacitive susceptance.*

Figure 11 shows the principal features of the bridge arrangement, and figure 12 shows the auxiliary admittances in place for balancing the bridge.

Although the two voltage sources derived from a transformer are easily procurable, the third source 90° out of phase with them presented some design problems. Our equipment uses a passive phase-shifting network driven by a separate winding on the main transformer to produce this voltage. The phase-shifting network is adjustable to allow the complex components of z to be varied in small increments and set within a few parts in a million of zero.

The assumptions leading to the bridge equations require only that the proper voltage at junction C be produced and maintained, and place no restriction on the equivalent series impedance of the 90° source. However, if its impedance is too large, variation of one balancing component such as C_1 in figure 9 changes not only the voltage at D_1, but also the voltage at junction C and hence at D_2. This mutual dependence between the two bridges makes it very difficult to balance both bridges simultaneously unless the impedance of the 90° source is less than $\frac{1}{10}$ the impedance of the bridge arms, or in this case less than 1000 ohms. Based on these considerations, the circuit of figure 13 was chosen to provide the three sources for the bridge. With A, B, and C connected to the bridge. the voltage at C may be adjusted, with the controls provided, to the proper value.

Power for driving the bridge is provided by a commercial tuning fork oscillator driving a power amplifier as shown in figure 14. The filter is designed to reduce harmonic content of the signal. The tuning fork frequency is adjustable in a small range around $\omega = 10^4$.

4.3. Frequency Measurement

The frequency is measured with the circuit of figure 15. The pulse former preceding the preset counter proper is part of the preset counter assembly. The sharp pulse produced therein goes through the gate when the preset counter registers the desired

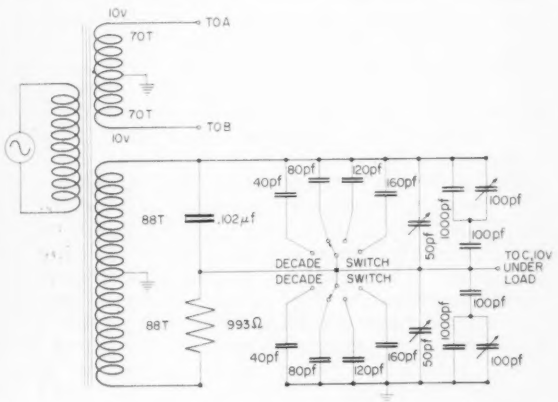

FIGURE 13. *Bridge voltage sources.*

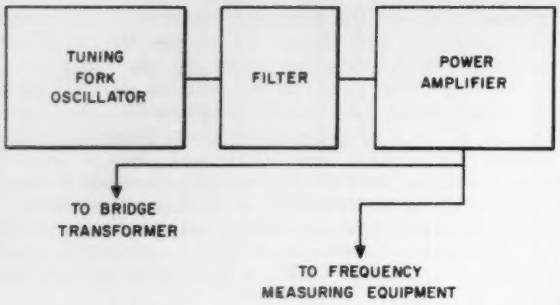

FIGURE 14. *Bridge power supply.*

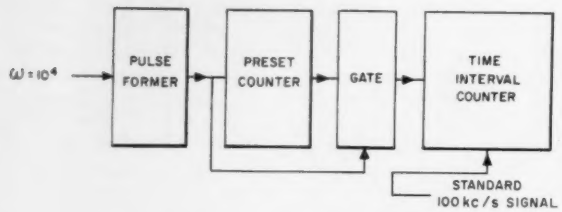

FIGURE 15. *Frequency measuring system.*

number of counts, and the time interval counter measures the time between two such pulses. The preset counter is automatically reset after 10^4 cycles at the input. For $\omega = 10^4$ the time interval between pulses reaching the time interval counter is 2π sec, during which time a 10-Mc/s signal derived from the 100-kc/s standard frequency source is counted and displayed by the time interval counter. The system may be checked for internal consistency by using it to measure 10^4 periods of a standard 1000-cycle signal. This equipment monitors the tuning fork output while the bridge is in use, and allows the frequency to be measured with an accuracy better than 5 parts in 10^8.

4.4. Detectors

Since the bridge balance is strongly frequency dependent, the harmonics of the driving frequency may have relatively high signal levels at the detector inputs. Sharp tuning of the detectors is not sufficient to eliminate trouble from this source, since two or more harmonics may mix in the nonlinear first stages of the amplifiers to produce apparent fundamental frequency signals [8].

Figure 16 shows the circuit of filters which precede the electronic amplifiers used with detectors D_1 and D_2. With the exception of the input transformer, all inductors are 0.1-henry commercial dust-core toroidal inductors. The input transformer must have a very high Q to preserve high signal strength, and was constructed from a similar inductor by removing a few turns and adding a primary; the turns ratio being chosen to give a good impedance match between the bridge and the filter. The filter forms a bridge which is balanced at the second harmonic

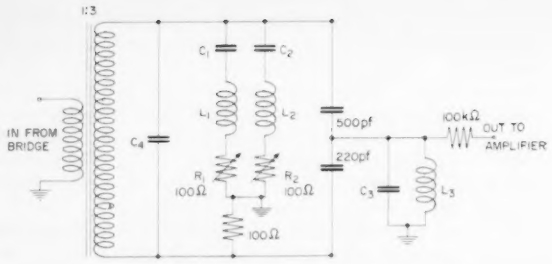

FIGURE 16. *Filters for harmonic rejection.*

by adjusting C_1 so that C_1 and L_1 resonate, and by adjusting R_1. Also, C_2 and R_2 are adjusted to produce balance at the third harmonic. Tuning the input transformer with C_4 and the output circuit with C_3 to the fundamental completes the adjustment of the doubly-tuned filter which attenuates harmonics higher than the third sufficiently for our purposes. The filters are housed in boxes constructed of $\frac{1}{16}$ in. sheet steel for magnetic shielding.

It has been found that with these filters, second and third harmonic signal levels are attenuated 140 db with respect to the fundamental, and all higher harmonics by at least 95 db. Experimentation with filter orientation shows that stray pickup to the filters cannot produce an error as large as one part in 10^7.

The effectiveness of the filters has been investigated by greatly increasing the harmonic content of the power signals reaching the bridge. For this purpose a diode rectifier was placed between the tuning-fork filter and the power amplifier. Harmonic levels at the bridge center were measured with and without this diode. It was found that although the levels of all measured harmonics were greatly increased, the bridge balance change was less than one part in 10^7.

Following the detector filters, commercial tuned amplifiers are used, which drive the vertical deflection plates of cathode-ray tubes. The horizontal plates of the cathode-ray tubes are driven by constant amplitude sinusoidal voltages derived from the tuning-fork oscillator but passing through variable phase shifters. At balance a straight horizontal line appears on the cathode-ray tube, and the phase shifter may be adjusted so that an unbalance in a main component (C_1 or C_2) opens the line into an ellipse, and an unbalance in phase (q_1 or p_1) tilts the line. This provides a phase sensitive detection scheme which allows the bridge to be balanced with a minimum of time consumed. The detector sensitivity is sufficient to observe unbalances of one part in 10^7 in magnitude or 10^{-7} radians in phase angle.

4.5. Resistance Comparisons

The bridge system described allows the mean of two a-c conductances G_1 and G_2 to be measured in terms of a measured frequency and two capacitors C_1 and C_2 whose values are obtained from a computable capacitor. The conductance standards G_1 and

G_2 each consists of a commercial 10^4-ohm woven-wire resistor mounted in a shielded hermetically-sealed box and placed in the oil bath. The reciprocal of their measured conductance values is a resistance, which must be stepped down and compared with the bank of 1-ohm reference resistors which maintain the unit of resistance [9].

The conductance standards G_1 and G_2 are completely shielded, and are measured in the a-c bridge as direct conductances. In section 5 we will describe measurements performed to evaluate the difference between their conductances as measured with 1592 c/s alternating current, and their conductances as measured with direct current. This difference may be expected to be small, and will certainly remain constant over long periods of time. We will, at this time, tentatively assume that the difference is zero, and apply a correction later.

The d-c direct conductances of G_1 and G_2 are compared with the resistance of a stable 10^4-ohm d-c resistor in the circuit of figure 17, which shows the provision for eliminating the effect of leakage resistances R_3 and R_4 to the shield. The bridge is balanced first with point (1) grounded, which shorts R_4 and places R_3 in parallel with G_1; and then with point (2) grounded, which places R_4 across the battery and places R_3 across the 10^4-ohm standard R#505. Neither balance depends upon R_4, and a large R_3 affects the two balances equally with opposite sign; hence the average balance gives the ratio[3]

$$\frac{r_4+1/G_1}{r_3+R\#505}=\frac{B}{\overline{A}_1}$$

Interchanging the link and standard, moving the galvanometer to D_1, and repeating the two balances gives

$$\frac{r_4+R\#505}{r_3+1/G_1}=\frac{B}{\overline{A}_2},$$

so that to the accuracy desired $R\#505=1/G_1(\times[1+(\overline{A}_1-\overline{A}_2)/2B]$, which allows the resistance of G_1 to be compared with the resistance of the d-c standard. The measurement is made with G_1 connected to the bridge center, and measurements are made between the same junctions used in the a-c measurement. A similar measurement of G_2 allows the 10^4-ohm d-c standard to be measured in terms of $\overline{G}=\frac{1}{2}(G_1+G_2)$, which is obtained from the a-c bridge. The measurement method involves the well-known double substitution technique with provision for eliminating the errors which might be caused by leakage resistance.

The variable arm A is constructed from a 100-ohm direct reading ratio set with a smallest step of one ppm, but is connected in series with a 900-ohm resistor to give a smallest step of one part in 10^7.

[3] This relationship is actually an approximation, and depends upon R_3 being large compared with R#505. Since the two values of A_1 differed in our measurements by only a few parts per million, the approximation introduces no significant error.

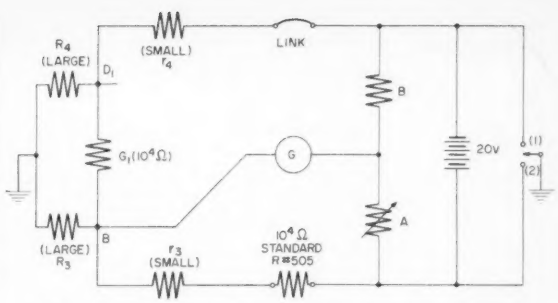

FIGURE 17. *Circuit for three-terminal d-c resistance measurement.*

This 900-ohm resistor, a 10^3-ohm resistor B, the 10^4-ohm standard, and the link rest on a mercury stand in the oil bath.

Table 2 shows the results of several comparisons of the 10^4-ohm d-c resistor with the 1-pf reference capacitor, using the frequency-dependent bridge. Recalling that the reference capacitor was measured in terms of the computable capacitor in May and July 1960, it will be noted that groups of runs were made immediately preceding and immediately following each cross capacitor measurement.

Each set of one cross capacitor measurement and two groups of resistance-capacitance bridge runs constitutes an evaluation of the resistance of the 10^4-ohm standard R#505.

5. Frequency Dependence of Bridge Resistors

The measurements of the a-c–d-c resistance differences of G_1 and G_2 were made by comparing them with a standard resistor of simple geometry having predictable frequency characteristics, using both direct current and 1592 c/s alternating current. Figure 18 shows the cross section of such a standard

TABLE 2. *Resistance of 10^4 ohm d-c resistor #505*

Based on 1 pf reference capacitor #NBS 89790–B neglecting a-c–d-c differences

Date (1960)	R#505	Average phase angle of 10^4 ohm a-c resistors
		Microradians
May 5	10^4 ohms −73.6 ppm	+15.0
May 10	−73.4	+15.4
May 11	−74.3	+14.8
May 19	−74.1	+15.4
May 20	−74.0	+15.2
Average	−73.9 ppm	+15.2

True value of 1 pf reference capacitor = 1 pf −54.0 ppm.
Resistance of R#505 = 10^4 ohms −19.9 ppm.

Date (1960)	R#505	Average phase angle of 10^4 ohm a-c resistors
		Microradians
July 18	10^4 ohms −72.2 ppm	+14.7
July 19	−71.8	+15.0
July 28	−72.5	+14.8
July 29	−71.6	+14.7
Average	−72.0 ppm	+14.8

True value of 1 pf reference capacitor = 1 pf −51.4 ppm.
Resistance of R#505 = 10^4 ohms −20.6 ppm.

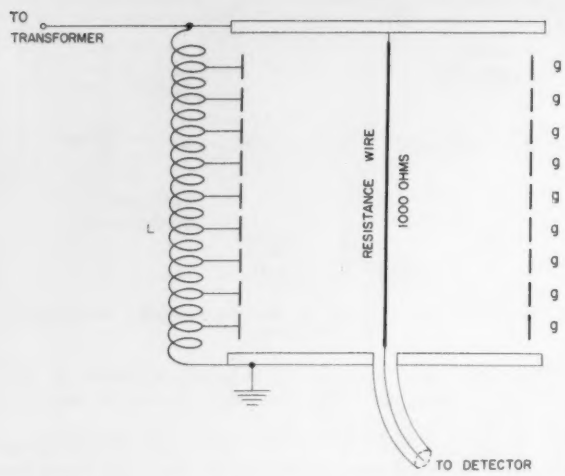

FIGURE 18. *A-c–d-c resistance transfer standard.*

whose resistance element consists of a single straight wire 0.0008 in. in diameter and 9.5 in. long having a resistance of 1000 ohms. The structure is cylindrical with the resistance wire down the center. The large phase angle expected from a conventional coaxial line resistor is eliminated by the use of a set of guard rings, *g*, about 4 in. in diameter, which surround the resistance wire. The potentials of the guard rings are defined with a tapped inductor *L* placed between the line terminal and ground. The inductor taps are placed to provide a uniform potential gradient down the center of the cylinder in the absence of the resistance wire.[4]

When a bridge containing the transfer resistor is balanced with the resistance wire in place, the detector voltage is zero, and the potential gradient along the wire is still uniform. Since the wire does not change the electric field within the resistor assembly, we may expect no capacitance contribution to the resistor phase angle and a-c–d-c resistance difference. The effectiveness of the guard rings may be checked by connecting adjacent guards in parallel to cut the effective number of them in half, and by suitably reconnecting them to the tapped inductor. If the apparent resistance and phase angle measured in these two ways are the same, we may assume that the number of guard rings is sufficient to eliminate the effects of capacitance within the resistor. In practice it is found that even with all of the guard rings grounded, the measured a-c resistance is equal to the a-c resistance with all guards connected properly to the tapped inductor, and the phase angle change between the two-guard arrangements is less than 3 microradians.

The inductance of the standard resistor was measured by replacing the fine resistance wire with a larger low resistance wire and measuring, with a Maxwell-Wien bridge, the inductance including that of the coaxial leads between the junction points

[4] Similar arrangements applied to high voltage transformer testing have been described by Silsbee [10] and Weller [11].

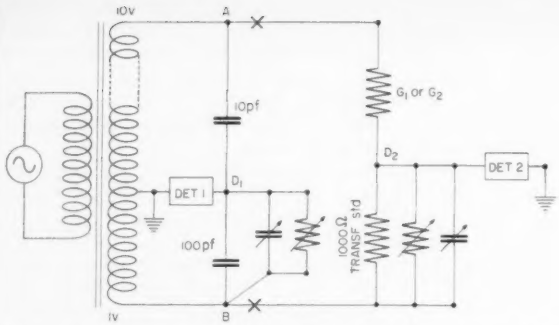

FIGURE 19. *Circuit for comparing the transfer resistor with the bridge resistors, using ac.*

of the bridge center used in the measurements to be reported below. A simple computation [12] yields the difference between the inductances of the fine wire and the low resistance wire. We find for the series inductance of the resistor attached to the bridge center $L=1.1$ microhenries. This inductance has a negligible effect on the a-c resistance, but produces a phase angle of 11 microradians.

Figure 19 shows the bridge used for the a-c comparison of the 1000-ohm transfer resistor, R_T, with G_1 or G_2. The 10:1 transformer is the one used for the capacitance step-up, and has a known ratio. A balance is observed on detector 1 with the resistors disconnected at "X" to compare the 100-pf capacitor with the 10-pf capacitor. When the resistors are placed in the circuit and both bridges are balanced, a change in the balance at detector 1 indicates a change in the transformer ratio between the junctions *A* and *B*, and allows the loaded voltage ratio between these points to be calculated. This figure combined with the readings of the admittances required to balance detector 2 allows the a-c ratio of the resistances of G_1 or G_2 to the resistance of the 1000-ohm transfer standard to be determined, and also allows the phase angles of G_1 and G_2 to be determined from the known phase angle of the transfer standard.

Figure 20 shows the bridge used for comparing the d-c resistance of the transfer standard with G_1 or G_2. Since the tapped inductor of the transfer resistor presents a low d-c impedance to ground, it must be removed from the circuit for the d-c measurement. With this done, the leakage resistances R_1, R_2, and R_3 are all high. Series resistances r_1 and r_2 in connecting wires are small. Two balances are made with points 1 and 2 grounded in turn. The direct reading ratio set readings are called A_1 and A_2, respectively.

The bridge is then connected as in figure 20, where R_1' and R_3' are low resistance "shorts." The bridge is balanced with the galvanometer connected to 3 and 4 in turn; the readings of the DRRS are called A_3 and A_4, respectively. An analysis shows that for G_1,

$$R_T G_1 = \frac{R\#400}{R\#505}\left[1+\frac{100(A_1-A_3)}{11B}+\frac{10(A_2-A_4)}{11B}\right].$$

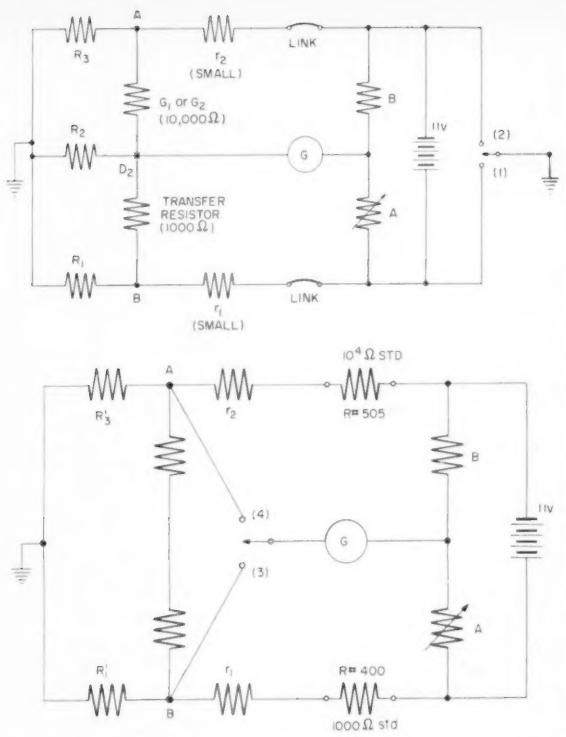

FIGURE 20. *Circuits for comparing the transfer resistor with the bridge resistor, using dc.*

Provided that the resistance ratio of the d-c standards is known, measurements of this form yield the a-c–d-c differences of both G_1 and G_2. Since the 10^4-ohm resistor #505 was used for both this measurement and for the direct d-c comparison between it and G_1 and G_2 in connection with the frequency dependent bridge, one finds that resistor #505 serves only to maintain the unit between the two measurements, and that in effect the 10:1 transformer is used five times to step up the impedance of the 1-pf standard capacitor to the 1000-ohm transfer resistor. The d-c step-up is then needed only from the bank of one-ohm reference resistors to the 10^3-ohm d-c standard resistor #400. An error in the d-c step-up from 10^3 ohms to 10^4 ohms would cause no error in the final value assigned to the one-ohm reference resistors, but would only cause an error in the measured a-c–d-c differences of G_1 and G_2, which in this sense is not needed for our work. In fact, the only reason for including 10^4-ohm #505 in the measurements is that it is much more stable than G_1, G_2, and the transfer resistor. The use of 10^4-ohm #505 allows the complete determination to be broken up into smaller steps which may be completed more quickly and with higher accuracy. Subject to the above comments, we find that G_1 and G_2 have identical a-c–d-c differences and that their a-c resistances are 0.85 ppm higher than their d-c resistances. The average of their phase angles is found from the a-c measurement using the phase angle calculated for the transfer resistor to be 16.6 microradians (capacitive).

6. Conclusion

Combining the results of table 2 with the measured a-c–d-c difference of G_1 and G_2 we find $R\#505 = (10^4 \text{ ohms} - 19.4 \text{ ppm})$. Comparison of this resistor with the NBS bank of one-ohm reference standards yields the value (10^4 ohms -21.7 ppm) in terms of the ohm as adopted in 1948 [13] and as maintained at NBS. Our measurements therefore indicate that the NBS unit of resistance is 1.000002_3 ohms.

Two values have been obtained for the phase angles of the 10^4-ohm woven-wire resistors; 16.6 microradians from the computed phase angle of the straight wire a-c–d-c transfer resistor and 15.0 microradians based on the assumption that the 1-pf reference capacitor has no phase angle. The discrepancy of 1.6 microradians may be ascribed to the actual phase angle of the 1-pf capacitor, an error of 0.16 microhenry in the measurement of the transfer resistor series inductance, or a combination of these two effects. The agreement is considered satisfactory in view of the uncertainties in these measurements.

Table 3 summarizes the steps of this determination and lists the estimated uncertainties associated with each step. The estimates are in most cases little more than guesses, since they must include allowances for possible systematic errors. The estimates are in all cases given as "50 percent errors," meaning that in the experimentor's judgment the chances of the error being greater or less than this amount are approximately equal. It is judged to be almost certain that the error is less than four times the stated 50-percent error. No allowance is made for the possibility of error in the assigned value of the speed of light, which is taken as a predetermined constant, $c = 2.997925 \times 10^{10}$ cm/sec.

With the exception of the speed of light, all measurement uncertainties may be reduced with suitable refinements in measurement techniques. It is believed that with the development of an improved cross capacitor and with minor changes in the rest of the equipment, the measurement uncertainties not including the contribution from the speed of light may be reduced below 1 ppm.

TABLE 3. *Uncertainties associated with steps followed in this determination*

	50% error
	ppm
Measurement of the reference capacitor in terms of the computable capacitor, neglecting the contribution from the uncertainty in the speed of light	2.0
Instability of the reference capacitor	0.3
Ten-to-one step-up using alternating current (times 5)	.1
Frequency dependent bridge	.3
Dependence of bridge resistors upon frequency	.3
Step-down from 10^3 ohms to 1 ohm using direct current	.3
Measurement uncertainty neglecting the uncertainty in the speed of light	2.1

7. Comparision With Other Determinations

In order to compare several recent evaluations of the 1948 resistance unit with each other, it is necessary to know the relative values of the units in terms of which these evaluations were made. Figure 21 shows the results of comparisons made at the International Bureau of Weights and Measures (BIPM) of resistors embodying the units as maintained by NBS (Ω_{EU}), NRC (Ω_{Ca}), and NPL (Ω_{GB}) in terms of the unit as maintained at the International Bureau (Ω_{BIPM}) [14, 15, 16, 17].

No information is yet available concerning the 1960 intercomparisons, so it is impossible to compare the present work with Ω_{BIPM} at this time. For this reason and for consistency in the table to follow, all measurements will be referred to the unit as maintained at NBS, Ω_{EU}.

Table 4 contains values assigned to Ω_{EU} by several recent investigations [18, 19, 20]. The values have been adjusted to allow for the difference between Ω_{EU} and the units used for the measurements. The results obtained by Thomas et al have been referred to Ω_{EU} instead of the international ohm, and also revised upwards by 3 ppm. This revision represents the results of a new evaluation of the current distribution in the primary winding of the mutual inductor, and is based on measurements of the dependence of resistivity upon strain in a sample of the wire used for the winding. These measurements were made in 1956 by Wells [21]. The revised current distribution correction was also calculated by him, but the result was not published.

The National Bureau of Standards was fortunate in receiving a visit in April and May of 1960 from Mr. G. H. Rayner of the National Physical Laboratory in England. Mr. Rayner helped perform the May measurements reported in this paper, and contributed greatly to the early success of this method. His contributions are gratefully acknowledged.

Others contributing substantially to the work described in this paper were Mr. John C. Clark, Mr. Lai H. Lee, Mr. John Q. Shields, and Mr. Thomas E. Wells.

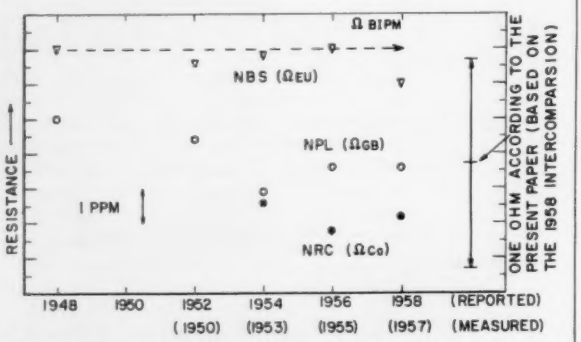

FIGURE 21. *Resistance units maintained by NBS, NPL, and NRC in terms of the unit maintained at the International Bureau of Weights and Measures* (Ω_{BIPM}).

TABLE 4. *Values assigned to the resistance unit maintained at NBS* (Ω_{EU}) *by several recent investigations*

(See text.)

Date of measurements	Reference	Laboratory	Value of the resistance unit Ω_{EU} maintained at NBS
1938 to 1949	Thomas, Peterson, Cooter, & Kotter	NBS	0.999997
1951	Rayner	NPL	1.000004
1957	Romanowski & Olson	NRC	.999996
1960	Present paper	NBS	1.000002_3

8. References

[1] Thompson, A. M., and Lampard, D. G., A new theorem in electrostatics and its application to calculable standards of capacitance, Nature, **177,** 888 (1956).

[2] Lampard, D. G., A new theorem in electrostatics with applications to calculable standards of capacitance, Proc. I.E.E., Mono. No. 216M, January 1957.

[3] Thompson, A. M., The cylindrical cross capacitor as a calculable standard, Proc. I.E.E., Vol. 106, Pt. B, No. 27, May 1959.

[4] Lampard, D. G., and Cutkosky, R. D., Some results on the cross capacitances per unit length of cylindrical 3-terminal capacitors with thin dielectric films on their electrodes, Proc. I.E.E., Mono. No. 351M, January 1960.

[5] Thompson, A. M., The precise measurement of small capacitances, I.R.E. Trans. Instr., vol. **I-7,** Nos. 3 and 4, December 1958.

[6] McGregor, M. C., et al, New apparatus at the National Bureau of Standards for absolute capacitance measurement, ibid.

[7] Cutkosky, R. D., and Shields, J. Q., The precision measurement of transformer ratios, Paper presented at the 1960 Conference on Standards and Electronic Measurements at Boulder, Colorado, IRE Trans. Instr. **I-9,** 243 (1060).

[8] Johnson, G. J., and Thompson, A. M., Intermodulation in bridge detector amplifiers, Proc. I.E.E., Mono No. 210M, November 1956.

[9] Thomas, J. L., Precision resistors and their measurement, NBS Circular 470, 1948.

[10] Silsbee, F. B., A shielded resistor for voltage transformer testing. Scientific Papers NBS No. 516, 1925.

[11] Weller, C. T., A 132-KV shielded potentiometer for determining the accuracy of potential transformers, A.I.E.E. **48,** 1929.

[12] Grover, F. W., Inductance Calculations, Van Nostrand Co., Inc., New York, N.Y., 1946.

[13] Comité International des Poids et Mesures, Procès-Verbaux Deuxième Serie, **TXX,** 1945–1946.

[14] Comité International des Poids et Mesures, Procès-Verbaux Deuxième Serie, **TXXIII,** 1952.

[15] Comité International des Poids et Mesures, Procès-Verbaux Deuxième Serie, **TXXIV,** 1954.

[16] Comité International des Poids et Mesures, Procès-Verbaux Deuxième Serie, **TXXV,** 1956.

[17] Comité International des Poids et Mesures, Procès-Verbaux Deuxième Serie, **TXXVI,** 1958.

[18] Thomas, J. L., et al, An absolute measurement of resistance by the Wenner method, NBS Research Paper 2029, 1949.

[19] Rayner, G. H., An absolute measurement of resistance by Albert Cambell's bridge method, I.E.E., Mono. No. 95, 1954.

[20] Romanowski, M., and Olson, N., An absolute determination of resistance, Can. J. Phys., **35,** 1957.

[21] Wells, T. E., Measurement of the resistance-strain relation and Poisson's ratio for copper wires, Proc. Instr. Soc. Am., **11,** 1956.

(Paper 65A3–97)

JOURNAL OF RESEARCH of the National Bureau of Standards—A. Physics and Chemistry
Vol. 65A, No. 3, May–June 1961

Wavelengths and Intensities in the First Spectrum of Bromine, 2000 to 13000 A

Jack L. Tech and Charles H. Corliss

(December 19, 1960)

The first spectrum of bromine, Br I, has been newly investigated using electrodeless discharge tubes as light sources. The observations have led to a list of wavelengths and estimated intensities of 1056 lines emitted by neutral atoms in the region from 12965 A in the infrared to 3325 A in the ultraviolet. Most of the wavelengths are given to 0.01 A and the intensities are estimated on a relative scale between 1 and 75,000. Lines of Br I were not found in the ultraviolet between 3325 and 1700 A.

1. Introduction

Electrodeless discharge tubes containing an iodide or bromide of an element are now widely used as light sources in the study of spectra. In particular, such lamps containing halides are frequently used in this and other laboratories in the study of the spectra of the rare-earth group of elements. An increasing need has therefore been felt for accurate line lists of the spectra emitted by iodine and bromine, in order that wavelengths emitted by these atoms can be successfully deleted from the line list of whatever other element is under investigation. For this reason, and because the halogen spectra present many problems interesting in their own right, this laboratory undertook a program of extending and improving the descriptions and analyses of the arc and first spark spectra of both iodine and bromine. Results of the research on the first spectrum of iodine have already appeared [1] and the results for the first spark spectrum are now in press [2]. The spectrum of singly ionized bromine, Br II, has been observed in the vacuum ultraviolet region as well as in much the visible region, and work on this spectrum is continuing.

The most comprehensive list of Br I wavelengths hitherto available is that contained in the excellent paper on the structure of the arc spectrum of bromine published thirty years ago by C. C. Kiess and T. L. deBruin [3]. Improvements in apparatus and experimental procedures have now permitted a considerable augmentation of this earlier work. Specifically, we have been able to increase the number of lines observed in the spectra region described here to 1056 compared with the 330 lines reported by Kiess and deBruin. It must be mentioned that extensive observations have been completed also in the vacuum ultraviolet and the far infrared regions of the spectrum. These data, together with some Zeeman-effect observations, have already resulted in a well advanced analysis of the first spectrum of bromine and in some revisions of its term structure as reported by Kiess and deBruin. Since this work on the analysis, however, must be temporarily interrupted, it seemed advisable to report separately at this time the complete description of the spectrum in the range from 12965 A to 3325 A, especially in view of its probable usefulness to workers in other laboratories who are using bromides for excitation in electrodeless discharge tubes. The other data, together with the completed analysis of the first spectrum of bromine will be reported at a later time.

2. Experimental Procedure

The wavelengths of Br I presented here are derived from two essentially independent sets of observations made at two different times at the Bureau. The first series of observations was made several years ago using as light source an electrodeless discharge tube of the type described by Corliss, Westfall, and Bozman [4]. The vicious attacking of hot metal internal electrodes by the chemically very active bromine, which plagued many early observers of this spectrum, was thus avoided.

The electrodeless tube contained $BeBr_2$, produced by evacuating of air a lamp blank containing Be filings and then heating the filings after bromine vapor had been admitted into the blank. To obtain the spectrograms, these lamps were excited in a field of 2,450 Mc/s provided by a microwave oscillator. Spectrograms were made in the first and, where possible, the second orders of 7,500, 15,000, and 30,000 lines per inch concave gratings mounted in parallel light (Wadsworth mounting) at first order reciprocal dispersions of 10, 5, and 2.4 A/mm respectively. Eastman Kodak spectroscopic plates of types 103a–O, 103a–F, I–N, I–Q, and I–Z were used in the appropriate regions.

The line list thus obtained was regarded as fairly complete until the fall of 1959 when W. F. Meggers pointed out that some bromine lines of intensity one in our list appeared much more strongly than that on some plates he was measuring which had been exposed to a lamp containing YbBr. It was then decided to prepare some new lamps and to obtain at least one more set of observations in the entire range of wavelengths. In fact, however, except for the

region extending from 4264 to 5721 A and except for the fainter new lines, at least two new measurements were made on each line. The lamps used in this second series of observations were also of the electrodeless type. They contained, however, not a salt, but bromine vapor at a few millimeters pressure. The bromine used was of ACS purity. To avoid the presence of objectionable water vapor in the lamps, which also had often been a source of annoyance in the early observations of the spectrum, the bromine was thoroughly dried. This drying was accomplished on a vacuum system by means of a U-tube terminated at both ends by stopcocks and leading on one side to a reservoir into which bromine had been admitted and on the other side to another reservoir, the lamp blank, and finally the pumps. The U-tube was filled in a dry-box with P_2O_5. The bromine vapor made several passes through the drying agent before it was finally collected in the lamp blank. By setting up the microwave oscillator at the vacuum system, the pressure of bromine vapor was adjusted until the most complete arc spectrum was obtained, as judged by observing the discharge visually through a small spectroscope. The pressure was of the order of several millimeters of mercury and the discharge exhibited a reddish color. At much below this optimum pressure the discharge changed to a white color, and there appeared a continuous emission spectrum interrupted only by the strongest Br I lines and apparently arising from the Br_2 molecule. In the other direction, as the pressure was increased above the optimum pressure, the spectrum remained pure, but the length of the discharge became shorter and eventually the lamp ceased to operate. This same behavior at lower pressures could be observed after the lamp was sealed off the vacuum system, of course, by immersing the side limb with which the lamp had been provided into a coolant. The white discharge appeared and the molecular background became objectionable at temperatures of the order of −60 °C, which corresponds to a bromine vapor pressure of slightly less than 1 mm of mercury.

Despite this procedure, the molecular background appeared throughout the visible region of the spectrum on plates bearing long exposures. It is thus possible that some of the fainter lines in the appended table of wavelengths, especially in the region from 5000 A to 7000 A, actually are characteristic of molecular, rather than atomic bromine. Further, bromine exhibits continuous emission which begins strongly at about 3800 A and extends to shorter wavelengths although on one set of plates of emulsion type EK I–F exposed for 5 hours this continuous emission already began faintly at about 4400 A. Above that wavelength, discrete molecular lines appear on these plates.

Within this region of continuous emission, atomic emission lines could still be observed and measured. It was discovered, however, that it was more satisfactory in the region below 4000 A to reduce the pressure in the lamp by immersing the side limb in a mixture of solid carbon dioxide and alcohol at about −70 °C. This procedure had the result that the continuous emission spectrum disappeared and was replaced by a weaker background of discrete molecular lines upon which the atomic emission lines, now enhanced, could more easily be identified and measured.

All of the spectrograms bore exposures to an electrodeless lamp containing thorium or iron, or to the iron arc, to serve as standards in the determination of bromine wavelengths. In the first series of observations, the plates were reduced by linear interpolation with a correction curve, whereas in the second series, the micrometer readings of the bromine lines and of the standard lines on each plate were punched on cards so that the computation of bromine wavelengths could be accomplished by an IBM–704, which adjusted all wavelengths by least squares to fit a fourth degree equation.

3. Results

In the table are listed the wavelengths of the lines of Br I, together with their character and estimated intensities. It includes all the lines observable by photography in air, since there are no lines of Br I between 1700 A and 3300 A. The given wavelengths of most lines are weighted means of from two to eight different measurements. The character of a line is indicated by inserting the following symbols after the intensity of the line:

bl	blend
c	partially resolved hyperfine structure
d	double line
h	hazy, diffuse
H	very hazy, very diffuse
w	widened line, probably owing to unresolved hfs
W	very wide line

The intensities are visual estimates on an approximately linear scale where the faintest line is assigned an intensity 1. It must be emphasized that these relative intensities are valid only over small wavelength ranges, and no attempt has been made to adjust the values in accordance with the varying sensitivity of the photographic emulsions. In the case of lines which are separated by just a few angstrom units and which thus all appeared at once in the field of view of the microscope of the comparator used to measure the spectrograms, finer variations of intensities have been indicated, which, however, are meaningless over a wider range. For example, a group of four lines in the field, all of which appear with an intensity of about 200 when compared with other lines on the same plate, might be assigned intensities 180, 195, 205, and 200, to give an approximate index of their own relative intensities.

In conclusion, the authors thank William R. Bozman, who very kindly guided them in the preparation of data for computation by the IBM–704. Further, we wish to express our gratitude to William F. Meggers and especially C. C. Kiess, both of whom have generously provided us counsel and encouragement throughout the course of this work.

TABLE 1. *Wavelengths and intensities of* Br I

Wavelength	Intensity	Wavelength	Intensity	Wavelength	Intensity
A		*A*		*A*	
3325. 307	10 *w*	3942. 026	2 *h*	4412. 49	100
3347. 990	4	3943. 776	2	4423. 03	200
3348. 566	15	3943. 835	8	4425. 14	1500
3400. 050	40 *c*	3945. 565	4	4427. 20	40
3402. 420	20 *c*	3969. 430	1 *c*	4431. 59	1
3409. 740	20 *c*	3973. 967	5	4441. 74	10000
3418. 888	15 *w*	3991. 363	300	4446. 08	15
3425. 577	60	3992. 363	1500	4466. 21	200
3428. 605	15	3993. 177	5	4469. 98	150
3429. 809	8	3998. 492	35	4471. 67	80
3472. 200	30 *c*	3999. 070	200	4472. 61	10000
3496. 366	5	4000. 599	2 *w*	4475. 87	15
3497. 430	1	4009. 310	2 *c*	4477. 72	20000
3516. 144	40	4012. 570	75 *c*	4479. 59	15
3541. 173	100	4016. 453	1 *h*	4490. 42	1000
3556. 530	40 *c*	4018. 316	2	4513. 44	3000
3557. 461	250	4021. 772	250	4513. 82	150
3558. 616	75	4033. 762	1 *h*	4525. 59	15000
3563. 706	50	4037. 324	500	4528. 61	400
3564. 480	15 *c*	4056. 420	35 *c*	4529. 79	600
3579. 081	40	4057. 020	30	4575. 74	3000
3581. 712	15	4058. 406	75	4592. 16	200
3589. 818	100	4064. 150	4	4614. 58	2500
3599. 962	100	4075. 503	50	4640. 92	40
3606. 518	20	4076. 956	75	4641. 02	70
3608. 864	7	4083. 149	50	4643. 52	900
3644. 190	10 *c*	4094. 643	35	4693. 56	300
3646. 620	100 *c*	4106. 352	25	4703. 42	50
3658. 486	2 *h*	4113. 132	4	4706. 36	12 *h*
3659. 970	20	4114. 165	25	4720. 03	100
3735. 800	500	4124. 233	75	4722. 97	9
3745. 419	50	4143. 974	600	4727. 05	4
3751. 287	10	4157. 425	250	4752. 28	2500
3753. 351	5	4164. 158	4	4757. 19	2
3756. 032	30	4164. 270	15	4762. 04	4
3757. 265	5	4168. 115	10	4763. 84	5
3761. 746	2	4175. 786	750	4765. 18	8 *h*
3761. 847	1	4179. 322	100	4765. 63	250
3770. 880	150 *c*	4191. 935	50	4775. 20	750
3794. 030	900 *c*	4196. 468	50	4780. 31	4000
3798. 805	5 *w*	4199. 473	35	4785. 19	1600
3810. 950	1 *h*	4202. 487	450	4796. 85	5
3811. 440	30 *h*	4220. 701	5 *h*	4802. 67	250
3815. 650	1200	4220. 859	2	4803. 47	5
3828. 505	700	4231. 643	4	4804. 64	4 *h*
3829. 750	200 *c*	4240. 366	40	4806. 03	6
3844. 035	100	4242. 497	2 *h*	4806. 57	7
3847. 360	2 *h*	4248. 414	50	4807. 61	350
3850. 619	10	4250. 818	40	4809. 46	5
3850. 740	1	4250. 924	15	4812. 09	6
3851. 654	3	4260. 625	40	4812. 21	6
3854. 702	90	4261. 964	3	4814. 80	7
3896. 653	200	4334. 54	20	4817. 21	3
3899. 767	25	4342. 45	2	4818. 71	7
3905. 850	20 *c*	4358. 33	1	4834. 46	500
3909. 385	175	4365. 14	2000	4848. 39	25
3913. 560	12	4369. 22	75	4860. 04	250
3917. 810	200 *c*	4391. 60	800	4906. 49	10
3929. 196	5	4399. 73	450	4920. 98	300
3934. 090	125 *c*	4404. 57	10	4921. 80	10 *w*

TABLE 1. *Wavelengths and intensities of* Br I—Continued

Wavelength	Intensity	Wavelength	Intensity	Wavelength	Intensity
A		*A*		*A*	
4954. 73	300	5529. 01	175	5898. 96	90
4979. 76	4000	5532. 22	100	5905. 45	900
4983. 25	75	5536. 37	300	5905. 66	80
5002. 72	500	5544. 72	6	5909. 31	250
5029. 37	200	5546. 90	20	5937. 85	90
5063. 74	40	5558. 13	40	5940. 48	1600
5083. 83	6 *w*	5558. 40	10	5943. 71	140
5092. 60	4	5588. 17	160	5945. 50	600
5099. 79	20	5590. 56	50	5950. 32	750
5138. 55	10	5597. 26	15	5953. 92	750
5139. 47	10 *w*	5602. 41	8 *h*	5982. 90	12
5148. 78	10	5604. 96	4	5983. 35	5
5150. 47	6 *h*	5609. 83	10 *h*	5985. 32	125
5220. 71	8	5611. 62	125	5992. 89	100
5222. 32	12	5627. 24	200	5999. 73	95
5226. 91	20	5633. 97	140	6007. 96	200
5241. 43	5	5637. 27	130	6018. 17	200
5245. 12	350	5640. 86	35	6022. 66	30
5261. 80	5	5645. 31	30	6025. 24	10 *h*
5285. 22	50	5645. 96	45	6048. 15	5
5297. 32	15	5667. 75	9	6057. 87	200
5310. 04	5 *h*	5667. 92	8	6059. 74	5
5314. 18	10	5685. 77	15 *W*	6061. 46	5
5315. 85	8	5697. 29	18	6062. 88	4
5317. 25	20	5705. 74	85	6064. 35	200
5318. 83	7	5709. 44	9	6067. 36	5
5323. 20	12	5716. 26	225	6095. 74	700
5328. 92	200	5721. 11	100	6107. 69	125
5329. 30	12	5722. 97	40 *h*	6111. 10	80
5337. 10	40	5764. 66	45	6116. 19	60
5345. 42	600	5771. 30	5	6118. 80	300
5348. 29	10	5777. 69	10	6122. 14	2400
5354. 67	120	5779. 97	4	6126. 53	30 *W*
5356. 74	12 *w*	5783. 32	500	6132. 71	800
5364. 19	300	5784. 02	30	6134. 70	75
5365. 20	5 *h*	5793. 98	100	6137. 49	150
5370. 34	300	5801. 50	40	6141. 04	100 *w*
5379. 13	15	5803. 82	30	6142. 73	100
5382. 96	120	5805. 04	30	6146. 00	25 *cw*
5384. 27	8	5809. 59	250	6148. 60	40000
5393. 58	7	5819. 56	80	6151. 10	50 *d*
5395. 50	1500 *c*	5821. 45	12	6158. 19	750
5414. 26	4	5826. 07	5	6177. 39	2000
5420. 43	13	5827. 07	10	6184. 09	200
5420. 80	18	5828. 51	150	6199. 74	50
5424. 61	8 *h*	5828. 89	7	6203. 08	900
5432. 47	60	5830. 39	400	6204. 35	90
5434. 22	7	5833. 39	900	6204. 49	90
5450. 09	550	5836. 84	150	6205. 40	120
5453. 03	90	5852. 08	1800	6208. 26	100
5455. 16	60	5861. 20	120	6216. 71	5
5455. 96	70	5864. 82	90	6225. 51	65
5463. 72	80	5867. 05	60	6235. 87	10
5466. 22	1200	5869. 47	18	6244. 39	400
5469. 76	15	5877. 15	50 *w*	6248. 24	200
5470. 90	5	5886. 87	60 *cw*	6251. 32	300
5504. 46	35 *h*	5889. 87	60	6253. 69	400
5512. 98	5 *h*	5894. 28	18	6282. 46	600
5520. 86	20	5898. 32	8	6284. 69	8
5522. 53	90	5898. 51	8 *d*	6290. 13	550

TABLE 1. *Wavelengths and intensities of* Br I—Continued

Wavelength	Intensity	Wavelength	Intensity	Wavelength	Intensity
A		*A*		*A*	
6296. 71	700	6646. 59	120	6927. 34	8
6301. 36	275	6653. 82	15	6929. 78	400
6315. 12	5	6666. 93	150	6936. 76	20
6331. 99	300	6672. 15	600	6962. 99	10
6335. 48	1500	6676. 54	15	6971. 96	250
6336. 48	500 *cw*	6676. 72	8	6992. 25	5
6337. 85	60	6682. 28	20000	6992. 83	5
6343. 79	35 *w*	6684. 22	100 *cw*	6993. 31	20
6345. 30	500	6687. 33	90	7005. 19	10000
6349. 82	500	6688. 08	90	7011. 53	50
6350. 73	60000	6690. 35	120 *cw*	7015. 15	75
6371. 60	200 *w*	6692. 13	10000	7024. 70	20
6392. 57	35 *W*	6694. 62	10	7026. 53	2
6394. 67	7	6700. 71	60 *h*	7031. 36	15
6398. 03	30	6702. 07	110	7054. 88	50
6399. 99	10 *W*	6706. 79	60	7058. 38	200
6405. 65	15 *cw*	6712. 12	30	7061. 71	1
6410. 32	2500	6713. 06	125	7066. 33	4
6418. 28	45	6714. 86	90	7076. 71	5
6418. 97	35 *cw*	6719. 97	8	7082. 34	2
6426. 30	500	6720. 68	75 *h*	7082. 63	3
6435. 81	15	6723. 65	400	7091. 12	4
6436. 60	10	6728. 28	8000	7101. 80	5 *h*
6438. 02	600	6738. 61	100	7111. 62	200 *cw*
6458. 92	25 *h*	6739. 66	8	7113. 22	50
6462. 32	500	6740. 83	5	7113. 60	100
6470. 41	200	6752. 67	6	7117. 59	15
6475. 23	100 *h*	6760. 06	2000	7120. 78	10
6483. 56	1800	6761. 92	25	7120. 87	10 *c*
6483. 96	35	6765. 12	8	7133. 95	5
6488. 62	800	6771. 95	175	7138. 05	2
6493. 80	20 *h*	6774. 63	30 *h*	7138. 19	4
6501. 50	4	6778. 57	60	7142. 25	500 *c*
6514. 32	12	6779. 48	2000	7145. 56	2
6514. 62	1000	6785. 23	10	7147. 06	4
6531. 39	70 *bl* *with* Cl	6785. 74	900	7149. 08	15
6532. 29	600	6786. 74	2200	7150. 00	8
6541. 30	600	6787. 34	175	7150. 30	75
6544. 57	20000	6787. 77	8	7153. 13	5 *h*
6548. 09	1500	6790. 04	6500	7160. 74	15
6551. 57	12	6791. 48	1600 *c*	7162. 10	750
6559. 80	50000 *cw*	6801. 35	60	7172. 22	25
6571. 31	1000	6816. 72	50	7175. 74	5 *H*
6574. 29	15	6820. 39	800 *c*	7177. 89	5 *h*
6576. 24	10 *W*	6826. 02	400	7184. 30	300
6579. 14	1800	6840. 62	175	7194. 40	15 *cw*
6579. 36	300	6844. 82	5	7214. 95	5 *c*
6582. 17	20000	6845. 24	40	7217. 78	20
6584. 14	600	6845. 30	40	7222. 31	50
6589. 62	10 *w*	6846. 27	150	7232. 45	100
6604. 80	15	6858. 22	45	7236. 86	7
6613. 05	4	6859. 43	20	7247. 29	5 *h*
6620. 47	1500	6861. 15	1800	7255. 47	10 *cw*
6621. 44	8	6875. 22	20 *w*	7255. 63	15 *W*
6624. 26	20	6887. 99	12 *h*	7257. 40	4
6631. 62	50000 *cw*	6888. 73	80 *h*	7257. 82	10
6635. 10	60	6895. 65	1 *w*	7260. 45	2000
6636. 62	150	6904. 95	400	7261. 46	20
6639. 57	40	6922. 86	30	7262. 40	25
6645. 17	40	6923. 04	1	7265. 16	5

TABLE 1. *Wavelengths and intensities of* Br I—Continued

Wavelength	Intensity	Wavelength	Intensity	Wavelength	Intensity
A		*A*		*A*	
7272.58	3 *w*	7711.68	5	8111.55	50
7284.41	5	7713.28	200	8113.02	20 *h*
7288.40	150	7713.53	45	8131.52	30000
7291.92	1	7715.30	500 *cw*	8137.88	150
7305.03	75	7721.45	300	8142.79	40 *h*
7310.45	4	7726.16	125 *cw*	8152.65	1000 *c*
7311.48	100 *d*	7733.61	900	8153.75	10000
7319.44	50 *cw*	7734.60	25	8153.98	25000
7323.35	10	7742.00	1	8166.30	175
7329.20	10 *hw*	7795.00	15	8170.19	200 *d*
7333.72	50 *c*	7803.02	30000	8172.07	200
7344.53	100	7807.66	125 *cw*	8173.70	20
7348.51	10000	7821.09	30	8175.57	25
7378.41	20 *d*	7827.23	1200	8179.62	40
7383.69	5	7835.09	30	8179.98	100
7385.54	4 *h*	7841.87	30	8183.49	450
7420.69	2	7843.58	600	8189.91	1 *hw*
7425.85	750	7844.04	150 *d*	8190.05	1 *hw*
7452.11	60	7869.52	10	8190.25	40
7453.41	70	7881.52	4000 *c*	8197.71	175 *h*
7458.22	50 *h*	7889.85	600	8210.48	3 *h*
7461.84	70	7903.66	50	8215.11	200
7464.67	8	7905.69	50	8237.94	500
7495.46	15 *hw*	7925.81	2500	8246.86	5000
7497.79	5	7929.68	250	8247.97	30
7512.96	40000	7932.97	30 *W*	8252.38	30
7532.76	50	7938.68	30000 *c*	8253.87	35
7535.78	400	7940.04	60	8258.32	300
7551.49	500 *cw*	7947.94	3000	8264.96	15000
7559.97	70	7950.18	3000	8272.45	75000 *c*
7569.07	500	7961.33	350	8280.23	100
7570.85	550	7966.94	900 *c*	8280.75	100 *w*
7575.22	15 *w*	7978.44	8000 *bl*	8291.05	900
7582.55	10 *h*	7978.57	10000 *bl*	8293.56	100
7582.98	100 *h*	7987.12	30	8304.59	10
7586.59	25	7989.94	30000	8308.48	20
7591.59	1600	7997.01	80	8313.09	10
7594.50	25	7998.74	175	8334.70	20000
7595.06	1800	8004.35	25	8343.69	10000
7598.00	4	8008.87	30 *h*	8357.53	10
7604.02	70	8009.36	75	8359.05	5
7606.26	120	8010.00	800 *cw*	8361.71	300
7607.37	400 *cw*	8014.72	500 *cw*	8362.38	100 *h*
7616.39	2000	8021.70	500 *cw*	8367.19	15
7617.90	20 *cw*	8022.51	800	8369.00	20
7632.85	50	8023.13	20	8372.77	150
7641.62	600	8023.91	900	8378.63	100 *w*
7647.67	40	8026.45	5000 *c*	8384.02	1200
7652.82	150 *cw*	8028.21	18	8387.97	100
7663.51	100 *cw*	8028.79	400	8389.73	300
7680.71	10 *hw*	8029.66	500 *cw*	8392.76	75
7681.74	20	8030.91	250 *h*	8397.61	50
7685.08	50	8033.40	40	8402.07	20
7698.71	35	8034.94	250 *cw*	8408.67	250
7699.56	80	8037.32	40	8410.79	10 *w*
7704.32	60 *h*	8037.63	60	8411.61	5 *w*
7706.68	15 *hw*	8050.40	15	8421.88	4
7708.38	8	8066.36	200	8428.76	75
7709.34	15 *h*	8072.87	300	8430.50	50
7709.54	15 *h*	8101.20	150	8432.49	10

TABLE 1. *Wavelengths and intensities of* Br I—Continued

Wavelength	Intensity	Wavelength	Intensity	Wavelength	Intensity
A		*A*		*A*	
8434. 83	150	8839. 98	20	9314. 85	30
8435. 33	75	8842. 84	125	9320. 86	15000
8441. 25	100	8861. 69	85	9325. 32	20
8446. 55	40000	8869. 64	300	9352. 55	175
8454. 25	75	8870. 45	200	9354. 56	15
8463. 32	4	8877. 89	90	9369. 96	100
8470. 62	100	8878. 41	90	9379. 22	30
8471. 51	500	8882. 86	30	9399. 57	5
8477. 45	4000	8883. 46	15	9400. 18	90
8484. 40	30	8886. 35	40	9409. 56	20
8491. 52	4	8888. 98	4000	9438. 22	80
8503. 78	400	8890. 27	50	9460. 14	500 *d*
8513. 38	1500	8895. 21	20	9470. 67	20 *h*
8515. 68	100	8895. 88	150	9475. 08	80
8529. 38	8 *h*	8897. 62	30000	9476. 32	30
8557. 73	1000	8909. 72	300	9477. 48	60
8560. 57	300	8932. 40	6000	9488. 66	120
8565. 28	200	8933. 29	25	9495. 30	50
8566. 28	1000	8936. 96	15	9498. 32	20
8578. 84	400	8944. 84	50	9503. 78	6 *w*
8580. 00	20	8945. 19	15	9504. 53	3
8592. 32	250	8949. 38	1800	9507. 03	75
8595. 49	50	8955. 44	30	9517. 27	100
8595. 66	50	8964. 00	9000	9543. 04	40
8603. 69	100	8972. 82	350	9552. 65	175
8604. 06	20 *hw*	8979. 59	200	9560. 58	6
8606. 68	20	8984. 56	100	9570. 32	2
8608. 97	30 *hw*	8995. 22	50	9588. 60	300
8610. 48	100	9005. 21	50 *h*	9590. 33	20
8611. 83	250	9012. 23	20	9598. 78	60
8612. 48	75	9029. 94	300	9603. 62	35
8625. 39	750 *c*	9045. 08	40	9604. 30	6
8628. 84	200	9066. 26	400	9621. 02	35 *h*
8638. 66	20000	9078. 64	700	9623. 33	15
8655. 10	100	9079. 29	125	9625. 17	8
8658. 84	10	9084. 29	25	9627. 54	4
8668. 84	300	9086. 81	100	9631. 29	60
8698. 53	4000	9107. 39	10	9635. 05	20
8708. 68	75	9123. 17	50	9662. 00	40
8708. 95	100	9129. 31	70	9662. 99	20
8725. 33	500	9147. 05	75 *h*	9710. 64	12
8726. 75	100 *c*	9151. 49	4	9717. 44	40
8741. 63	50	9166. 06	30000	9719. 18	600
8742. 98	75	9173. 62	15000	9725. 39	40
8749. 09	10	9178. 16	20000	9731. 73	350
8757. 22	10	9183. 14	30	9732. 86	50
8760. 46	700	9193. 46	20	9740. 38	15
8764. 19	500	9197. 16	50	9745. 83	100
8775. 70	250	9201. 22	80 *w*	9751. 41	90
8779. 16	50	9201. 78	80	9793. 43	6000
8793. 47	10000 *c*	9202. 48	80	9810. 63	60
8801. 03	150	9220. 55	200	9817. 98	60 *bl*
8803. 40	100	9221. 20	35	9818. 15	70 *bl*
8804. 77	20	9226. 57	15	9828. 34	15
8807. 57	100 *c*	9229. 11	5	9844. 13	7
8808. 85	500	9254. 06	70	9864. 92	2
8810. 57	10	9254. 39	30	9896. 37	10000
8819. 96	15000	9265. 42	40000	9944. 04	400 *c*
8825. 22	25000	9282. 78	100	9945. 19	1
8833. 32	175	9288. 56	200	9962. 04	35 *c*

TABLE 1. *Wavelengths and intensities of* Br I—Continued

Wavelength	Intensity	Wavelength	Intensity	Wavelength	Intensity
A		*A*		*A*	
9963. 86	1	10529. 48	3 *h*	11093. 46	250
10001. 92	10	10539. 14	6	11094. 19	100
10002. 15	5 *h*	10554. 72	1	11096. 54	20
10025. 20	4 *h*	10566. 12	250	11100. 59	1
10045. 67	3 *h*	10566. 85	100	11101. 30	1
10056. 86	15	10569. 62	2	11161. 68	1 *w*
10061. 57	25 *d*	10591. 48	20 *w*	11194. 94	100
10079. 72	10	10608. 64	40	11197. 00	2
10085. 97	35	10616. 27	1	11197. 11	3
10087. 92	1	10619. 62	1	11225. 04	250
10088. 27	10	10624. 28	1	11247. 46	2
10102. 79	12	10629. 43	18	11286. 92	2
10107. 76	150 *d*	10634. 04	1	11292. 69	2
10113. 72	2	10638. 80	15	11297. 98	2
10119. 17	3	10660. 76	3	11316. 92	10 *w*
10128. 76	4	10718. 80	100	11325. 97	1
10139. 04	3000	10723. 07	15	11330. 17	3
10174. 72	12	10742. 09	1000	11350. 02	65
10175. 44	20	10742. 43	100	11367. 21	4 *w*
10183. 98	300	10747. 17	20	11367. 88	4 *w*
10184. 45	200	10753. 88	200 *cw*	11436. 18	3
10197. 58	18	10755. 86	3000	11437. 59	9
10208. 88	300	10757. 76	6	11447. 25	18
10225. 20	1	10795. 01	10 *cw*	11464. 56	35
10231. 58	8	10798. 06	25	11501. 27	1
10232. 36	15	10804. 38	3	11508. 75	30
10237. 11	75	10810. 04	300	11583. 66	10
10237. 72	6000	10815. 63	6	11597. 58	1
10243. 28	3	10840. 04	500 *d*	11631. 30	2
10248. 24	3	10869. 65	100	11636. 05	1
10265. 85	15 *h*	10871. 58	90	11640. 91	1
10293. 63	50	10891. 37	250	11666. 17	20 *d*
10299. 62	1000	10892. 74	100	11742. 82	400
10305. 96	10	10896. 75	200	11810. 27	1
10310. 50	800	10908. 58	60 *w*	11819. 31	2
10310. 72	600	10973. 40	500	11833. 03	1
10310. 91	700	10978. 52	40	11870. 75	4
10312. 87	40	10978. 93	300	11883. 89	4
10314. 01	8	10982. 25	100	11902. 60	5
10320. 06	15	10991. 07	2	11903. 57	8
10324. 93	3	10997. 78	600	11928. 09	8
10329. 99	100 *cw*	10998. 23	400	11990. 51	15
10374. 35	12 *cw*	11007. 36	10	12088. 15	2
10377. 61	1500	11010. 38	600	12285. 46	2
10390. 71	175	11012. 27	5	12303. 82	35
10392. 49	25	11013. 17	20	12349. 26	1
10415. 05	12 *w*	11024. 19	10	12354. 35	1
10457. 90	30000	11039. 75	60	12368. 85	1 *w*
10483. 31	8	11045. 69	800 *d*	12450. 44	1
10505. 02	8	11047. 15	10	12809. 50	1
10507. 87	12	11047. 57	17	12826. 01	1
10513. 64	1	11074. 04	40	12965. 11	4

4. References

[1] C. C. Kiess and C. H. Corliss, J. Research NBS **63A,** 1 (1959).

[2] W. C. Martin and C. H. Corliss, J. Research NBS **64A,** 443 (1960).

[3] C. C. Kiess and T. L. deBruin, BS J. Research **4,** 667 (1930).

[4] C. H. Corliss, W. R. Bozman and F. O. Westfall, J. Opt. Soc. Am. **43,** 398 (1953).

(Paper 65C3–98)

JOURNAL OF RESEARCH of the National Bureau of Standards—A. Physics and Chemistry
Vol. 65A, No. 3, May–June 1961

Torsional Resonance Vibrations of Uniform Bars of Square Cross Section

Wayne E. Tefft and Sam Spinner

(February 14, 1961)

Relations by which the shear modulus may be computed from the fundamental and overtones of the torsional resonance frequencies of square bars have been established empirically.

The results are analyzed in terms of a proportionality factor, R, defined by the equation $G=(2l\,f_n/n)^2\rho R$. R is found to increase with increasing cross section to length ratio. Also, the overtones are less than integral multiples of the fundamental by an amount which increases with increasing cross section to length ratio.

1. Introduction

1.1. General Background

This is the third in a series of papers [1, 2] [1] dealing with the relations between various mechanical resonance frequencies of uniform bars and their elastic moduli. The general method of approach has been described in the previous papers. Essentially this approach consists in determining the mechanical resonance frequencies of a series of specimens, all having the same intrinsic elastic moduli and density, but having dimensions which differ from each other in a consistent manner. Then, relations are developed from which the elastic moduli can be computed from the associated resonance frequencies in terms of properly selected dimensional and elastic parameters. These empirically established relations are compared with corresponding theoretical ones (based on the classical theory of elasticity) whenever feasible. The theoretical relations serve as a guide in the selection of these foregoing parameters. Also, it is only because the experimental methods for determining these resonance frequencies have been developed to a high degree of accuracy (see sec. 2.2) that it has become possible to develop the empirical relations with comparable accuracy, and to check the classical theory more carefully than has been possible heretofore.

Since the uniformity of specimens with respect to elastic modulus and density is a necessary condition for the entire development, considerable care must be taken in the selection of specimens to realize this condition experimentally. If, in the course of the investigation, an opportunity presents itself for checking this uniformity independently, it is clearly of the utmost value, since, as just indicated, failure of the specimens to conform to this condition would render the entire subsequent analysis invalid. Such an opportunity occurred in a previous study (specimens of set II in [2]) and again in this study, as will be shown.

Generally, steel specimens have been chosen because this material possesses certain desirable properties in fulfilling the purposes of these investigations. These include,

1. Steel can be machined to high dimensional accuracy fairly easily.
2. The material is inexpensive. (For these reasons steel is chosen over tungsten, for instance.)
3. It is dimensionally staple.
4. It has been found that if reasonable care is taken, the fundamental condition of maintaining the uniformity among the different specimens with respect to intrinsic modulus and density can be achieved to the high accuracy necessary for the subsequent analysis.
5. Also, if sufficient care is taken, steel can be selected which satisfactorily fulfills the assumptions on which the empirical and corresponding theoretical equations are based, namely, that the material be homogeneous and isotropic. Even though the individual grains of which the steel is composed are anisotropic, and chemically, the material is not "pure", nevertheless, the orientation and distribution of the grains is random. On the macroscopic scale of the experiments and analysis, this material may safely be considered to be isotropic and homogeneous, and equations based on this condition are valid.
6. Steel gives excellent elastic responses under the experimental conditions used, so that resonance frequencies of up to about 50 kc/s can be realized. This applies for higher overtones of longer specimens or lower overtones or the fundamental of the shorter specimens. Consequently, a fairly wide range of experimental data can be analyzed. This is of considerable importance, because it is usually only at higher frequencies that departures from the theory are large enough to be observed.

[1] Figures in brackets indicate the literature references at the end of this paper.

It is emphasized, however, that although steel specimens have been used almost entirely in these investigations (and will be used in this one), the results are not peculiar to steel, but should apply to any elastic, homogeneous, isotropic material. The only qualification to this statement is that for Young's modulus and its related modes of vibration, flexural and longitudinal, Poisson's ratio must also be considered. This complication presumably does not arise in the determination of shear modulus from measurements in the first torsional mode of any order.

1.2. Particular Problem of This Study

It is recalled from the previous paper [1] on torsion that the first overtone of rectangular specimens was found to deviate from the exact double of the fundamental, and that the amount of deviation varied with the width to depth ratio of the cross section. Even for a specimen of square cross section the data revealed that the first overtone was slightly lower than the exact double of the fundamental. However, the data of that paper [1] were limited to one length of specimen (about 6 in.) and to only the first overtone. The purpose of the present paper is to consider this problem more fully by investigating specimens of square cross section of different lengths and at higher overtones.

To give a fuller picture, the fundamental and higher overtones of torsional resonance of some cylindrical specimens were also investigated.

2. Experiment

2.1. Specimens

All the specimens listed were cut from a single bar of steel, designated as SAE 1010. It was the same bar mentioned in footnote 4 in [2]. Its composition, as determined by spectroscopic analysis was, carbon 0.10 percent, manganese 0.30 percent, phosphorus 0.011 percent, sulfur 0.022 percent, and the remainder, iron. The original bar was about 2 ft long and about 1½ in. square in cross section. The steel was specially heat treated to be as homogeneous as possible and to have a minimum of preferred crystal orientation. As a further precaution to insure uniformity, the original specimens were cut from the center of the stock, since preferred crystal orientation, when it does occur, is usually most pronounced at the periphery.

First, two cylindrical and one square specimen were machined from the original stock. After the fundamental and as many overtones as possible were determined for these specimens, the square one was subdivided in length and the torsional resonances were similarly determined for the two new shortened specimens thus formed. The larger of these two specimens was again subdivided and the resonances once more determined. The subdivisions were so performed that the resulting specimens were all of different lengths. In this manner, a large number of specimens (and, therefore of experimental points) was made available from the original bar stock. The subscripts in the specimen designations indicate the history of the subdivision process. Thus A12, indicates that the specimen was cut from A1, A1 was cut from A, which in turn was cut from the original bar.

The dimensions of all the specimens were true to ± 0.0003 cm. This was a higher order of accuracy than that achieved in the previous investigations. The accuracy of the dimensions and the intrinsic uniformity of the specimens was such that the standard deviation in the density of four randomly selected specimens, calculated from the mass and volume (obtained from the dimensions) was less than 0.0002 g/cm^3, the average density being 7.8541/g/cm^3.

2.2. Resonance Frequencies

The torsional resonance frequencies were obtained in the manner previously described [1]. In addition to the precautions previously taken to insure accuracy, sufficient time was allowed to elapse for the specimens to arrive at equilibrium with the ambient temperature which was controlled at 25.0 ± 0.5°C. This often took from 2 to 3 hr since it was found that significant frequency variations could be observed during this time interval. The specimen was considered to have come to equilibrium when successive measurements at one-half hour intervals showed no change in the measured resonance frequencies (i.e., one in the last significant figure). When this additional (temperature) precaution was taken, a conservative figure for the accuracy of the resonance frequency determinations was about 1 part in 10,000. This figure is about 2½ times better than that given previously [1,2].

Table 1 lists the dimensions, and torsional resonance frequencies, both fundamental and overtones, of the specimens used in this investigation.

3. Results and Discussion

3.1. General Theory

All rods, whether cylindrical, square or rectangular in cross section conform to the following equation relating the shear modulus, G, to the density, ρ, the first (nondispersive)-mode torsional resonance frequency, f, and the length, l, of the specimens,

$$G=(2lf_n/n)^2\rho R \qquad (1)$$

n signifies the overtone of the resonance frequency; for the fundamental, $n=1$, first overtone, $n=2$, etc. R is a proportionality factor which depends upon the shape of the specimen and n.

3.2. Cylindrical Specimens

For cylindrical specimens, the theory states that $R=1$ exactly for all length to cross section ratios and

TABLE 1. *Dimensions and torsional resonance frequencies of steel bars of square cross section*

Specimen [a]	t/l [b]	Resonance frequencies, c/s [c]						
		f_1	f_2	f_3	f_4	f_5	f_6	f_7
A	0.12225	5182.0	10362.7	15542	20719	25892	31058	
A 1	.17497	7417.9	14832.0	22241	29637			
A 12	.21609	9161.5	18315.6	27456	36573	45653	54700	63621
A 2	.42339	17937	35785	53430				
A 11	1.00000	41995						
B	0.45039	28233						
C	.27871	17471	34946					

[a] Specimens designated A are bars of square cross section, those designated B and C are cylinders of circular cross section.
[b] l=length of specimen, for square specimens t=cross-sectional edge=3.4950 cm; for cylindrical specimens t=diameter=2.5737 cm.
[c] f_1=fundamental torsional resonance frequency,
f_2=first overtone, etc.

for all overtones. Also torsional waves in cylinders conform to the following two equations (which are exactly analogous to the ones for longitudinal waves in cylinders),

$$n\lambda=2l \text{ and } v_t=\frac{2lf_n}{n} \tag{2}$$

where λ=wavelength and v_t=velocity, of torsional waves.

In contrast with longitudinal waves in cylinders, however, the velocity of torsional waves is not reduced as the length of the specimen is reduced with respect to the cross section. For all lengths, then,

$$G=v_t^2\rho. \tag{3}$$

The constancy of R was checked from the experimental data by substituting the appropriate values for the two cylindrical specimens, in eq (1) and assuming G/ρ to be the same for both specimens. R was found to be constant with a coefficient of variation of 1.2×10^{-7} percent. Since these two specimens were not long enough to provide enough overtones for an extended range of data, the constancy of R was further checked experimentally by using another pair of specimens, about 12 in. and 8 in. long, both about 1 in. in diameter from an earlier source (specimens I–19 and I–16 from [2]). For the longer of these specimens, torsional resonances up to the fourth, and for the shorter specimen, up to the third overtone could be detected; and R was similarly computed from these 9 resonances. Again, R was found to be constant with a coefficient of variation of 1.1×10^{-7} percent. Furthermore, R showed no tendency to drift systematically for either pair of specimens.

The equations for torsional waves in cylinders are not only exact but so clear cut and simple (requiring no qualifying correction factors) that, had the experimental results not been in accord with the theory, one would be more inclined to suspect the data than the theory. Consequently, the excellent agreement found in this respect is reassuring evidence of the reliability of the experimental data.

G/ρ for the specimens may now be obtained by substituting the 3 sets of values for the two cylindrical specimens in eqs (2) and (3). The average of these 3 values so obtained is,

$$\frac{G}{\rho}=v_t^2=(104.117\pm.008)\times10^9\left(\frac{\text{cm}}{\text{sec}}\right)^2. \tag{4}$$

Since ρ is known from section 2.1, G may also be computed. It turns out to be 817.7×10^9 dynes/cm^2. However, this information is not necessary for the further development.

3.3. Square Bars

For torsional waves in bars of square cross section, unfortunately, the situation is not so simple as in cylinders. (Not only is the theory more complex requiring uncertain approximations, but the experimental results obtained here do not agree too well with the theory.)

Timoshenko [3] has derived exact expressions for the stress, strain and dimensional relations of square bars in static torsion. Timoshenko's equations have been solved for a shape factor, k_1, which when substituted into Pickett's [4] equation for R, ($R=I_p/k_1$ where I_p is the polar moment of inertia of the cross-sectional area) leads to a value of $R=1.18559$, which is accurate to the number of places given. This particular value of R is henceforth designated as R_0. For the dynamic case (i.e., a square bar vibrating in torsion) R_0 may be safely used in eq (1) as long as the cross section of the specimen is small in comparison with the wavelength. For shorter specimens in torsional resonance, however, as the cross section becomes a significant part of the wavelength, the strain pattern departs sufficiently from the static case to require modification (increase) in the value of R_0.

Davies [5] has considered theoretically this problem of change in R for shorter square specimens along with the possible departure of the overtones from integral multiples of the fundamental. His concluding equation, which involves a number of approxi-

mations, may be expressed, in the notation of this paper, as follows:

$$R/R_0=1+.00851\left(n\frac{t}{l}\right)^2 \qquad (5)$$

where t=the length of a cross sectional edge.

It is clear from Davies' equation and eq (1), that as t/l increases R/R_0 will increase and the overtones will decrease by greater amounts from integral multiples of the fundamental. These results are in qualitative agreement with the experimental data. However if one attempts to fit the experimental results to Davies' equation, one finds significant quantitative disagreement, especially at higher values of t/l and at higher overtones.

After considerable manipulation, it was found that a satisfactory fit could be obtained if R, or preferably R/R_0, was not assumed to be a function of $(nt/l)^2$ as Davies does, nor any other function of (nt/l), but rather a function of n and t/l separately. Figure 1 is a plot of R/R_0 as a function of $n^2(t/l)^3$.

For any given value of n, R/R_0 varies very nearly as $(t/l)^3$. Therefore the solid lines in the figure for $n=1$, $n=2$, and $n=3$ (which plot R/R_0 as functions of $(t/l)^3$) are very nearly straight lines. The 5 dashed lines represent the variations in R/R_0 for given values of t/l (represented by the values for the 5 square specimens) as a function of their overtones.

It is seen from the figure that for constant t/l, R/R_0 is not a linear function of n^2, but requires further modification. The equation finally arrived at, for most accurately representing all the data, was of the form,

$$R/R_0=A+n^2(t/l)^3\ (B+Cn+Dn^2). \qquad (6)$$

The constant, A, in this equation would equal one, if the two basic assumptions made in arriving at the equation are correct. These are (1) that it is legitimate to substitute R_0, solved from the static case, into the dynamic one for a long specimen, i.e., that $R/R_0\rightarrow 1$ as $t/l\rightarrow 0$ and (2) that the numerical value of G/ρ given in eq (4) and contained implicitly in R is correct, for the square bars as well as for the cylinders.

In order for A to equal one, both of these assumptions must be correct, except in the unlikely possibility that both are incorrect in such a manner as to cancel each other. Also the second of these assumptions is recognized to be the one mentioned earlier as the basic condition for the entire analysis. Therefore if $A=1$ is not assumed but is solved for, along with the constants B, C, and D from the available data, then the degree to which A approaches one, will be a critical indication of the correctness of these assumptions. This agreement of A with one

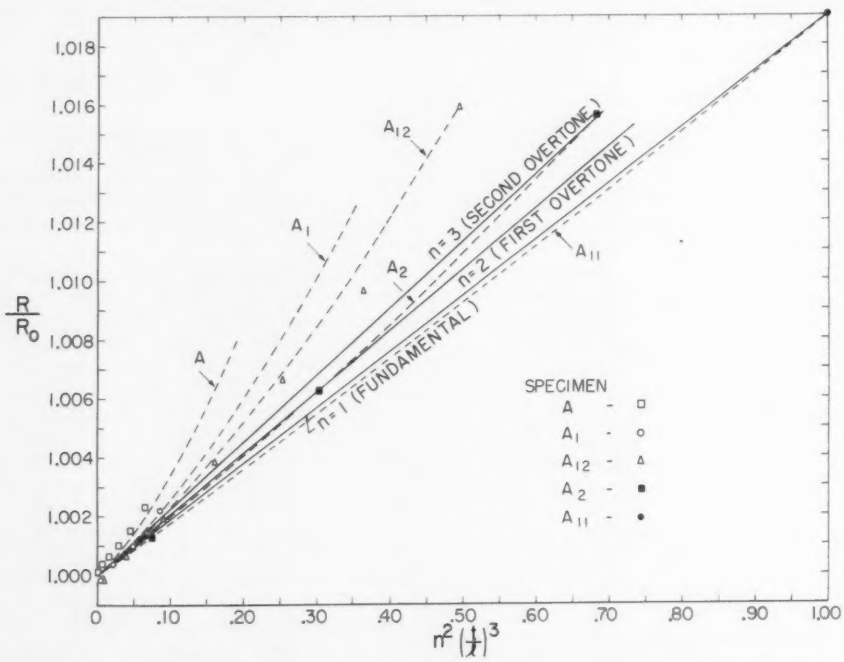

FIGURE 1. *Plot of correction factor* R/R_o *for computing the shear modulus of square bars from their torsional resonance frequencies.*

R/R_o is a function of n, t, and l where; n is the order of the overtone, t is length of the cross sectional edge, and l is the length of the specimen. The dashed lines are for constant t/l. The solid lines are for constant n. All the lines are actually drawn by solving the equation, $R/R_o=1+n^2(t/l)^3\ (0.01746+0.00148n+0.00009n^2)$ for selected values of n or t/l. $R_o=1.18559$.

is also the independent check mentioned earlier (sec. 1.1) on the uniformity of the specimens with respect to modulus and density (actually G/ρ).

The constants, A, B, C, and D were determined by a least squares routine on an automatic computer. For this purpose, the data from the same specimens, as plotted in figure 1, 21 measurements on 5 specimens were used.

The values so obtained for these constants are given below,

Constant	Value	Standard error
A	1.00010	0.00006
B	0.01745	.00045
C	.00148	.00036
D	.00009	.00005

Standard deviation for R/R_0=0.00022.

The value for A is seen to depart only insignificantly from one. If $A=1$ were used with the same standard error actually obtained for A, then G/ρ would come out to be 104.107 ± 0.006. Had this value turned out to be significantly different from the one actually used, ($G/\rho=104.117\pm0.008$) then a readjustment in the values for B, C, and D would be necessary. However, the difference between the two values for G/ρ, the one actually used, and the one resulting from assuming $A=1$, is not statistically significant, being not greater than (actually equal to) the standard error of the difference which is

$$\sqrt{(0.006)^2+(0.008)^2}.$$

Therefore no such readjustment is necessary. It appears then that, except in the unlikely possibility mentioned above, the assumptions made in arriving at eq (6) are valid. Also, the standard deviation in R/R_0, is well within the error to be expected on the basis of the accuracies given for the resonance frequencies and the dimensions of the specimens. The standard deviation of this variable is most critical since it is the test of whether the form of equation selected (eq (6)), accurately represents the data. Had the standard deviation of R/R_0 been larger than that to be expected from the experimental error, it would have meant that the form of equation chosen was incorrect. The entire analytical expression corresponding to figure 1 may now be written as,

$$R/R_0=1+n^2(t/l)^3(0.01746+0.00148n+0.00009n^2) \tag{7}$$

Actually the curves in the figure are not drawn through the experimental points but through values obtained by solving eq (7) for selected values of n and t/l. This gives a graphical indication of the degree of agreement between the equation and the experimental points.

4. Summary

Accurate relations have been developed from which the shear modulus may be computed from the torsional resonance frequencies of uniform bars of square cross section. These relations are in qualitative agreement with Davies' corresponding theoretical formulation which recognizes that the proportionality factor R varies for different ratios of cross section to length and also for higher overtones. However the accurately determined empirical relations given here are shown to depart from Davies' equation especially at these higher cross section to length ratios and higher overtones.

5. References

[1] S. Spinner and R. C. Valore, Jr., Comparison of theoretical and empirical relations between the shear modulus and torsional resonance frequencies for bars of rectangular cross section, J. Research NBS **60,** 459 (1958) RP2861.

[2] S. Spinner, T. W. Reichard, and W. E. Tefft, A comparison of experimental and theoretical relations between Young's Modulus and the flexural and longitudinal resonance frequencies of uniform bars, J. Research NBS **64A,** 147 (1960).

[3] S. Timoshenko and J. N. Goodier, Theory of elasticity, 2d ed., p. 278 (eqs 160 and 163) (McGraw-Hill Book Co., New York, N.Y., 1951).

[4] G. Pickett, Equations for computing elastic constants of prisms and cylinders, Am. Soc. Testing Materials Proc. **45,** 846 (1945).

[5] R. M. Davies, The frequency of longitudinal and torsional vibration of unloaded and loaded bars, Phil. Mag. 7 Series, **25,** 364–386 (Jan.–June 1938).

(Paper 65A3–99)

JOURNAL OF RESEARCH of the National Bureau of Standards—A. Physics and Chemistry
Vol. 65A, No. 3, May–June 1961

Infrared Studies of Aragonite, Calcite, and Vaterite Type Structures in the Borates, Carbonates, and Nitrates

C. E. Weir and Ellis R. Lippincott

(January 10, 1961)

Infrared absorption spectra have been obtained on the alkali nitrates, the divalent metal carbonates, and the rare earth borates which assume the aragonite, calcite, or vaterite crystal structures. It was observed that similar structures give rise to analogous spectra except for the carbonate and borates having the vaterite structure. The marked differences observed in these latter spectra are discussed. Frequency shifts produced by cation substitution are ascribed to repulsion between closed electron shells of oxygen atoms. It is concluded that this repulsive force determines the structure type in the rare earth borates.

1. Introduction

Although a considerable amount of work has been devoted to the study of the infrared spectra of calcite and aragonite type structures [1,2],[1] relatively little attention has been given to vaterite [3]. The scarcity of the data on vaterite type structures is apparently due to the relative rarity of this structure. However, a large number of compounds with the vaterite-type structure have been prepared recently by Levin and Roth [4] in their studies of the rare-earth borates. They found that all rare-earth borates from $SmBO_3$ to $YbBO_3$ inclusive normally had the vaterite-type structure. Larger cations, such as Nd^{3+} formed borates with the aragonite-type structure and only the smallest, Lu^{3+}, normally formed a borate with the calcite structure.

The availability of the borate compounds suggested a detailed study of the infrared spectra of the calcite-aragonite-vaterite type structures using a diamond infrared cell. This cell has the advantage that spectra are obtained routinely with no concern about interaction between the material studied and the diamond. Although some of the experiments on the calcite and aragonite spectra were performed with thin single crystals, most were run using pellet and mull techniques. In the latter methods there is uncertainty as to the effect on the spectrum of interaction between the pellet or mull material and the substance being studied.

The present report contains data on the spectra of calcite, aragonite, and vaterite type structures in the borate, carbonate, and nitrate series which were available. The data are analyzed to correlate the spectra with structure in order to obtain information on the interatomic forces and the reasons for the occurrence of the different structure types in the rare earth borates. Representative data for a few other structures of interest are also included.

[1] Figures in brackets indicate the literature references at the end of this paper.

2. Apparatus and Experimental Method

All absorption spectra were obtained using a type-II diamond cell [1] in a commercially available infrared spectrometer. The region from 6μ to 20μ was covered in these experiments.

In a given experiment a few milligrams of powder or a small crystal of the specimen was placed on one diamond surface. The cell was assembled and a maximum pressure of a few hundred atmospheres was applied to produce a clear film. The pressure was decreased to a few atmospheres, e.g., less than 50 atm, before obtaining the spectra. Since the specimen was in contact with diamond alone no shift in bands from interaction with the diamond is to be expected. Previous studies have shown that the positions of the bands are essentially unaffected by the low pressures used in these measurements.

All nitrates studied were reagent grade chemicals. All carbonates except vaterite were of natural origin with the small specimens required being obtained from small single crystals. The structure type was verified by X-rays in those instances where there was any uncertainty. Most of the natural minerals have been in use here for several years as optical and X-ray standards. Vaterite [2] was prepared according to the procedure described by Wray and Daniels [5] and the structure was confirmed by X-ray analysis. The X-ray pattern indicated the presence of a small amount of calcite and this was confirmed microscopically. The borate samples were prepared by Levin and Roth [4] from the rare-earth oxides and orthoboric acid by ordinary solid state reaction techniques. A contaminant consisting of a $3R_2O_3 \cdot B_2O_3$ high temperature phase may have been present in some of the borates.

[2] Vaterite was obtained through the courtesy of Dr. Robert Likins of the National Institutes of Health.

3. Infrared Spectral Analysis

For the isolated planar ion XO_3 having trigonal symmetry there are four fundamental modes of vibration; the symmetric stretching, ν_1, the out of plane bending, ν_2, the doubly degenerate antisymmetric stretching, ν_3, and the doubly degenerate planar bending, ν_4 [6]. Of these fundamentals, three are inherently active in the infrared while the fourth, the symmetric stretching, is inactive in isolated ions. In a crystalline solid containing more than 1 molecule per unit cell, symmetry considerations indicate that all modes may be active and coupling between various modes may even remove degeneracies [7, 8]. In the calcite structure it is expected that ν_2, ν_3, and ν_4 will be observed with ν_1 inactive and both ν_3 and ν_4 doubly degenerate. In aragonite, six bands are expected since in this structure ν_1 is active and the degeneracies are removed from ν_3 and ν_4. Vaterite is reported to have a hexagonal cell containing two or more molecules per unit cell [9, 10, 11]. However, the structural details of the unit cell have not been established so far as can be ascertained. Therefore, the expected spectrum cannot be predicted.

The errors associated with measuring the frequencies may be assessed as follows: All values recorded represent average peak positions. In general, ν_1 (not usually observed in calcite), is very sharp and its position can be determined with little error. Both ν_2 and ν_4 are reasonably sharp and occur in a region of high dispersion. These values are also considered to be known with little error. In all specimens, ν_3 is extremely strong and broad and is distinctly asymmetrical. The broadness coupled with the location of ν_3 in a region of low dispersion imply that the tabulated ν_3 values are subject to some uncertainty. In particular, it is to be noted that as a result of asymmetry, ν_3 values corresponding to positions of maximum absorption will differ considerably from the values tabulated. Comparison of the data of this report with the data of Huang and Kerr [15] for carbonates shows that ν_2 and ν_4 values agree within ± 2 cm^{-1} but that corresponding values of ν_3 may differ by as much as 40 cm^{-1}.

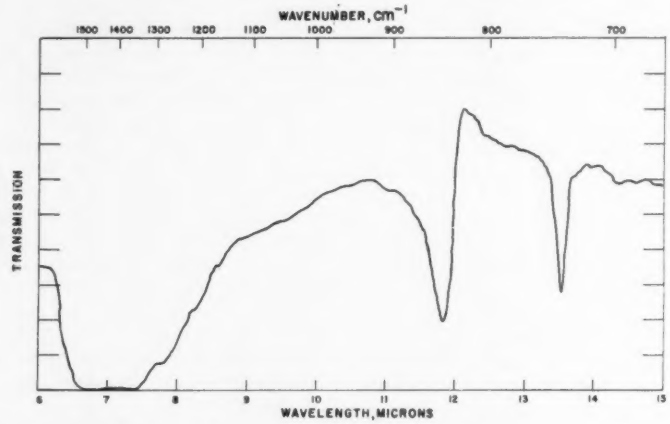

FIGURE 1. *Infrared absorption spectrum of $LiNO_3$ (calcite structure).*

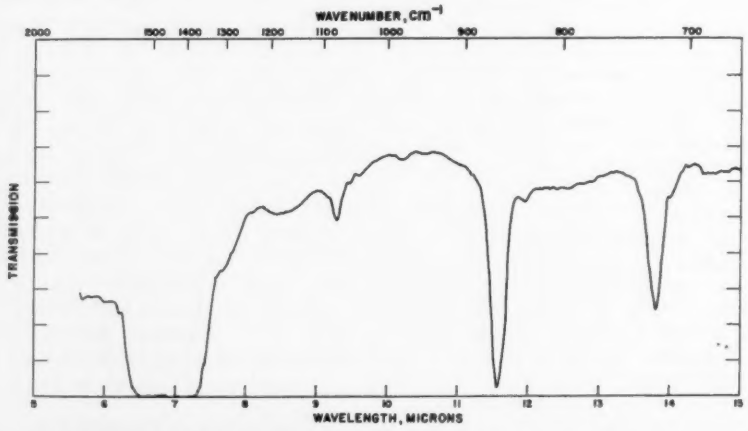

FIGURE 2. *Infrared absorption spectrum of $CdCO_3$ (calcite structure).*

4. Results

4.1. Calcite

Typical spectra for the calcite structures are shown in figures 1 to 3 and the data for all calcite structures studied are given in table 1. The tabular data consist of the frequencies in cm^{-1}, the force constants calculated from the observed frequencies assuming a simple valence force potential for the isolated XO_3 ion [6], the ionic radius of the cation [11], and the unit cell constants [12, 13]. Values for ν_1, which is inactive in calcite type structures, are available for $NaNO_3$ and $CaCO_3$ from Raman spectra [14]. In $CdCO_3$ and $CoCO_3$ bands were observed in the position expected for ν_1 and these are listed in the table. All other values for ν_1 are given in parentheses and are assumed to be identical with the corresponding values found for $NaNO_3$, $CaCO_3$ or $NdBO_3$ (aragonite type structure). From data to be given later, it appears that the error arising from the assumed values of ν_1 do not exceed a few percent. However, force constants involving the assumed values of ν_1 will reflect the error and such values are also enclosed in parentheses. The arrangement in table 1 is in the order of increasing valence of anion with subarrangement in the order of increasing ionic radius of cation.

In general, the results listed in table 1 are in agreement with the spectra predicted on the planar ion model. Several unexpected bands are found, however, i.e., weak low frequency satellites of the ν_2 bands in $CdCO_3$ and $CoCO_3$ and the appearance of the ν_1 band in these materials. There is also a reasonably strong high frequency satellite of ν_2 in the borates. This band has been shown by Steele and Decius [16] to arise from the B^{10} isotope. Decius [17]

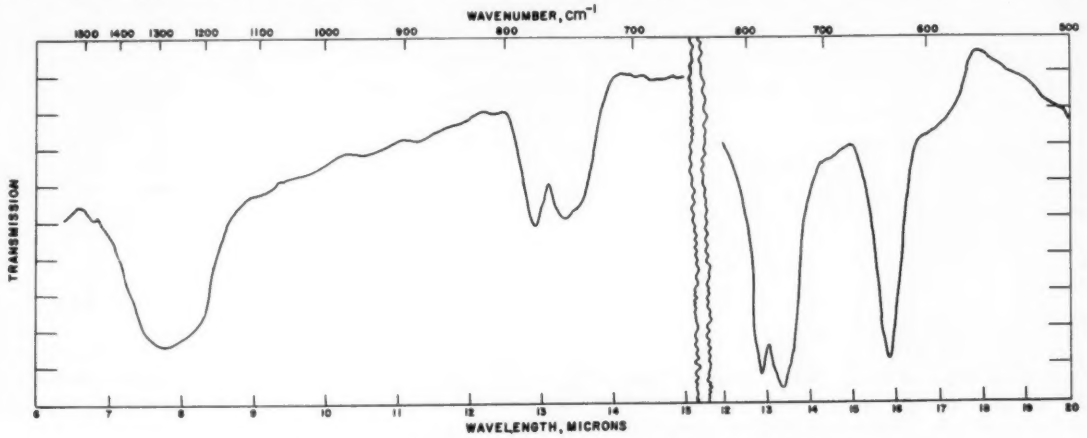

FIGURE 3. *Infrared absorption spectrum of $LuBO_3$ (calcite structure).*

TABLE 1. *Infrared frequencies and related data for calcite structures*

Compound	Frequency, cm^{-1}				Force constant,[1] dyne/cm$\times 10^{-5}$			Ionic radius of cation,[2] A	Unit cell constants,[3] A	
	ν_1	ν_2	ν_3	ν_4	k	k_{Δ/l^2}	k_{δ/l^2}		a	c
$LiNO_3$	(1068)	843	1420	738	(10.1)	1.51	(0.727)	0.68	4.692	15.22
$NaNO_3$	1068	838	1395	727	10.1	1.50	.683	.94	5.070	16.829
$MgCO_3$	(1087)	892	1478	749	(11.2)	1.50	(.646)	.67	4.633	15.015
$CoCO_3$	1090	838 869	1485	747	11.2	1.32 1.42	.650	.73	4.659	14.957
$ZnCO_3$	(1087)	873	1480	745	(11.2)	1.44	(.643)	.74	4.653	15.028
$FeCO_3$	(1087)	869	1470	738	(11.2)	1.42	(.623)	.74	4.711	15.436
$MnCO_3$	(1087)	870	1480	728	(11.2)	1.43	(.615)	.80	4.777	15.67
$CdCO_3$	1075	837 862	1462	724	10.9	1.32 1.40	(.609)	.97	4.930	16.27
$MgCa(CO_3)_2$	(1087)	883	1480	730	(11.2)	1.47	(.618)	.82 (avg)	4.832	15.92
$CaCO_3$	1087	881	1432	712	11.2	1.46	.554	.99	4.989	17.062
$InBO_3$	(951)	743 768	1288	676	(8.5)	0.97 1.04	(.493)	.81	4.823	15.456
$LuBO_3$	(951)	748 773	1275	630	(8.5)	0.98 1.05	(.420)	.85	4.913	16.214

[1] Calculated assuming simple valence force potential function for isolated ions.
[2] L. H. Ahrens, Geochim. Cosmochim. Acta **2**, 155 (1952).
[3] Unit cell data from standard X-ray diffraction powder patterns, NBS circ. 539, vols. **1** to **9**, Dana's system of mineralogy Vol II, 7th ed; and E. M. Levin and R. Roth in preparation.

TABLE 2. *Infrared frequencies and related data for Aragonite structures*

Compound	Frequency, cm^{-1}				Force constant,[1] dyne/cm$\times 10^{-5}$			Ionic radius of cation,[2] A	Unit cell constants,[3] A		
	ν_1	ν_2	ν_3	ν_4	k	$k_{\Delta/\beta}$	$k_{\beta/\beta}$		a	b	c
KNO_3	1050	827	1420	714	10.4	1.46	.655	1.33	5.414	9.164	6.431
$CaCO_3$	1087	866	1430 1550	703 715	11.2	1.41	.53 0.63 .55 .65	0.99	4.959	7.968	5.741
$SrCO_3$	1074	845 863	1496	701 707	10.9	1.35 1.40	.597 .608	1.12	5.107	8.414	6.029
$PbCO_3$	1053	826 840	1450	670 678	10.4	1.29 1.33	.537 .550	1.20	5.195	8.436	6.152
$BaCO_3$	1060	845 858	1470	695 709	10.6	1.35 1.38	.582 .607	1.34	5.314	8.904	6.430
$NdBO_3$	951	720 791	1307	598 619	8.52	0.91 1.10	.40 .43	1.04	5.037	7.968	5.741
$LaBO_3$	944	725 790	1310	597 613	8.39	0.92 1.09	.40 .42	1.14	5.104	8.252	5.872

[1] Calculated assuming simple valence force potential function for isolated ions.
[2] L. H. Ahrens, Geochim. Cosmochim. Acta **2**, 155 (1952).
[3] Unit cell data from standard X-ray diffraction powder patterns, NBS Circ. 539 vols. **1** to **9**, Dana's system of mineralogy Vol II, 7th ed; and E. M. Levin and R. Roth in preparation.

has discussed the splitting and coupling of the out of plane bending modes to be expected under these conditions. The low frequency satellite of ν_2 in the carbonates is probably not due to a similar isotope effect because of the rarity of C^{14}. It would appear that the band might arise from coupling of out of plane modes of adjacent XO_3 ions, but according to the treatment of Decius [17], electrostatic coupling is not to be expected in the vibrations unless mass differences exist in the XO_3 ions. There is little doubt that a similar satellite of the ν_2 band occurs in most of the carbonates although it is of low intensity and is not listed in table 1. That coupling of modes between adjacent $CO_3^=$ ions may be the cause of the satellite is indicated by the fact that the distance between adjacent $CO_3^=$ ions along the c axis of $CoCO_3$ is smaller than that in $MgCO_3$; and is smaller in $CdCO_3$ than in $CaCO_3$. Whatever the origin of the satellite of ν_2, interaction effects appear to be responsible for the appearance of ν_1 in $CdCO_3$ and $CoCO_3$ since the band obviously contains fine structure, being much broader than observed in any other similar materials. The broad, asymmetric appearance of ν_3 is also indicative of coupling or interaction between the antisymmetric mode and other vibrations.

The data for dolomite are of particular interest inasmuch as alternate cation positions are occupied by Ca and Mg ions [13]. From the crystal structure it might be expected that the larger Ca ion would influence the out of plane and antisymmetric vibrations and that the average field of both ions would affect the in-plane vibration. It is found that in dolomite ν_2 agrees with that for calcite and ν_4 is approximately the average of the corresponding values for calcite and magnesite. However, contrary to expectations, ν_3 for dolomite is almost identical with ν_3 for magnesite.

The data of table 1 do not illustrate clearly the trend of frequency with ionic radius of cation. There is some indication that the in-plane frequency increases as the cation radius decreases. However, it is most likely that all the carbonates listed are not equally ionic and effects due to variation in the ionic character of the compound will probably be superimposed on effects arising from ionic size. In the alkaline earth carbonates and the alkali nitrates which may be considered to be completely ionic it appears from the tabulated frequencies that smaller cations produce frequency shifts to higher energies. This trend will become more apparent in data presented later.

4.2. Aragonite

Typical absorption spectra of aragonite type structures are shown in figures 4 to 6 and the pertinent data are compiled in table 2. The arrangement in table 2 follows that of table 1. The tabular data show that only for $CaCO_3$ is there good evidence for the splitting of ν_3. For all other materials, however, it is apparent that the ν_3 band contains internal structure unresolved by the spectrometer which is consistent with the predicted splitting. The two components of ν_4 appear in all specimens except KNO_3 in which ν_4 is very weak and apparently unsplit. It should be noted that in all cases where the ν_4 band is split into two components that the higher frequency component is invariably much the stronger. As in the calcite structure there is evidence for a low frequency component on most of the ν_2 bands in the carbonates. In the borates the second component of ν_2 is quite strong and most probably due to B^{10} [16]. The effect of change in ionic radius of cation and differences in packing in the unit cell is shown by the trends of ν_1 and k in the alkaline earth carbonates. The increase in ν_1 and k as the unit cell decreases in size may be attributed to shortening of the C—O bond by repulsion of closed shells of the oxygen atoms. It will be noted that

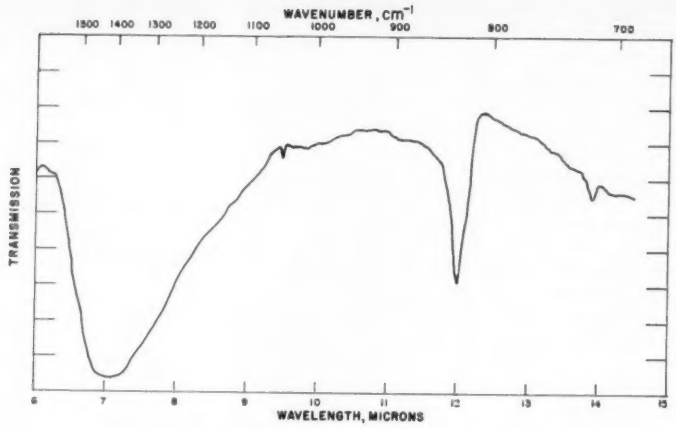

FIGURE 4. *Infrared absorption spectrum of KNO_3 (aragonite structure).*

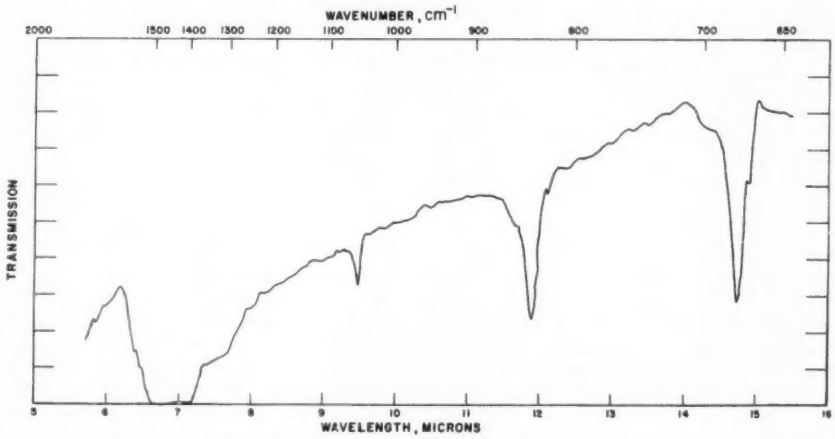

FIGURE 5. *Infrared absorption spectrum of $PbCO_3$ (aragonite structure).*

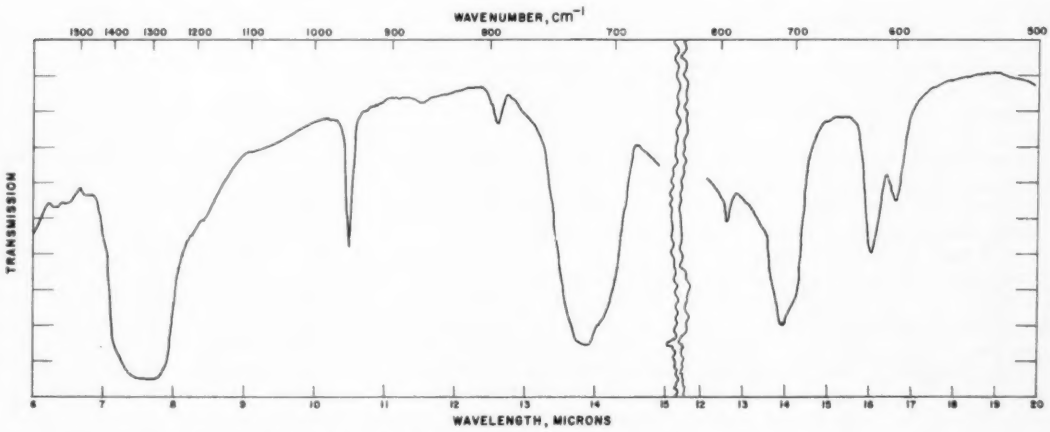

FIGURE 6. *Infrared absorption spectrum of $NdBO_3$ (aragonite structure).*

$PbCO_3$ does not follow the trend for the alkaline earth carbonates, a behavior which is probably due to the greater covalency of the Pb—O bonds.

Comparison of the force constants and frequencies for $CaCO_3$ in the aragonite and calcite structures shows that there is little change. This is particularly true in the stretching force constants. A similar conclusion is reached by comparing data for $NaNO_3$ and KNO_3. Since the cation coordination number is six in calcite and nine in aragonite [18] it is concluded that the electrostatic forces around the ionic cations have little effect on the internal vibrations of the much more tightly bonded anions. It can also be concluded that changes in vibrational frequencies are primarily due to anion-anion forces rather than anion-cation interactions.

4.3. Vaterite

Typical absorption spectra for the vaterite type structures are shown in figures 7 to 10 and the data are compiled in table 3. The spectrum of the vaterite form of $CaCO_3$ is analogous to those for calcite and aragonite, and the frequency assignments appear straight forward. Accordingly, the complete tabular data are given for $CaCO_3$. The spectra of the borate type vaterites are considerably different from those for the borates in the calcite and aragonite structures. The borate vaterites are characterized by an extremely broad and intense absorption band extending from 800 cm^{-1} to 1,200 cm^{-1}. Studies made on extremely thin films showed that this one intense band consisted most probably of four broad bands. Of these four, the existence of three is unequivocal and the average positions of the bands could be located with reasonable accuracy. The fourth band, however, appeared to be definite for some specimens but doubtful for others. This band occurs near 1,000 cm^{-1}, is weaker than the adjoining bands and is partially obscured. Inasmuch as it was not observed definitely in all samples and could not be located with reliability when it appeared, the data for the fourth band near 1,000 cm^{-1} are omitted from the table. The band assignments have not been listed in table 3 for the vaterite type borates. It seems likely that the bands below 800 cm^{-1} arise from distortion and bending modes and they are so tabulated. Bands above 800 cm^{-1} are designated as stretching modes. It is possible that the symmetric stretching band is that near 930 cm^{-1} in the vaterites in analogy with the value found in the borate type aragonites. However, this is by no means certain since the character of the band is quite different in the two instances, i.e., sharp and of medium intensity in aragonite, and broad and very intense in vaterite.

The analysis of the spectra on the borates was believed originally to be complicated by the existence of the $3R_2O_3 \cdot B_2O_3$ compound and the high temperature forms of low symmetry reported by Levin and Roth [4]. Patterns containing high percentages of Tm_2O_3 were used to identify the spectrum of $3Tm_2O_3 \cdot B_2O_3$. It was found that a broad, very strong band near 1,300 cm^{-1} was the most prominent feature in the spectrum of this material. Traces of this band were observed in most spectra of the borate type vaterites, but the other bands being weaker were not observed. The band near 1,300 cm^{-1} is not listed in table 3, as it is believed to arise from the 3:1 compound.

TABLE 3. *Infrared frequencies and related data for vaterite structures*

Compound	Frequency, cm^{-1}				Force constant,[1] dyne/cm×10^{-5}			Ionic radius of cation,[2] A	Unit cell constants,[3] A	
	ν_1	ν_2	ν_3	ν_4	k	k_{Δ/l^2}	k_{δ/l^2}		a	c
CaCO	1090	850 878	1450	741 747	9.09	1.46	0.755	0.99	4.12	8.56
	Distortion frequencies, cm^{-1}				Stretching frequencies, cm^{-1}					
$LuBO_3$	578, 723				884, 952, 1093			.85	3.725	8.71
$YbBO_3$	579, 722				881, 940, 1110			.86	3.732	8.74
$TmBO_3$	576, 719				875, 940, 1080			.87	3.748	8.76
$ErBO_3$	571, 716				876, 937, 1103			.89	3.761	8.79
$HoBO_3$	569, 711				870, 931, 1096			.91	3.776	8.80
$DyBO_3$	570, 708				872, 928, 1086			.92	3.791	8.84
YBO_3	551, 714				874, 935, 1105			.92	3.777	8.81
$GdBO_3$	567, 698				862, 922, 1082			.97	3.829	8.89
$EuBO_3$	568, 693				860, 922, 1049			.98	3.845	8.94
$SmBO_3$	568, 692				851, 910, 1035			1.00	3.858	8.96

[1] Calculated assuming simple valence force potential function for isolated ions.
[2] L. H. Ahrens, Geochim. Cosmochim. Acta **2**, 155 (1952).
[3] Unit cell data from R. W. G. Wykoff, The structure of crystals, 2d ed (1931), and E. M. Levin and R. Roth in preparation.

The infrared patterns of the carbonate and borate vaterite type structures are so strikingly dissimilar that it is difficult to believe that they arise from isostructural compounds. However, the X-ray data show that it would be equally difficult to conclude that the compounds are not isostructural [4]. The absorption pattern of the carbonate type vaterite agrees in detail with a spectrum published previously [3]. Comparison of the data for the carbonate type vaterite with aragonite and calcite shows that the stretching force constant and the out-of-plane bending constant are essentially unchanged. However, the in-plane constant has increased in vaterite. If the analysis of the effects of different types of forces in solution by Benson and Drickamer [19] is considered to apply here, the marked change in the in-plane bending constant is indicative of repulsion between oxygen atoms in the plane of the ion.

Ordinarily the borate type vaterite spectrum would be interpreted in terms of an increase in B—O distances as compared with the corresponding distances in the other polymorphic forms. This change would imply that an increase in coordination of boron had occurred in the transition from the calcite or aragonite to the vaterite type structure. The indication from the data of strong shifts of all bands to lower frequencies in the borate type vaterite structure supports these conclusions. However, the indication of such shifts is not necessarily correct as it is not possible to identify the modes of vibration. Boron is known to assume a tetrahedral fourfold coordination in many compounds and may exhibit both 3- and 4-fold coordination simultaneously in some materials [20, 21]. It is found that as the radius of

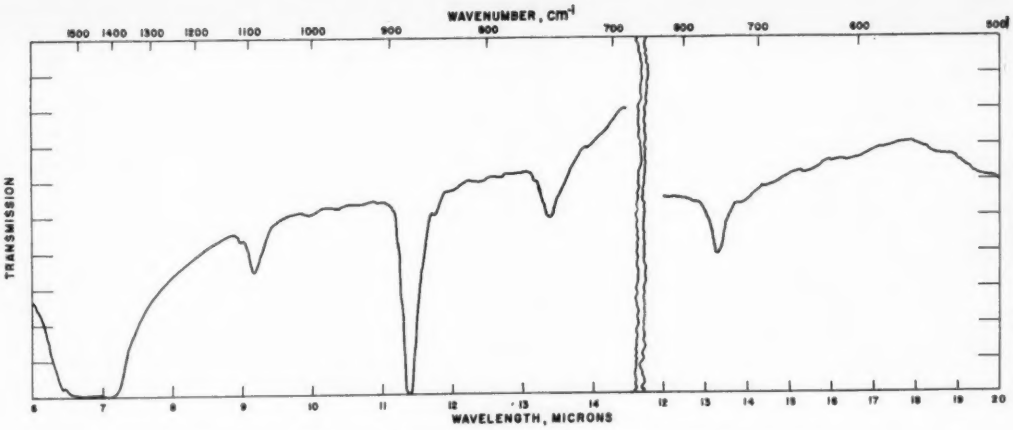

FIGURE 7. *Infrared absorption spectrum of $CaCO_3$ (vaterite structure).*

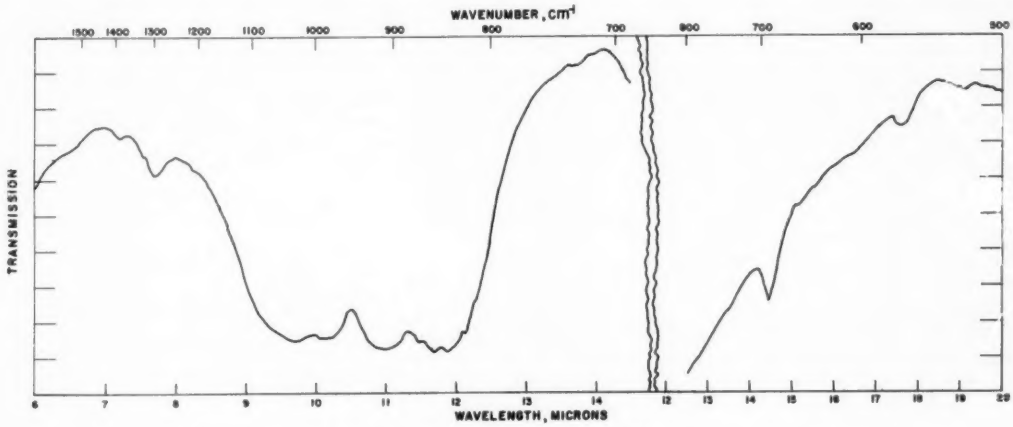

FIGURE 8. *Infrared absorption spectrum of $SmBO_3$ (vaterite structure).*

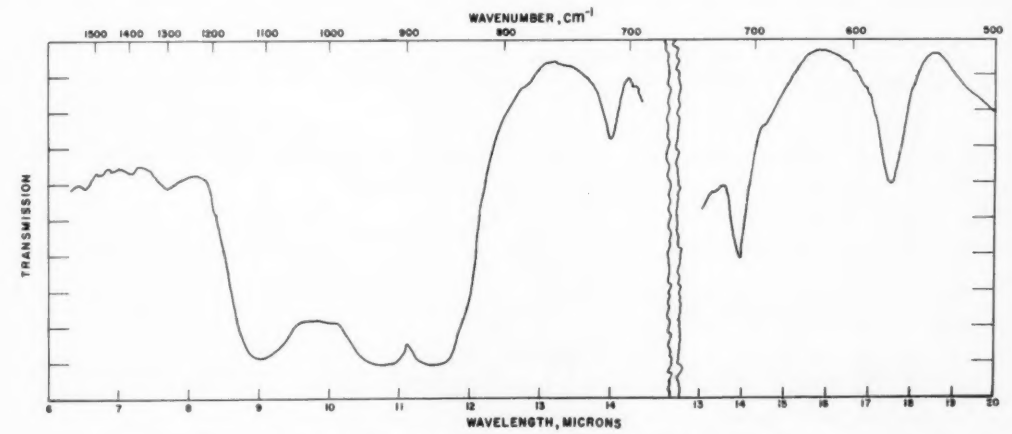

FIGURE 9. *Infrared absorption spectrum of YBO_3 (vaterite structure).*

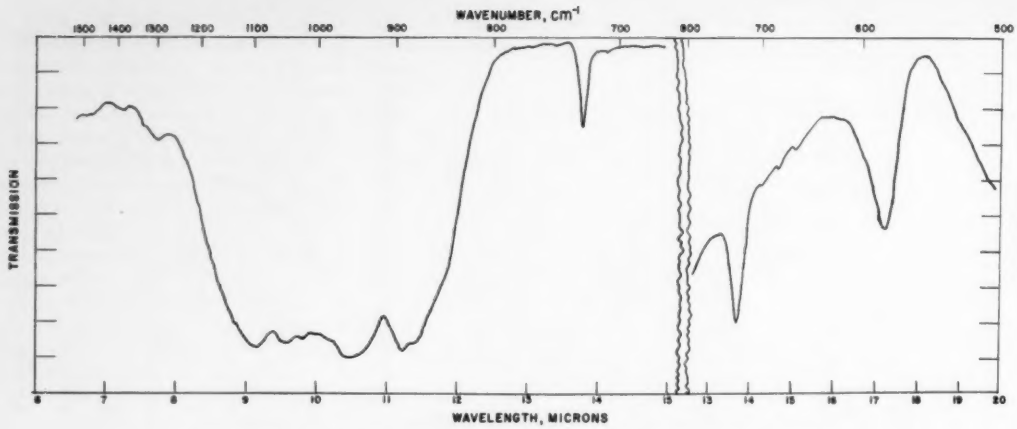

FIGURE 10. *Infrared absorption spectrum of $LuBO_3$ (vaterite structure).*

the rare earth ion decreases, the structure of the rare earth borate changes from aragonite type to vaterite type, and then to calcite type. It seems very improbable that the coordination number of the boron should change from three to four and then revert to three again as the size of the cation decreases monotonically. Therefore, despite the indications of the infrared data, it appears unwise to ascribe the spectrum of the borate to boron in 4-fold coordination. Under the present circumstances it is possible to conclude only that borate and possibly carbonate ions are subjected to severe perturbations in the vaterite type structure. The dissimilarity of the infrared spectra and the similarity of the structures of the borates as shown by X-ray data raise interesting questions to be answered in future studies.

4.4. Miscellaneous Structures

Absorption spectra for other materials in this series are given in figures 11 to 13 and the data are compiled in table 4. For $CsNO_3$ the data are arranged as in table 1. The high temperature borates exist metastably at room temperature and the spectra were obtained at room temperature. These materials are of unknown structure type of low symmetry and the spectral assignments are unknown. By analogy with other borates it would appear that the sharp band near 950 cm^{-1} represents the symmetric stretching mode, but further assignments are not obvious. In general, the complexity of the spectrum confirms the low symmetry found by X-ray analysis [4].

5. Discussion

5.1. Effect of Mass of Cation

It has been suggested [15, 22] that change in the mass of the cation is reflected by a change in the observed internal frequencies of the anion through a modified inverse square root relationship. It would appear that the mass of the cation should have a small effect on the internal anion frequencies since the bond between the anion and cation for purely

TABLE 4. *Infrared frequencies and related data for miscellaneous structures*

Compound	Frequency, cm^{-1}				Force constant,[1] dyne/cm$\times 10^{-5}$			Ionic radius of cation,[2] A	Unit cell constants,[3] A	
	ν_1	ν_2	ν_3	ν_4	k	k_{Δ/l^2}	k_{δ/l^2}		a	c
$CsNO_3$	1050	835	1380	716	10. 4	1. 48	0. 623	1. 67	10. 950	7. 716
	Distortion frequencies, cm^{-1}				Stretching frequencies, cm^{-1}					
$LaBO_3$	582, 588, 634, 757				952, 1215, 1280			1. 14		
$NdBO_3$	563, 575, 667, 737, 762				935, 1172, 1215, 1310, 1390			1. 04		
$SmBO_3$	561, 571, 674, 732, 760				939, 1055, 1085, 1338, 1388			1. 00		
$EuBO_3$	564, 573, 675, 733, 763				925, 1066, 1180, 1210, 1360			0. 98		

[1] Calculated assuming simple valence force potential function for isolated ion. For details of notation see reference 6 in text.
[2] L. H. Ahrens, Geochim. Cosmochim. Acta **2**, 155 (1952).
[3] Unit cell data from standard X-ray diffraction powder patterns, NBS Circ. 539, Vol. **9**, p. 25 (Feb. 1960).

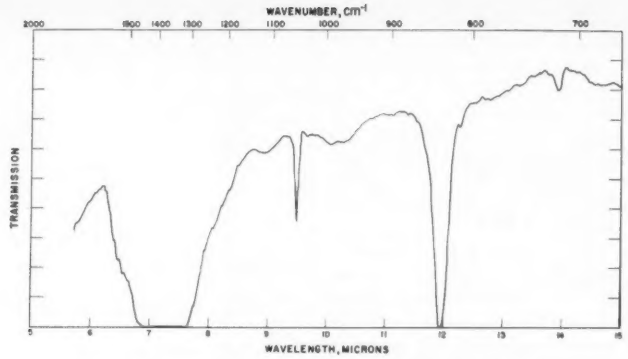

FIGURE 11. *Infrared absorption spectrum of $CsNO_3$.*

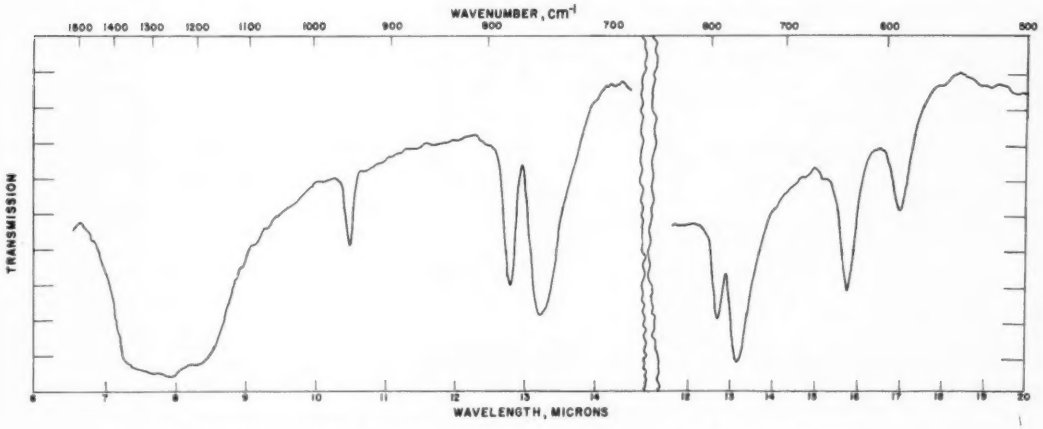

FIGURE 12. *Infrared absorption spectrum of $LaBO_3$ (high temperature structure).*

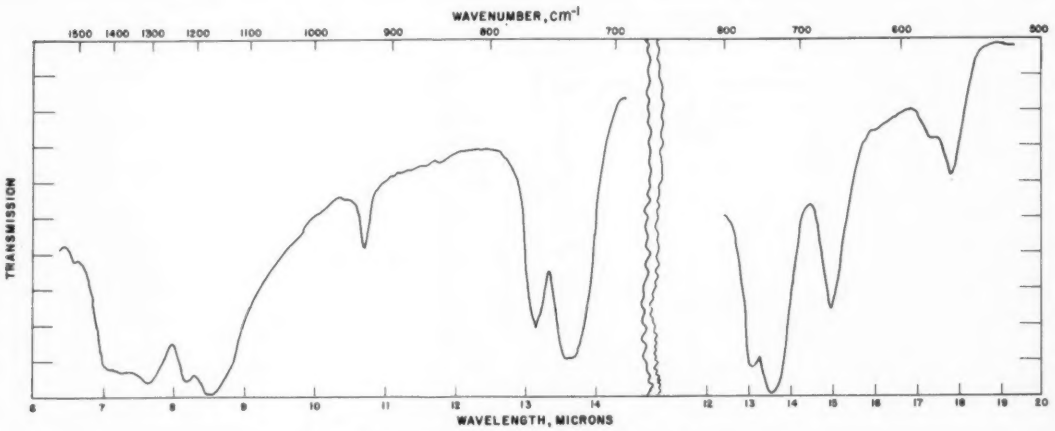

FIGURE 13. *Infrared absorption spectrum of $NdBO_3$ (high temperature structure).*

ionic bonding is much weaker than the internal covalent bonds of the anion. It was noted previously that in calcium carbonate a change in coordination number of the calcium ion in the transition from calcite to aragonite produces a negligible frequency shift. The data on the borate type vaterites refute the idea of a conventional mass effect. Although the mass of the cation increases from Sm^{3+} to Lu^{3+}, it is apparent that the frequencies increase also from $SmBO_3$ to $LuBO_3$. Considering YBO_3, in which the cation has a mass approximately half that of the rare earth ions, it is observed that the frequencies are not much higher as expected by conventional mass effects but close to what would be expected on the basis of the radius of the cation. Similarly, there is no correlation of frequency with mass of cation in the carbonate type calcites. There appear to be irregularities in the carbonates which are most readily interpreted as change in ionic character of the cation-oxygen bond such as in $PbCO_3$. It seems quite reasonable to conclude that as this bond becomes more covalent the cation mass may play a greater role in affecting the internal vibrations of the anion.

5.2. Effect of Volume

The data on the rare earth borates of the vaterite structure type lead to other interesting conclusions. The rare earth ions form a series whose external electron configurations are quite similar. Quantitatively these ions should show very small differences in the character of their interactions with their neighbors in the crystal. In the vaterite structures, as the cation is changed from Sm^{3+} to Lu^{3+}, the ionic radius decreases by some 15 percent. This result may be considered to be produced by an increase in the *effective* nuclear charge tending to reduce the size of the electron shells.

The unit cell dimensions also become smaller as the cation radius decreases and as a consequence the cation-oxygen nuclear distance becomes less. Both

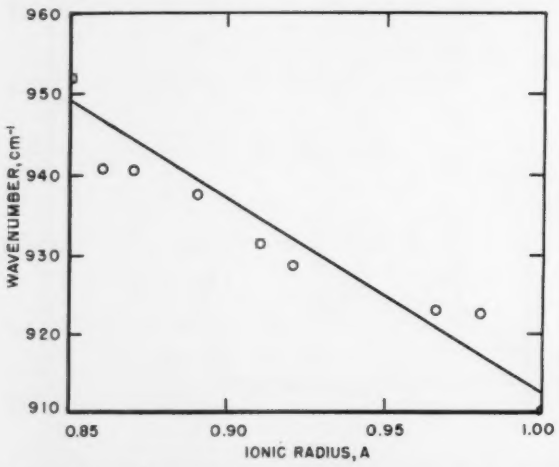

FIGURE 14. *Effect of ionic radius of cation on position of 930 cm^{-1} band in borate type vaterites.*

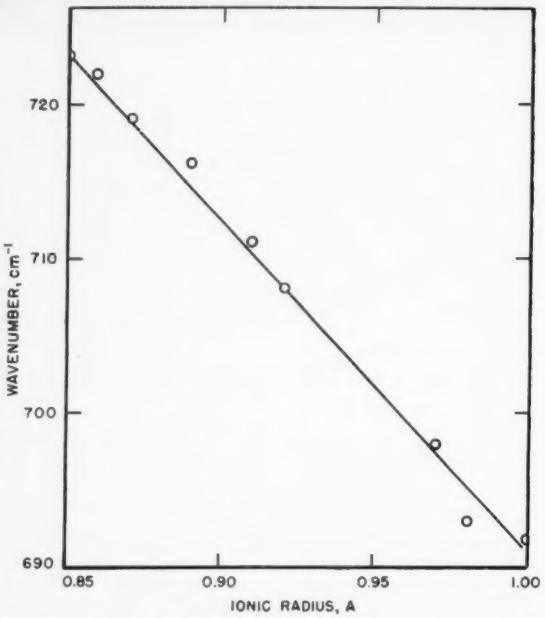

FIGURE 15. *Effect of ionic radius of cation on position of 710 cm^{-1} band in borate type vaterites.*

the increase in effective charge and the smaller cation-oxygen distance cause an increase in *electrostatic* attraction of cation for oxygen. The increased attractive force must be balanced by an increased repulsion that is most readily attributed to overlap of closed electron shells of the oxygen atoms which comprise the major portion of the unit cell volume. However, an increase in the oxygen-oxygen repulsion should be reflected in a corresponding shortening of the B—O bond and an increase in the frequencies of

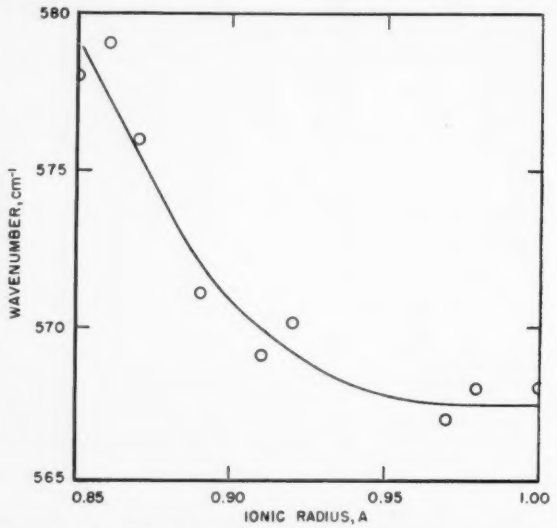

FIGURE 16. *Effect of ionic radius of cation on position of 570 cm^{-1} band in borate type vaterites.*

vibration of the borate ion. This trend is illustrated by the data on the borate type vaterites, the alkaline earth type aragonites, the nitrate type calcites, etc. Data on garnets with various cations [22] also show the same effect. It will be noted that the data for YBO_3 do not conform exactly to the order of the rare earth borates. Since Y^{3+} has a different electronic configuration than the rare earth ions, this is not surprising. The differences may readily be attributed to the difference in the oxygen-oxygen interactions caused by the variation in the outer shell electrons of the Y^{3+} and the rare earth ions.

5.3. Effect of Ionic Radius on Structure Type

The present data shed some light on the causes of changes in structure produced by variation in the ionic radius. As noted, the frequency trend observed in these studies is readily interpreted as arising from repulsion of oxygen atoms in the crystals. Figures 14 to 16 show the frequency-ionic radius dependence for three bands in the borate type vaterites. For the 900 cm^{-1} and 700 cm^{-1} bands, the frequencies increase essentially linearly as the ionic radius diminishes. The 550 cm^{-1} band, however, shows a rapidly accelerating increase in frequency as the ionic radius decreases. From figure 16 it is apparent that the energy associated with this vibration is rising rapidly. It seems most reasonable to suppose that eventually a different arrangement of the structural units becomes energetically more favorable, and the new structure will be assumed if the energy barrier can be surmounted. Thus, as the cation is changed from Yb^{3+}, for which vaterite is stable to the slightly smaller Lu^{3+}, the vaterite structure is not stable because of the greater repulsive forces, and the more open calcite structure is formed. Conversely as the atomic number of the cation is decreased, the closed shell repulsive forces decrease very rapidly whereas the electrostatic attractive forces decrease at a slower rate, and the energy will rise along the attractive leg of the potential energy curve until a point is reached, at which another more dense structure (aragonite) becomes stable. This occurs between Sm^{3+} and Nd^{3+}. That these ideas are qualitatively consistent is indicated by the fact that at elevated temperatures at which the O—O repulsive forces will decrease because of thermal expansion, the calcite form of $LuBO_3$ reverts to the vaterite type structure which is more stable in the expanded lattice.

The considerations outlined apply only to structure type changes produced by ionic substitution. The question of a general polymorphic transition when produced by a change in pressure or temperature, or both, is considerably more complex inasmuch as kinetic as well as potential energies are involved. However, it appears that repulsive energy considerations discussed here may well be the governing factor in "abnormal" transitions in which the high temperature phase is denser than the low temperature phase.

6. References

[1] C. E. Weir, E. R. Lippincott, A. Van Valkenburg, and E. N. Bunting, J. Research NBS **63A,** 55 (1959).
[2] R. M. Hexter, Spectrochim. Acta **10,** 281 (1958).
[3] G. Baron, S. Cailliere, R. Lagrange, and T. Pobeguin, Bull. Soc. Fran. Min. Cryst. **82,** 150 (1959).
[4] E. M. Levin and R. Roth—in preparation.
[5] J. L. Wray and F. Daniels, J. Amer. Chem. Soc. **79,** 2031 (1957).
[6] G. Hertzberg, Molecular spectra and molecular structure vol. II, Infrared and raman spectra of polyatomic molecules, 7th ed., p. 178 (D. van Nostrand Co. New York, N.Y., 1956).
[7] D. F. Hornig, J. Chem. Phys. **16,** 1063 (1948).
[8] R. S. Halford, J. Chem. Phys. **14,** 8 (1946).
[9] R. W. G. Wykoff, The structure of crystals, 2d ed. p. 280 (The Chemical Catalog Co., New York, N.Y., 1931).
[10] Hans-Jurgen Meyer, Angew. Chem. **71,** 678 (1959).
[11] L. H. Ahrens, Geochim Cosmochim Acta **2,** 155 (1952).
[12] Standard X-ray diffraction powder patterns, NBS Circ. 539 vols. **1** to **9**.
[13] C. Palache, H. Berman, and C. Frondel, Dana's system of mineralogy Vol. II, 7th ed., (John Wiley & Sons, New York, N.Y., 1951).
[14] S. Bhagavantam and T. Venkatarayudo, Proc. Indian Acad. Sci. **A9,** 224 (1939); **A13,** 543 (1941).
[15] C. K. Huang and P. F. Kerr, Am. Mineral. **45,** 311 (1960).
[16] W. C. Steele and J. C. Decius, J. Chem. Phys. **25,** 1184 (1955).
[17] J. C. Decius, J. Chem. Phys. **23,** 1290 (1955).
[18] L. Pauling, The nature of the chemical bond, ch. X. (Cornell Univ. Press, Ithaca, N. Y., 1948).
[19] A. M. Benson and H. G. Drickamer, J. Chem. Phys. **27,** 1164 (1957).
[20] J. R. Clark, Acta Cryst. **12,** 69 (1958).
[21] C. L. Christ, Am. Mineral. **45,** 334 (1960).
[22] H. Adler et al., Reference Clay Minerals A.P.I. Research Project 49, Infrared spectra of reference clay minerals, p. 15 (Columbia University New York, N.Y., July, 1950).

(Paper 65A3–100)

JOURNAL OF RESEARCH of the National Bureau of Standards—A. Physics and Chemistry
Vol. 65A, No. 3, May–June 1961

Dielectric Properties of Polyamides: Polyhexamethylene Adipamide and Polyhexamethylene Sebacamide

Alexander J. Curtis

(January 6, 1961)

The dielectric relaxation in two polyamides has been studied over a temperature range from −100 to 175 °C and a frequency range from 50 c/s to 10 Mc/s. The effects of various thermal treatments on the relaxation behavior and density, X-ray diffraction, and intrinsic viscosity have been studied. The polyamides were poly(hexamethylene adipamide) and poly(hexamethylene sebacamide). Four relaxation phenomena have been identified. Mechanical relaxation processes are compared with the dielectric phenomena and possible molecular mechanisms are discussed.

1. Introduction

The dielectric properties of polyamides have received widespread interest in recent years. Boyd [1] [1] has reported measurements of the dielectric loss of poly(hexamethylene adipamide), 66 nylon, and discussed in detail the high temperature relaxation process in terms of molecular structure. McCall and Anderson have described measurements on a series of seven linear polyamides [2], and Rushton and Russell [13] have studied 66 nylon. The much earlier measurements of the dielectric properties of a number of polyamides by Baker and Yager [3] should also be mentioned.

The polyamides, or as they are commonly called, the nylons, have attracted the attention of a wide group of investigators for a number of reasons. Quite aside from their commercial importance, the nylons are of interest because they possess a highly complex structure and, as expected, have a complicated dielectric relaxation spectrum. The crystalline regions of 66 nylon and of 610 nylon, poly(hexamethylene sebacamide), have been studied by means of X-ray diffraction by Bunn and Garner [4]. It was shown that in the highly ordered crystalline regions, the polymer molecules lie in sheets in which adjacent molecules are joined through hydrogen bonds involving amide protons and carbonyl groups. The two principal lateral spacings determined from X-ray diffraction are, therefore, related to the interchain spacing within the hydrogen-bonded sheets and the intersheet spacing. It has been reported by a number of observers [5, 6, 7] that these two spacings merge and become indistinguishable above some temperature well below the melting point: in 66 nylon this temperature was reported to be 160 °C while the crystalline melting point was observed at 260 °C [6]. The structure above the transition temperature apparently corresponds to a disordered crystal in which the molecules have some rotational freedom about their long axes. It has also been shown that it is possible to obtain samples of nylon in which part or all of the ordered regions are in this rotationally disordered condition at room temperature [7]. This structural feature has been discussed in detail by Sandeman and Keller [8].

The present study of dielectric relaxation in two polyamides, 66 nylon and 610 nylon, is an attempt to correlate dielectric properties with pretreatment variables and in turn to show how these are related to such measurable quantities as crystallinity, moisture content, and molecular weight.

2. Experimental Details

2.1. Dielectric Measurements

All the dielectric measurements reported here were made with a cell specifically designed for measurements on disk-shaped solids, (fig. 1). All measurements were two-terminal. There is no reason to suspect that the present results, which are consistent with three-terminal measurements on similar materials [1], would have been different if three-terminal measurements had been made.

In figure 1 the cell is shown with the protective enclosure removed. In use, the electrodes were surrounded by this enclosure with heaters built into the walls to provide necessary heating. Temperature control was effected by independent sets of heaters in the top, the sides, and bottom of the enclosure. Thermocouples at the side and top were sensing elements for the controller. Two calibrated chromel-constantan junctions, one below the lower electrode and the other at the upper electrode, served to measure the temperature. The tempera-

[1] Figures in brackets indicate the literature references at the end of this paper.

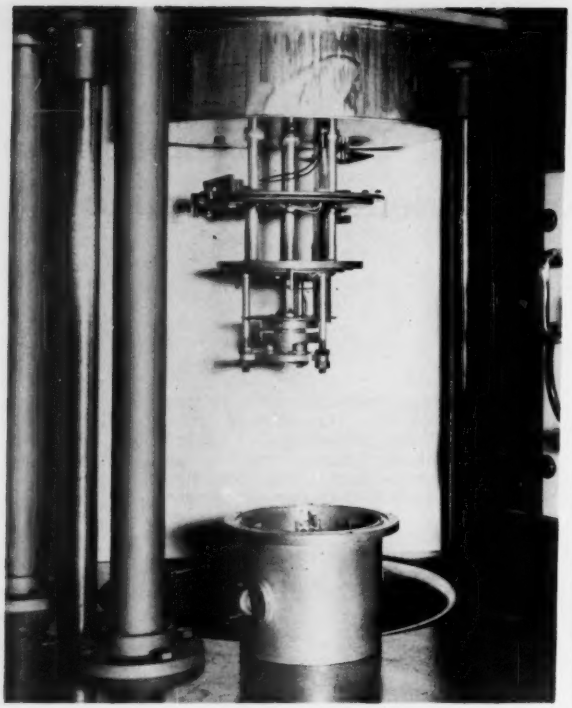

FIGURE 1. *Cell for dielectric measurements shown with sample between electrodes.*

ture difference between the upper and lower electrodes was never greater than a tenth of a degree at any of the temperatures at which dielectric measurements were carried out.

Below room temperature the entire cell and enclosure were surrounded by a large Dewar cylinder containing either dry ice or liquid nitrogen, without actually immersing the enclosure in the coolant. The controller supplied whatever current was necessary to maintain the desired temperature. Dry nitrogen was kept flowing through the cell at all times during measurements. At high temperatures, this prevented oxidation of the samples and at low temperatures it prevented condensation of moisture in the system.

Dielectric measurements from 50 c/s to 100 kc/s were carried out using a modified General Radio Schering Bridge (716–C). The higher frequency measurements up to 10 Mc/s were made using a Boonton Q-meter (Type 260–A). The details of the modifications and calibrations will be published elsewhere [9]. The precision and accuracy of the data reported here are in part a function of the dimensions of the samples used. Thus, although capacitance can easily be measured to better than 0.1 percent in almost all cases, the equivalent vacuum capacitance of a sample, as computed from the measured dimensions may involve greater uncertainties, which enter into the computation of each dielectric constant value. In order to reduce probable errors, samples having large equivalent vacuum capacitance were chosen for the low temperature measurements where dielectric constant and loss were relatively small and, correspondingly, samples of small equivalent vacuum capacitance were selected for the high temperature measurements, where extremely large values of dielectric constant and loss were encountered.

For samples having properly selected dimensions, it is estimated that the precision of the measurements on 66 nylon was 0.1 percent in the dielectric constant and 5 percent in the loss index. The measurements on 610 nylon involved the use of a more limited number of samples and similar precision was estimated for all but the low temperature measurements. The errors at low temperatures may have been as great as 1 percent in the dielectric constant, and as large as 10 percent in the loss index.

The principal factor involved in causing errors in measurement of dielectric properties of solids, aside from pretreatment and impurities, is the computation of the equivalent vacuum capacitance of a given disk. The error has been greatly reduced by measuring the diameter of each disk sample with a traveling microscope and computing the thickness from the diameter, the sample weight, and specific volume. This technique which has been described elsewhere [9] has been shown to give equivalent vacuum capacitances to better than 0.1 percent.

2.2. Preparation and Characterization of Specimens

The specimens of 66 nylon were pressed from a batch of nylon, in the form of chips, supplied by Dr. Albert Goodman and Miss Helen Anderson of the Du Pont Company. Disk shaped specimens were formed in a special mold designed for this purpose. In this mold, the nylon chips were melted under vacuum and pressed into disks. Because of the large heat capacity of the mold, it was not possible to cool the samples rapidly; generally it took about two hours to cool the mold and sample to room temperature. Because of this unavoidable annealing process, all the 66 nylon samples were quite highly crystalline, as indicated below.

The samples of 610 nylon were supplied by Dr. D. W. McCall of Bell Telephone Laboratories. These samples were from the same lot of polymer used in his work [2], and were supplied as injection molded disks. Some samples for the present study were formed by machining these disks to suitable dimensions. Others were formed by remelting and molding as in the case of the 66 samples.

All the samples were stored in a dessicator over phosphorus pentoxide. Before electrodes were applied, the samples were heated to about 110 °C in an evacuated container (*circa* $5\text{–}10\times10^{-3}$ mm) for three days. Evaporated gold electrodes were applied to most of the samples. Painted silver electrodes were used in some cases. The latter type of electrodes has been found to introduce a very small extraneous dielectric loss in previous studies [23],

but this effect is certainly negligible in measurements of a material as lossy as the polyamides. In the present study, samples with the two types of electrodes gave identical results. After the electrodes were applied, the samples were again heated to 110 °C in vacuum for about one day. A variety of further annealing processes were used for the various samples with consequent variations in physical properties, as indicated below.

Specific volume measurements were carried out by a buoyancy technique. The measurements at room temperature and lower were carried out in *n*-heptane, while those at higher temperatures were in a silicone oil bath (Dow Corning "710"). Specific volumes were determined by comparing the measurements with those made simultaneously on a piece of fused silica. The apparatus employed was that described by Hoffman and Weeks [10]. Results obtained at room temperature (23 °C), together with specimen descriptions, are given in table 1. A typical plot of specific volume as a function of temperature used for the determination of thickness is shown in figure 2 for sample 610–8. Degrees of crystallinity were computed on the basis of the specific volume scale of Starkweather and Moynihan [11]. It is worth noting that very reproducible specific volumes were obtained for various specimens when nearly identical heat treatments were employed.

Intrinsic viscosities were obtained from measurements on *m*-cresol solutions at 30 °C. These measurements were undertaken to check on possible alterations in molecular weights resulting from the various treatments involved in the preparation of the specimens. The data are listed in table 2, together with sample descriptions. End group analysis gave a number average molecular weight of 16,000 for the 66 nylon chips as received. (Analysis showed 98 moles carboxyl end groups and 38 moles amine end groups per 10^6 g of polymer.)

Flory [12] has developed the following relationship between number-average molecular weight (determined by end group analysis) and intrinsic viscosity in *m*-cresol for 66 nylon:

$$\overline{M}_n = 17{,}800[\eta] - 3{,}300.$$

The above expression demonstrates the well-known monotonic relationship between molecular weight and intrinsic viscosity for polymers. Using the

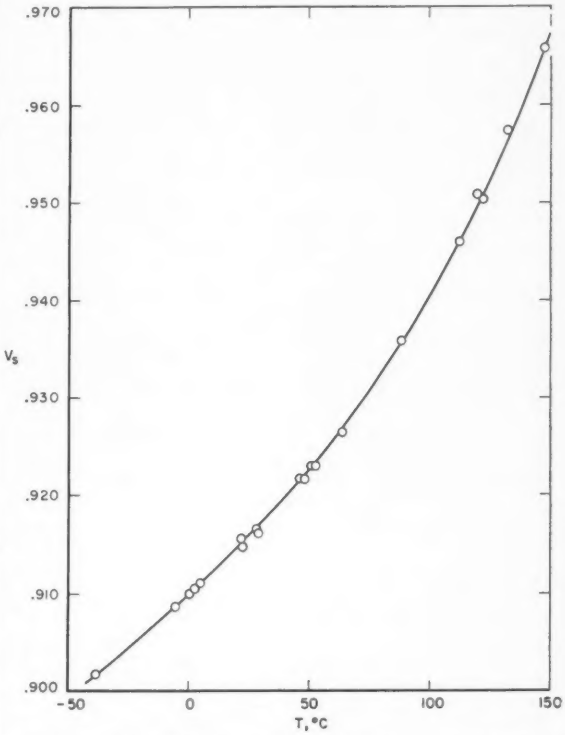

FIGURE 2. *Specific volume (cm³/g) of 610 nylon as a function of temperature.*

TABLE 1. *Sample descriptions and specific volumes*

Number	Mode of preparation and thermal history	Specific volume at 23 °C	% Crystallinity (see text)	Thickness	Area
		cm³/g		*cm*	*cm²*
66–1	Melted in vacuum, compression molded, heated in vacuum for three days at 130 °C.	0. 8709	56	0. 3540	10. 372
66–2	Same as 66–1.	. 8637	62	. 3823	5. 0623
66–3	Same as 66–1.	. 8676	58	. 1461	10. 525
66–4	Cut from same disc as 66–3	. 8676	58	. 1485	10. 535
66–6	Melted in vacuum, compression molded. (Heated in vacuum for subsequent measurements, no perceptible change in V_s.)	. 8685	58	. 3365	7. 9118
610–1	Injection molded, stored one month over P_2O_5.	. 9289	34	. 3197	7. 285
	After heating in vacuum to 110 °C for three days.	. 9287	34	———	———
	After heating to 210 °C for one day.	. 9138	50	———	———
610–2	Melted in vacuum, heated five days in vacuum at 130 °C.	. 9181	46	. 2545	7. 905
610–7	Injection molded, stored over P_2O_5.	. 9289	34	———	———
	After drying at 130 °C in vacuum for five days.	. 9248	38	———	———
	After heating in vacuum at 210 °C for one day.	. 9156	48	. 2924	7. 785
610–8	Melted in vacuum, heated five days at 130 °C in vacuum.	. 9150	49	. 1745	10. 616
610 9	Injection molded and heated three days at 110 °C.	———	—	. 1578	11. 445

intrinsic viscosity value obtained on polymer "as received" from table 2 (1.18), one obtains $\overline{M}_n = 17{,}700$ which is in fair agreement with the value obtained from end group analysis.

It is evident from the data in table 2 that the various heat treatments carried out to dry the specimens have caused a definite increase in molecular weight. This effect will be dealt with subsequently.

The X-ray diffraction properties of the various samples were also measured with a North American Phillips diffractometer. Sample traces of X-ray intensity as a function of diffraction angle are shown in figure 3. These, and specific volume data, show that high temperature annealing is necessary to obtain maximum crystallinity in these polyamides.

The d-c resistance measurements were made with a Beckman Ultrohmeter with an external 200 v potential for resistances greater than 10^9 ohms. Resistances below this value were measured with a General Radio Type 544–B megohm bridge. In the temperature region where the d-c conduction was of particular interest, i.e., above about 80 °C, it was found that there was such a large drift in resistance after applying the measuring potential that the results were of questionable value and low reproducibility.

TABLE 2. *Intrinsic viscosities*

In *m-cresol* at 30 °C.

Sample description	
66 Nylon samples:	
Chips, as received	1.18
Chips, dried in vacuum at 130 °C for 3 days	1.26
Vacuum melted, dried in vacuum at 130 °C for 3 days	1.69
Vacuum melted, dried in vacuum at 130 °C for 3 days	1.73
610 Nylon samples:	
Injection molded, as received	0.96
Injection molded, dried at 130 °C for 3 days	.96
Melted in vacuum, dried at 130 °C for 3 days	1.26
Melted in vacuum, dried at 210 °C for 1 day	1.33

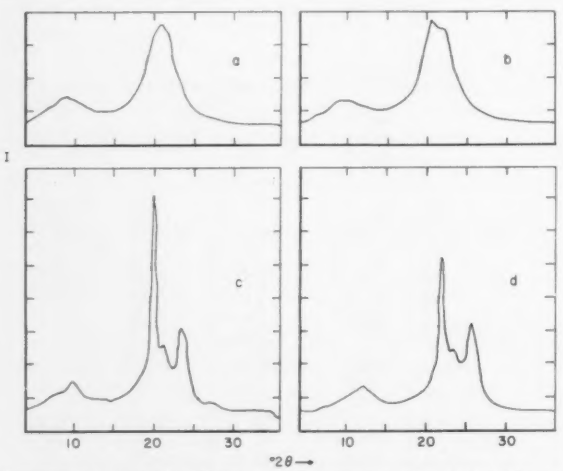

FIGURE 3. *Relative X-ray intensity versus 2θ, (nickel-filtered copper K radiation).*

6-10 Nylon; (A) injection molded, no heat treatment; (B) after five days in vacuum at 130 °C; (C) melted in vacuum, cooled slowly in mold; (D) injection molded, heated 1 day in vacuum to 210 °C.

The data shown in figure 4 are computed from the only set of measurements made.

2.3. Experimental Results

The dielectric constants and losses of the various 66 nylon specimens are listed in table 3. Similar measurements on the 610 nylon samples are given in table 4. Thermal history of each specimen is briefly described in the tables.

There are several cases of nearly identical samples. The differences in the dielectric properties of these samples reflect the difficulty of obtaining semicrystalline polymer samples in identical physical states: for example, nylon specimen 610–1, after drying at 210 °C, had $\epsilon' = 8.311$ and $\epsilon'' = 0.950$ while specimen 610–7, given similar treatment had $\epsilon' = 8.391$ and $\epsilon'' = 0.984$, all measured at 1 kc/s and 80 °C.

The data in table 3 have not been corrected for the effect of d-c conduction on observed dielectric loss. As noted above, in the temperature region in which this correction would become significant, the measurement of d-c resistance becomes somewhat arbitrary. The significance of d-c conduction

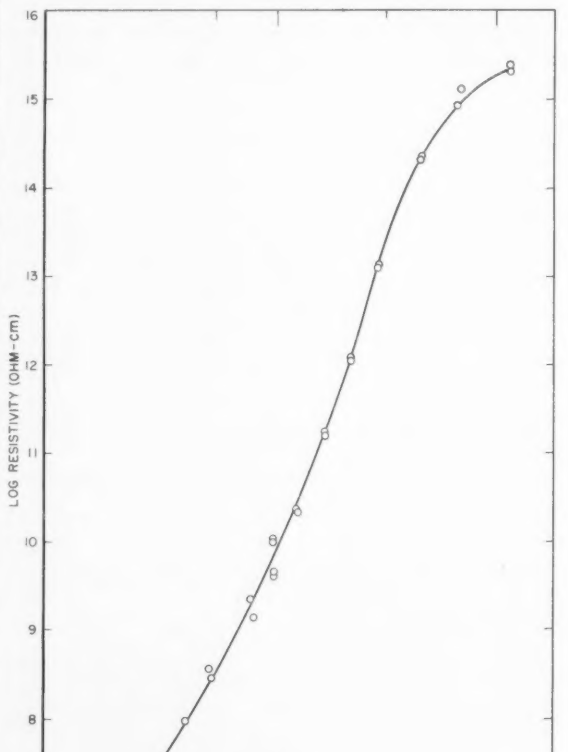

FIGURE 4. *D–C resistivity of 66 nylon as a function of the reciprocal temperature.*

TABLE 3. *Dielectric constants and loss indexes of 66 nylon samples*

	66-1											
	23 °C		51.3 °C		75.2 °C		99 °C		125.4 °C		149.6 °C	
Frequency	ϵ'	$\epsilon''\times10^4$	ϵ'	$\epsilon''\times10^4$	ϵ'	ϵ''	ϵ'	ϵ''	ϵ'	ϵ''	ϵ'	ϵ''
50 c/s	3.570	278.7	3.926	842	7.526	1.969						
100	3.560	327.4	3.900	771	6.961	1.529	20.56	19.04				
200	3.546	346.2	3.873	685	6.487	1.101	16.94	11.77	50.72	100.1		
500	3.522	397.6	3.834	666	5.991	0.8045	13.27	6.49				
1 kc/s	3.505	421	3.800	683	5.728	.6765	11.85	4.30	26.78	29.38	60.32	140.1
2	3.486	458	3.780	714	5.495	.584	10.91	2.96	21.78	18.60	43.62	82.0
5	3.455	499	3.733	795	5.186	.499	9.82	1.95	16.44	9.78	30.55	39.7
10	3.432	514	3.698	841	4.987	.455	9.24	1.60	14.55	6.118	24.82	24.3
20	3.411	516	3.661	865	4.810	.428	8.717	1.47	13.44	4.035	19.31	14.92
50	3.376	541	3.664	919	4.550	.393	7.881	1.34	12.22	2.445	15.89	7.66
100	3.352	566	3.563	948	4.389	.374	7.315	1.34	11.63	1.976	14.51	4.79
310	3.292	570	3.493	902	4.144	.2959	6.516	1.102	10.75	1.496		
1 Mc/s	3.261	612	3.436	901	3.963	.2560	5.558	0.953	9.43	1.603		
3.2	3.211	647	3.374	888	3.743	.2200	4.817	.750	7.79	1.678		
10	3.165	708	3.305	921	3.593	.2041	4.313	.593	6.19	1.505		

	66-2									
	23.5 °C		51.3 °C		61.4 °C		66.0 °C		71.3 °C	
Frequency	ϵ'	$\epsilon''\times10^4$	ϵ'	$\epsilon''\times10^4$	ϵ'	$\epsilon''\times10^4$	ϵ'	$\epsilon''\times10^4$	ϵ'	$\epsilon''\times10^4$
50 c/s	3.641	328	3.956	840	4.538	3120	5.067	5600	5.770	9330
100	3.627	365	3.931	763	4.441	2590	4.892	4560	5.491	7290
200	3.612	372	3.910	716	4.357	2040	4.754	3540	5.265	5570
500	3.587	401	3.874	699	4.249	1670	4.575	2760	4.979	4170
1 kc/s	3.572	438	3.845	709	4.187	1500	4.474	2400	4.826	3510
2	3.549	451	3.817	755	4.130	1430	4.388	2160	4.700	3120
5	3.516	480	3.770	801	4.044	1390	4.262	1990	4.524	2750
10	3.494	496	3.735	827	3.985	1380	4.181	1890	4.416	2580
20	3.473	476	3.700	846	3.928	1350	4.106	1860	4.316	2460
50	3.441	499	3.642	859	3.838	1330	3.985	1790	4.162	2320
100	3.418	529	3.608	885	3.776	1340	3.905	1770	4.065	2260
310	3.293	526	3.481	851	3.635	1240	3.693	1620	3.868	1980
1 Mc/s	3.276	534	3.455	850	3.559	1180	3.625	1440	3.749	1820
3.2	3.259	584	3.404	858	3.491	1120	3.574	1330	3.605	1610
10	3.191	683	3.303	962	3.389	1170	3.438	1300	3.503	1540

	66-2 (Cont.)											
	75.8 °C		80.0 °C		99.8 °C		125.9 °C		150.2 °C		175.2 °C	
Frequency	ϵ'	ϵ''	ϵ'	ϵ''	ϵ'	ϵ''	ϵ'	ϵ''	ϵ'	ϵ''	ϵ'	ϵ''
50 c/s	6.989	1.677	8.497	2.798	22.99	23.76						
100	6.508	1.253	7.698	2.052	18.60	15.29	40.64	168.3				
200	6.137	0.9413	7.122	1.456	15.24	9.962	36.44	89.13				
500	5.694	.6750	6.468	0.997	12.284	5.920	28.73	44.42	44.68	262.62		
1 kc/s	5.461	.5642	6.135	.803	10.828	3.902	23.70	26.40	37.67	138.23		
2	5.270	.4963	5.862	.690	9.857	2.659	19.297	16.61	32.57	74.09	41.35	322.31
5	4.992	.4257	5.477	.577	8.992	1.767	15.199	9.157	26.21	35.81	35.05	135.22
10	4.827	.3862	5.243	.5228	8.461	1.421	13.288	5.692	21.447	21.63	30.86	73.47
20	4.682	.3645	5.042	.4847	7.969	1.250	12.061	3.667	17.647	13.210	26.15	40.71
50	4.459	.3361	4.745	.4399	7.150	1.204	11.082	2.223	14.461	7.053	17.98	18.87
100	4.320	.3193	4.562	.4120	6.535	1.009	10.510	1.756	12.804	4.334	16.80	12.55
310	4.087	.2735	4.245	.3526	6.13	1.030	9.80	1.513	12.15	2.141	13.90	5.295
1 Mc/s	3.909	.2411	4.008	.2968	5.37	0.868	8.63	1.623	11.23	1.572	12.63	2.320
3.2	3.663	.2073	3.779	.2467	4.70	.679	7.41	1.656	10.24	1.704	11.94	1.501
10	3.570	.1839	3.601	.2181	4.18	.522	5.97	1.497	8.87	2.091	11.07	1.726

will be discussed below. In this particular case, we prefer not to alter the data in an arbitrary manner by using an assumed value of the d-c conduction.

3. Discussion of Results

The important features of the dielectric relaxation behavior of the two polyamides examined in this study may be summarized as follows:

(1) Both polymers exhibit a relaxation phenomenon which appears as a loss maximum at temperatures above about 80 °C and at frequencies above 1 kc/s. Some of the data from tables 3 and 4 are plotted in figures 5 and 6. It is seen that the relaxation process is similar in the two materials. This is the same relaxation effect identified as the "α" process by Boyd [1] and studied in detail by him in 66 nylon. It is also the same as that studied by McCall and Anderson [2] in 66 nylon as well as in six other polyamides.

(2) Above about 50 °C, both polymers exhibit a low frequency polarization as manifested by a large dielectric constant and also a large loss. The appearance of this process is clearly shown by some of the data from table 3 for 66 nylon as plotted in figure 7. This phenomenon has been observed and reported previously [1, 2, 3], and is also apparent in figures 5 and 6.

TABLE 3. *Dielectric constants and loss indexes of 66 nylon samples*—Continued

	66-3													
	23 °C		0.3 °C		−25.1 °C		−49.5 °C		−79.6 °C		−98.0 °C		23.2 °C	
Frequency	ϵ'	$\epsilon''\times10^4$	ϵ'	$\epsilon''\times10^4$	ϵ'	$\epsilon''\times10^4$	ϵ'	$\epsilon''\times10^4$	ϵ'	$\epsilon''\times10^4$	ϵ'	$\epsilon''\times10^4$	ϵ'	$\epsilon''\times10^4$
50 c/s	3.554	213	3.508	339	3.421	353	3.337	323	3.235	287	3.162	282	3.535	218
100	3.545	239	3.495	355	3.405	352	3.323	317	3.223	293	3.149	285	3.526	251
200	3.534	275	3.480	380	3.390	357	3.310	328	3.210	311	3.137	285	3.515	291
500	3.515	326	3.456	394	3.367	362	3.289	336	3.190	324	3.118	280	3.496	347
1 kc/s	3.500	360	3.439	408	3.351	363	3.275	348	3.176	335	3.106	266	3.480	375
2	3.484	386	3.422	412	3.336	373	3.260	357	3.162	341	3.095	260	3.463	400
5	3.458	422	3.380	427	3.312	382	3.237	382	3.139	341	3.078	235	3.435	441
10	3.439	435	3.378	437	3.295	397	3.221	396	3.124	330	3.068	211	3.416	453
20	3.420	444	3.360	442	3.278	413	3.204	406	3.110	309	3.059	197	3.396	457
50	3.391	469	3.331	461	3.251	440	3.176	418	3.090	292	3.047	176	3.366	473
100	3.371	484	3.311	481	3.232	461	3.157	415	3.078	269	3.040	158	3.346	489
310	3.364	488	3.302	501	3.227	465	3.138	366	3.062	223	3.048	129	3.324	488
1 Mc/s	3.308	535	3.248	534	3.172	457	3.108	331	3.039	189	3.026	104	3.268	529
3.2	3.265	583	3.205	556	3.136	421	3.078	285	3.032	156	3.013	87	3.238	570
10	3.215	644	3.163	542	3.112	379	3.069	248	3.021	126	3.004	78	3.196	625

	66-4		66-3						66-2			
	23 °C		23 °C		23 °C with .72% H_2O		22.8 °C redried		23 °C		100.6 °C with .69% H_2O	
Frequency	ϵ'	$\epsilon''\times10^4$	ϵ'	$\epsilon''\times10^4$	ϵ'	$\epsilon''\times10^4$	ϵ'	$\epsilon''\times10^4$	ϵ'	$\epsilon''\times10^4$	ϵ'	ϵ''
50 c/s	3.554	213	3.542	214	4.088	1348	3.533	204	3.753	624	----------	----------
100	3.545	239	3.533	257	4.036	1248	3.525	232	3.723	620	----------	----------
200	3.534	275	3.523	278	3.983	1219	3.516	272	3.697	667	----------	----------
500	3.515	326	3.504	330	3.913	1247	3.497	321	3.652	686	----------	----------
1 kc/s	3.500	360	3.489	365	3.856	1265	3.482	348	3.620	706	14.15	7.539
2	3.484	386	3.473	394	3.799	1289	3.467	373	3.589	745	12.26	5.041
5	3.458	422	3.445	431	3.721	1313	3.442	407	3.538	794	10.66	3.027
10	3.439	435	3.426	445	3.661	1316	3.424	417	3.503	804	9.827	2.182
20	3.420	444	3.407	447	3.602	1288	3.406	429	3.467	796	9.188	1.676
50	3.391	469	3.379	464	3.526	1212	3.379	449	3.412	803	8.478	1.410
100	3.371	479	3.359	472	3.471	1145	3.360	468	3.376	763	7.904	1.343
310	3.364	488	----------	----------	3.418	939	3.324	471	3.29	687	7.18	1.282
1 Mc/s	3.308	535	----------	----------	3.337	805	3.273	514	3.25	611	6.21	1.193
3.2	3.265	583	----------	----------	3.276	715	3.232	589	3.20	573	5.26	0.988
10	3.215	584	----------	----------	3.229	628	3.180	719	3.12	569	4.49	.695

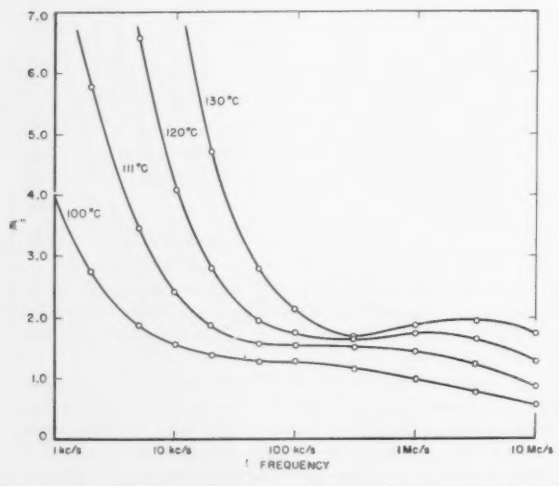

FIGURE 5. *Dielectric loss index of 66 nylon as a function of frequency at high temperatures.*

The high-temperature dipole relaxation process appears as a maximum at the high frequency end.

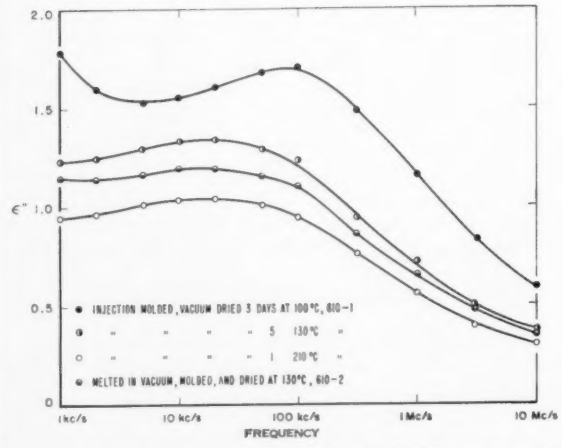

FIGURE 6. *Dielectric loss of 610 nylon at 80 °C as a function of frequency.*

TABLE 3. *Dielectric constants and loss indexes of 66 nylon samples*—Continued

	66-6													
	23 °C not dried		100.5 °C not dried		23 °C vacuum dried		100 °C vacuum dried		111.0 °C vacuum dried		120.3 °C vacuum dried		130.3 °C vacuum dried	
Frequency	ϵ'	$\epsilon''\times10^4$	ϵ'	ϵ''	ϵ'	$\epsilon''\times10^4$	ϵ'	ϵ''	ϵ'	ϵ''	ϵ'	ϵ''	ϵ'	ϵ''
50 c/s	3.650	406			3.600	297								
100	3.628	440	23.779	22.08	3.585	322	19.66	15.95						
200	3.608	499	18.924	14.35	3.571	372	16.02	10.46						
500	3.573	564	14.956	8.273	3.547	407	13.02	6.01						
1 kc/s	3.547	610	13.055	5.598	3.529	430	11.58	3.98	15.69	9.19	20.93	18.35	28.96	36.48
2	3.518	668	11.758	3.817	3.510	465	10.52	2.77	14.11	5.80	17.23	11.66	22.89	22.39
5	3.472	741	10.528	2.410	3.478	495	9.649	1.89	11.96	3.476	14.314	6.587	18.151	12.22
10	3.435	752	9.899	1.891	3.457	510	9.057	1.55	11.12	2.417	12.940	4.090	15.170	7.429
20	3.402	743	9.263	1.617	3.434	529	8.503	1.38	10.45	1.887	12.020	2.814	13.710	4.709
50	3.355	731	8.471	1.477	3.400	548	7.784	1.28	9.671	1.579	11.153	1.950	12.537	2.805
100	3.322	704	7.850	1.457	3.376	571	7.221	1.27	9.060	1.547	10.558	1.748	11.883	2.133
310	3.261	584	6.992	1.329	3.381	566	6.463	1.14	8.138	1.499	9.720	1.624	11.117	1.663
1 Mc/s			5.916	1.151	3.280	621	5.573	0.985	6.917	1.443	8.373	1.728	9.920	1.880
3.2	3.156	737	5.102	.891	3.237	658	4.869	.770	5.82	1.216	6.970	1.643	8.377	1.931
10	3.098	712	4.455	.691	3.160	665	4.326	.566	4.91	0.893	5.633	1.282	6.68	1.737

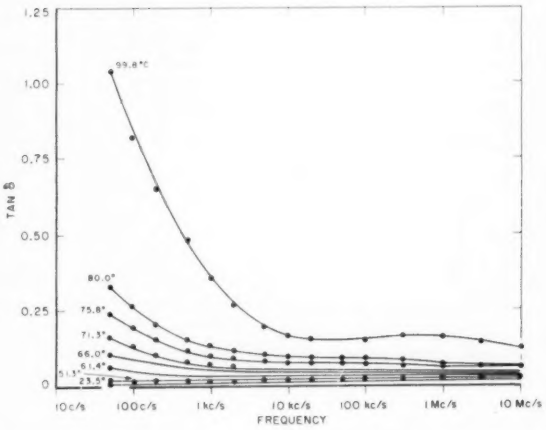

FIGURE 7. *Loss tangent of 66 nylon as a function of frequency.*

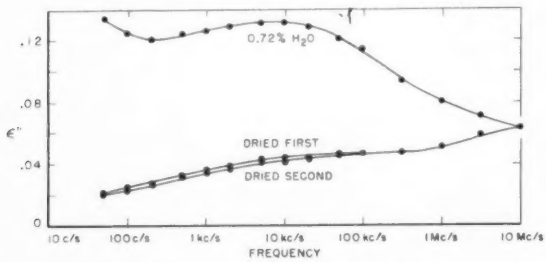

FIGURE 8. *Dielectric loss index of 66 nylon at 23 °C as a function of frequency.*

(3) There is a relaxation process observable at room temperature at about 10 kc/s in both systems. This process virtually disappeared in the case of 66 nylon after prolonged drying. The relaxation process could be made to reappear after absorption of very small quantities of water, and then to disappear again on drying as shown in figure 8. In the case of 610 nylon there was no case in which, even after prolonged drying, this relaxation process was completely removed. Rushton and Russell [13] have reported dielectric measurements that showed the pronounced effect that small amounts of water have on this process is 66 nylon, but in no case did they observe an absence of a maximum in their dielectric loss curves.

(4) There is a dipole relaxation process observed between −100 °C and 0 °C in the frequency range studied here. This process, which has not been previously studied by dielectric methods, is present in both polymers, and is characterized by an energy of activation of about 13 kcal per mole of active dipole. Some of the low temperature data for 66 nylon which exhibit the loss peak due to this process are plotted in figure 9. This relaxation phenomenon is quite probably related to the mechanical relaxation observed in these and other polyamides by Woodward and coworkers [14], Willbourn [15], and Illers and Jenckel [16].

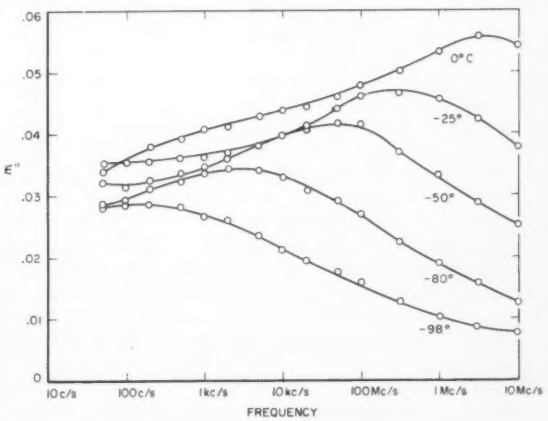

FIGURE 9. *Dielectric loss index of 66 nylon at low temperatures as a function of frequency.*

TABLE 4. *Dielectric constants and loss indexes of 610 nylon samples*

	610-1						After vacuum drying five days at 130 °C				After 1 day vacuum drying at 210 °C	
	23 °C		80.7 °C		100 °C		23 °C		80.1 °C		80.2 °C	
	ϵ'	$\epsilon''\times10^4$	ϵ'	ϵ''	ϵ'	ϵ''	ϵ'	$\epsilon''\times10^4$	ϵ'	ϵ''	ϵ'	ϵ''
Frequency												
50 c/s	3.665	561	16.34	6.780	----------	----------	3.558	526	----------	----------	----------	----------
100	3.640	627	15.05	4.480	----------	----------	3.533	574	----------	----------	----------	----------
200	3.614	683	13.89	3.150	----------	----------	3.509	601	----------	----------	----------	----------
500	3.569	748	12.843	2.180	----------	----------	3.468	654	----------	----------	----------	----------
1 kc/s	3.535	782	12.165	1.780	15.990	4.570	3.438	660	9.786	1.230	8.311	0.950
2	3.501	829	11.543	1.600	14.954	3.070	3.410	687	9.255	1.250	7.885	.970
5	3.448	888	10.749	1.530	14.046	2.030	3.365	685	8.546	1.300	7.307	1.020
10	3.407	895	10.078	1.560	13.498	1.690	3.336	674	7.940	1.331	6.825	1.040
20	3.367	894	9.374	1.610	12.865	1.560	3.306	645	7.321	1.332	6.338	1.050
50	3.308	879	8.392	1.680	12.059	1.640	3.265	641	6.518	1.290	5.702	1.010
100	3.270	844	7.583	1.720	11.330	1.840	3.236	645	5.931	1.240	5.219	0.960
310	3.138	677	6.480	1.490	10.064	2.090	3.163	621	5.221	0.950	4.725	.752
1 Mc/s	3.109	630	5.337	1.170	8.137	2.200	3.104	625	4.563	.730	4.169	.570
3.2	3.094	617	4.562	0.840	6.407	1.840	3.064	650	4.081	.510	3.776	.410
10	3.009	629	4.036	.561	5.142	1.285	3.024	671	3.697	.355	3.510	.284

610-2

	23 °C		80.9 °C		+0.2 °C		−25.3 °C		−50.0 °C		−83.1 °C		−106.2 °C	
	ϵ'	$\epsilon''\times10^4$	ϵ'	ϵ''	ϵ'	$\epsilon''\times10^4$	ϵ'	$\epsilon''\times10^4$	ϵ'	$\epsilon''\times10^4$	ϵ'	$\epsilon''\times10^4$	ϵ'	$\epsilon''\times10^4$
Frequency														
50 c/s	3.324	393	----------	----------	3.311	380	3.212	364	3.119	312	3.031	283	2.943	245
100	3.306	429	----------	----------	3.293	401	3.195	357	3.107	314	3.020	293	2.935	244
200	3.287	450	----------	----------	3.276	419	3.180	363	3.096	324	3.009	289	2.922	240
500	3.257	482	----------	----------	3.247	406	3.157	341	3.079	317	2.991	301	2.913	228
1 kc/s	3.236	495	9.177	1.153	3.229	403	3.143	329	3.067	317	2.978	320	2.903	226
2	3.214	504	8.689	1.149	3.211	400	3.128	326	3.055	317	2.965	316	2.896	206
5	3.180	524	8.035	1.170	3.185	399	3.108	329	3.037	354	2.951	325	2.884	199
10	3.157	514	7.499	1.200	3.169	399	3.093	328	3.024	361	2.934	312	2.877	185
20	3.136	495	6.942	1.200	3.152	390	3.080	328	3.010	374	2.923	285	2.870	161
50	3.102	495	6.207	1.160	3.127	391	3.058	350	2.989	397	2.907	266	2.861	149
100	3.082	496	5.684	1.120	3.111	402	3.043	377	2.972	405	2.893	247	2.856	140
310	3.040	469	5.060	0.870	3.063	413	2.987	382	2.932	351	2.881	181	2.804	110
1 Mc/s	2.978	499	4.420	.667	2.997	446	2.958	413	2.847	318	2.833	145	2.789	76
3.2	2.939	520	4.010	.480	2.983	472	2.954	395	2.925	280	2.833	127	2.785	72
10	2.898	539	3.654	.341	2.949	470	2.880	359	2.832	238	2.807	124	2.763	73

610-7

	After vacuum drying at 210 °C for one day			
	23 °C		79.5 °C	
	ϵ'	$\epsilon''\times10^4$	ϵ'	ϵ''
Frequency				
50 c/s	3.381	399	10.164	1.466
100	3.363	430	9.727	1.210
200	3.344	464	9.288	1.061
500	3.313	478	8.791	0.990
1 kc/s	3.291	488	8.391	.984
2	3.271	505	7.938	.998
5	----------	504	7.367	1.055
10	3.215	497	6.899	1.072
20	3.194	483	6.376	1.074
50	3.163	486	5.738	1.040
100	3.141	478	5.284	0.973
310	3.067	465	4.721	.766
1 Mc/s	3.008	479	4.212	.578
3.2	2.991	510	3.770	.403
10	2.953	581	2.981	.286

Although further investigation will be necessary before an unambiguous explanation in terms of molecular structure for all of these phenomena can be given, it is possible at this time to rule out some possibilities and to suggest others.

3.1. High Temperature Dipole Relaxation Process

The high temperature relaxation process seen in figures 5 and 6 has been extensively studied by Boyd [1] and McCall and Anderson [2], who referred to it as α'. The results presented here are in no way contradictory to their results. The absence of a clear maximum in the loss index at 80 °C, or even 100 °C, in 66 nylon indicates that the samples studied here were more highly ordered than those used by Boyd. He found a crystallinity of 45 percent while the samples used in this work were 57 percent. These values can be compared, since specific volumes and the same crystallinity scale were used in each case.

TABLE 4. *Dielectric constants and loss indexes of 610 nylon samples*—Continued

610–8

	23 °C		0 °C		−26.1 °C		−50.1 °C		−75.6 °C		−100.1 °C		80.5 °C
Frequency	ϵ'	$\epsilon''\times10^4$	ϵ'	$\epsilon''\times10^4$	ϵ'	$\epsilon''\times10^4$	ϵ'	$\epsilon''\times10^4$	ϵ'	$\epsilon''\times10^4$	ϵ'	$\epsilon''\times10^4$	ϵ''
50 c/s	3.429	455	3.254	364	3.189	350	3.120	304	3.048	241	2.972	238	----------
100	3.409	487	3.241	378	3.173	348	3.107	287	3.038	249	2.962	238	----------
200	3.388	504	3.227	394	3.159	346	3.093	280	3.028	252	2.953	238	----------
500	3.355	536	3.205	399	3.136	341	3.076	281	3.011	272	2.938	227	----------
1 kc/s	3.331	543	3.188	395	3.123	323	3.062	283	2.999	282	2.927	222	1.178
2	3.308	546	3.174	390	3.109	317	3.050	286	2.988	285	2.918	221	1.184
5	3.273	559	3.150	398	3.089	324	3.032	312	2.968	304	2.904	209	1.208
10	3.248	549	3.132	392	3.075	320	3.018	319	2.954	297	2.896	188	1.238
20	3.224	529	3.116	381	3.062	320	3.004	329	2.941	285	2.888	169	1.242
50	3.192	535	3.092	393	3.041	349	2.982	356	2.923	276	2.878	155	1.203
100	3.169	535	3.076	393	3.026	365	2.965	359	2.911	257	2.871	139	1.130
310	3.155	503	3.035	393	2.981	374	2.923	332	2.871	221	2.847	119	----------
1 Mc/s	3.054	509	2.987	432	2.941	398	2.840	313	2.824	195	2.815	97	----------
3.2	3.030	523	2.963	474	2.901	391	2.859	286	2.832	171	2.812	85	----------
10	2.986	502	2.937	494	2.886	372	2.837	240	2.821	135	2.821	120	----------

610–9

	23° C		0 °C		−25.3 °C		−50.9 °C		−75.2 °C	
Frequency	ϵ'	$\epsilon''\times10^4$	ϵ'	$\epsilon''\times10^4$	ϵ'	$\epsilon''\times10^4$	ϵ'	$\epsilon''\times10^4$	ϵ'	$\epsilon''\times10^4$
50 c/s	3.507	454	3.345	462	3.229	446	3.133	350	3.050	272
100	3.488	498	3.324	485	3.209	442	3.119	338	3.037	279
200	3.466	537	3.304	493	3.191	425	3.105	329	3.025	287
500	3.429	584	3.271	515	3.165	405	3.085	325	3.006	307
1 kc/s	3.402	620	3.249	509	3.147	385	3.071	326	2.993	315
2	3.376	626	3.226	499	3.131	376	3.057	328	2.979	324
5	3.322	641	3.195	496	3.108	376	3.036	355	2.957	342
10	3.294	644	3.173	475	3.092	372	3.020	370	2.942	338
20	3.267	624	3.154	458	3.077	374	3.004	379	2.927	320
50	3.227	616	3.125	460	3.052	404	2.978	408	2.905	309
100	3.200	610	3.105	461	3.035	428	2.960	411	2.892	275
310	3.130	565	3.054	448	2.989	431	2.904	370	2.846	239
1 Mc/s	3.071	577	2.996	502	2.924	457	2.865	342	2.811	206
3.2	3.029	608	2.957	533	2.885	433	2.832	297	2.791	175
10	2.991	637	2.921	540	2.851	383	2.821	253	2.797	149

The relationship between order, thermal treatment, and the magnitude of the high temperature dipole relaxation process for 610 nylon may be seen by comparison of figure 6, which shows the loss indexes of several specimens of different degrees of order, and figure 3, which shows the X-ray diffraction intensities of the same specimens. The high temperature loss peak is evidently associated with disordered regions. The specific volume data for these specimens also supports this interpretation.

Sandeman and Keller [8] have pointed out the existence of a disordered crystalline phase in these polyamides. If such a structure exists as a separate phase in the polyamides, it would seem likely that a dipole relaxation phenomenon distinct from that for the even more disordered amorphous phase might be observed. The high temperature relaxation process could be associated with such a disordered crystalline phase. Boyd's observation that cross linking by high energy electron irradiation caused a progressive disappearance of this dielectric relaxation process in 66 nylon, with very little effect on the relaxation time, can more readily be understood in terms of such a phase. It is reasonable to suppose that a few cross links in a disordered crystalline region would more effectively prevent chain rotation than in the amorphous phase. Chemical cross linking in amorphous polymers is known in some instances to raise the glass transition temperature [24]. If this relaxation process were related to such a transition, one might have expected a definite lowering of the frequency of the loss maximum at a given temperature due to cross linking. The data presented in this study do not prove or substantiate the hypothesis that the high temperature relaxation is due to a disordered crystalline region; they do indicate that this relaxation process is definitely not associated with the highly ordered regions of these polyamides, in agreement with both Boyd, and McCall and Anderson.

3.2. High Temperature, Low Frequency Polarization

The low frequency polarization process that is evident above about 50 °C in both 610 and 66 nylon (see, for example fig. 7 for 66 nylon) has a number of interesting features. The very high loss indexes observed at lower frequencies in both polyamides above this temperature cannot be entirely accounted for in terms of d-c conduction attributable to a simple ionic mechanism. This is readily shown by simple computation from the measured d-c resistance. For example, for 66 nylon at 100 °C, the contribution to the loss index due to d-c conduction is approximately 4.0 at 100 c/s, while the observed loss indexes for the various specimens listed in table 3 in this frequency range are between 15.29 and 22.08, depending on the amount of annealing and drying. This point is further demonstrated by the tremendous rise in dielectric constants. It is noteworthy that the highest loss index at 100 °C and 100 c/s is observed for specimen 66–6 before drying (22.08) while the lowest value is for 66–2 which had been dried

(15.29). The value for specimen 66–6 closely approached this latter value after drying (15.95).

The high dielectric constants and loss indexes are evidently not simply due to electrode polarization; if this were the case, the values of dielectric constant and loss would be roughly proportional to sample thickness under comparable conditions.[2] The present data, which do show considerable sensitivity to thermal history of the samples show no such trend. Compare for example, the high temperature data in table 3 for samples 66–1 and 66–2 in which the ratio of thickness of 66–1 to 66–2 is 0.926. At about 100 °C and 100 c/s for example, for 66–1 and 66–2, the dielectric constants were 20.56 and 18.60 respectively. In this case the comparison shows, as do the data at room temperature, that 66–2 was more nearly dry than 66–1. This low frequency polarization, then, must be largely a bulk property of these polyamides. Consideration of the dielectric properties of the two types of nonpolymeric substances mentioned below suggest the reasonableness of this conclusion.

Hoffman and Smyth [17] have described measurements of the dielectric properties of long chain, solid alcohols. A number of these compounds exhibit the interesting property of existing over some temperature range in "rotator" phases. In these rotator phases, the molecules exhibit hindered rotation with consequent dipole orientation. The hydroxyl groups in the crystal structure are arranged in sheets and are joined by hydrogen bonds. In the rotator phases, these hydrogen bonds occasionally break and reform to allow molecular orientation. The dielectric constants and losses were unusually high for these materials, and both quantities increased by as much as a factor of four in passing from the liquid to the rotator solid. These losses were interpreted in terms of a large proton drift mobility in the sheets of hydroxyls in the disordered rotator phase. The high dielectric constant was evidently a result of polarization due to a bound anion together with cation (proton) mobility.

Leader and Gormley [18, 19] have reported measurements of a number of amides and *N*-substituted amides in the liquid state. They observed exceedingly high dielectric constants for the *N*-monosubstituted amides: *N*-methylformamide had a dielectric constant of 182.4 at 25 °C while that of *N*-methylproprionamide was 172.2 at the same temperature. They observed that unsubstituted amides had lower dielectric constants, 110 for formamide and 74 for acetamide. The disubstituted amides had much lower dielectric constants: 36.71 for *N*, *N*-dimethylformamide and 37.78 for *N*, *N*-dimethylacetamide. It is clear that the polyamides under consideration have structures analogous to those of the monosubstituted amides. It might be expected, therefore, that in the liquid state, the amide groups of polyamides might associate into orientable structures of high dipole moment due to hydrogen bonding similar to those proposed by Leader and Gormley for the monosubstituted amides.

These hypotheses suggested a number of further experiments on the nature of the low frequency polarization mechanism, two of which will be briefly described here. It was thought that a slow relaxation process such as this might be "frozen in" at sufficiently low temperatures, resulting in a very slowly decaying polarization. In effect, it was thought that polyamides should make unusually strong electrets. The classical electret forming treatment was given to some samples: the sample disk was heated up to about 125 °C and a d-c electric field applied. Then, while maintaining the field, the sample was slowly cooled. Strong electrets were formed in this manner with both 66 and 610 nylon, and the electric field remained for many months when stored at room temperature. On reheating above about 80 °C, a small current could be withdrawn from the specimen over a period of hours, and resulted in the disappearance of the electret field.

It was only after these observations had been made that it was found that Wieder and Kaufman [20] had noted the strong electret forming properties of nylon some years previously.

It is also interesting to note that when a d-c field was applied at elevated temperatures to a specimen on which evaporated gold electrodes had been formed that, although the side towards the positive electrode appeared unchanged, the gold on the side toward the negative electrode was loose and readily flaked off. This phenomenon might well be due to the formation of hydrogen gas due to the electrolysis of the current carrying protons.

3.3. Water-Sensitive, Room Temperature Process

The relaxation process observed at about 10 kc/s at room temperature is clearly very sensitive to moisture. In figure 8, it is evident that, at least for 66 nylon, it is possible to remove enough of the water to cause the relaxation process to be almost completely absent. In the case of the 610 nylon, there was a maximum in the loss index curve for all specimens studied. However, careful drying greatly reduced the magnitude of the maximum in this case also.

It is noteworthy that although exposure of a dried specimen to moisture caused a reappearance of the maximum in 66 nylon, such exposure did not alter the appearance of the high temperature α' process in these highly crystalline specimens. (In table 3 there was no loss maximum in sample 66–2 containing 0.69 percent water at 100 °C although the losses are generally higher than in comparable dry samples. This overall increase in loss is in agreement with the already noted effects of moisture on the low frequency, high temperature polarization process.) Thus, since the measurements of Rushton

[2] This is so because electrode polarization would introduce a polarization confined to the immediate area of the electrodes, independent of sample thickness. If this effect were pronounced, it would outweigh the effect of bulk polarization. Thus the measured dielectric constant would equal some capacitance caused by electrode polarization divided by the equivalent vacuum capacitance of the volume occupied by the sample: $\epsilon' = C_p/C_v$. The capacitance, due to electrode polarization, C_p, would be independent of sample thickness; the equivalent vacuum capacitance, C_v, is inversely proportional to sample thickness. Therefore, if pronounced electrode polarization occurs, the measured dielectric constant should tend to be proportional to thickness.

and Russell [13] and of Boyd [1] indicate a loss maximum at room temperature in their driest samples, it seems doubtful that all water had been removed.

The strong hydrogen bonding character of the amide groups in these polymers makes understandable their tenacious absorption of water. This effect is aggravated by the nature of the mechanism of forming these polymers, which results in formation of water as a by-product, and the fact that water-forming end groups (amine and carboxyl groups), remain after polymerization to a finite molecular weight. Thus, chemical equilibrium predicts the presence of small quantities of water which are inversely proportional to the molecular weight of the polyamide. The intrinsic viscosity results indicate that the most severe drying conditions have resulted in a shift of the equilibrium to higher molecular weight and, of course, the removal of some water. However, the fact that this dielectric relaxation process is not due to the end groups themselves but is due to water associated with the polymer, is shown by the fact that it may be made to reappear immediately on absorption of small amounts of water. Hydrolysis to reform end groups under the conditions used for these experiments is very improbable.

The fact that the relaxation process under consideration appeared in all the 610 nylon specimens apparently indicates that none of these were as dry as the 66 nylon. It is also significant that the highest intrinsic viscosity ($[\eta]=1.33$) observed for any of the 610 nylon specimens was significantly lower than that for any of the 66 nylon specimens used in dielectric measurements ($[\eta]=1.69$). Comparison of intrinsic viscosities of different polymers cannot be absolutely quantitative where other information is lacking, but in this case, where the chemical structures are so closely similar, it seems safe to say that the molecular weights of the 610 samples were lower in all instances than the 66 samples used for dielectric measurements.

If one makes certain simple assumptions, it is possible to compute the amount of dispersion in the dielectric constant to be expected from a given quantity of water. Assuming that the water absorbed in the nylon has the same polarizability as in the pure state, for which a dielectric constant of 78 is generally quoted at room temperature (21), then one might expect 0.72 percent of water to increase the low frequency dielectric constant by about 0.56. The data in table 3 for specimen 66–3 shows a difference in the dielectric constant of about 0.54 with and without this amount of water at 50 c/s. The difference in the dispersion of the dielectric constants in the frequency range studied, namely 50 c/s to 10 Mc/s, is 0.506 for the specimen with water and after drying. These figures demonstrate the reasonableness of the proposal that this relaxation process is due to the water-polymer complex. (Pure water shows dielectric dispersion in the microwave region at this temperature.)

This water-sensitive dispersion region is almost certainly closely related to the so called β process observed in mechanical measurements of polamides [14, 16], as noted earlier. Some of the mechanical data of Illers and Jenckel [16] are shown in figure 10, together with one dielectric point. In this plot of frequency of loss maximum against reciprocal of absolute temperature, it is evident that there is a correspondence between the mechanical β process and the room temperature dielectric loss maximum. It is evident from the dielectric and mechanical measurements that the relaxation process is characteristic of the water-polyamide complex and not of the pure polymer. The opinion has been expressed that a small quantity of swelling agent, such as water in this case, does not result in a new relaxation process but rather modifies processes characteristic of the pure polymer. In this case, such a view is not substantiated, and it is worth pointing out that Scheiber and Mead [22] have reported a similar situation with respect to the effect of water on dielectric dispersion in poly(methyl methacrylate).

3.4. Low Temperature Relaxation Process

The low temperature relaxation process observed in these data, as plotted in figure 9, is evidently related to the mechanical relaxation process observed in the same temperature region [14, 16]. The plot of the frequency of the maximum loss versus reciprocal of absolute temperature for the 66 nylon data is shown at the right-hand side of figure 10. The activation energy is 13 kcal/mole. Also included in this figure are some of the mechanical relaxation data of Illers and Jenckel, together with those of Woodward and coworkers, on what they have called the γ process. It is evident that the dielectric data do not exactly match the mechanical data, the latter having an activation energy of 9 kcal/mole. Further, the displacement of the two sets of data indicate a difference in entropy of activation. To understand these differences, it is first necessary to decide what molecular motions are responsible for this process.

The mechanical relaxation process has been widely attributed to motions of the hydrocarbon portions of the polymer chains. Various arguments have been proposed to support this hypothesis [15]. The present results indicating the existence of a dipolar

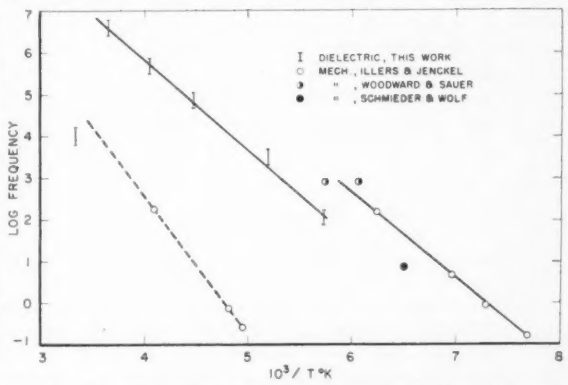

FIGURE 10. *Frequency of loss maximum of 66 nylon as a function of reciprocal temperature.*

Water or β process indicated by dashed line, low temperature process by solid line.

relaxation process necessitate some modification of this view. The difference in entropy of activation as well as the slightly higher energy of activation for the dielectric process suggest a possible mechanism. It seems reasonable that motions of the hydrocarbon segments might be accompanied by motions of the polar amide groups. Because of intermolecular hydrogen bonding, however, such combined motions would be less likely and would also involve a somewhat higher activation energy to break hydrogen bonds. A different entropy for the activated complex would be expected in the two cases. Thus, while the mechanical measurements undoubtedly "see" the relaxation of polar groups to some extent, the much more active motions of the hydrocarbon segments overshadow the process observed in the dielectric measurements.

The hypothesis that this relaxation process is due to motions of molecular end groups can be almost eliminated on the basis of two arguments. First, if such a mechanism were involved, the dielectric and mechanical relaxation processes should coincide at any given temperature and frequency, which is not the case. Second, the magnitude of the polarization associated with this process is not inversely proportional to molecular weight, at least within the limited range covered in the nylon 610 data presented here. However, it is difficult to separate effects of crystallinity and molecular weight. Therefore, the latter argument is not proven, and further work is in progress with other polyamide specimens covering a wider range of molecular weights. It should be pointed out that it is not a simple matter to relate the magnitude of the polarization with the known type and number of polar end groups since in this hydrogen bonded material, the relationship between dipole moment and polarizability cannot be predicted with sufficient accuracy.

4. Conclusions

Four relaxation phenomena have been identified in 610 and 66 nylon: (1) Above about 80 °C a dipolar relaxation process is apparent in both polymers. The earlier suggestion that this process does not occur in highly ordered regions is confirmed by comparison of dielectric, specific volume, and X-ray diffraction data. (2) There is a very-low-frequency polarization characterized by an extremely high loss index and dielectric constant above about 60 °C in both polyamides. This process, also observed by previous authors, is undoubtedly due to motions of amide group hydrogens involved in intermolecular hydrogen bonds. This process has been found to give rise to electret formation in these polyamides. (3) There is a relaxation process observed at room temperature at about 10 kc/s. This is evidently a result of the presence of water and, in one case, was almost completely absent after prolonged drying. This process has been shown to be the dielectric manifestation of the "β process" observed in dynamic mechanical measurements. (4) There is a low temperature relaxation process closely related to the "γ process" observed in mechanical measurements. This process, observed in both polyamides, necessarily involves dipolar motions and probably requires modification of the proposal that the "γ process" involves only motions of the hydrocarbon segments in these polymers.

The author is grateful to William P. Harris, who carried out many of the measurements on 66 nylon, and to Benjamin Furst, who carried out the X-ray diffraction measurements.

5. References

[1] R. H. Boyd, J. Chem. Phys. **30,** 1276, (1959).

[2] D. M. McCall and E. W. Anderson, J. Chem. Phys. **32,** 237 (1960).

[3] W. O. Baker and W. A. Yager, J. Amer. Chem. Soc. **64,** 2171 (1942).

[4] C. W. Bunn and E. V. Garner, Proc. Roy. Soc. (London) **A189,** 39 (1947).

[5] W. P. Slichter, J. Poly. Sci. **25,** 77 (1958).

[6] G. F. Schmidt and H. A. Stuart, Z. Naturforsch. **13,** 222 (1958).

[7] P. W. Allen, Research (London) **5,** 492 (1952).

[8] I. Sandeman and A. Keller, J. Poly. Sci. **19,** 401 (1956).

[9] A. H. Scott, D. J. Scheiber, A. J. Curtis, J. D. Hoffman, and J. I. Lauritzen, Jr., J. Research NBS, to be published.

[10] J. D. Hoffman and J. J. Weeks, J. Research NBS **60,** 465 (1958).

[11] H. W. Starkweather and R. E. Moynihan, J. Poly. Sci. **22,** 363 (1956).

[12] P. J. Flory, J. Amer. Chem. Soc. **58,** 1884 (1936).

[13] E. Rushton and G. Russell, Brit. Elect. and Allied Indust. Research Assoc. Report L/T 355.

[14] A. E. Woodward, J. A. Sauer, C. W. Deeley and D. E. Kline, J. Coll. Sci. **12,** 363 (1957).

[15] A. E. Willbourn, Trans. Faraday Soc. **54,** 717 (1958).

[16] K. H. Illers and E. Jenckel, I.U.P.A.C. Kurzmitteilungen, Sec. 1: Physik Makromolekular Stoffe, Verlag Chemie, GmbH, Weinheim, (1959), K. H. Illers, Makromoel. Chem. **38,** 168, (1960), and K. H. Illers, private communication.

[17] J. D. Hoffman and C. P. Smyth, J. Amer. Chem. Soc. **71,** 431 (1949).

[18] G. R. Leader and J. F. Gormley, J. Amer. Chem. Soc. **73,** 5731 (1951).

[19] G. R. Leader, J. Amer. Chem. Soc. **73,** 856 (1951).

[20] H. H. Wieder and S. Kaufman, J. Appl. Phys. **24,** 156 (1953).

[21] C. P. Smyth, Dielectric Behavior and Structure, p. 86, (McGraw-Hill, New York, N.Y., 1955).

[22] D. J. Scheiber and D. J. Mead, J. Chem. Phys. **27,** 326 (1957).

[23] A. H. Scott, private communication.

[24] E. B. Baker, P. Auty, and G. J. Ritenour, J. Chem. Phys. **21,** 159 (1953).

(Paper 65A3–101)

JOURNAL OF RESEARCH of the National Bureau of Standards—A. Physics and Chemistry
Vol. 65A, No. 3, May–June 1961

Heat of Formation of Calcium Aluminate Monocarbonate at 25 °C

H. A. Berman and E. S. Newman

(January 14, 1961)

The heat of formation of $3CaO{\cdot}Al_2O_3{\cdot}CaCO_3{\cdot}10.68H_2O$ at 25 °C was determined by the heat-of-solution method, with 2*N* HCl as the solvent and $3CaO{\cdot}Al_2O_3{\cdot}6H_2O$ and $CaCO_3$ as the reactants. The heat of solution of $CaCO_3$, to form dissolved CO_2, was obtained by a new technique and a modified calculation which served to include the heat of vaporization of the gas escaping in the reaction and resulted in a higher value than those obtained by Wells and Taylor and by Bäckström in determinations representing only partial solution of CO_2. The results obtained were:

	kj/mole	*kcal/mole*
$3CaO{\cdot}Al_2O_3{\cdot}CaCO_3{\cdot}10.68H_2O$		
Heat of formation		
from elements, ΔH_f°		−1956
from reactants and H_2O		−18.9
Heat of solution in 2*N* HCl	−532.9	−127.4
$3CaO{\cdot}Al_2O_3{\cdot}6H_2O$		
Heat of solution in 2*N* HCl	−576.6	−137.8
$CaCO_3$		
Heat of solution in 2*N* HCl	−35.0	−8.4

1. Introduction

Hydrated calcium aluminate monocarbonate, $3CaO{\cdot}Al_2O_3{\cdot}CaCO_3{\cdot}11H_2O$, is one member of a series of complex salts represented by the general formula $3CaO{\cdot}Al_2O_3{\cdot}CaX{\cdot}nH_2O$, in which *X* is a divalent anion or two units of a monovalent anion, and *n* is 10 to 12. Turriziani and Schippa [1] [1] have observed and identified the monocarbonate in a film which formed on the surface of water in which cubes of aluminous cement paste were stored. The limited possibility of its formation in setting mortar and concrete is indicated by its stability only at CO_2 pressures below the partial pressure of CO_2 in air [2]. It has nevertheless been observed in test borings from portland cement concrete road surfaces [3].

As part of a continuing investigation of the thermochemical properties of substances occurring in hydraulic cements and their reaction products, the heat of formation of hydrated calcium aluminate monocarbonate has been determined.

It should be noted that the formula $3CaO{\cdot}Al_2O_3{\cdot}CaCO_3{\cdot}11H_2O$ is an idealized formula in which the number of moles of H_2O has been rounded off. This compound, as with many similar compounds encountered in portland cement chemistry, does not always have a definite water content. The actual water content in the samples prepared varied from 10.58 to 10.88. The average figure of $10.68H_2O$ was used in the calculations.

Measurements were made of the heat evolved at 25 °C in the reaction

$$3CaO{\cdot}Al_2O_3{\cdot}6H_2O + CaCO_3 + 4.68H_2O \xrightarrow{\Delta H_1} 3CaO{\cdot}Al_2O_3{\cdot}CaCO_3{\cdot}10.68H_2O \quad (1)$$

The heat of this reaction is the difference between the sum of the heats of solution of the reactants and the heat of solution of the product, in accordance with the following equations:

$$3CaO{\cdot}Al_2O_3{\cdot}6H_2O + 12HCl \xrightarrow{\Delta H_2} [3CaCl_2 + 2AlCl_3 + 12H_2O] \quad (2)$$

[1] Figures in brackets refer to the literature references at the end of this paper.

$$CaCO_3+[3CaCl_2+2AlCl_3+12H_2O]+2HCl \xrightarrow{\Delta H_3} [4CaCl_2+2AlCl_3+13H_2O]+CO_2 \quad (3)$$

$$[4CaCl_2+2AlCl_3+13H_2O]+4.68H_2O \xrightarrow{\Delta H_4} [4CaCl_2+2AlCl_3+17.68H_2O] \quad (4)$$

$$[4CaCl_2+2AlCl_3+17.68H_2O]+CO_2 \xleftarrow{\Delta H_5} 3CaO\cdot Al_2O_3\cdot CaCO_3\cdot 10.68H_2O+14HCl \quad (5)$$

Summation:

$$3CaO\cdot Al_2O_3\cdot 6H_2O+CaCO_3+4.68H_2O \xrightarrow{\Delta H_1} 3CaO\cdot Al_2O_3\cdot CaCO_3\cdot 10.68H_2O \quad (1)$$

$$\Delta H_1=\Delta H_2+\Delta H_3+\Delta H_4+\Delta H_5$$

The heat of solution of each of the reactants and of the product of this reaction was measured in $HCl\cdot 26.61H_2O$ (2.00*N* HCl at 25 °C). The heats of formation of the reactants were taken from Circular 500 [4] of the National Bureau of Standards.

All calculations in this paper are based on the 1957 atomic weight table, and on the thermochemical calorie, defined as exactly 4.184 absolute joules.

2. Materials, Apparatus, and Procedure

2.1. Preparation of $3CaO\cdot Al_2O_3\cdot CaCO_3\cdot 11H_2O$

Three samples, two of which closely approached the stoichiometric composition $3CaO\cdot Al_2O_3\cdot CaCO_3\cdot 11H_2O$, were prepared and studied. Their properties and details of their preparation are listed in table 1. They were obtained by mixing solutions of calcium aluminate, calcium hydroxide (prepared from reagent calcium carbonate), and reagent sodium carbonate, according to the method of Turriziani and Schippa [1]. The calcium aluminate solution was prepared by shaking aluminous cement with distilled water for periods up to 3 hr. The solution, containing up to 2.0 g Al_2O_3 and 1.2 g CaO per liter, is metastable and becomes cloudy soon after its maximum concentration is reached. It was filtered quickly and the filtrate used immediately to prepare the monocarbonate compound. A sample of the filtrate was taken at the same time to determine the concentration of CaO and Al_2O_3. Eight to nine liters of saturated $Ca(OH)_2$ solution were added to 2 liters of the calcium aluminate solution, the mixture stirred a few seconds, after which 3.50 to 3.75 g Na_2CO_3 in 250 ml of water was added slowly with continued stirring. After the mixture had been allowed to stand about 2 months, the precipitate was filtered off and dried over saturated $MgCl_2$ solution (33% relative humidity) until the ignition loss was constant (requiring about 2 months).

Precautions were taken to exclude atmospheric CO_2 during every step of the process including preparation of the reagents, mixing, filtration, and drying. These precautions are described in another publication [5].

X-ray diffraction patterns of the samples were obtained by the powder method on a Geiger-counter diffractometer with copper Kα radiation. The patterns, one of which has been published [2], agree closely with the original pattern of Turriziani and Schippa [1].

The oxide composition of the samples was obtained by chemical analysis. The designation and calculation of the amounts of compounds present as impurities was based on the chemical analysis and optical microscopic examination.

2.2. Preparation of Hydrated Tricalcium Aluminate

Tricalcium aluminate hydrate, $3CaO\cdot Al_2O_3\cdot 6H_2O$, was prepared by autoclaving $3CaO\cdot Al_2O_3$ at 150 °C for several days, according to the method of Thorvaldson, Brown, and Peaker [6]. The hydrated aluminate was dried over potassium hydroxide. Chemical analysis gave the composition $3CaO\cdot Al_2O_3\cdot 5.859H_2O$ (plus 0.007 mole $CaCO_3$ per mole as impurity). The anhydrous aluminate had been prepared by repeated heating of lime and alumina with intervening moistening of the material to aid in dispersing the CaO, as described by the same authors.

2.3. Preparation of the Calcium Carbonate

Low-alkali reagent calcium carbonate was used. The reagent was moistened with 3 percent of its weight of distilled water, pelleted at 4,000 psi, and dried at 110 °C to constant weight. This treatment served to agglomerate the fine particles and decrease (but not completely eliminate) the tendency of the $CaCO_3$ to adhere to the glass funnel through which samples were normally introduced into the calorimeter.

The $CaCO_3$ was largely calcite. Since the difference between the heats of formation of calcite and aragonite [4] is smaller than the reproducibility of the calorimetric measurements, the presence of aragonite in the $CaCO_3$ would have no effect on the results of the heat-of-solution determinations.

2.4. Heat-of-Solution Measurements

The heats of solution of the compounds were determined in $HCl{\cdot}26.61_4H_2O$ (2.00*N* HCl at 25 °C). A precision calorimeter, described by Newman [7], was used for determinations on all the materials except the $CaCO_3$. For this compound an improved calorimeter was used, which is shown in figure 1. The major advantage of the newer calorimeter is its one-piece design, except for the stirring tube and stirrer (A) which fit over and close a 1.5-in. diam opening (B) in the upper surface. Two stirrers can be used, a 4-in. stirrer with a 4-blade propeller, and a 6¼-in. stirrer (shown with dashed line in the figure) with an additional 2-blade propeller at the end. The 4-in., single-propeller, stirrer was used for the heat of solution of $CaCO_3$. Thermal equilibrium in the calorimeter is reached much sooner than in the older design, which featured a heavy cover and large temperature lags. The sample is introduced through opening

TABLE 1. *Preparations of* $3CaO{\cdot}Al_2O_3{\cdot}CaCO_3{\cdot}nH_2O$

Sample	1	2	3
Original concentration of mixture:			
CaO, g/liter	1.129	1.158	1.473
Al_2O_3, g/liter	0.358	0.355	0.370
Na_2CO_3, g/liter	.342	.337	.386
Molar ratio:			
$CaO:Al_2O_3$	5.74	5.93	7.72
$CO_2:Al_2O_3$	0.92	0.91	1.00
Final concentration of solution:			
CaO, g/liter	.387	.414	0.653
Al_2O_3, g/liter	.007	.008	.001
Composition of product:			
Weight percent [a]			
CaO	40.19	39.66	40.38
Al_2O_3	18.04	18.22	17.78
CO_2	7.95	7.74	8.56
H_2O	33.82	34.38	33.28
Molar ratio:			
$CaO:Al_2O_3$	4.05	3.96	4.13
$CO_2:Al_2O_3$	1.02	0.98	1.12
$H_2O:Al_2O_3$	10.61	10.68	10.59
Molar ratios of compounds present to Al_2O_3:			
$3CaO{\cdot}Al_2O_3{\cdot}CaCO_3{\cdot}nH_2O$	1.00	0.96	1.00
where $n=$	10.58	10.88	10.58
$CaCO_3$	0.02		0.12
$3CaO{\cdot}Al_2O_3{\cdot}6H_2O$		0.04	
$Ca(OH)_2$	.03		.01
CO_2		.02	
Heat of solution of the sample:			
$-\Delta H$ (from table 4), cal/g	226.07	229.25	224.74
Standard deviation of average	0.21	0.54	0.18
Corrected Heat of Solution of the			
$3CaO{\cdot}Al_2O_3{\cdot}CaCO_3{\cdot}nH_2O$, $-\Delta H$, cal/g	225.75	225.86	227.48
kcal/mole	126.62	127.89	127.59

[a] The CaO/Al_2O_3 ratios were determined on wet samples, and the CO_2 and H_2O were determined on samples conditioned over saturated $MgCl_2$ solution. For this reason, the analyses total exactly 100 percent.

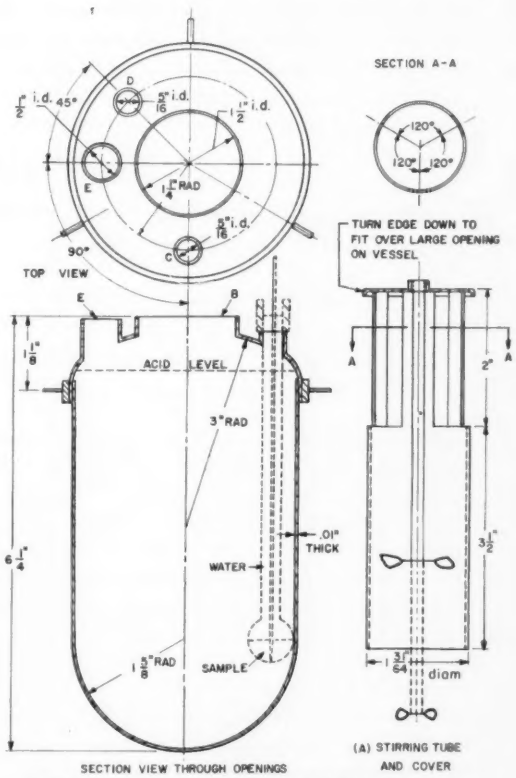

FIGURE 1. *Improved heat-of-solution calorimeter.*
The glass bulb shown with dashed lines was used for determinations of the heat of solution of $CaCO_3$. Opening C normally contains a funnel instead of a glass bulb.

C, either by means of a funnel or in a glass bulb as indicated by the dashed lines in the drawing. The glass bulb was used with $CaCO_3$, as described in section 2.5. The entire calorimeter assembly, except for the bulb or funnel and for the outer supporting ring, is made of platinum. The calorimeter otherwise is similar to the earlier design. Opening D is fitted with an electric heater for calibration purposes and for setting the initial temperature range, and opening E contains the resistance thermometer. The calorimeter is placed inside an air jacket and the jacket-calorimeter assembly is submerged in a constant-temperature water bath controlled to ± 0.005 °C.

Since it was inconvenient to prepare the calcium aluminate monocarbonate in large quantities, 1–g samples of the compound were used with the normal quantity of acid (600 g) for the older calorimeter. With the newer calorimeter, 0.2–g samples of $CaCO_3$ were used with 740 g of acid (corresponding to 0.18 g in 600 g acid), and 0.7 g of hydrated tricalcium aluminate was added to the acid before the addition of $CaCO_3$. These quantities are required by the stoichiometry of eqs (1) and (3).

In the determination of the heat of solution of $3CaO{\cdot}Al_2O_3{\cdot}6H_2O$, the sample size was 0.2 to 0.4 g. These determinations had been made previously to calculate the heat of formation of calcium aluminate trisulfate (calcium trisulfoaluminate) [5]. In accordance with eq (1), the proper sample size should be 0.67 g. However, the value obtained for the smaller samples (370.4 cal/g) is not inconsistent with values obtained by Thorvaldson, Brown, and Peaker [6] from determinations in which 2.9–g samples were used. When their results are adjusted to allow for the use of $HCl{\cdot}26.6H_2O$ instead of $HCl{\cdot}20H_2O$, thermochemical calories (4.1840 abs j/cal) instead of 20° calories (4.181 abs j/cal), and a final temperature of 25 °C instead of 20°, the result is 373.1 cal/g. The difference, 2.7 cal/g, or 1.0 kcal/mole, is in the wrong direction to be attributed to differences in sample size. There is thus no measurable dilution effect due to variations in sample size. The value obtained with the smaller samples was therefore used.

The heat effect of adding the 4.68 moles of water appearing in eqs (1) and (4) was estimated as the partial molal heat content of water in $2N$ HCl [4], neglecting the contribution of the small amounts of other solutes present.

2.5. Heat of Solution of the $CaCO_3$

The determination of the heat of solution of $CaCO_3$ presents problems because of the evolution of CO_2 when the sample is dissolved in acid. Two reactions take place:

$$CaCO_3\ (c) + 2HCl\ (aq) \xrightarrow[\text{(exothermic)}]{} CaCl_2\ (aq) + H_2O\ (l) + CO_2\ (aq) \qquad (6)$$

$$CO_2\ (aq) \xrightarrow[\text{(endothermic)}]{} CO_2\ (g) \qquad (7)$$

The problem is twofold: (a) the evolution of CO_2 from solution is endothermic; an uncertain amount of heat is lost depending on how much CO_2 escapes. (b) The CO_2 gas carries with it some of the sensible heat produced by equation (6) if it is not in complete thermal equilibrium with the solution before it is evolved. The sensible and latent heat of water vapor in the CO_2 gas is lost as well. All these effects produce low results for the heat of solution and an inaccurate final rating period for the calculation of thermal leakage.

Various investigators have attacked the first difficulty by determining the heat of solution of $CaCO_3$ both in HCl saturated with CO_2 and in HCl not saturated with CO_2. A smaller heat of solution is obtained in the first solvent because all the CO_2 escapes. The second solvent retains some of the CO_2 and gives a larger value. Working with 1.5-g samples in 640 g of CO_2-saturated $2N$ HCl, Wells and Taylor [8] obtained $-\Delta H = 59.2$ cal/g CaO or 33.2 cal/g $CaCO_3$ (3.32 kcal/mole) at 25 °C. Working with 10-g samples in 800 g of CO_2-saturated N HCl at the same temperature, Bäckström obtained 3.26 kcal/mole [9, 10].

The agreement between these two investigators was not as good when the HCl was not saturated with CO_2, principally because the sample and acid weights were different, resulting

in different ratios of CO_2 dissolved in the acid to CO_2 escaping from the calorimeter in each case. Wells and Taylor, using $2N$ HCl at 25 °C and the same relative weights as for CO_2-saturated HCl, obtained a heat of solution of $-\Delta H = 105.0$ cal/g CaO or 58.9 cal/g $CaCO_3$ (5.89 kcal/mole). Bäckström, using N HCl at 25 °C and the same relative weights he had used before, obtained 4.50 kcal/mole.

The heats of solution of the aluminate monocarbonate and of the tricalcium aluminate had been determined in $2N$ HCl not saturated with CO_2. It was therefore necessary to determine the heat of solution of the $CaCO_3$ in the same acid and to adopt a sample size that would result in the same concentration of CO_2 as for the aluminate carbonate. A $CaCO_3$ sample of 0.2 g does not release enough CO_2 to saturate 740 g of $2N$ HCl at 25 °C. (The solubility of CO_2 in $2N$ HCl at 25 °C is 0.8 g/liter CO_2 in the liquid for each g/liter in the gas phase or 1.6 g/liter at 760 mm pressure [11].) Therefore, it should be expected that all the CO_2 would dissolve, thus producing the maximum heat of solution, that is, the heat effect of eq (6). However, CO_2 determinations made on the calorimeter acid before and after the calorimetric determinations showed that only about two-thirds of the available CO_2 dissolved completely even though saturation was not attainable. Presumably this is due to the fact that chemical equilibrium was not established owing to the rapid solution of the sample.

It is difficult to introduce powdered $CaCO_3$ into a calorimeter through a funnel because it adheres to the glass and forms lumps at the bottom of the funnel stem, even after the pressure treatment described in section 2.3. It was therefore introduced in a glass bulb (see fig. 1) placed in the acid before assembling the calorimeter. After an initial rating period to determine the stirring energy of the calorimeter, the bulb was broken by a glass rod actuated by a 10-g weight falling through a distance of 69 cm. The temperature of the calorimeter was read at 1-min intervals until the rise was steady, then at 2-min intervals for a total of about 1 hr. Corrections were made to the observed temperature rises by subtracting the stirring energy and the thermal leakage between the bath and the calorimeter. The thermal-leakage constant had been determined previously in the calorimeter calibration.

The corrected rises obtained in this manner for a typical calorimeter run are plotted against time (open circles) in figure 2. The corrected temperature rise for $CaCO_3$ increases rapidly at the start and reaches a maximum (about 95% of the rise occurs in the first half-minute). It then falls as CO_2 is evolved, approaching a constant value. A first-order decay law

$$d\theta/dt = -c(\theta - \theta_f) \tag{8}$$

fits the descending curve quite well; θ represents the corrected temperature rise at any time t, θ_f the final temperature rise. From this relationship it is possible to calculate θ_0, the corrected temperature rise at zero time when no CO_2 has escaped. This rise, multiplied by the heat capacity of the calorimeter, is taken as the true heat of solution of $CaCO_3$ in $2N$ HCl in accordance with eq (6).

The tendency of sensible heat to escape with the CO_2 was reduced by covering the sample of $CaCO_3$ in the bulb with a few milliliters of distilled water. Any bubbles rising in the bulb stem give up their sensible heat to the water. At the same time, the water pushes the sample directly into the calorimeter acid, causing most of the bubbles to escape through the acid surrounding the bulb. Thermal equilibrium is thereby facilitated. Blank runs were made to determine the energy of dilution of the acid with the small quantity of water. Figure 2 (closed circles) shows the corrected rise for the blank run plotted against the time after introduction of the sample.

3. Results and Discussion

3.1. Heats of Solution of the Preparations

The heats of solution obtained on the preparations of calcium aluminate monocarbonate were corrected for the small quantities of impurities present. The heats of solution of the preparations and the corrected heats of solution of the pure monocarbonates themselves are summarized in table 1.

The heats of solution of the reactants, $3CaO \cdot Al_2O_3 \cdot 5.859H_2O$ and $CaCO_3$, are shown in table 2.

The heat capacities obtained in the calorimeter calibrations are listed in tables 3 (a and b). Additional data from the heat-of-solution determinations are shown in table 4 and 5.

TABLE 2. *Reactants*

	$3CaO \cdot Al_2O_3 \cdot 6H_2O$	$CaCO_3$
Composition		
Weight percent:		
CaO	44.52	56.00
Al_2O_3	26.93	
CO_2	0.11	43.93
H_2O	27.88	
Molar ratio:		
$CaO:Al_2O_3$	3.007	
$CO_2:Al_2O_3$	0.009	
$H_2O:Al_2O_3$	5.859	
$CaO:CO_2$		1.00
Molar ratios of compounds:		
$3CaO \cdot Al_2O_3 \cdot 5.859H_2O$	1.000	
$CaCO_3$	0.007	
CO_2	.002	
Heat of solution of the materials (from tables 4 and 5)		
$-\Delta H$ cal/g	369.73±0.33	83.61±0.51
Corrected heat of solution of the reactant		
$-\Delta H$ cal/g	$370.35_1 \pm 0.33$	83.61±0.51
kcal/mole	$139.16_3 \pm 0.12$	8.37±0.05

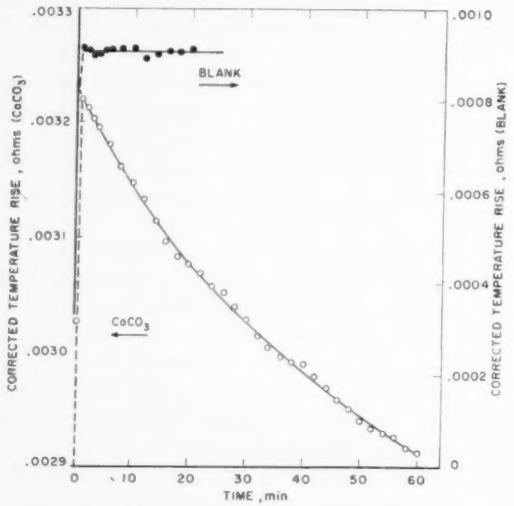

FIGURE 2. *The corrected temperature rise of a 0.2247-g sample of $CaCO_3$ plotted against the time after the sample was introduced into the calorimeter.*

The curves for both blank and sample start from the origin, representing zero temperature rise at zero time. Open circles and ordinates on left refer to the $CaCO_3$. Closed circles and ordinates on right refer to a blank run. The sample was placed in a glass bulb and covered with water. The blank contained water alone.

TABLE 3a. *Calibration of calorimeter and 600 grams 2N* HCl, *used for determining the heat of solution of* $3CaO \cdot Al_2O_3 \cdot 6H_2O$ *and the samples of* $3CaO \cdot Al_2O_3 \cdot CaCO_3 \cdot nH_2O$

Run	Time	I	E	Q	ΔR_s	Heat capacity
	sec	*amp*	*Volts*	*j*	*Ohm*	*j/ohm*
1	599.91	0.188960	17.2276	1952.903	0.079767	[a] $24,482.5_9$
2	599.85	.188982	17.2293	1953.128	.079847	$24,460.8_8$
3	600.15	.188959	17.2272	1953.629	.079779	$24,488.0_1$
4	600.21	.201466	18.3474	2218.603	.090500	$24,514.9_4$
5	599.79	.196921	17.9510	2120.215	.086527	$24,503.5_1$
6	660.04	.192244	17.5261	2223.865	.090897	$24,465.7_6$
7	639.95	.191276	17.4388	2201.345	.090058	$24,443.6_4$
Mean heat capacity						j/ohm 24,479.9₈±9.43
Mean heat capacity						cal/ohm 5,850.8₄±2.25

[a] It is not the authors' intention to imply that the heat-capacity values are either precise or accurate to the number of figures tabulated. These figures are carried through the calculations and the heat-of-solution values obtained from them in tables 4 and 5 are rounded off.

TABLE 3b. *Calibration of calorimeter and 740 grams 2N* HCl, *used for determining heat of solution of* $CaCO_3$. *Average heater resistance 69.0995 ohms*

Run	Time	I	$I^2RT=Q$	ΔR_s	Heat capacity
	sec	*amp*	*j*	*Ohm*	*j/ohm*
1	720.24	0.239042	2843.810	0.099817	[a] $28,490.2_4$
2	720.32	.236182	2776.476	.097375	$28,513.2_3$
3	780.21	.233174	2931.208	.102977	$28,464.6_9$
4	960.20	.232667	3591.751	.126155	$28,470.9_3$
5	839.72	.232183	3128.025	.109968	$28,444.8_7$
Mean heat capacity					j/ohm 28,476.7₉±11.64
Mean heat capacity					cal/ohm 6,806.1₂±2.78

[a] See footnote, table 3a.

3.2. Correction for Impurities

The calculation of the composition of a sample and of the heat of solution of the pure aluminate carbonate present in a sample is shown in the appendix, with sample 1 as the example.

The spread for the heat of solution of the three preparations is 4.51 cal/g before correction for impurities. After correction, the spread is 1.73 cal/g. The average corrected heat of solution of the three samples is $-\Delta H = 226.36 \pm 0.56$ [2] cal/g or 127.37 ± 0.38 kcal/mole. The average water content of the pure compound in the 3 samples is $10.68H_2O$.

[2] The estimates of standard deviation quoted in this paper represent the standard deviation of the average, using n-1 degrees of freedom.

TABLE 4. *Heat-of-solution determinations. Heat capacity of calorimeter, 24,479.90 joules/ohm*

	Run	Corrected rise	Sample weight	Heat of solution, uncorrected $-\Delta H$	Correction for heat capacity of sample $-\Delta H$	Heat of solution, corrected $-\Delta H$
		Ohm	*g*	*j/g*	*j/g*	*j/g*
$3CaO \cdot Al_2O_3 \cdot CaCO_3 \cdot nH_2O$ Sample 1	1	0. 038552	0. 9976	946. 02	0. 00	946. 02
	2	. 039513	1. 0206	947. 75	+. 13	947. 88
	3	. 019889	0. 5158	943. 93	−. 38	943. 55
	4	. 021232	. 5492	946. 39	−. 29	946. 10
Mean, before correction for impurities					j/g	945. 89±0. 88
					cal/g	226. 07±0. 21
Sample 2	1	0. 039698	1. 0186	954. 06	−0. 79	953. 27
	2	. 039823	1. 0196	956. 12	−. 13	955. 99
	3	. 039254	0. 9940	966. 73	−. 08	966. 65
	4	. 020605	. 5258	959. 32	−. 08	959. 24
	5	. 019594	. 4994	960. 47	+. 21	960. 68
Mean, before correction for impurities					j/g	959. 17±2. 26
					cal/g	229. 25±0. 54
Sample 3	1	0. 038027	0. 9909	939. 45	−0. 21	939. 24
	2	. 038923	1. 0147	939. 03	−. 13	938. 90
	3	. 020396	0. 5298	942. 42	−. 33	942. 09
	4	. 020225	. 5256	941. 98	−. 88	941. 10
Mean, before correction for impurities					j/g	940. 33±0. 75
					cal/g	224. 74±0. 18
$3CaO \cdot Al_2O_3 \cdot 5.859H_2O$	1	0. 019390	0. 3057	1552. 72	+0. 92	1553. 64
	2	. 018995	. 3001	1549. 47	+. 50	1549. 97
	3	. 019701	. 3122	1544. 77	+. 46	1545. 23
	4	. 027583	. 4384	1540. 21	+. 25	1540. 46
	5	. 016714	. 2647	1545. 74	+. 33	1546. 07
	6	. 018847	. 2980	1548. 23	+. 38	1548. 61
	7	. 016869	. 2669	1547. 21	+. 25	1547. 46
	8	. 019520	. 3085	1548. 94	+. 46	1549. 40
	9	. 023494	. 3732	1541. 08	+. 46	1541. 54
Mean, before correction for impurities					j/g	1546. 93±1. 34
					cal/g	369. 73±0. 33

3.3. Heat of Solution of the $CaCO_3$

The heat of solution eventually determined for the $CaCO_3$ was higher ($-\Delta H$=83.6 cal/g) than the values of Wells and Taylor (58.9 cal/g) [8] and Bäckström (44.9 cal/g) [10], obtained by these authors with partial evolution of CO_2. The accuracy of the higher figure obtained in this work may be checked in two different ways.

The heat of the reaction

$$CaO\ (c) + CO_2\ (aq) \xrightarrow{\Delta H_9} CaCO_3\ (c) \qquad (9)$$

may be calculated by several methods, one of which requires the heat of solution of $CaCO_3$ which is to be checked:

a. From the heats of formation of the three compounds in equation 9 [4], ΔH_9=−37.9 kcal/mole.

TABLE 5. *Heat-of-solution determinations,* $CaCO_3$

Heat capacity of calorimeter, without bulb and sample assembly, 28,476.79 j/ohm

Run	Sample weight	Water	Corrected rise	Blank correction	Net rise	Heat capacity corrections		Total heat capacity of calorimeter	Heat of solution $-\Delta H$
						Sample + glass	Water		
	g	*g*	*Ohm*	*Ohm*	*Ohm*	*j/ohm*	*j/ohm*	*j/ohm*	*j/g*
1	0.0000	4.0286	0.000456		[a] 0.0001132				
2	.0000	7.9910	.000906		[a] .0001134				
3	.2247	5.2820	.003334	0.000598	.002736	+80.79	+212.17	28,769.75	350.31
4	.2247	4.5413	.003230	.000515	.002715	+79.87	+182.42	28,739.08	347.25
5	.2110	7.8531	.003486	.000890	.002596	+79.83	+315.43	28,872.05	355.22
6	.2068	6.0117	.003146	.000681	.002465	+78.58	+241.46	28,796.83	343.25
7	.2277	4.7903	.003339	.000543	.002796	+81.59	+192.42	28,750.80	353.04
Mean heat of solution								j/g	349.81±2.13
								cal/g	83.61±0.51

[a] Net rise, ohm, of blank per g water.

b. From the heat of the same reaction, but with CO_2 (g) as a reactant instead, and from the heat of vaporization of CO_2 from solution, both values obtained from Bäckström's work [10, 12]:

$$\begin{aligned} CaO\ (c) + CO_2\ (g) &\longrightarrow CaCO_3\ (c) & \Delta H_{10} &= -42.6 \\ CO_2\ (aq) &\longrightarrow CO_2\ (g) & \Delta H_{11} &= +\ 4.9 \\ & & \Delta H_9 &= -37.7 \end{aligned}$$

If the heat-of-formation figures for CO_2 from NBS Circular 500 [4] are used, ΔH_{11} is calculated to be +4.64. If this figure is added to Bäckström's value for ΔH_{10}, ΔH_9 becomes −38.0.

c. From the heats of solution of CaO and $CaCO_3$ in 2*N* HCl, based on Wells and Taylor's value for CaO of −46.7 kcal/mole. [8] and the heat of solution of $CaCO_3$ obtained in this work, $\Delta H_9 = -38.3$ kcal/mole.

A second check on the value reported here may be made by calculating the heat of solution of $CaCO_3$ in 2*N* HCl not saturated with CO_2 from the heat of solution in CO_2-saturated acid and from the heat of vaporization of CO_2 from solution (ΔH_{11}). To Wells and Taylor's value of −3.32 [8] or Bäckström's value of −3.26 [10] for the heat of solution may be added −4.9 (Bäckström) or −4.64 (NBS Circ. 500) [4] to obtain values ranging from −7.9 to −8.2 kcal/mole for the heat of solution in 2*N* HCl not CO_2-saturated. This compares with −8.4 kcal/mole determined in this work.

There may still be a residual error in this determination. The corrected temperature rise extrapolated analytically to zero time represents the correct enthalpy change for equation 6 only if all the CO_2 has dissolved at the start. Some of the CO_2 may, however, be evolved as a gas almost immediately without preliminary solution. The result obtained by this technique may therefore still be somewhat low. An error in the opposite direction results from the fact that the solution of the $CaCO_3$ takes place in finite time so that the extrapolation should really be made to some point between zero time and 1 min.

The heat of solution of $3CaO \cdot Al_2O_3 \cdot CaCO_3 \cdot nH_2O$ was not materially different when determined by ordinary methods or by the technique used for $CaCO_3$. This is attributed to the fact that the aluminate monocarbonate is slower to react with acid, and the CO_2 is released more slowly. Chemical equilibrium is presumably obtained more easily, with complete solution of the CO_2. The difference in activity is further evidence that CO_2 is bound differently in the monocarbonate than in $CaCO_3$, as concluded from differential thermal analysis and infrared patterns by Carlson and Berman [2].

3.4. Heat of Formation of the Product from the Reactants

The heat of the reaction

$$3CaO{\cdot}Al_2O_3{\cdot}5.859H_2O\ (c) + CaCO_3\ (c) + 4.82H_2O\ (l) \rightarrow 3CaO{\cdot}Al_2O_3{\cdot}CaCO_3{\cdot}10.68H_2O\ (c) \quad (10)$$

is calculated from the heats of solution of the reactants and products as follows:

$$3CaO{\cdot}Al_2O_3{\cdot}5.859H_2O\ (c) + 654.375\ (HCl{\cdot}26.614H_2O)\ (aq) \rightarrow [3CaCl_2 + 2AlCl_3 + 642.375\ (HCl{\cdot}27.130H_2O)]\ (aq);\ -\Delta H = +139.16\ \text{kcal.} \quad (11)$$

$$CaCO_3\ (c) + [642.375\ (HCl{\cdot}27.130H_2O) + 3CaCl_2 + 2AlCl_3]\ (aq) \rightarrow CO_2\ (aq) + [4CaCl_2 + 2AlCl_3 + 640.375\ (HCl{\cdot}27.216H_2O)]\ (aq);\ -\Delta H = +8.37\ \text{kcal.} \quad (12)$$

$$CO_2\ (aq) + [4CaCl_2 + 2AlCl_3 + 640.375\ (HCl{\cdot}27.223H_2O)] \leftarrow 3CaO{\cdot}Al_2O_3{\cdot}CaCO_3{\cdot}10.68H_2O\ (c) + 654.375\ (HCl{\cdot}26.614H_2O)\ (aq);\ -\Delta H = -127.37\ \text{kcal.} \quad (13)$$

$$640.375\ (HCl{\cdot}27.216H_2O)\ (aq) + 4.82H_2O\ (1) \rightarrow 640.375\ (HCl{\cdot}27.223H_2O)\ (aq);\ -\Delta H = +0.07\ \text{kcal.} \quad (14)$$

The heat of reaction (eq (10)) is the sum of the heat effects of eqs (11), (12), (13), and (14), or $-\Delta H = 20.23$ kcal/mole $3CaO{\cdot}Al_2O_3{\cdot}CaCO_3{\cdot}10.68H_2O$.

3.5. Correction for the Water Content of the Tricalcium Aluminate

This correction is found by adding to the heat of reaction for equation 10 the heat of the following reaction:

$$3CaO{\cdot}Al_2O_3{\cdot}6H_2O \rightarrow 3CaO{\cdot}Al_2O_3{\cdot}5.859H_2O + 0.141H_2O. \quad (15)$$

This correction has been estimated previously as $-\Delta H = -1.36$ kcal/mole $3CaO{\cdot}Al_2O_3$ [5]. The heat of reaction is therefore $-\Delta H = 20.23 - 1.36 = 18.87$ kcal, for the equation

$$3CaO{\cdot}Al_2O_3{\cdot}6H_2O + CaCO_3 + 4.68H_2O \rightarrow 3CaO{\cdot}Al_2O_3{\cdot}CaCO_3{\cdot}10.68H_2O. \quad (16)$$

3.6. Heat of Formation

The heat of formation of the calcium aluminate monocarbonate is the sum of the heat effect of equation 16 and the heats of formation of the reactants in that equation [4], and is calculated as follows:

ΔH_f° $3CaO{\cdot}Al_2O_3{\cdot}6H_2O$	$= -1329$
ΔH_f° $CaCO_3$	$= -\ 288.45$
ΔH_f° $4.68H_2O$	$= -\ 319.72$
ΔH $3CaO{\cdot}Al_2O_3{\cdot}CaCO_3{\cdot}10.68H_2O$ from these reactants	$= -\ \ 18.87$
ΔH_f° $3CaO{\cdot}Al_2O_3{\cdot}CaCO_3{\cdot}10.68H_2O$	$= -1956$ kcal/mole

The calculated uncertainty of this result, based on a standard deviation for the heat of solution of 0.38 kcal/mole for the aluminate carbonate, 0.12 for the tricalcium aluminate hydrate, and 0.05 for the calcium carbonate, is 0.40 kcal/mole. This value does not include the uncertainty in the heat of formation of the reactants, which is certainly of the order of 1 kcal/mole for the hydrated tricalcium aluminate, nor the uncertainties due to chemical analysis.

4. Summary

Determinations were made of the heat of solution of $3CaO \cdot Al_2O_3 \cdot CaCO_3 \cdot 10.68H_2O$ in 2.00*N* HCl at 25 °C. Calculations were made of the heat of formation of this compound from $3CaO \cdot Al_2O_3 \cdot 6H_2O$, $CaCO_3$, and H_2O; and from the elements. A new technique was employed to determine the heat of solution of $CaCO_3$, in which most of the sensible heat lost by escaping CO_2 gas was retained by improved thermal equilibrium between the solution and the gas. By a modified type of calculation, the heat of solution determined included the latent heat of the evolved gas as well. The heat of solution thus calculated is greater than values obtained for $CaCO_3$ by Wells and Taylor and by Bäckström in determinations in which only part of the CO_2 went into solution. It is consistent with other thermochemical data in the literature.

The authors acknowledge with thanks the help of Howard E. Swanson and coworkers, who made the X-ray diffraction measurements.

5. Appendix. Calculation of the Impurities, H_2O Content, and Heat of Solution of a Preparation of Calcium Aluminate Monocarbonate

Sample 1

From the mole ratios of the oxides (table 1), the mole ratio of $3CaO \cdot Al_2O_3 \cdot CaCO_3$ to Al_2O_3 was taken as 1.00. This accounts for 4.00 moles of CaO and 1.00 mole of CO_2, leaving a remainder of 0.05 mole of CaO and 0.02 mole of CO_2. Since calcite was observed in the microscope in very small quantities, the remainder was calculated to 0.02 mole of $CaCO_3$ and 0.03 mole of excess $Ca(OH)_2$. The 0.03 mole of H_2O corresponding to the $Ca(OH)_2$ was deducted from the 10.61 moles of H_2O, leaving 10.58 moles of H_2O in the hydrated aluminate carbonate, or a composition of $3CaO \cdot Al_2O_3 \cdot CaCO_3 \cdot 10.58H_2O$.

The heat of solution of each impurity was multiplied by its weight per mole of Al_2O_3 to obtain the calories produced by the impurity. The sum of the heats of solution of all the impurities was subtracted from the total heat (heat of solution of the sample multiplied by its total weight per mole of Al_2O_3) to obtain the heat effect of the pure aluminate carbonate. This result, divided by the mole ratio of pure compound to Al_2O_3 (in this case 1.00) is the corrected heat of solution in calories per mole. If this quotient is further divided by the formula weight of the pure compound, the heat of solution is obtained in calories per gram. Thus, for sample 1:

1.00 mole $3CaO \cdot Al_2O_3 \cdot CaCO_3 \cdot 10.58H_2O$	$\times 560.90 =$	560.90 g
0.02 mole $CaCO_3$	$\times 100.09 =$	2.00 g
0.03 mole $Ca(OH)_2$	$\times 74.096 =$	2.22 g
Total weight of sample per mole Al_2O_3		565.12 g
Total heat of solution per mole Al_2O_3		
$= 226.07$ cal/g $\times 565.12 =$		127,757 cal.
$-$Heat of solution of $CaCO_3 = 83.61 \times 2.00$	$=$	-167 cal
$-$Heat of solution of $Ca(OH)_2 = 436.41 \times 2.22$	$=$	-969 cal
Net heat of solution of aluminate carbonate	$=$	126,621 cal
Heat of solution of aluminate carbonate	$=$	126.62 kcal/mole
	$=\frac{126{,}621}{560.90} =$	225.75 cal/g

The calculation in the case of sample 2 was based on the presence of $3CaO \cdot Al_2O_3 \cdot 6H_2O$ and CO_2 as impurities. A small quantity of the tricalcium aluminate hexahydrate was observed under the microscope.

6. References

[1] R. Turriziani and G. Schippa, On the existence of hydrated calcium monocarboaluminate (in Italian), Ricerca Sci. **26,** 2792 (1956).

[2] E. T. Carlson and H. A. Berman, Some observations on the calcium aluminate carbonate hydrates, J. Research NBS **64A,** No. 4, 333 (1960).

[3] Katharine Mather, private communication.

[4] F. D. Rossini, D. D. Wagman, W. H. Evans, S. Levine, and I. Jaffe, Selected values of chemical thermodynamic properties, NBS Circ. 500, U.S. Govt. Printing Office, Washington (1952), pp. 11, 99, 386, 395, 401.

[5] H. A. Berman and E. S. Newman, Heat of formation of calcium trisulfoaluminate at 25 °C, presented to the Fourth International Symposium on the Chemistry of Cement (Washington) 1960, estimated publication by NBS in 1962.

[6] T. Thorvaldson, W. G. Brown, and C. R. Peaker, Studies on the thermochemistry of the compounds occurring in the system CaO–Al_2O_3–SiO_2, J. Am. Chem. Soc. **52,** 3927 (1930).

[7] E. S. Newman, Heat of formation of potassium calcium silicate, J. Research NBS **62,** 207 (1959) RP2955.

[8] L. S. Wells and K. Taylor, Hydration of magnesia in dolomitic hydrated limes and putties, J. Research NBS **19,** 215 (1937) RP1022.

[9] K. K. Kelley and C. T. Anderson, Contributions to the data on theoretical metallurgy IV—Metal carbonates, U.S. Bureau of Mines, Bulletin 384, p. 14; U.S. Govt. Printing Office, Washington (1935).

[10] H. L. J. Bäckström, The thermodynamic properties of calcite and aragonite, J. Am. Chem. Soc. **47,** 2432 (1925).

[11] G. Geffcken, Contributions to the knowledge of factors affecting solubility (in German), Z. Phys. Chem. **49,** 257 (1904).

[12] H. L. J. Bäckström, The heat of dissociation of calcium carbonate and the entropy of carbon dioxide, J. Am. Chem. Soc. **47,** 2443 (1925).

(Paper 65A3–102)

JOURNAL OF RESEARCH of the National Bureau of Standards—A. Physics and Chemistry
Vol. 65A, No. 3, May–June 1961

Thermodynamic Constants for Association of Isomeric Chlorobenzoic and Toluic Acids With 1,3-Diphenylguanidine in Benzene [1]

Marion Maclean Davis and Hannah B. Hetzer

(January 16, 1961)

This paper reports values of ΔF_{25}, ΔH, and ΔS_{25} for the association of diphenylguanidine with the isomeric monochlorobenzoic acids and the isomeric toluic acids in benzene from spectrophotometric measurements at 25 and 30 °C, using bromophthalein magenta E (3′, 5′, 3″, 5″-tetrabromophenolphthalein ethyl ester) as the indicator. The results are compared with available data for other donor-acceptor associations in aprotic solvents which include the monomer-dimer equilibrium of benzoic acids, the association of tertiary amines with iodine, and the association of certain oxygen bases with phenols. The comparisons indicate that the value of the ratio $\Delta H/298\Delta S$ is approximately constant in the following associations in aprotic solvents: (1) Association of phenolic or carboxylic acids with nitrogenous bases to form hydrogen bonded ion-pairs; (2) hydrogen bonding of weakly acidic phenols to nitrogenous bases; (3) association of tertiary amines with iodine. A somewhat smaller value for this ratio seems to apply to most associations of phenols with oxygen bases. Possible applications of these findings include estimation of other thermodynamic constants when one of the constants ΔF, ΔH, or ΔS is known, and clarification of the relative importance of ionic and covalent contributions in hydrogen bond formation.

1. Introduction

A spectrophotometric procedure was described earlier [1],[2] by means of which the relative strengths of 40 carboxylic acids of the benzoic acid series were determined when in benzene solution at 25 °C. The strengths were expressed as values of $K_{assoc.}$ or log $K_{assoc.}$ for the reaction

$$\text{B (base)} + \text{HA (acid)} \rightleftarrows \text{BH}^{+}\ldots\text{A}^{-}, \qquad (1)$$

in which the base used was 1,3-diphenylguanidine. The phenolic acid, bromophthalein magenta E (3′,5′,3″, 5″- tetrabromophenolphthalein ethyl ester) served as the indicator dye. An essential step was determining K for the association of diphenylguanidine with bromophthalein magenta E. After completion of the experimental work at 25 °C [1], analogous measurements at 30 °C were made for part of these acids, namely, bromophthalein magenta E, benzoic acid, the isomeric chlorobenzoic acids, and the isomeric toluic acids. This paper reports thermodynamic constants derived from the combined data at 25 and 30 °C, and discusses their significance.

2. Experimental Procedure and Results

Among the possible sources of error in studies of acid-base equilibria in benzene by spectrophotometry are the volatility of the solvent and effects of adventitious moisture or oxygen. Such errors can be minimized by making absorbance measurements very soon after the preparation of solutions.[3] To facilitate speed in obtaining optical data, as well as to reduce errors arising from imprecise temperature control, the temperature in our laboratory is automatically controlled to match closely the temperature within the thermostated air bath which serves as the absorption cell compartment [3]. Throughout most of the year, a laboratory temperature of 25±0.5 °C can be maintained. During summer and winter weather, respectively, the laboratory temperature can be held as high as 30 °C or as low as 20 °C.

Qualitative observations of thermal effects on the extent of association of bromophthalein magenta E with bases [4] had made it seem likely that enthalpy and entropy changes involved in the kinds of acid-base associations which have been under study could be estimated from optical measurements covering the temperature range 20 to 30 °C, and plans were made to extend the measurements already made at 25 °C [1] to these two additional temperatures. In August and September of 1955 some of the experiments (see introduction) were repeated at 30 °C, using the same materials and following the same experimental technique as at 25 °C, but the work had to be interrupted without performance of the intended measurements at 20 °C.

The combined results of the experiments at 25 and 30 °C are summarized in table 1.[4] The steps

[1] This research was supported in part by the United States Air Force, through the Air Force Office of Scientific Research of the Air Research and Development Command, under contract No. CSO–670–55–21.

[2] Figures in brackets indicate the literature references at the end of this paper.

[3] For example, leakage of atmospheric oxygen into glass-stoppered absorption cells containing the base tribenzylamine in benzene solution was found to cause its partial conversion to tribenzylamine oxide. To determine the equilibrium constant for association of tribenzylamine with bromophthalein magenta E, the benzene was freshly boiled to remove dissolved air and the measurements were made as quickly as possible [2].

[4] The raw data reported for 25 °C [1] are typical of those obtained at 30 °C.

followed in calculating association constants corresponding to eq (1), and then applying a correction for the amount of carboxylic acid dimer presumed to be present, were the same as previously explained [1]. As noted in table 1, parallel studies of the association of diphenylguanidine with bromophthalein magenta E and with benzoic acid at 25 and 30 °C have been made in this laboratory [5], with very similar results.

The dimer-monomer data used in making the corrections are not known with certainty to be accurate. Self-association of diphenylguanidine, formation of complex anions $(RCOOHOCOR)^-$, the "secondary" reaction of diphenylguanidine with bromophthalein magenta E [6], and adsorption of solutes on glass- or silicaware are additional possible causes of errors. However, it is believed that experimental uncertainties in the optical data are the main obstacle to the attainment of high accuracy; these have more effect when the association constants are relatively great in magnitude (10^5 to 10^6), as in the present work.[5]

Values for the thermodynamic constants ΔF_{25}, ΔH, and ΔS_{25} were calculated in the conventional way from the $K_{assoc.}$ values at the two temperatures. These results are summarized in table 2.[6]

[5] See [5], footnote 10.

TABLE 2. *Thermodynamic constants for association of acids with 1,3-diphenylguanidine in benzene*[a]

Acid	ΔF_{25}	ΔH	ΔS_{25}	$\frac{\Delta H}{298\Delta S_{25}}$
	kcal mole^{-1}	*kcal mole*$^{-1}$	*cal mole*$^{-1}$ *deg*$^{-1}$	
Bromophthalein magenta E	−7.38	−15.8	−28.2	1.9
Benzoic	−7.24	−16.2	−30.1	1.8
o-Chlorobenzoic	−8.32	−18.8	−35.1	1.8
m-Chlorobenzoic	−8.30	−19.0	−36.0	1.8
p-Chlorobenzoic	−7.97	−18.0	−33.7	1.8
o-Toluic	−6.78	−16.5	−32.5	1.7
m-Toluic	−7.06	−16.5	−31.5	1.8
p-Toluic	−7.00	−16.0	−30.1	1.8

[a] Calculated from association constants expressed in liter mole^{-1} units. See discussion in section 2 of the text.

[6] The values of ΔH and ΔS_{25} given in table II of [5] for the association of diphenylguanidine with bromophthalein magenta E and benzoic acid were based on $K_{assoc.}$ values at 20, 25, and 30 °C. Unaccountably the value of $K_{assoc.}$ found at 20 °C for the reaction of diphenylguanidine with bromophthalein magenta was lower than the value expected ($\sim 4\times10^5$) and, as a result, the value of $K_{assoc.}$ for the reaction of diphenylguanidine with benzoic acid was also lower than expected. If 4×10^5 is assumed to be approximately the correct K value for the association of diphenylguanidine with bromophthalein magenta at 20 °C, K for its association with benzoic acid acquires the expected magnitude, and the thermodynamic constants obtained agree closely with the ones given in table 2 of this paper.

TABLE 1. *Equilibrium constants for association of acids with 1,3-diphenylguanidine in benzene at 25 and 30 °C*

Acid	t (°C)	No. expts.	Range of n[a]	Range of n''[a]	10^3K_{21}[b]	$10^{-5}K_{cor.}$[b]	St. dev.	Coeff. var. %
Bromophthalein magenta E	25	10	0. 25 to 3	----------	----------	2. 55 2. 57[c]	0. 098	3. 8
	30	8	. 75 to 3	----------	----------	1. 64 1. 66[c]	. 070	4. 3
Benzoic	25	25	1 to 3	0. 5 to 5	1. 6	2. 01 2. 09[c]	. 045	2. 2
	30	8	0. 5 to 3	. 5 to 3	2. 0	1. 28 1. 31[c]	. 081	6. 3
o-Chlorobenzoic	25	9	. 5 to 3	. 5 to 4	3. 7	12. 5	. 047	3. 8
	30	8	. 5 to 3	. 5 to 4	4. 7	7. 42	. 235	3. 2
m-Chlorobenzoic	25	16	. 5 to 3	. 5 to 5	2. 4	12. 1	. 023	1. 9
	30	8	. 5 to 3	. 5 to 4	3. 0	7. 13	. 116	1. 6
p-Chlorobenzoic	25	8	. 5 to 3	. 5 to 4	(1. 7)	6. 94	. 133	1. 9
	30	9	. 5 to 3	. 5 to 4	(2. 0)	4. 20	. 108	2. 6
o-Toluic	25	19	. 5 to 3	. 5 to 8	2. 4	0. 930	. 179	1. 9
	30	8	1 to 3	. 25 to 4	3. 0	. 588	. 112	1. 9
m-Toluic	25	11	1 to 3	1 to 8	1. 4	1. 50	. 041	2. 7
	30	9	0. 5 to 3	0. 5 to 4	1. 8	0. 948	. 219	2. 3
p-Toluic	25	10	1 to 3	1 to 4	0. 415	1. 34	. 084	6. 3
	30	6	0. 5 to 3	0. 5 to 3	0. 53	0. 859	. 288	3. 4

[a] The molar concentration (C_a) of bromophthalein magenta E (3′, 5′, 3″, 5″-tetrabromophenolphthalein ethyl ester) was 5.0×10^{-5} throughout. The molar concentrations of 1,3-diphenylguanidine (nC_a) and of the aromatic carboxylic acid ($n''C_a$) varied within the ranges indicated. Experimental procedure and apparatus were as described in [1].

[b] K_{21} is the equilibrium constant for dissociation of dimeric carboxylic acid into the monomer in benzene, while $K_{cor.}$ is the equilibrium constant for the association A(acid) + B(base) ⇆ S(salt) in benzene after the raw data have been corrected by taking into consideration the dimer-monomer equilibrium of the carboxylic acid; for method of calculating $K_{cor.}$ see [1], especially sections 3.2 and 4.1. The values of K_{21} used in correcting the association constants were based on data in the literature except in the cases of *m*- and *p*-chlorobenzoic acids, for which K_{21} values have not been reported. In the case of *m*-chlorobenzoic acid, data for *m*-iodobenzoic acid were applied; in that of *p*-chlorobenzoic acid, K_{21} values at 25 and 30 °C were estimated by trial and error. All equilibrium constants given in this table are in molar units.

[c] Reference [5].

3. Discussion

Two well-known thermodynamic equations,

$$-RT\ln K=\Delta F \tag{2}$$

and

$$\Delta F=\Delta H-T\Delta S, \tag{3}$$

are frequently utilized in efforts to develop generalizations about the effects of structural modifications on reaction rates and equilibria (for example, see [7 to 13]). The great majority of the attempts to assess relative contributions of changes in enthalpy and entropy to free energy changes have been made in connection with studies of reaction kinetics. In some instances, a structural change apparently leads to an increase in the energy of activation, with little or no effect on the entropy factor.[7] In other cases, an increase in the energy of activation is accompanied by a parallel effect on the entropy factor.[8]

A class of chemical equilibria which is of major interest is the ionization of acids of the benzoic acid series in water, since this reaction series was adopted for evaluating substituent constants in the Hammett equation [8]. Thermodynamic constants for the aqueous ionization of some benzoic acids pertinent to this paper are compiled in table 3. The ΔH values for these acids, except in the case of *o*-toluic acid, are much less than one kcal mole^{-1} in magnitude. Clearly, the values of ΔF_{25} for aqueous ionization of the acids depend almost solely on the temperature-entropy term, $T\Delta S$.

The thermodynamic constants obtained in this work for association of benzoic acids with 1,3-diphenylguanidine in benzene (table 2) contrast greatly with the corresponding constants for aqueous ionization.[9] Values of ΔH are in the approximate range 16 to 19 kcal mole^{-1}, are all negative in sign, and the variations in numerical magnitude parallel those in the temperature-entropy term, the ratio $\Delta H/298\Delta S_{25}$ being 1.8, or very close to this value, in all cases. For five of the reactions $\Delta H/\Delta F_{25}$ is 2.3 the extreme values being 2.1 and 2.4.

TABLE 3. *Thermodynamic constants for ionic dissociation of selected benzoic acids in water*

Acid	ΔF_{25}	ΔH	ΔS_{25}	$298\Delta S_{25}$
	kcal mole^{-1}	*kcal mole*$^{-1}$	*cal mole*$^{-1}$ *deg*$^{-1}$	*kcal mole*$^{-1}$
Benzoic	5.74	0.11 [a] 0.104 [c] 0.09 [d]	−18.9 [a c d]	−5.64
m-Chlorobenzoic	5.22	.019 [b]	−17.4 [b]	−5.19
m-Iodobenzoic	5.26	.190 [b]	−17.0 [b]	−5.07
p-Chlorobenzoic	5.43	.226 [b]	−17.5 [b]	−5.22
o-Toluic	5.33	−1.50 [d]	−22.9 [d]	−6.83
m-Toluic	5.78	0.07 [b d]	−19.2 [b d]	−5.72
p-Toluic	5.92	0.30 [b] 0.24 [d]	−19.0 [d]	−5.67

[a] T. L. Cottrell, G. W. Drake, D. L. Levi, K. J. Tully, and J. H. Wolfenden, J. Chem. Soc. (London) **1948,** 1016.
[b] G. Briegleb and A. Bieber, Z. Elektrochem. **55,** 250 (1951).
[c] A. V. Jones and H. N. Parton, Trans. Faraday Soc. **48,** 8 (1952).
[d] T. W. Zawidski, H. M. Papée, and K. J. Laidler, Trans. Faraday Soc. **55,** 1743 (1959).

For comparison, available values of ΔH and ΔS_{25} for the monomer-dimer equilibrium of the same or closely related benzoic acids are presented in table 4. It is of considerable interest that the ratio $\Delta H/298\Delta S_{25}$ has practically the same value for the self-association of the benzoic acids in benzene as for their association with diphenylguanidine in this solvent.[10] The enthalpy-entropy relationship for the two kinds of association reactions is also brought out in figure 1, in which $-\Delta S_{25}$ is plotted against $-\Delta H$. In this figure the equation for the *solid* line was calculated by the method of least squares, using data for all seven of the carboxylic acids.[11] The *dashed* line is an extension of the solid line. For the monomer-dimer equilibrium, $\Delta H/\Delta F_{25}$ varies from 2.1 to 2.5, with the exception of *p*-toluic acid where the value is 1.9.[12]

A few additional investigations of thermodynamic properties of acid-base associations in aprotic solvents have been reported. Table 5 is a compilation of most of the published data. Several tentative conclusions may be drawn:

(1) In most associations in which nitrogen is the proton acceptor (electron donor), the value of $\Delta H/298\Delta S_{25}$ is not far from 1.8.[13]

TABLE 4. *Thermodynamic constants for self-association of aromatic acids in benzene* [a]

Acid	ΔF_{25}	ΔH [d]	ΔS_{25} [d]	$\frac{\Delta H}{298\Delta S_{25}}$ [d]
	kcal mole^{-1}	*kcal mole*$^{-1}$	*cal mole*$^{-1}$ *deg*$^{-1}$	
Benzoic	−3.81	−8.37	−15.3	1.8
o-Chlorobenzoic [b]	−3.31	−8.31	−16.8	1.7
m-Iodobenzoic [b]	−3.57	−7.6 [8]	−13.7	1.9
o-Toluic [c]	−3.58	−8.39	−16.1	1.7
m-Toluic [c]	−3.91	−9.26	−17.9	1.7
p-Toluic [b]	−4.61	−8.72	−13.8	2.1

[a] Calculated from monomer-dimer equilibrium constants (K_{12}) expressed in liter mole^{-1} units.
[b] Computed from data of G. Allen and E. F. Caldin (ref. [18]), after converting monomer-dimer constants from mole fraction units to liter mole^{-1} units.
[c] From data of F. T. Wall and F. W. Banes, J. Am. Chem. Soc. **67,** 898 (1945).
[d] Dividing these values of ΔH and ΔS_{25} by two, so as to obtain the average values per hydrogen bond has no effect, of course, on the ratio $\Delta H/T\Delta S$.

[7] For example, in the *alkaline* hydrolysis of *m*- and *p*-substituted ethyl benzoates in 85-percent aqueous ethanol [14].
[8] An illustration is the *acidic* hydrolysis of *m*- and *p*-substituted ethyl benzoates in 85-percent aqueous ethanol [15].
[9] In comparing relative acidic strengths in water and benzene, one must bear in mind that the primary acid-base reaction eq (1) is a shift of the acid proton toward the base to form hydrogen-bonded ion-pairs. Formation of independently moving ions occurs to a very minor extent unless the ions can become hydrogen-bonded to molecules of solvent or solute [3, 6]. This "secondary reaction" is likely to hamper study of the main acid-base interaction.

[10] Others have recognized a linear correlation of ΔH and ΔS in the dimerization of carboxylic acids, as well as in some additional instances of hydrogen bond formation [16, 17], but the units of concentration were not the same as those used here, thus leading to different values for ΔH and ΔS.
[11] Omitting data for *o*-toluic acid would have given a still better correlation of ΔH with ΔS_{25} values.
[12] *p*-Toluic acid shows anomalous behavior in the comparison of K_{12} values for carboxylic acids in benzene with the K_{ion} values in water [16]. Its tendency to dimerize in benzene [18] seems surprisingly great.
[13] The thermodynamic constants for the three base-acid systems in cyclohexane are small, and the authors regarded the values as being rough. Nevertheless, the agreement of two of the values of $\Delta H/298\Delta S_{25}$ with those for stronger acid-base interactions is very good.

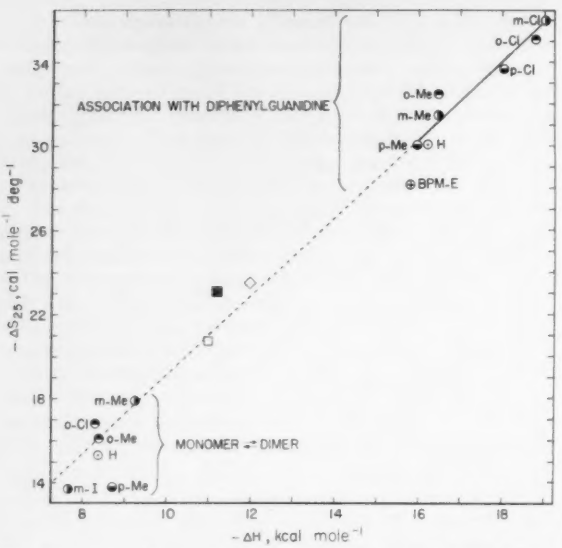

FIGURE 1. *$-\Delta S_{25}$ versus $-\Delta H$ for association of some benzoic acids with 1,3-diphenylguanidine and for self-association (dimerization) of the same or analogous acids, in benzene.*

H, Benzoic acid; *o*-, *m*-, and *p*-Me, the toluic acids; *o*-, *m*-, and *p*-Cl, the monochlorobenzoic acids; BPM-E, bromophthalein magenta E; see table 2. The unlabeled symbols refer to the following associations (see table 5): open square, triethylamine with benzoic acid in benzene; filled square, tribenzylamine with picric acid in benzene; open diamond, triethylamine plus iodine in *n*-heptane.

(2) Statement (1) holds irrespective of whether the acid is a Brønsted acid (phenol, carboxylic acid) or the Lewis acid iodine.

(3) In most associations in which oxygen is the proton acceptor (electron donor), the value of $\Delta H/298\Delta S_{25}$ is 1.4.[14] Results with dioxane and methyl or ethyl acetate as the base indicate that the values of both $-\Delta H$ and $-\Delta S_{25}$ increase on changing from carbon tetrachloride to a saturated hydrocarbon solvent, but without affecting the ratio of the two values.

(4) With benzene as base (π-electron donor), the value of $\Delta H/298\Delta S$ seems to be smaller.[15]

A linear relationship of $-\Delta H$ and $-\Delta S$ in a related series of association reactions has been interpreted as signifying that with increasing strength of the bond between donor and acceptor there is increased restraint on motions of the component parts.[16] Per-

[14] The monomer-dimer equilibrium of benzoic acids (see table 4) does not conform to this generalization.

[15] The very interesting thermodynamic data for formation of alkylbenzene-iodine [19] and alkylbenzene-iodine monochloride [20] complexes in carbon tetrachloride solution, which show a linear correlation of ΔH and ΔS, are in other units of concentration, and raw data necessary for conversion to molar units were not published. Consistent use of molar units of association in presenting thermodynamic properties of such association reactions would have the advantage of facilitating comparisons with systems containing both donor and acceptor compounds in concentrations much too low for use of mole fraction units.

[16] For example, see [17, 19, 20].

TABLE 5. *Thermodynamic constants for miscellaneous acid-base associations in aprotic solvents* [a]

Solvent	Base	Acid	ΔF_{25}	ΔH	ΔS_{25}	$\frac{\Delta H}{298\Delta S_{25}}$
			kcal mole^{-1}	*kcal mole*$^{-1}$	*cal mole*$^{-1}$ *deg*$^{-1}$	
Benzene [b]	Triethylamine	Bromophthalein magenta E	−6.1	−15.3	−30.9	1.7
Benzene [b]	Triethylamine	Benzoic acid	−4.9	−11.0	−20.7	1.8
Benzene [c]	Tribenzylamine	Picric acid	−4.4	−11.2	−23.1	1.6
Carbon tetrachloride [d]	Benzene	Iodine	+1.1	−1.1	−7.4	0.5
Carbon tetrachloride [e]	Dioxane	Phenol		−4.7	−11.5	1.4
Carbon tetrachloride [f]	Diethyl ether	Phenol		−3.7	−7.6	1.6
Carbon tetrachloride [g]	Ethyl acetate	Phenol		−4.8	−11.9	1.4
Carbon tetrachloride [f]	Hexamethylenetetramine	Phenol		−6.9	−13.6	1.7
Chlorobenzene [b]	*n*-Butylamine	2,4-Dinitrophenol	−3.1	−12.2	−30.5	1.3
Chlorobenzene [b]	Di-*n*-butylamine	2,4-Dinitrophenol	−4.6	−11.4	−22.8	1.7
Chlorobenzene [b]	Tri-*n*-butylamine	2,4-Dinitrophenol	−5.1	−14.4	−31.3	1.5
Cyclohexane [i]	Trimethylamine	Phenol	−2.6	−5.8	−10	1.9
Cyclohexane [i]	Trimethylamine	*p*-Chlorophenol	−3.1	−7.0	−13	1.8
Cyclohexane [i]	Trimethylamine	*p*-Cresol	−2.4	−3.8	−5	2.6
n-Heptane [j] [o]	Pyridine	Iodine	−3.3 [j]	−7.8	−15.5 [j]	1.7 [j]
n-Heptane [k] [o]	Triethylamine	Iodine	−5.0	−12.0	−23.5	1.7
n-Heptane [l]	Methyl acetate	Phenol		−5.3	−12.8	1.4
Isooctane [m]	*N,N*-Dimethylacetamide	Phenol		−7.7	−14.8	1.8
Petroleum ether [e]	Dioxane	Phenol		−5.4	−13.1	1.4
Petroleum ether [g]	Ethyl acetate	Phenol		−5.7	−13.7	1.4
Nitrobenzene [n]	Pyridine	Methanesulfonic acid		−17.1		

[a] From thermodynamic constants or association constants (converted where necessary to liter mole^{-1} units) given in the references cited below.
[b] Reference [5].
[c] A. A. Maryott, J. Research NBS **41,** 7 (1948); M. M. Davis and E. A. McDonald, J. Research NBS **42,** 595 (1949).
[d] See reference [5], table II, footnote *f*.
[e] S. Nagakura, J. Chem. Soc. Japan, Pure Chem. Sect. **74,** 153 (1953), through reference [17], appendix B.
[f] M. Tsuboi, Bull. Chem. Soc. Japan **25,** 60 (1952).
[g] S. Nagakura, J. Am. Chem. Soc. **76,** 3070 (1954).
[h] See reference [5], table II, footnote *d*.
[i] R. L. Denyer, A. Gilchrist, J. A. Pegg, J. Smith, T. E. Tomlinson, and L. E. Sutton, J. Chem. Soc. (London) **1955,** 3889; see table 5.
[j] C. Reid and R. S. Mulliken, J. Am. Chem. Soc. **76,** 3869 (1954). ΔF and ΔS are for 17 °C instead of 25 °C.
[k] S. Nagakura, J. Am. Chem. Soc. **80,** 520 (1958).
[l] S. Nagakura, J. Chem. Soc. Japan, Pure Chem. Sect. **75,** 734 (1954), through reference [17], appendix B.
[m] S. Mizushima, M. Tsuboi, T. Shimanouchi, and Y. Tsuda, Spectrochim. Acta **7,** 100 (1955).
[n] H. C. Brown and R. R. Holmes, J. Am. Chem. Soc. **77,** 1727 (1955).
[o] The method used in calculating $K_{\text{assoc.}}$ values has been criticized (see R. S. Drago and N. J. Rose, J. Am. Chem. Soc. **81,** 6141 (1959).

haps the different values which $\Delta H/298\Delta S_{25}$ seems to have (see table 5) for bases with nitrogen as the electron donor atom and those with oxygen as the electron donor (approximately 1.8 and 1.4, respectively) result chiefly from variations in $-\Delta H$.

The existent thermodynamic data for donor-acceptor reactions in aprotic solvents are not extensive enough to determine the scope of the relationships indicated above, or accurate enough to detect possible small effects resulting from variations in structure as, for example, isomerism in the toluic acids or the chlorobenzoic acids. Two important areas of possible application may be suggested, however.

(1) If one of the three constants ΔF, ΔH, and ΔS is known, it should be possible to estimate values for the other two. To illustrate, from the value of ΔH which has been determined for association of pyridine with methanesulfonic acid in nitrobenzene (see table 5), estimated values for ΔS_{25}, ΔF, and $K_{\text{assoc.}}$, in the units used above, are -32, -7.6, and 3.7×10^5, respectively. The assumption must be made that nitrobenzene does not affect the association differently from other solvents listed in the table. A further example concerns association of triethylamine with phenol in *n*-heptane. The reported value of $K_{\text{assoc.}}$ at 25 °C is 83.8 [21]. This leads to the following approximate values for ΔF, ΔH, and ΔS_{25}, respectively: -2.6, -5.9, and -11. These agree well with the constants reported for association of trimethylamine with phenol in cyclohexane (see table 5).

(2) The theory of hydrogen bond formation still needs clarification (see [17], chs. 7 and 8). Evidence for hydrogen bonding in ion-pairs of salts that are formed by union of nitrogenous bases with hydrogen acids (and therefore have one or more protons attached to the nitrogen of the cation) has been pointed out ([4,2,5] and references cited), but has not received wide consideration in discussions of hydrogen bonding. The thermodynamic data in tables 2, 4, and 5 point to a relationship of such systems with the more weakly bonded systems which so far have been the basis for speculations about the nature of hydrogen bonding and the relative importance of ionic and covalent contributions.

4. References

[1] M. M. Davis and H. B. Hetzer, J. Research NBS **60,** 569 (1958) RP2871.
[2] M. M. Davis and H. B. Hetzer, J. Am. Chem. Soc. **76,** 4247 (1954).
[3] M. M. Davis and H. B. Hetzer, J. Research NBS **48,** 381 (1952) RP2326.
[4] M. M. Davis and P. J. Schuhmann, J. Research NBS **39,** 221 (1947) RP1825.
[5] M. M. Davis and M. Paabo, J. Am. Chem. Soc. **82,** 5081 (1960).
[6] M. M. Davis and H. B. Hetzer, J. Research NBS **46,** 496 (1951) RP2219.
[7] A. E. Stearn and H. Eyring, J. Chem. Phys. **5,** 113 (1937).
[8] L. P. Hammett, Physical organic chemistry, chs. III and IV (McGraw-Hill Book Co., Inc., New York, N.Y., 1940).
[9] K. F. Laidler and H. Eyring, Ann. N.Y. Acad. Sci. **39,** 303 (1940).
[10] C. K. Ingold, Structure and mechanism in organic chemistry, ch. II, 6c and 6d (Cornell University Press, Ithaca, N.Y., 1953).
[11] J. E. Leffler, J. Org. Chem. **20,** 1202 (1955).
[12] J. Hine, Physical organic chemistry, chs. 2–4 and 3–3 (McGraw-Hill Book Co., Inc., New York, N.Y., 1956).
[13] R. P. Bell, The proton in chemistry, ch. V (Cornell University Press, Ithaca, N.Y., 1959).
[14] (a) C. K. Ingold and W. S. Nathan, J. Chem. Soc. (London) **1936,** 222; (b) D. P. Evans, J. J. Gordon, and H. B. Watson, J. Chem. Soc. (London) **1937,** 1430.
[15] E. W. Timm and C. N. Hinshelwood, J. Chem. Soc. (London) **1938,** 862.
[16] G. Allen and E. F. Caldin, Quart. Revs. (London) **7,** 255 (1953).
[17] G. C. Pimentel and A. L. McClellan, The hydrogen bond, ch. 7 (W. H. Freeman and Co., San Francisco, Calif., 1960).
[18] G. Allen and E. F. Caldin, Trans. Faraday Soc., **49,** 895 (1953).
[19] R. M. Keefer and L. J. Andrews, J. Am. Chem. Soc. **77,** 2164 (1955).
[20] N. Ogimachi, L. J. Andrews, and R. M. Keefer, J. Am. Chem. Soc. **77,** 4202 (1955).
[21] S. Nagakura and M. Gouterman, J. Chem. Phys. **26,** 881 (1957).

(Paper 65A3–103)

JOURNAL OF RESEARCH of the National Bureau of Standards—A. Physics and Chemistry
Vol. 65A, No. 3, May–June 1961

Heats of Combustion and Formation of Trimethylborane, Triethylborane, and Tri-*n*-butylborane

Walter H. Johnson, Marthada V. Kilday, and Edward J. Prosen

(January 3, 1961)

The heats of combustion at 25 °C of trimethylborane (liquid), triethylborane (liquid), and tri-*n*-butylborane (liquid), to form crystalline boric acid, liquid water, and gaseous carbon dioxide have been determined to be −2989.4 ±22.4 kj/mole (−714.48 ±5.36 kcal/mole), −4975.6 ±15.1 kj/mole (−1189.2 ±3.6 kcal/mole), and −8901.0 ±10.2 kj/mole (−2127.4 ±2.4 kcal/mole), respectively. These data, combined with the heats of formation of boric acid, carbon dioxide, and water give −34.79 ±5.40, −47.2 ±3.7, and −83.2 ±2.5 kcal/mole at 25 °C for the standard heats of formation of trimethylborane, triethylborane, and tri-*n*-butylborane, respectively. The data of other investigators are discussed briefly.

1. Introduction

The alkyl boranes comprise a unique and rather extensive group of compounds somewhat analagous to the hydrocarbons. As in the case of the hydrocarbons, a knowledge of the thermochemistry of the lower members is necessary for calculating the thermodynamic properties of the other members of groups from bond energies and for determining the effects of molecular structure. The lower members of the group are extremely pyrophoric; trimethylborane and triethylborane ignite immediately upon exposure to air. Tri-*n*-butylborane also oxidizes rapidly in air but takes fire only when spread over a fairly large surface.

2. Materials

The samples of trimethylborane, triethylborane, and tri-*n*-butylborane were obtained from the Olin Mathieson Chemical Corporation. The trimethylborane was purified by means of fractional crystallization [1] and the purity was determined to be 99.9 mole percent from calorimetric freezing-point determinations.[2] The material was stored in a stainless steel cylinder at −80 °C.

The purities of the triethylborane and tri-*n*-butylborane were estimated to be about 99 percent from the quantities of carbon dioxide produced in the combustions. The samples were prepared by the reaction of the appropriate alkyl magnesium bromide with boron trifluoride. The most likely impurities were the mono- and di-alkyl substitution products. Therefore, the quantity of carbon dioxide found in the combustion products was assumed to be an indication of the purity of the sample. No attempts were made to purify these materials further because of the small quantities of material available.

[1] Pure Substances Section of the Chemistry Division.
[2] Thermodynamics Section of the Heat Division.

The oxygen was purified by passing it through an oxidizer (containing copper oxide at 600 °C) and through an absorber containing Ascarite.

3. Apparatus

The calorimeter, the thermometric system, and the general calorimetric procedure have been described previously [1, 2, 3].[3] A twin-valve stainless-steel bomb, fitted with a gold gasket, was used for the combustion experiments on trimethylborane; the volume of the bomb was 376 ml. A similar bomb, with a Teflon gasket and having a volume of 385 ml, was used for the experiments on triethylborane and on tri-*n*-butylborane. The apparatus used for determination of the quantity of carbon dioxide has been described [2].

4. Procedure

4.1. Trimethylborane

Spherical Pyrex-glass bulbs, having capacities of 0.5 to 1.0 ml, were sealed to standard taper joints, weighed, and attached to a distillation manifold with wax (Apiezon "W"). Samples of trimethylborane, weighing 0.2 to 0.4 g, were distilled into the bulbs which were then sealed in vacuo, warmed to room temperature, and weighed. The bulbs were then stored at −80 °C.

The bulb containing the sample was wrapped with glass wool, placed in a platinum crucible and weighed. About 0.1 g of *n*-hexadecane (NBS Standard Sample 568) was dropped on the glass wool and the quantity determined by re-weighing the crucible. A platinum wire fuse, 0.076 mm in diameter and 50 mm long, was connected between the bomb electrodes so that it was located slightly above and near the side of the crucible. A weighed strip of filter paper was then

[3] Figures in brackets indicate literature references at the end of this paper.

attached to the fuse and placed so that it extended to the bottom of the crucible.

Two milliliters of water were placed in the bomb which was then closed and placed in the calorimeter can with enough water to cover the surface of the bomb. The bomb was then flushed with purified oxygen (to remove nitrogen) and filled with oxygen to a pressure of 30 atm at 25 °C. The can, together with the water and the charged bomb, was weighed and the quantity of water adjusted to 1,000.0 g less than the total amount required for the "standard" calorimeter system. The can with its contents was then transferred to the calorimeter and 1,000 g of water was added from a weighed flask. After the transfer of water the empty flask was re-weighed to determine accurately the amount of water added.

It was necessary to keep the bomb submerged during and after filling to avoid the danger of an accident if the bulb broke under the oxygen pressure. Because of the difficulty of manipulating the completely filled calorimeter can, the 1,000 g portion of water was added after the can was inserted into the calorimeter. Because the quantity of water was not exactly reproduced from experiment to experiment, a small but accurately determined correction for the resulting deviation in the heat capacity of the calorimeter system was made in each case.

The gaseous contents of the bomb were analyzed after each experiment to determine the quantity of carbon dioxide [2]. In the trimethylborane experiments, the liquid and solid materials remaining in the bomb were washed with hot water into a boron-free beaker. The resulting solution was filtered through a sintered-glass funnel to remove the glass fragments and the insoluble residue. The filtrate was titrated for nitric acid, and for boric acid in the presence of mannitol, using standard alkali solution; the end points of the titrations were determined by means of a Beckman *p*H-meter.

The solid portion collected in the filter was digested with nitric acid to dissolve elemental boron; analysis of the resulting solution showed no measurable quantity of boric acid, although the solution was so highly buffered that precise measurements were not possible. Portions of the insoluble residue were found by X-ray diffraction studies [4] to contain traces of B_4C, the only crystalline material identified.

4.2. Triethylborane and Tri-*n*-butylborane

The samples were placed in spherical soft-glass bulbs by means of a hypodermic syringe; this operation was performed in a dry-box containing an argon atmosphere. Rubber caps were placed over the tips of the bulbs which were then removed from the dry-box, cooled in an ice-bath, and sealed.

The bulb containing the sample was placed in a platinum crucible. An iron wire fuse, 50 mm long and 0.127 mm in diameter, was connected between the electrodes and adjusted to be about 1 mm directly above the sample bulb. One milliliter of water was placed in the bomb which was then closed. The flushing, filling and transfer operations, and the subsequent analyses of the gaseous combustion products were the same as described for the experiments on trimethylborane.

[4] Constitution and Microstructure Section of the Mineral Products Division.

4.3. Calibration

The calorimetric systems were calibrated by means of a series of combustion experiments on benzoic acid, NBS Standard Sample 39 g. The certified value for the heat of combustion of this sample in the standard bomb process is 26433.8 ±2.2 j/g at 25 °C. This value, when corrected for deviations from the standard bomb conditions, gave 26430.9 j/g at 28 °C [4]. The energy equivalent of the calorimetric system used for the experiments on trimethylborane was determined to be 141754.7 ±7.0 j/ohm.

The energy equivalent of the calorimetric system used for the experiments on triethylborane and tri-*n*-butylborane differed significantly from that used with trimethylborane because of the substitution of a larger bomb. The certified value for the heat of combustion of benzoic acid in the bomb process, corrected for deviations from the standard bomb process, was determined to be 26427.1 j/g at 29.8 °C. The energy equivalent of the calorimeter system was determined to be 136080.6 j/ohm.

5. Units and Conversion Factors

All atomic weights were taken from the 1957 International Table of Atomic Weights [5]. All weighings were corrected to weight in a vacuum.

The unit of energy was the joule; for conversion to the conventional thermochemical calorie, one calorie was taken as 4.1840 joules.

6. Results and Calculations

The heat of combustion of *n*-hexadecane was taken as −47155.2±7.7 j/g for the bomb process at 28 °C [6]. The heat of combustion of the filter paper was determined, in a separate series of experiments, to be 17084.5±8.0 j/g for the bomb process at 28 °C; analyses of the combustion products gave 1.599 g CO_2/g. The density of trimethylborane (liquid) at 25 °C was taken as 0.625 g/cm³ [7]; the heat capacity for the liquid at 25 °C was estimated as 30.8 cal/mole °C [8]. The densities of triethylborane and of tri-*n*-butylborane were taken as 0.74 and 0.68 g/cm³ respectively from the volumes and weights of the sample bulbs; the heat capacity of triethylborane was taken as 57.6 cal/mole °C [8], and the heat capacity of tri-*n*-butylborane was estimated to be 107 cal/mole °C.

The results of the experiments on the combustion of trimethylborane are given in table 1 where ΔRc is the corrected temperature rise of the calorimetric system [4], Δe is the deviation in the energy equivalent of the actual calorimetric system from that of the calibrated system, q_N is a correction for the heat of formation of nitric acid [4], WC is the Washburn correction [4], $q_{B(am)}$ is the correction for con-

TABLE 1. *Results of the experiments on the combustion of trimethylborane*

Experiment	ΔRc	Δe	n-$C_{16}H_{34}$	Filter paper	CO_2	H_3BO_3 titr.	q_N	WC	$q_{B(am)}$	S	$-\Delta E°$ (28 °C)
	Ohm	*j/ohm*	*g*	*g*	*g*	*Mole*	*j*	*j*	*j*	*Mole*	*kj/mole*
1	0.144332	72.5	0.12816	0.01085	1.04646	0.004726	0.5	3.0	40	0.0047855	2983.6
2	.125478	41.2	.13063	.01145	0.92999	.003657	1.0	2.6	174	.0039160	2964.0
3	.116465	24.0	.14520	.01136	.88888	.003053	0.4	2.4	113	.0032211	2974.4
4	.156235	68.8	.09554	.01185	1.08877	.005668	.0	3.2	129	.0058611	2998.8
5	.127848	34.4	.14098	.01030	0.95582	.003633	.0	2.6	107	.0037929	3007.7
6	.183669	38.7	.10816	.00837	1.26985	.006805	.2	3.0	190	.0070885	2960.6
Mean											2981.5
Standard deviation of the mean											±7.7

verting amorphous boron to crystalline boric acid, and $\Delta E°$ is the heat of the constant-volume process at 28 °C with all reactants and products in their respective thermodynamic standard states. The Washburn correction has been modified for these calculations to include the heat of solution of the combustion products in the aqueous portion. The mass of n-$C_{16}H_{34}$, of CO_2, and of sample, S, given in table 1 are corrected to vacuum; the weight of filter paper is not corrected to vacuum. Boron in the sample which was not found as boric acid was assumed to be present in the insoluble products as amorphous boron. For the conversion of amorphous boron, gaseous oxygen, and liquid water to crystalline boric acid, we used −670 kj/mole of amorphous boron as the heat of reaction. The calculation of $\Delta E°$ was based on the moles of trimethylborane calculated from the sample weight, because the use of auxiliary materials introduced errors in the determination of carbon dioxide formed in the combustion of the sample. The average ratio of the mass of carbon dioxide found in the products of combustion to the mass of carbon dioxide calculated from the masses of sample and n-hexadecane, and weight of filter paper was 0.9943 where the standard deviation of the mean was ±0.0024.

TABLE 2. *Results of the experiments on the combustion of triethylborane*

Experiment	ΔRc	Δe	q_{ign}	q_N	WC	CO_2	$-\Delta E°$ (29.8 °C)
	Ohm	*j/ohm*	*j*	*j*	*j*	*g*	*kj/g* CO_2
1	0.062858	−23.8	33.9	0.6	0.4	0.45323	18.793
2	.102274	1.6	34.0	1.0	.9	.73851	18.797
Mean							18.795

TABLE 3. *Results of the experiments on the combustion of tri-n-butylborane*

Experiment	ΔRc	Δe	q_{ign}	q_N	WC	CO_2	$-\Delta E°$ (29.8 °C)
	Ohm	*j/ohm*	*j*	*j*	*j*	*g*	*kj/g* CO_2
1	0.123530	−20.8	33.4	1.0	2.0	0.99797	16.805
2	.101518	1.6	33.1	1.0	1.6	.81913	16.822
Mean							16.814

The results of the experiments with triethylborane and with tri-n-butylborane are given in tables 2 and 3 respectively. In each case the calculations were based on the mass of carbon dioxide produced in the combustion process.

The results, corrected to the constant-pressure process at 25 °C, correspond to the reactions:

$$B(CH_3)_3(liq)+6\ O_2(g)\rightarrow H_3BO_3(c)+3CO_2(g)+3H_2O(liq), \quad (1)$$

$$\Delta H°(25\ °C)=-2989.4\pm22.4\ \text{kj/mole}=-714.48\pm5.36\ \text{kcal/mole},$$

$$B(C_2H_5)_3(liq)+21/2\ O_2(g)\rightarrow H_3BO_3(c)+6CO_2(g)+6H_2O(liq), \quad (2)$$

$$\Delta H°(25\ °C)=-4975.6\pm15.1\ \text{kj/mole}=-1189.2\pm3.6\ \text{kcal/mole},$$

$$B(n\text{-}C_4H_9)_3(liq)+39/2\ O_2(g)\rightarrow H_3BO_3(c)+12CO_2(g)+12H_2O(liq), \quad (3)$$

$$\Delta H°(25\ °C)=-8901.0\pm10.2\ \text{kj/mole}=-2127.4\pm2.4\ \text{kcal/mole}.$$

The uncertainties assigned to the above values have been taken as twice the standard deviation (or twice the average deviation) of the mean of the experimental values, combined with reasonable estimates of all other known sources of error.

The heats of formation of carbon dioxide (gas) and of water (liquid) were taken from the literature [9]; the heat of formation of crystalline boric acid was taken as −262.16±0.32 kcal/mole [10]. These were combined with the values given above to obtain the heats of formation of the liquids given in table 4.

The heat of vaporization of trimethylborane at 25 °C was calculated to be 4.83 kcal/mole from the calorimetric data of Furukawa and Park [8] and the vapor pressure data reported by Furukawa and Park [8] and by Stock and Zeidler [7]. The heat of vaporization of triethylborane at 25 °C was calculated to be 8.8 kcal/mole from the vapor pressure

data of Furukawa and Park [8]. The heat of vaporization of tri-*n*-butylborane was calculated to be 13.8 kcal/mole at 25 °C from the vapor pressure equation reported by Skinner and Tees [11]. These values were used to obtain the heats of formation in the gas phase for trimethylborane, triethylborane, and tri-*n*-butylborane given in table 4.

TABLE 4. *Heats of formation of trialkylboranes* $\Delta Hf°$ *(25 °C) in kcal/mole*

	Liquid	Gas
$(CH_3)_3B$	−34.79	−29.96
$(C_2H_5)_3B$	−47.2	−38.4
$(n\text{-}C_3H_7)_3B$		−52.3
$(i\text{-}C_3H_7)_3B$		−57.4
$(n\text{-}C_4H_9)_3B$	−83.2	−69.4
$(i\text{-}C_4H_9)_3B$		−74.5
$(sec\text{-}C_4H_9)_3B$		−72.6
$(t\text{-}C_4H_9)_3B$		−85.6

These heats of formation have been combined with the data on the hydrocarbons [12] to obtain values for the average B—C bond energy. The heats of formation at 25 °C of B(g), H(g), and C(g) were taken as 135.2, 52.1, and 171.3 kcal/g-atom, respectively [13]. The heat of formation of methane was used to obtain the average bond energy of the C—H bond in the methyl group. Combination of this value with the heat of formation of trimethylborane leads to 84.4 kcal/mole for the B—C bond. The data for ethane, propane, and butane were used to obtain values of the average bond energies of the C—H and C—C bonds in the higher alkyl groups. Combination of these values with the heats of formation of triethylborane and tri-*n*-butylborane leads to values of 84.3 and 84.3 kcal/mole, respectively, for the B—C bond. This value, together with the values of the C—C and C—H bond energies obtained for C_2H_6, C_3H_8, and $n\text{-}C_4H_{10}$, was used to calculate the heat of formation of tri-*n*-propylborane given in table 4.

The values for the isomeric propyl and butyl compounds given in table 4 were obtained from a comparison with the data on hydrocarbons [12]. The values, except for tri-*t*-butylborane, include only the effects of isomerization in the alkyl groups. The value for tri-*t*-butylborane includes a repulsive energy of 1 kcal for interaction between each pair of groups. It is felt that the uncertainty of these calculated values is ±5 kcal/mole.

Long and Norrish [14] have also measured the heat of combustion of liquid trimethylborane, but under slightly different conditions. A correction of their data for the value taken for the heat of combustion of the benzoic acid with which they calibrated their calorimetric system, for the heat of solution of the boric acid formed, for the atomic weight of carbon, and to 25 °C yields for the liquid: $\Delta Hc° = -714.80$ kcal/mole and $\Delta Hf° = -34.47$ kcal/mole.

Tannenbaum and Schaeffer [15] measured the heat of combustion of tri-*n*-butylborane and obtained for the reaction:

$$B(n\text{-}C_4H_9)_3\ (liq) + 39/2\ O_2(g) \rightarrow 1/2\ B_2O_3(c) + 12CO_2(g) + 27H_2O(liq)$$

$$\Delta H°\ (25\ °C) = -2117.6\ \text{kcal/mole}.$$

This value yields −2124.6 kcal/mole for the process corresponding to equation 3.

The data reported by Long and Norrish and by Tannenbaum and Schaeffer are in excellent agreement with the results of this investigation.

7. Discussion

Measurements of the heats of combustion of the alkylboranes, as well as of boron compounds in general, are subject to several uncertainties regarding the nature and thermodynamic states of the combustion products. The major portion of the boron is burned to form boric oxide which is then hydrated to boric acid; it is not known, however, if the hydration process is completed during the period when calorimeter temperatures are being observed. There is also some uncertainty regarding the amount and the concentration of aqueous boric acid. Although the assumption was made that the liquid water in the bomb was saturated with respect to boric acid at the final calorimeter temperature, this is very probably not true. Later we plan to do more work to supplement the two experiments reported for triethylborane and for tri-*n*-butylboran , and we hope at that time to obtain more information regarding the final state of the products.

It was necessary to use rigid Pyrex bulbs for the trimethylborane samples because of the high vapor pressure of the compound and to permit transfer of the material in vacuo. The use of flexible soft-glass bulbs for the triethylborane and tri-*n*-butylborane samples was attempted but they invariably broke during filling of the bomb; it appears that these liquids have abnormally high compressibility coefficients.

The use of soft glass for containing the sample is generally preferred, except in those cases which require the sample to be frozen or cooled to very low temperatures, because the bulbs are usually fused into small globules during the combustion process. Rigid Pyrex bulbs are usually not fused and some method must be employed to shatter the bulb completely; the sample may otherwise be entrapped within the bulb and burn in a limited supply of oxygen.

In the case of trimethylborane, the residues contained small amounts of a dark material, which was not soluble in water, and which indicated the presence of elemental carbon, elemental boron, or boron carbide. Although the amounts of elemental boron were too small for determination by the analytical methods employed, the possibility of its presence could not be eliminated. The quantity of boron carbide, although detected in the residue, was assumed to be negligible.

The residues from the triethylborane combustions appeared to contain extremely small amounts of

water-insoluble materials; the residues from the tri-*n*-butylborane contained no visible traces of insoluble material. This trend was to be expected, however, since the quantities of elemental boron or of boron carbide would be a function of the total amount of boron in the sample.

The heats of combustion and formation given in this paper are believed to be accurate within the limits of the assigned uncertainties. Additional measurements on compounds of higher purity would not appreciably reduce these uncertainties because they are chiefly caused by our inability at the present time to characterize accurately the nature and thermodynamic states of the combustion products.

8. References

[1] H. C. Dickinson, Bull. BS **11,** 189 (1915) S230.
[2] F. J. Prosen and F. D. Rossini, J. Research NBS **27,** 289 (1941) RP1420.
[3] M. V. Kilday, W. H. Johnson, and E. J. Prosen, J. Research NBS **65A,** 101 (1961).
[4] E. J. Prosen, Chapter 6, Experimental thermochemistry, F. D. Rossini, ed., (Interscience Publishers, Inc., New York, N.Y., 1956).
[5] E. Wichers, J. Am. Chem. Soc. **80,** 4121 (1958).
[6] F. M. Fraser and E. J. Prosen, J. Research NBS **55,** 329 (1955) RP2638.
[7] A. Stock and F. Zeidler, Ber. **54,** 531 (1921).
[8] G. T. Furukawa and R. P. Park, unpublished data, NBS, 1955.
[9] F. D. Rossini, D. D. Wagman, W. H. Evans, S. Levine, and I. Jaffe, Selected values of chemical thermodynamic properties, NBS Circ. **500** (U.S. Government Printing Office, Washington 25, D.C., 1952).
[10] E. J. Prosen, W. H. Johnson, and F. Y. Pergiel, J. Research NBS **62,** 43 (1959) RP2927.
[11] H. A. Skinner and T. F. S. Tees, J. Chem. Soc. **1953,** 3378.
[12] F. D. Rossini, K. S. Pitzer, R. L. Arnett, R. M. Braun, K. Li, H. J. Ries, P. A. Cowie, J. Mitchell, L. A. Parcella, M. B. Epstein, A. L. McClellan, M. H. Sarao, C. R. Decelles, and H. M. Flanagan, Selected values of physical and thermodynamic properties of hydrocarbons and related compounds (Carnegie Press, Pittsburgh, Pa., 1953).
[13] G. T. Armstrong, H. W. Woolley, W. H. Evans, and L. A. Krieger, private communication, 1960.
[14] L. A. Long and R. G. W. Norrish, Trans. Roy. Soc. (London) [A] **241,** 587 (1949).
[15] S. Tannenbaum and P. F. Schaeffer, J. Am. Chem. Soc. **77,** 1385 (1955).

(Paper 65A3–104)

JOURNAL OF RESEARCH of the National Bureau of Standards—A. Physics and Chemistry
Vol. 65A, No. 3, May–June 1961

Pyrolysis of Linear Copolymers of Ethylene and Propylene [1]

Sidney Straus and Leo A. Wall

(December 15, 1960)

The rates of volatilization of linear polymers of ethylene and propylene and their copolymers are somewhat characteristic of random degradation in that a maximum occurs in the rate curve for all polymers studied. Increasing amounts of propylene in the copolymer showed increases in the maximum rate on thermal decomposition. Minute inorganic and organic impurities added to the polypropylene have considerable effect on the thermal stability of the polymer by lowering the rates of volatilization and increasing the activation energy. Possibly there is an inhibition of the free-radical chain process, and the overall reaction becomes more like that for the initiation process. Rate studies and volatile decomposition products for a fully deuterated linear polyethylene were also determined, and its activation energy was calculated to be 70 kcal/mole, which is very close to the value (72 kcal/mole) calculated for the nondeuterated polymer. The effect of a large dose of beta-radiation on a linear polyethylene was also determined. Results suggest that scissions in the chain, as well as cross links, are caused by the radiation.

1. Introduction

Although the overall decomposition of linear polyethylene exhibits features indicating random degradation, the decomposition of branched polyethylene shows an entirely different pattern of behavior [1].[2] Theoretical treatment [2] of the degradation of branched chains, assuming various ratios for the probabilities of rupture of the bonds at the roots and at points distant from the roots of the branches, did not predict the experimentally observed behavior. More recently the same differences were observed between the results obtained from the decomposition of linear polypropylene and of branched polypropylene [3]. The experimental evidence suggests an increase of intramolecular transfer over intermolecular transfer in the decomposition of the branched polymers. A series of polyethylenes with different numbers and lengths of branches were studied earlier [3].

In the present work a linear polyethylene, a linear polypropylene, and four copolymers of ethylene and propylene combined in different percentages were thermally decomposed in order to study the kinetics of the various reactions involved and also to determine the effect on stability of systematically adding methyl side groups to a linear chain. The effects on thermal decomposition were also determined wherein inorganic impurities had been added to the polymers. In addition, thermal studies were made on a fully deuterated polyethylene polymer and on irradiated linear polyethylene.

[1] Presented in part before the 136th meeting of the American Chemical Society, Atlantic City, New Jersey, Sept. 13–18, (1959).
[2] Figures in brackets indicate the literature references at the end of this paper.

2. Experimental Procedures

The experimental polymers used in this work are listed in table 1. The first six polymers were obtained from the B. F. Goodrich Co. The last two were prepared in our own laboratory. Available data on weight percent of propylene in the copolymers and on approximate molecular weight are indicated. They were all checked for ash content. Another linear polypropylene was also studied which had an appreciable ash content. In this paper it will be referred to as polypropylene-B.

The polytetradeuteroethylene was prepared by polymerizing tetradeuteroethylene in sealed thick-walled hard-glass tubes at 20 °C by exposure to gamma rays for several days. The material received a total dose of approximately 0.5 Mr (megaroentgen). Polyethylenes produced under these conditions

TABLE 1. *Polymers investigated*

Polymer	Propylene content	Approx. mol wt
	wt %	
Polyethylene [a]	0.0	50,000
Polyethylene-propylene [a]	5.9	100,000
Do [a]	10.9	100,000
Do [a]	21.3	100,000
Do [a]	33.9	100,000
Polypropylene [a]	100.0	50,000
Polytetradeuteroethylene [b]		cross linked
Irradiated linear polyethylene [c]		cross linked; (10^6 before irradiation)

[a] Linear Ziegler-type polymers obtained from the B. F. Goodrich Co.
[b] Prepared with γ-irradiation.
[c] Irradiated with 800 kv electrons to a dose of 30 Mr.

show no methyl groups by infrared analysis. However, the polytetradeuteroethylene used in this work was somewhat cross linked.

Linear polyethylene used in previous work (1), which was prepared from diazomethane using boron trifluoride etherate as a catalyst, was irradiated and then pyrolyzed. It was irradiated with 800 kv electrons to a total dose of 30 Mr under nitrogen at the General Electric Co., through the courtesy of Dr. E. J. Lawton.

All the polymers were pyrolyzed in an apparatus wherein loss of sample in weight per minute could be determined by means of a tungsten spring balance inside a heated furnace [4]. In addition, several of the polymers studied were also decomposed in a tube furnace [5], after which the volatile products were analyzed by mass spectrometry.

3. Results

Rates of volatilization were studied on the ethyleneпropylene polymers by means of the tungsten spring balance apparatus at 400 °C; the results are shown in figure 1. All the polymers exhibited degradation curves with maxima, which are characteristic of linear olefinic polymers [1, 3]. With increasing amounts of propylene in the polymer the maximum rate of volatilization is increased.

Figure 2 shows the maximum rates plotted as a function of the percentage of propylene in the polymers in order to ascertain the relationship between the rates and composition. The downward curvature indicates relatively slower rates for the copolymers than what would occur on an additive basis. This curve may be of some utility for approximating the rates of volatilization at this temperature for other copolymers of ethylene and propylene.

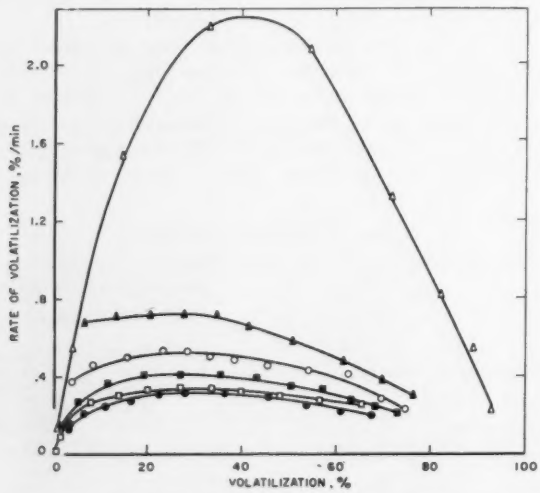

FIGURE 1. *Pyrolysis of copolymers of ethylene and propylene at 400 °C.*

Percentage of propylene in copolymers: ●, 0%; □, 5.9%; ■, 10.9%; ○, 21.3%; ▲, 33.9%; △, 100%.

Additional rate studies were made on the linear polyethylene and polypropylene polymers. The results are shown in figures 3 and 4. With increase of temperature, the maximum peak heights shift in position from about 25 percent volatilization at 400 °C to almost 35 percent at 420 °C in the case of polyethylene. Figure 3 indicates that some of the polymer is lost prior to the initial reading. This loss may arise from the fact that some of the polymer is degraded during the 15-min heating-up period that is required in order that the sample reach the temperature of pyrolysis [4], or from the presence of a small amount of low molecular weight material or some impurities in the polymer. Using the maximum rates at the three temperatures shown, an activation energy of 72 kcal/mole of linear polyethylene was calculated by means of the Arrhenius equation. This is the same value that was obtained by Madorsky on another linear polyethylene, after correction for temperature [6].

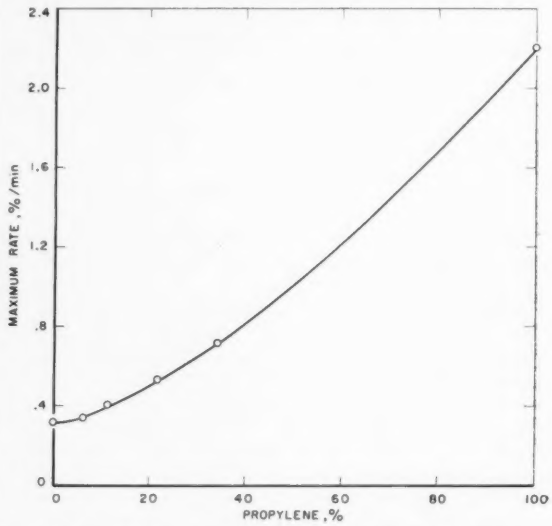

FIGURE 2. *Maximum rates of decomposition at 400 °C versus percent of propylene in copolymers of ethylene and propylene.*

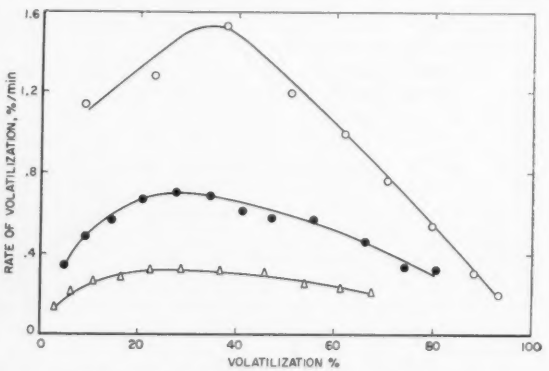

FIGURE 3. *Pyrolysis of linear polyethylene.*

△, 400 °C; ●, 410 °C; ○, 420 °C.

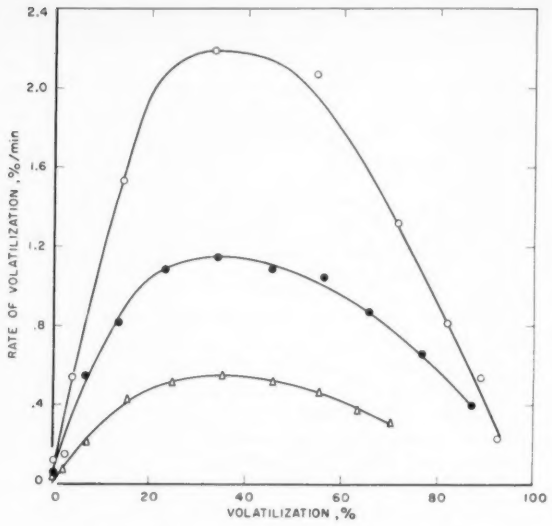

FIGURE 4. *Pyrolysis of linear polypropylene.*
△, 380 °C; ●, 390 °C; ○, 400 °C.

The maximum peak heights for the polypropylene polymer, as can be seen in figure 4, cover a broad area at approximately 30 to 40 percent volatilization. There is only a negligible loss of polymer during the heating-up period in this case, indicating a more clean-cut molecular weight distribution. An activation energy for polypropylene, likewise calculated on the basis of maximum rates at the three temperatures shown, was determined to be 59 kcal/mole, which compares with the value of 58 kcal/mole determined by Madorsky on another polypropylene polymer [6].

Another experimental polymer, designated here as polypropylene-B, was also studied for both rates of volatilization and analysis of its volatile products. The rates were found to be very inconsistent, depending upon the particular piece of sample selected. At similar temperatures the maximum peak heights varied considerably. In searching for the cause of this variability it was ascertained that the polymer contained some inorganic matter that was probably the cause for these inconsistencies. An "ash" analysis of the polymer showed from 1 to 2 percent of inorganic gray material. A spectrochemical analysis of this substance revealed the presence of relatively large amounts of aluminum, intermediate amounts of iron and silicon, and smaller amounts of titanium, magnesium, copper, calcium, tin, and zinc, in approximately that order. Apparently, an aluminum silicate catalyst or other catalysts had not been completely removed from the polymer in the polymerization process. In addition, the inorganic material was not uniformly mixed in the polymer, thus accounting for the conflicting results. Generally, the greater the ash content, the more stable was the particular sample.

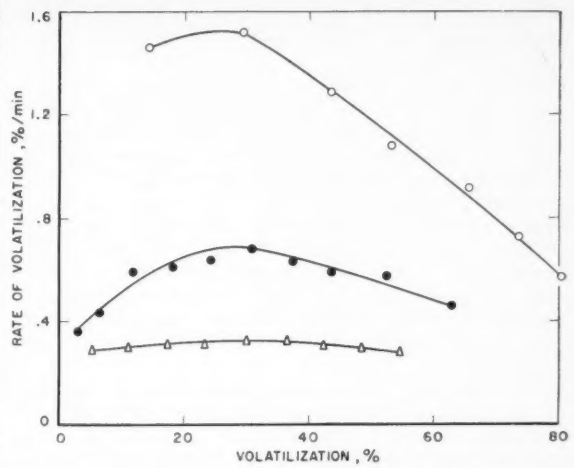

FIGURE 5. *Pyrolysis of polypropylene treated with hot xylene and in contact with inorganic impurities.*
△, 390 °C; ●, 400 °C; ○, 410 °C.

It was then decided to observe the effect of the presence of some of this inorganic material on the thermal decomposition of a relatively clean polypropylene polymer. The polypropylene previously studied was selected for this purpose. A very small amount of this inorganic material in the oxide form, approximately 0.2 mg, was allowed to remain at the bottom of the small platinum tray [4] after flaming to drive off the organic portion of the polypropylene-B. Approximately 5 mg of the uncontaminated polypropylene was then placed in the platinum tray and, as before, pyrolyzed at 400 °C. The polymer, in the form of a powder, melts at about 130 °C and flows to become a colorless glass. The rate of volatilization of the polypropylene was definitely lowered when in contact with the inorganic matter. The maximum rate of volatilization was reduced from 2.2 to less than 1 percent/min. In addition, the residue showed a definite brownish discoloration, whereas the pure polymer degraded to give a residue that remained colorless. Apparently a different depolymerization process was taking place while in contact with the inorganic material, and the pyrolysis of the original polymer was being inhibited.

Furthermore, it was also determined that after dissolving the pure linear polypropylene in hot xylene, evaporating off the solvent at 110 °C in a vacuum, placing the polymer in contact with the same inorganic material, and then pyrolyzing it at 400 °C the maximum peak height was reduced to approximately 0.70 percent/min. Rates of volatilization of the similarly treated polymer at temperatures of 390, 400, and 410 °C gave an activation energy of approximately 68 kcal/mole. The rates were reduced by a factor of approximately 3 and the activation energy increased by approximately 9 kcal/mole. These results can be seen in figure 5.

Figure 6 shows a comparison between the original polymer and the treated polymer when the percent

volatilized is plotted as a function of time for 400 °C pyrolysis in the tungsten-spring balance. The original polypropylene has a slower rate of volatilization initially; however, it then becomes rapid; over 90 percent of the polymer is degraded after 90 min. The treated polymer, dissolved in hot xylene, dried, and then pyrolyzed while in contact with the inorganic impurities degrades slightly faster initially but then progresses slower than the original polymer, until after 120 min of pyrolysis only 68 percent of the polymer has been degraded. The kinetics of this mechanism are not clear as yet, but apparently the original free-radical mechanism has been inhibited in some manner so that depolymerization under these new conditions has proceeded in a new direction.

The effect of xylene treatment alone on the rate of degradation of the polypropylene polymer is puzzling. When the polymer is dissolved in xylene and dried, it also yields a lower rate of volatilization at 400 °C, approximately 1.3 percent/min, except that initially there is a greater loss. In addition, the maximum peak heights cover a much broader area than in the case of pyrolysis of the untreated polypropylene. The xylene inclusion into the polymer might inhibit its breakdown if free radicals in the polypropylene react by removing a hydrogen atom from one of the methyl groups of the xylene. This would tend to stabilize the polymer by reducing its later transfer ability on thermal decomposition. The amount of xylene left in the polymer after drying is small, less than 0.1 percent by actual weight, but this evidently is sufficient to reduce the overall rate. The small amount of xylene present may also be the reason for the initial higher rate as compared to the case with no solvent in the polymer. It might be noted here that the presence of inorganic impurity in the linear polyethylene polymer or the treatment of this polymer in hot toluene has very little effect, if any, on its rate of decomposition.

As for the effect of the inorganic impurities, much more work will have to be done in this area of inhibition to polymers in general and to polypropylene in particular. Moreover, individual effects of inorganic materials as well as combined effects will have to be studied. In any event, the observed inhibition effect is most encouraging for future possibilities of stabilization, but theoretical interpretations will have to wait for more sophisticated kinetic experiments.

Polypropylene-B was also pyrolyzed in the tube furnace at 400 °C for a determination of the volatile products. The mass spectra of the light volatiles, about 13 percent of the total volatiles, was somewhat similar to that of a previous analysis obtained on a nonlinear polypropylene [7]. There were carbon compounds from C_1 through C_9, some of the larger components being pentane, hexene, pentene, butane, propylene, and ethylene, in diminishing order. The volatiles obtained from the clean polypropylene at 400 °C were also quite similar, except that the yield of monomer was somewhat greater than in the other two cases.

A study was also made on a fully deuterated linear polyethylene, both for the rate of decomposition and for a mass spectral analysis of its more volatile degradation products. Table 1 gives pertinent facts about the polymer. The rates of volatilization at 400, 405, 410, and 420 °C, shown in figure 7, all show maximum peaks similar to those for the undeuterated polyethylene (see fig. 3). The maximum peak heights are just slightly lower than those obtained for polyethylene at similar temperatures. The activation energy obtained for the deuterated polymer, based on these maxima, was calculated to be 70 kcal/mole.

This deuterated polyethylene was also pyrolyzed at 375, 425, 450, and 500 °C in the tube furnace and various fractions of the degradation products were collected. The monomer fraction, whose components are volatile at room temperature, amounted to about 3.5 percent of the total volatiles. Mass spectral analysis indicated deuterated compounds with up to 12 carbon atoms. No quantitative analysis could be made because of a lack of patterns

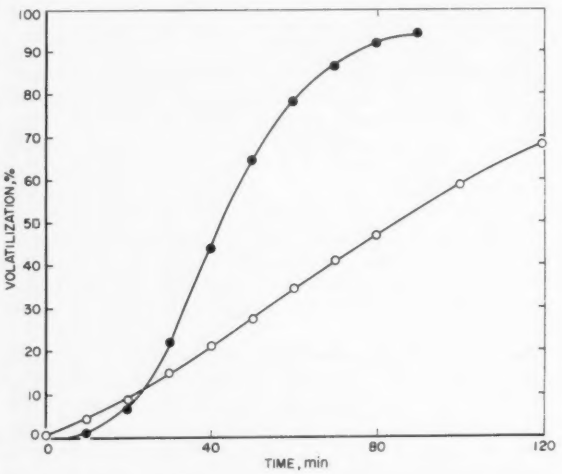

FIGURE 6. *Effect of impurities on amount volatilized versus time for polypropylene at 400 °C.*
●, Original polymer; ○, treated with hot xylene and in contact with impurities

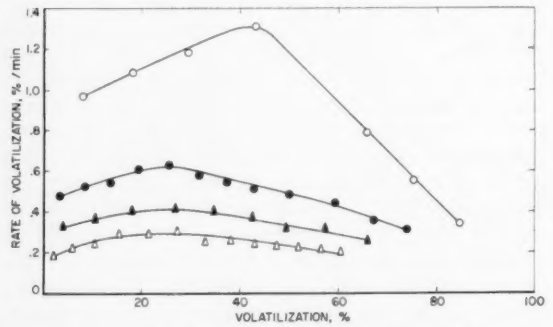

FIGURE 7. *Pyrolysis of polytetradeuteroethylene.*
△, 400 °C; ▲, 405 °C; ●, 410 °C; ○, 420 °C.

for deuterated compounds. However, there was a rough similarity between the spectra of the deuterated polymer and those of the hydrogen polymer. In that case, the heavier deuterated volatiles, the 97 percent waxlike fraction, should have had approximately the same average molecular weight as that previously determined cryoscopically for the hydrogen polymer volatiles, namely about 700 (8).

Finally, a linear polyethylene, approximately 1,000,000 molecular weight (see table 1) was given a large dose of radiation and then thermally decomposed at 400 °C in the tungsten-spring balance apparatus. A comparison of the rates with a nonirradiated polymer is shown in figure 8. The irradiated curve no longer shows a maximum as it does in the untreated polymer. Instead, the slope curves downward until about 35 percent volatilization and then almost coincides with the original polymer.

4. Discussion

The rates of volatilization, in percent of original sample per minute, for the linear polymers of ethylene and propylene and their copolymers, when plotted as a function of conversion to volatile products, produced curves characteristic, or nearly characteristic, of a net random degradation of linear chains [1,9]. It has been shown [3] recently that branched polyethylene and polypropylene do not exhibit the maximum-type curve but rather a continuously decreasing one, like curve A in figure 8.

Where maxima occur in the rate curves, they are used for evaluating the data because for random degradation a simple relation exists between the rate at the maximum and the overall rate constant for scission, k.

$$\left(\frac{dC}{dt}\right)_{\max} = \frac{kL}{e}.$$

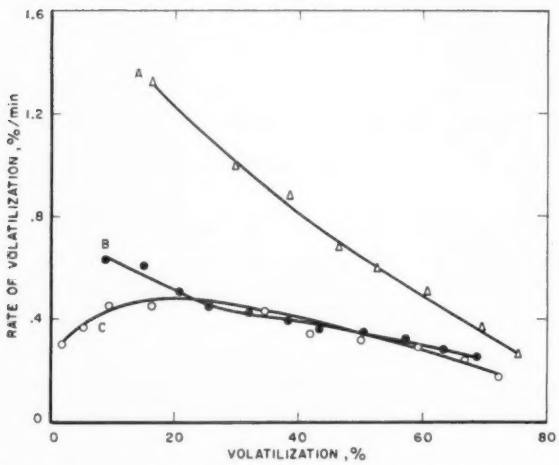

FIGURE 8. *Pyrolysis of beta-irradiated polyethylenes at 400° C.*
○, Linear unirradiated; ●, linear irradiated; △, branched unirradiated and irradiated.

The quantity L is the critical size for evaporation [10], i.e., species having a degree of polymerization equal to or greater than L must decompose before evaporating, and e is the base of the natural logarithms. The value of L for polyethylene has been determined to be 72, based on experimental measurement of the products of pyrolysis [10]. For polytetradeuteroethylene L is assumed to be same as for polyethylene. For polypropylene, where the monomer unit is larger, the molecular weight of the critical size for evaporation is assumed to be the same as for polyethylene, and therefore its L should be 48. A lower thermal stability will decrease L, while a lower cohesive energy density will increase it. Whatever assumption one makes as to the value of L, provided it is a reasonable one, the error in the calculated rate constant is unlikely to exceed 50 percent.

In table 2 the activation energies, E, and preexponential factors, A, for the overall rate constants are listed for the homopolyers studied. The copolymers of ethylene and propylene were compared only at 400 °C. Because of the lower activation energy for polypropylene it is clear that the difference in rates for the homopolymers of ethylene and propylene will be greater at lower temperatures. The trend in the copolymer rates (fig. 2) shows only a small tendency towards relatively increased stability for the copolymers; i.e., relative to a straight line between the rates for the homopolymers. This may be the result of the elimination of a small steric repulsion between methyl group of the propylene units when they are isolated from one another, as in the copolymers. The activation energies for polyethylene and polypropylene are large enough so that C—C bond dissociation may be occurring as the initiating step in the thermal decomposition. On the basis of a chain reaction for thermal decomposition one can roughly estimate [11] the dissociation energies as (99–2 E_2^1) for polyethylene and (85–2 E_2^1) for polypropylene, where E_2^1 is the activation energy for propagation in free-radical polymerization and is likely to be around 5 kcal/mole.

4.1. Irradiated Polyethylenes

Previously it has been observed (1) that branched polyethylenes, when pyrolyzed, produced rate-versus-conversion behavior of the type shown in figure 8, curve A, while linear polyethylene produced that in curve C. Irradiation of the branched polyethylene to a total dose of 30 Mr showed no

TABLE 2. *Activation energies for thermal decomposition*

Polymer	Rate at 400 °C	L	A	E
	%/min		*sec*$^{-1}$	*kcal/mole*
C_2H_4	0.32	72	$10^{17.6}$	72
C_2D_4	.30	72	$10^{16.9}$	70
C_3H_6	2.20	48	$10^{14.4}$	59
C_2H_6 (treated)	0.69	48	$10^{16.8}$	68

change in the rate of volatilization. However, it is now seen that, upon irradiation to 30 Mr, the linear polyethylene degrades to give curve *B*, which resembles *A*. The rates in the initial stages of pyrolysis are increased to an extent that the maxima in the curves are eliminated.

A priori, it is clear that cross linking alone would not lead to this behavior. Therefore some scission is indicated. It is possible that some very small molecules of the order of 1,000 to 5,000 molecular weight may contribute to the observed behavior; however, it is believed that scission combined with cross linking or primary radicals coupling with secondary ones produce a branched structure with long branches. The results support the speculation that long-chain branches are more effective in producing the behavior of the A-type curve than short-chain branching. The irradiation is not likely to produce short chain branches, and the amount of irradiation is unlikely to have produced many branches.

4.2. Polytetradeuteroethylene

The polymer polytetradeuteroethylene was produced by gamma-ray-initiated polymerization and was somewhat cross linked. The relatively high rates (see fig. 7) during the early stages of pyrolysis may be the result of the phenomena seen with the irradiated linear polyethylene (fig. 8). It was not expected that deuteration would produce a relatively large detectable effect in this polymer as it did in polystyrene [12]. Isotope effects on the elementary processes may cancel out and not affect the overall rate. For instance, the expected reduction in the rate of transfer may have been compensated by an increase in the rate of initiation. Evidence for an increase in the dissociation rate of hexadeuteroethane into trideuteromethyl radicals over that of ethane has been reported [13]. In polystyrene the monomer yield on degradation increases from 40 to 70 percent upon alpha deuteration [14]. Since the monomer yield for linear polyethylene is of the order 0.1 percent [15] the yield from polytetradeuteroethylene would not be expected to exceed 0.2 percent. Detection of such a change in the present experiments would be extremely difficult because of minor variations in the pyrolytic technique. Lack of mass spectra for larger deuterocarbons which interfere with the mass spectrometric analysis of tetradeuteroethylene also hindered monomer yield determination for this polymer. No appreciable difference was observed in the distribution of pyrolysis products between polyethylene and polytetradeuteroethylene.

4.3. Inhibition Effect

The inhibition effect of impurities derived from the catalytic agents used in preparing the polypropylene is difficult to understand. The changes produced in the activation energy and pre-exponential factor are compatible with an inhibition of a free-radical chain process, where the overall activation energy becomes closer to that for the initiation process. One suspects that the impurities may have some dehydrogenating effect. The fact that xylene has a small effect in spite of its volatility at the temperature of pyrolysis suggests radical abstraction of hydrogen in the methyl groups of xylene, producing some stable unreactive radicals. Unsaturated groups in the polymer may have a similar effect.

These results contrast those reported [16] for the polyamides, where traces of acid-polymerization catalyst tend to accelerate thermal decomposition. With polytetrafluorethylene some inhibition has been observed [17] when the material is pyrolyzed under fluorine or hydrogen.

5. References

[1] L. A. Wall, S. L. Madorsky, D. W. Brown, S. Straus, and R. Simha, J. Am. Chem. Soc. **76,** 3430 (1954).
[2] R. Simha, J. Chem. Phys. **24,** 796 (1956).
[3] L. A. Wall and S. Straus, J. Polymer Sci. **44,** 313 (1960).
[4] S. L. Madorsky, J. Polymer Sci. **9,** 133 (1952).
[5] S. Straus and S. L. Madorsky, Ind. Eng. Chem. **48,** 1212 (1956).
[6] S. L. Madorsky, J. Research NBS **62,** 219 (1959) RP2957.
[7] S. L. Madorsky and S. Straus, J. Research NBS **53,** 361 (1954) RP2553.
[8] S. L. Madorsky, S. Straus, D. Thompson, and L. Williamson, J. Research NBS **42,** 499 (1949) RP1989.
[9] R. Simha and L. A. Wall, J. Phys. Chem. **56, 707** (1952).
[10] R. Simha and L. A. Wall, J. Polymer Sci. **6,** 39 (1951).
[11] L. A. Wall, to be published.
[12] L. A. Wall, D. W. Brown, and V. F. Hart, J. Polymer Sci. **15,** 157 (1955).
[13] L. A. Wall and W. J. Moore, J. Am. Chem. Soc. **73,** 2840 (1951).
[14] S. Straus and S. L. Madorsky, J. Research NBS **50,** 165 (1953) RP2405.
[15] L. Wall and R. E. Florin, J. Research NBS **60,** 451 (1958).
[16] S. Straus and L. A. Wall, J. Research NBS **63A,** 269 (1959).
[17] L. A. Wall and J. D. Michaelsen, J. Research NBS **56,** 27 (1956).

(Paper 65A3–105)

JOURNAL OF RESEARCH of the National Bureau of Standards—A. Physics and Chemistry
Vol. 65A, No. 3, May–June 1961

Pyrolysis of Fluorocarbon Polymers*

Leo A. Wall and Sidney Straus

(December 15, 1960)

The thermal decomposition of various fluorocarbon polymers were investigated; volatile products of the decomposition were determined along with the overall rates of volatilization, and from these rates the activation energies were calculated for the thermal degradation reactions. The thermally most stable of all the polymers thus far studied are the completely fluorinated ones. However, evidence from a study of the decomposition of hexafluoropropylene telomers and from the study of a copolymer of tetrafluoroethylene and hexafluoropropylene suggests that the homopolymer of hexafluoropropylene, if it could be made, would be quite unstable. The photoinduced decomposition of polytrifluorochloroethylene was also investigated, and estimates of the activation energies were obtained for the various elementary steps of the decomposition mechanism. The photoinduced experiments indicated that mutual termination of the radical intermediates takes place and that a diffusion effect on depropagation becomes pronounced below 250 °C.

1. Introduction

Knowledge of the thermal decomposition mechanisms of fluorocarbon materials and the influence of molecular structure on their thermal stability is fairly limited. There is ample evidence that linear perfluoroaliphatic substances have a high thermal stability [1, 2][1] but few if any results are available for branched and aromatic perfluorocompounds or for the various copolymers containing fluorine, which are becoming important commercially. The mechanism of depolymerization or decomposition of these materials, with the possible exception of polytetrafluoroethylene [3 to 7], is also in need of extensive investigation, since such information would be useful in understanding the problems involved in the development of thermally more stable materials. There are numerous possible polymeric structures not yet synthesized. Studies on small molecules reported and discussed in this article will aid, it is hoped, in establishing the polymeric structures that are desirable for high-temperature polymers and hence will narrow down the number of objectives for synthesis research.

2. Materials Studied

Perfluoroamidine Polymers. These polymers were received from H. C. Brown of the University of Florida. They were prepared by heating perfluoroamidines [8] which then polymerized by splitting out ammonia and forming triazine rings. Three polymers were studied:

Polymer A1. A polymer of perfluoroglutarodiamidine alone. It was a hard brittle solid and was not soluble in any of the usual organic solvents. It was presumably a highly cross linked material composed mainly of the following structure:

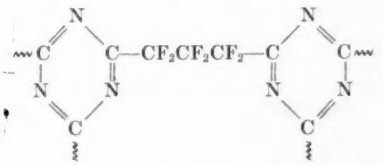

Polymer A2. A copolymer of perfluoroglutarodiamidine and perfluorobutyroamidine in a 1 to 1 molar ratio. It was a milky white, somewhat elastomeric solid, slowly soluble in pyridine and in ethylene diamine, with mainly the following structure:

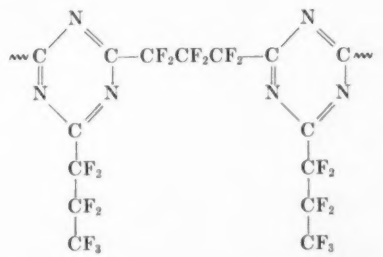

The polymer must, of course, be highly branched. A few solution measurements tended to support this conclusion. Viscosity measurements were made using pyridine as a solvent. Solution of the sample required 5 to 6 days at room temperature using a wrist-action mechanical shaker. The concentration of the solution was 1.53 wt-percent. Viscosity measurements were made on the 6th, 13th, 20th, and 27th day using a Ubbelohde viscometer. On the 6th day the specific viscosity was 0.094. On the 13th day the specific viscosity had dropped to 0.044 at which value it remained even after 27

*Based on research sponsored by the Office of Naval Research and the Bureau of Naval Weapons, U.S. Navy.

[1] Figures in brackets indicate the literature references at the end of this paper.

days. Assuming the molecules are spherical, one calculates a specific viscosity near 0.03. In view of the method of synthesis for this polymer, the close agreement between the calculated value and the experimental measurements suggests a highly branched molecule. The disaggregation indicated by the viscosity measurements between the 6th and 13th day may mean that solution in pyridine occurs with slow degradation. The material when recovered from solution was a brown wax and had none of the rubbery character of the original material.

FEP 100–X. A copolymer of tetrafluoroethylene and hexafluoropropylene. It is a thermoplastic material available from the DuPont Co.

VFHP–A. A copolymer of vinylidene flouride and hexafluoropropylene. It is a milky-white elastomeric gum available from the DuPont Co.

F. A polymer of chlorotrifluoroethylene. It is a thermoplastic material available from Minnesota Mining and Manufacturing Co. The sample used was Grade 300 molding powder with a reported number-average molecular weight of approximately 350,000. Data from previous work [10] on other samples of this polymer are used for comparison purposes in this article.

F 3700. A copolymer of chlorotrifluoroethylene and vinylidene fluoride. It is a white elastomeric gum. From analysis which showed that it contained 11.3 wt percent chlorine, it was calculated to be 24.4 mole percent chlorotrifluoroethylene.

F 5500. A copolymer similar to F 3700. Analysis showed that it contained 15.5 wt percent chlorine or 36.2 mole percent chlorotrifluoroethylene.

Polymer A3. A copolymer of perfluoroadipodiamidine and perfluorobutyroamidine in a ratio of 1 to 1.35. This copolymer was also a milky white, somewhat elastomeric substance, slowly soluble in pyridine. Its structure was presumably the same as that for A2, except for the additional difluoromethylene group, CF_2, in the diamidine unit. The compounds A2 and A3, when first prepared, were yellow tacky gums which became milky white some what elastomeric substances when heated in the air for several days at 350 °C. This behavior was somewhat erratic for certain samples of the yellow gums which when stored for several months failed to cure to white elastomeric substances when heated to 350 °C. Also heating for longer times tended to remove entirely the elastomeric character. The data reported here are for the two copolymers after curing at 350° C. The thermal stability of uncured samples was much poorer, indicating that curing does not occur under the vacuum conditions used in the test, at least not without a large amount of the material volatizing.

Polyhexafluoropentylene adipate. An experimental polymer [9] made at the Hooker Electrochemical Co. having the formula

$$\sim[(CH_2)_4\text{—}\overset{\overset{O}{\|}}{C}\text{—}O\text{—}CH_2(CF_2)_3CH_2O\text{—}\overset{\overset{O}{\|}}{C}]\sim$$

It is a milky-white tough gum with a reported number-average molecular weight of approximately 17,000.

Polytrifluoroethylene. Prepared for this study by polymerizing trifluoroethylene in a rocking bomb using aqueous persulfate as a catalyst and heating for 24 hr at 160 °C.

Telomers of Hexafluoropropylene. The pyrolysis of the following telomers of hexafluoropropylene [11,12] was also investigated.

Telomer PPF9A. A white wax having a number-average molecular weight of 1,541. Its average structure is represented by the formula

$$C_3F_7(CF_2CF)_9F.$$
$$\quad\quad\quad

The apparatus and experimental procedure for obtaining the rates of thermal decomposition for high polymers have been described in detail [14, 15]. It is essentially a technique for measuring the weight loss as a function of time. A very sensitive tungsten helical spring balance is used to suspend a 5 to 6 mg sample in an evacuated space. A small platinum or glass crucible is used to contain the polymer. The glass crucible gives better results when the sample does not melt and flow, presumably because radiant heat passes through the glass. The deflection of the tungsten spring is determined by means of a cathetometer. A thermoregulated furnace is raised to surround the suspended sample at the beginning of an experiment. A graph is made of the weight loss as a function of time, from slopes of which the rates at various times or conversions are obtained and plotted. From the shapes of these characteristic curves certain aspects of the thermal decomposition mechanism are obtainable [16–18].

The procedures described above were not applicable to the low molecular weight telomers of hexafluoropropylene. These materials would merely distill without decomposing. A variation of a technique that is often used [19, 20] for small molecules such as in a recent investigation of the thermal decomposition of certain phosphinoborines [21], was therefore employed.

The procedure used for the hexafluoropropylene telomers was as follows:

Samples of 100 ± 1 mg were weighed in a small bucket, and the bucket placed inside a 10 ml ampule. Ampules and weighing buckets of both glass and nickel were used in order to ascertain whether the container composition influenced the thermal decomposition. These ampules were then evacuated, generally eight at a time, to 10^{-4} mm of mercury. After evacuation, argon gas was introduced simultaneously into all eight tubes. The gas was previously purified by passing through a silica gel trap cooled to 197 °K in order to eliminate, as much as possible, water and oxygen. The amount of argon introduced was sufficient to give a pressure of about 50 to 100 mm of mercury. The moles of argon in each tube thus corresponded to approximately three times the moles of material to be pyrolyzed, and each tube contained to within ± 1 percent the same amount of telomer and argon. After introduction of the argon, each tube was sealed off. The nickel ampules were connected via a Kovar-Pyrex seal to a Pyrex tube. The ampules were pyrolyzed in a large copper furnace thermoregulated to ± 1 °C. The pyrolysis products and also a sample of the argon were analyzed by means of a mass spectrometer, and the ratio of product to argon permitted the calculation of yield of the products of pyrolysis.

4. Results

Pyrolysis of the three perfluoroamidine polymers for 30-min periods gave the data shown in table 1. It was found that quite high temperatures were required to cause an appreciable amount of volatilization. The first two columns list the temperature of pyrolysis and the initial weight of sample. The third column gives the weight loss in percent of original sample, and the final column gives the percent of the total products that were volatile at room temperature. The gas fraction was negligible and is not listed. The percent of heavy wax can be obtained by subtracting the percent light volatiles from 100. The residues in all cases were brown to black spongy solids, depending on temperature. The wax fraction which was brown in color, was obtained in greatest quantity from the elastomeric A3 material and least from the most cross linked brittle A1.

Mass spectrometric analysis of the light volatiles from the perfluoroamidine polymers are shown in table 2. The data for the A2 polymer were obtained at 489 °C, those for the other two at 470 °C. For all three polymers the major product found in the light volatiles was tetrafluoroethylene, the actual yields of which in weight percent of the total amount volatilized were 50, 20, and 4, respectively, for the polymers A1, A2, and A3. It is somewhat surprising that no nitrogen-containing product was identified in the light volatile fraction. The silicon tetrafluoride must come from reaction with the glass in the pyrolysis apparatus, either via the formation of hydrogen fluoride or from the reaction of the fluorocarbon fragments with the glass at the high temperatures of the furnace. The latter reaction may also account for some of the CO_2 found with the A3 polymer. The extent of reaction with the glass would be expected to depend, among other things, on the temperature. At 500 °C the A2 polymer showed 12 mole-percent silicon tetrafluoride in the light volatiles. In addition to the listed compounds, about 10 wt-percent of the light volatiles were unidentifiable compounds. The hydrocarbons listed for A1 must be the result of some solvent contamination. Most of the carbon dioxide probably comes from carboxyl groups in the polymer derived from the original amidine groups.

Infrared spectra were obtained on the original polymers, A1 and A2, and on their residues at about 11 to 14 wt-percent pyrolysis. The spectra in each case for the original and pyrolyzed polymer were

TABLE 1. *Pyrolysis of perfluoroamidine polymers* [a]

Polymer	Temperature	Weight of sample	Total volatilized products	Light volatiles [b]
	°C	mg	%	%
A1	430	20.4	3.5	70.4
	470	22.3	6.5	68.3
	503	18.5	13.8	66.7
A2	415	32.6	3.5	41.1
	455	27.4	6.0	34.5
	489	30.8	13.0	40.0
	505	20.9	21.1	46.0
A3	470	26.3	31.0	12.5
	510	20.9	62.7	15.9

[a] Thirty-minute periods of pyrolysis.
[b] Based on amount of total volatiles.

TABLE 2. *Representative analysis of light volatiles from pyrolysis of perfluoroamidine polymers*

Components	A1	A2	A3
	Mole %	*Mole %*	*Mole %*
C_3F_{10}			0.3
C_4F_8			.3
C_3F_8		0.9	1.5
C_3F_6	1.0	2.6	3.7
C_2F_6		14.0	3.6
C_2F_4	75.7	51.6	34.7
CF_4	6.3	17.3	17.5
SiF_4		0.7	15.0
CO_2	13.7	12.9	23.4
C_4H_8	0.7		
C_3H_6	.9		
C_2H_4	1.7		

essentially identical with the exception of minor differences related to particle size and clarity of the KBr pellet used in the infrared technique. There was, however, a small carbonyl band at about 5.7μ in the original samples which was eliminated during the pyrolysis.

Without analyzing or collecting products, a few longtime weight losses were measured on the A2 polymer at 355 °C and 400 °C. At 355 °C the polymer was heated for 180 hr, 136 hr of which were in a vacuum and the remainder in air. The sample lost 2.6 percent of its weight in the first hour and 5.2 percent during the remaining 179 hr. At 400 °C the polymer upon heating 41 hr in a vacuum lost 3.1 percent in the first hour and 7.7 percent of its initial weight in the remaining 40 hr. Thus, neglecting the weight losses in the first hour, the rate of weight loss at 355 °C and 400 °C were, respectively, 0.00048 and 0.0032 percent/min. These results agree quite well with those calculated using the Arrhenius relationship and the data obtained from the rate studies in the region of 500 °C. At 355 °C the calculated rate is 0.00054 percent/min.

In figures 1, 2, and 3, the rates of volatilization of the perfluoroamidine polymers are shown as a function of the conversion to volatile products. The shapes of these rate curves indicate a rather complex mechanism. Initially very fast, they drop at 20 to 30 percent conversion to a value which tends to be constant up to about 70 percent conversion. Arbitrary extrapolations were made as shown by the dashed lines to obtain an apparent initial rate. From such initial rates activation energies were calculated. Straight-line Arrhenius plots were obtained. Extrapolation from higher conversion portions of the curves (see figs. 1 and 2) would not greatly alter the activation energy calculated.

A study was made of the effect of small amounts of acid and methanol on the pyrolysis of the A2 polymer. After various treatments, the polymer was dried, preheated to 110 °C in vacuum for 1 hr, and then pyrolyzed at 500 °C. A small sample held in methanol containing 0.2 percent sulfuric acid for 50 days doubled the rate. However, methanol alone for 50 days also doubled the rate and a methanol

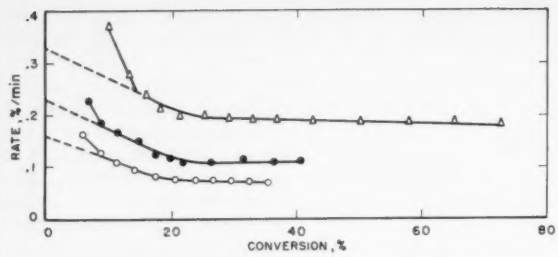

FIGURE 1. *Rate of volatilization versus conversion for polymer A1.*

△, 513 °C; ●, 501 °C; ○, 491 °C.

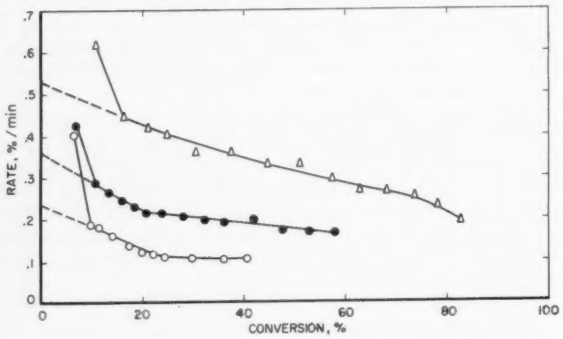

FIGURE 2. *Rate of volatilization versus conversion for polymer A2.*

△, 513 °C; ●, 502 °C; ○, 491 °C.

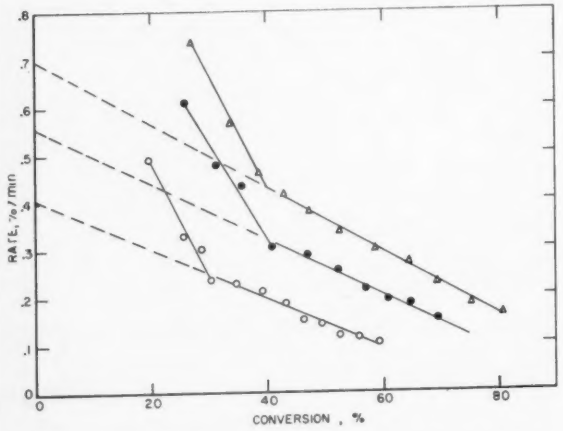

FIGURE 3. *Rate of volatilization versus conversion for polymer A3.*

△, 500 °C; ●, 490 °C; ○, 480 °C.

soaking for 7 days increased the rate by 50 percent. Methanol treatment for 30 min had no effect on the rate, i.e., the initial rate determined by extrapolation (see fig. 2). Methanol treatment tended to slow the actual high initial rate. The polymer A2 could be swollen in methanol, though it does not dissolve.

Possibly small molecules were washed out by the methanol treatments. Polymer swollen by methanol crumbled easily on touching, but when redried shrank back to its original shape and had apparently all its original elastomeric properties. All samples immersed in methanol slowly became yellow in color. The longer the material was immersed, the more intense was the color. The sample treated with methanol for 30 min became black when heated in vacuum at 400 °C for 1 hr. After a similar heating, an untreated sample would be tan in color.

These results suggest that methanol has a definite degrading effect on the polymer. Water in the methanol may be partly involved in the degradation, except that water alone would not swell the material.

4.1. Polyhexafluoropentyleneadipate

Pyrolysis of this material produced only a small quantity of light volatiles (see table 3). About 30 percent of the light volatiles for this polymer could not be identified; some of them contained fluorine, and the remainder were hydrocarbons and carbon dioxide. The relative proportions of the identified compounds are given in table 4. One would have expected some silicon tetrafluoride from this polymer. The rate of volatilization as a function of conversion is presented on figure 4. This polymer shows an unexpected rate behavior. Polyamides and polyesters usually produce rates that pass through a maximum [22, 23] when plotted against conversion or time.

4.2. FEP 100–X

This material produces somewhat less light volatiles (see table 3) than pure polytetrafluoroethylene, TFE, 75 to 84 percent as compared to about 95 percent for the latter. The main products (see table 4) are the two monomers tetrafluoroethylene and hexafluoropropylene, the latter being more abundant in the initial stages of degradation. At 10 percent decomposition the light volatiles analyzed 85 percent C_3F_6 and 9 percent C_2F_4, while at 92 percent decomposition analysis gave 19 percent C_3F_6 and 68 percent C_2F_4. From the results at the higher conversion it seems evident that the composition of FEP 100–X is about 22 mole percent hexafluoropropylene and 78 mole percent tetrafluoroethylene.

As seen also from the rate behavior (fig. 5), there appear to be two stages in the degradation. The rate at first drops quickly, but then after about 30 percent conversion it decreases much more slowly. With the exception of the first portion, the rate curves are similar to those found for polytetrafluoroethylene [3] and are compatible with the relatively high yield of monomer [16 to 18]. The initial more rapid degradation suggests a much lower stability of chain segments containing the hexafluoropropylene units. Also the somewhat lower monomer yield suggests more of the transfer type reactions [18] than occur in the pyrolysis of polytetrafluoroethylene.

TABLE 3. *Pyrolysis of fluorinated polymers* [a]

Polymer	Temperature	Wt. of sample	Total volatilized products	Light volatiles [b]
	°C	mg	%	%
Polyhexafluoropentyleneadipate	350	28.4	39.5	3.9
	415	28.4	98.9	2.6
FEP 100 X	455	38.5	10.8	83.9
	478	30.8	21.8	83.1
	505	21.5	39.4	79.2
	545	18.4	92.4	75.0
VFHP–A	385	16.4	12.5	40.0
	405	30.9	57.1	34.7
	500	19.8	94.9	30.0
F 3700	355	22.5	4.5	32.0
	380	17.6	24.2	25.5
	405	21.5	85.4	23.1
F 5500	375	24.6	10.8	17.4
	405	21.1	56.6	15.7
	435	19.3	99.2	10.6

[a] Thirty-minute periods of pyrolysis.
[b] Based on amount of total volatiles.

TABLE 4. *Representative analysis of light volatiles from the pyrolysis of various fluoropolymers in mole percent from mass spectrometer*

Components	Hexafluoropentyleneadipate polymer [a]	FEP 100–X	VFHP–A	F elastomers
	400 °C	478 °C	400 °C	400 °C
C_4F_8		2.0		
C_3F_8		0.4		
C_3F_6		54.8		
C_2F_6		0.5		
C_2F_4		35.6		
SiF_4		1.3	80.0	80.3
C_4H_{12}	2.8			
C_4H_8	12.7			
C_2H_4	7.8			
CH_4	3.3			
CO_2	73.4	5.4	14.7	7.8
HCl				11.9
SO_2			5.3	
Totals	100.0	100.0	100.0	100.0

[a] For this polymer, about 30 mole percent of the light volatiles were not identifiable.

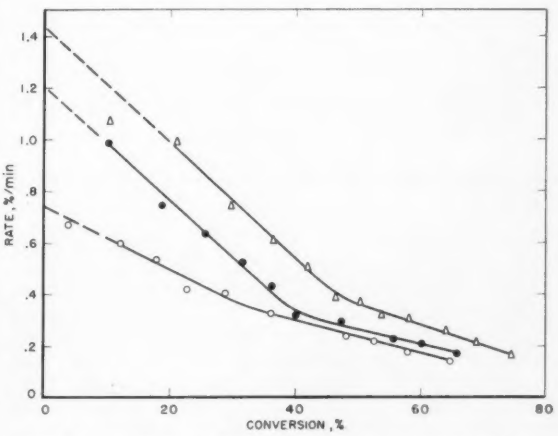

FIGURE 4. *Rate of volatilization versus conversion for polyhexafluoropentyleneadipate.*

△, 345 °C; ●, 340 °C; ○, 330 °C.

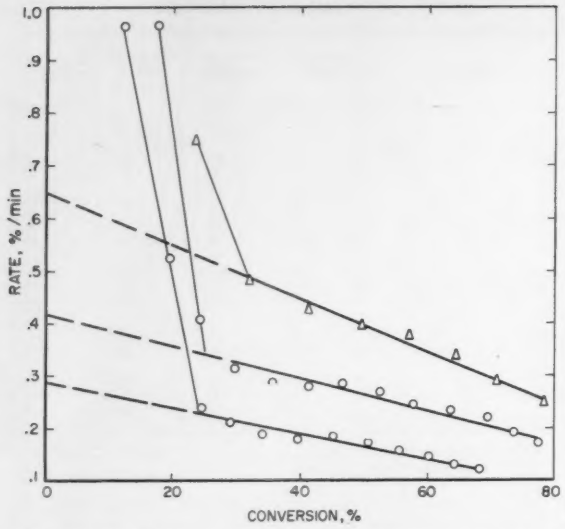

FIGURE 5. *Rate of volatilization versus conversion for FEP 100 X.*

△, 398 °C; ●, 499 °C; ○, 490 °C.

4.3. VFHP, F 3700, and F 5500

These three polymers gave very similar results on thermal decomposition, which is not surprising since all three are copolymers containing vinylidene fluoride as one of the monomers. In table 3 it is seen that the amount of light volatiles decreases in the order in which the polymers are listed above, or conversely, the amount of heavy volatiles or wax-fraction increases. The major volatile product is hydrogen fluoride, which reacts with the glass of the apparatus to form the silicon tetrafluoride listed in table 4. The rate curves (figs. 6, 7, and 8) are similar in character, all showing maximums which suggest that the mechanism of breakdown can be considered to be approximately a random one. An ideal random degradation would have the maximum occurring at 26 percent conversion. About the same range of temperatures is used to study the decomposition of all three polymers.

4.4. Polytrifluoroethylene and Poly-1,1-difluoroethylene

Polytrifluoroethylene has been partially investigated [24] previous to this work. Its major products of thermal decomposition are hydrogen fluoride and heavy unidentified species found in the wax fraction which comprised about 80 percent of the material volatilized during decomposition. The rate data are presented in figure 9. The curves are quite close in shape to those predicted for an ideal random decomposition of the main chain. Another process dehydrohalogenation, is, of course, simultaneously occurring, as is evidenced by the production of appreciable hydrogen fluoride [24].

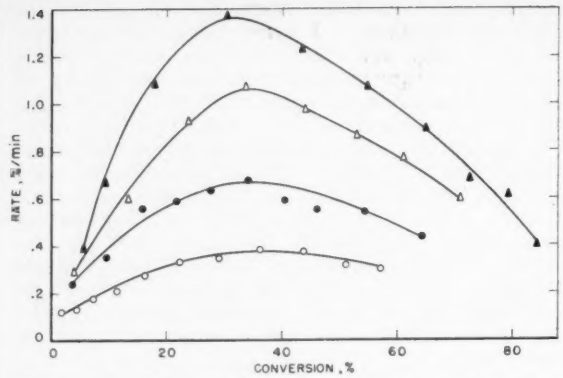

FIGURE 6. *Rate of volatilization versus conversion for VFHP–A*

▲, 405 °C; △, 400 °C; ●, 395 °C; ○, 385 °C.

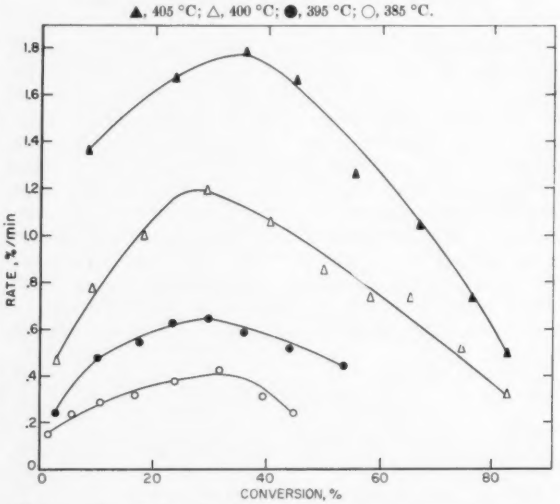

FIGURE 7. *Rate of volatilization versus conversion for F 3700.*

▲, 395 °C; △, 389 °C; ●, 380 °C; ○, 375 °C.

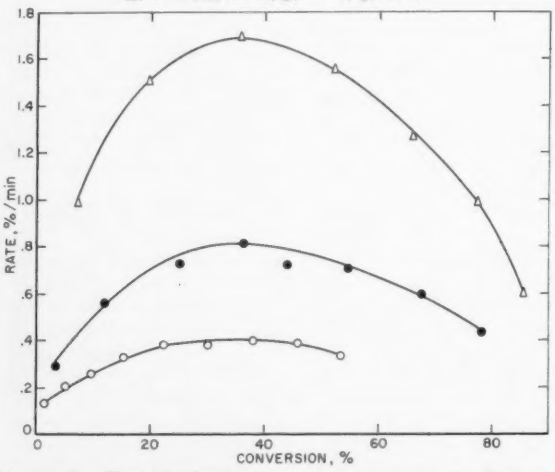

FIGURE 8. *Rate of volatilization versus conversion for F 5500.*

△, 395 °C; ●, 385 °C; ○, 375 °C.

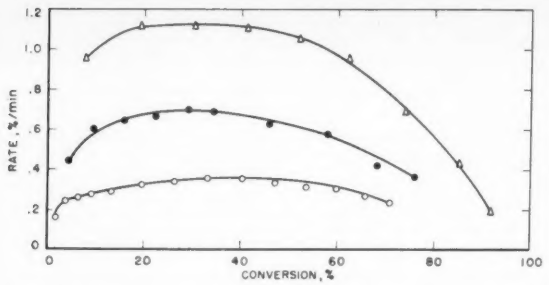

FIGURE 9. *Rate of volatilization versus conversion for polytrifluoroethylene.*

△, 420 °C; ●, 410 °C; ○, 400 °C.

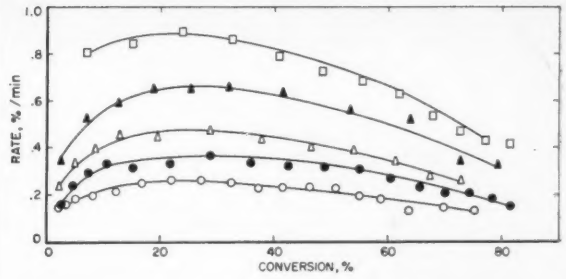

FIGURE 10. *Rate of volatilization versus conversion for polytrifluorochloroethylene.*

□, 371 °C; ▲, 366 °C; △, 361 °C; ●, 356 °C; ○, 351 °C.

Poly-1,1-difluoroethylene has been studied by other workers [25]. It produces more copious quantities of hydrogen fluoride and leaves a charred-appearing residue amounting to about 40 percent of the polymer sample pyrolyzed. However, over the first 60 percent of conversion the rate curves resemble those for polytrifluoroethylene in that a pronounced maximum in the rate occurs. Neither of these two polymers produce more than trace amounts of monomer.

4.5. Polytrifluorochloroethylene

Polytrifluorochloroethylene (F) has been the subject of a previous study [10]. The major fraction, 70 wt percent, produced was the wax or heavy fraction. The light volatiles amounted to approximately 28 wt percent of the material volatilized and was mainly monomer. The temperatures of previously reported rate studies have recently been corrected [26] and hence the activation energy also was corrected. The same data have been replotted in the manner used in this article and are presented in figure 10. The curves are again typical for random degradation and exhibit maximums in the rates. Our evaluation of the activation energy, discussed later in this article, is based on the maximum rates and is somewhat lower than all other values reported [10, 18, 26].

The photoinduced thermal depolymerization of F was explored using a medium-pressure quartz mercury lamp and a quartz window on the pyrolysis chamber. The apparatus was similar to that used previously [27], and a recording Pirani gauge was used to measure the rate of evolution of the light volatiles. The rate as recorded followed the pattern schematically shown in figure 11. Under appropriate conditions of temperature, usually about 100 °C below the normal pyrolysis temperatures, all polymers so far studied behave to some extent in the manner shown. The polymer, F, gave a fairly strong response to the ultraviolet light used and was studied in some detail because its light volatile fraction is mainly monomer. When the polymer is exposed to the light the rate rapidly rises to an essentially constant rate, which drops relatively

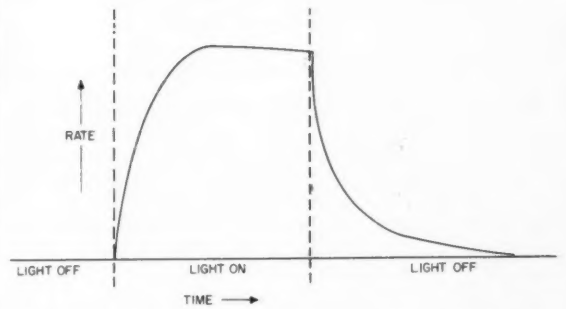

FIGURE 11. *Rate behavior during UV irradiation and post irradiation.*

slowly when the light is turned off. The time of the light and dark periods was roughly about 30 min. From both the photo rate, during continuous exposure to the light, and from the rate during the post-irradiation period, valuable information is obtained about the mechanism of decomposition. During post-irradiation the rate is in theory proportional to the concentration of intermediate radicals. From the time dependence of this rate, one can establish how this radical terminates. If the radical terminates bimolecularly, then a plot of the reciprocals of the rate of monomer production, V, during the post-irradiation against time should yield straight lines. In figure 12, such plots are shown for a series of temperatures. All things considered, the fit of the curves is excellent. Over the same time range a first-order plot of the same data gave markedly curved lines.

Polytetrafluorethylene showed only a feeble though definite response to the ultraviolet light used. This polymer does not absorb light except at shorter wavelengths and hence the result was not unexpected. The photo rate observed was probably the result of light absorption via impurities since, during successive runs on the same sample, the photo rate markedly decreased. Further experiments on this polymer are planned with shorter wavelengths and more intense ultraviolet radiation.

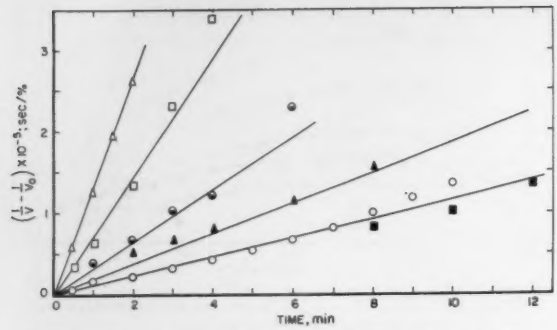

FIGURE 12. *Decomposition of polytrifluorochloroethylene during the post-irradiation period (V=rate of monomer production).*

■, 294 °C; ○, 277 °C; ▲, 247 °C and 261 °C; ○, 242 °C; □, 225 °C; △, 217 °C.

4.6. Telomers of Hexafluoropropylene

The telomer designated as PPF9A was studied the most extensively since it had the largest molecular weight among the telomers listed earlier. Decompositions were carried out in sealed tubes containing the materials with argon as an internal reference, so that mass spectral analysis would provide data on the extent of decomposition. At present, data on the mass spectra of fluorocarbons are fairly limited. Spectra of only twelve of the possible products were available for interpreting and computing the results. The products on the whole comprised a fairly complex mixture, and a complete analysis of the products could not be obtained. They were, however, paraffinic and olefinic fluorocarbons containing 1 to 6 carbon atoms per molecule. The original material contained an average of 30 carbon atoms, so these results indicate that decomposition takes place to give relatively small molecules.

Initial experiments were carried out at 350 °C; extensive decomposition occurred in the first 2 hrs and no marked change occurred at longer times. Other experiments were conducted at lower and at higher temperatures. The mass spectra showed that the main component in the products was hexafluoropropylene. From the amount of argon in the tubes and the weight of sample, it was estimated for the 350 °C run that 3 moles of hexafluoropropylene were produced per mole of starting material, i.e., about a 30 percent yield of this compound in 2 hr. Longer times gave the same result at this temperature.

The trend of decomposition at various temperatures can be seen from the data in table 5, where the ratio of the CF_3^+ ion to argon found in the mass spectra of each pyrolysis experiment is listed. Experiments were also performed at 150 °C, but no decomposition occurred. From table 5 it is seen that decomposition occurs as low as 200 °C, becomes appreciable at 250 °C for 24 hr, and appears to be essentially complete at 350 °C in less than 2 hr. The nickel tubes seem to give a little cleaner reaction and show slightly greater yields of hexafluoropropylene.

TABLE 5. *Mole ratio of the methyl to argon ions in the mass spectra of the pyrolysis products of telomer PPF9A*

Temperature	Time of pyrolysis	CF_3^+/A
°C	*hr*	
200	4	0. 0012
	8	. 0029
	24	. 0115
225	2	. 000[a]
	4	. 0054
	24	. 0630[a]
250	2	. 0948
	24	. 2830
275	2	. 3700
	4	. 5898
	24	. 4430
300	2	. 28
	4	. 35
	8	. 36
	24	. 52
350	2	1. 1
	4	1. 1
	8	1. 0
	24	0. 9
350	2	1. 2[a]
	4	1. 3[a]
	8	1. 3[a]
	24	1. 3[a]
400	2	1. 0
	4	0. 9
	8	. 9
	24	1. 0

[a] Nickel ampule.

However this effect is not large enough to change the general conclusions based on work with glass containers. It appears that at 350 °C and above the hexafluoropropylene reacts appreciably with the glass. At 8 and 24 hr at 350 °C and in all runs at 400 °C small amounts of silicon tetrafluoride were produced.

The results on the pyrolyses at 225 °C of the other telomers are shown in table 6. Their thermal stabilities appear to differ little from the PPF9A material, the latter being perhaps the least stable by a small degree. For the material PPCl6A, which contains one chlorine atom per molecule of telomer, the mass spectra showed a small quantity of HCl^+ ions. The telomer BVFC5A, which contains some hydrogen, produced considerable hydrogen fluoride and little or no hexafluoropropylene.

5. Discussion

The fluoropolymers examined in this investigation decompose by a wide variety of mechanisms. Before discussing the polymers studied, which in the main are copolymers, it will be useful to compare the thermal decomposition of fluorine-containing homo-

polymers for which data are available. For convenient comparison, the essential facts concerning the degradation of known fluorohomopolymers are listed in table 7. The replacement of fluorine in the Teflon structure by a phenyl group, chlorine atoms, or hydrogen atom is seen to change greatly the mechanism of decomposition and the thermal stability. The phenyl group produces the least change in monomer yield but shows the greatest change in thermal stabillty, although the activation energy is not greatly decreased. The monomer yield and the rate behavior give some insight into the mechanism of decomposition [16 to 18]. The mechanism for Teflon and poly-α, β, β-trifluorostyrene involves relatively long zip lengths [17], as indicated by the monomer yield and rate of volatilization curves [18]. Elucidation of other details of the mechanism such as the mode of initiation requires additional experiments not yet available for any fluoropolymers [28].

From the variation of rate with molecular size one can sometimes deduce whether the initial cleavage is at the end or at random along the chain. For polytetrafluoroethylene, studies of this type have so far been inconclusive, the rate being independent of molecular size [4, 6, 28]. Numerous polymers of tetrafluoroethylene prepared in various ways with various catalysts, including fluorine gas, all have essentially the same rate of volatilization [4].

Activation energies and estimated values of the preexponential factors are presented in tables 7 and 8, as well as the rates of volatilization at 350° C. For the purpose of calculation of the preexponential constants, rate data on all polymers not exhibiting a maximum in the rate are extrapolated to zero conversion in some manner which usually eliminates initial effects. The extrapolated values are then assumed to be the overall rate constants for thermal decomposition and assumed to be first order. For details and various possible relationships between the intercept and mechanisms reference should be made to various theoretical treatments [11, 17]. With random initiation the rate constants, and hence the preexponential factors, may contain a factor, N, the degree of polymerization of the decomposing molecules. Thus the extremely high values for the preexponential factors, 10^{19} listed in table 7 may indicate random initiation. However, correcting them by even the highest possible factor, 10^5, the 10^{14} values so obtained are still among the highest. With Teflon, low-molecular weight polymers gave the same rate values as those of high molecular weight; thus deductions based on this apparently high preexponential factor are extremely tenuous.

The substitution of a chlorine atom in the tetrafluoroethylene unit completely changes the decomposition in all respects. The rate of volatilization curve suggests a net random decomposition mechanism. Very likely a chlorine atom dissociates off the chain in the initiation step, followed by chain rupture and some depropagation. Competing with depropagation are transfer reactions in which a depropagating radical abstracts a chlorine atom from another chain. Some transfer, of course, may be intramolecular. The net effect, as seen from the rate of volatilization curve (fig. 10) and the products of decomposition, is a net random degradation. In such cases the maximum in the rate curve is used to calculate the pre-exponential factor and activation energy. Also, the rates at 350 °C listed in tables 7 and 8 are the maximum rates. All polymers ex-

TABLE 6. *Mole ratio of hexafluoropropylene produced from pyrolysis at 225 °C to internal reference gas, argon*

Telomer	Time of pyrolysis	Hexafluoropropylene/argon
	hr	
PPF6.5A	2	0.001
	2	.005
	24	.019
PPC16A	2	.003
	4	.008
	24	.029
PPC2A	2	
	4	.014
	24	.069
BVFC5A	2	
	4	
	24	.001

TABLE 7. *Thermal decomposition of fluorocarbon polymers*

Polymer unit	Monomer and other major products	Total light volatiles	Rate, 350 °C.	E	A (est)
	wt %	*wt %*	*min. %*	*kcal/mole*	*sec⁻¹*
CF_2CF_2 [3]	97 C_2F_4	100	2×10^{-6}	81	10^{16}
CF_2CF [10]	73 CF_2CF	74	4.8	64	10^{10}
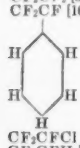	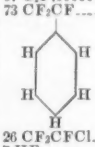				
CF_2CFCl [10]	26 CF_2CFCl	28	0.2	50	10^{12}
CF_2CFH [3]	7 HF	13	.02	53	10^{12}
CF_2CH_2 [25]	13 HF	25	.02	48	10^{10}
CH_2CHF_n [3]	7.2 HF	18	.1		

TABLE 8. *Thermal decomposition of fluorocarbon copolymers*

Polymer	Monomer and other major functions	Total light volatiles	Rate 350 °C	E	A (est)
	wt %	*wt %*	*%/min*	*kcal/mole*	*sec⁻¹*
FEP 100 X	52 C_2F_4, 22 C_3F_6	81	2×10^{-4}	55	10^{12}
Polymer A1	57 C_2F_4, 5 CO_2, 4 CF_4	68	6×10^{-4}	39	10^{8}
Polymer A2	21 C_2F_4, 8 C_3F_6, 6 CF_4, 2 CO_2	40	6×10^{-4}	43	10^{9}
Polymer A3	5 C_2F_4, 2 CF_4, 2 CO_2	13	8×10^{-3}	31	10^{5}
Polyhexafluoropentyleneadipate	1 C_4H_8, 2 CO_2	3	2.0	32	10^{8}
VFHP–A	24 HF	28	0.04	57	10^{13}
F 3700	16 HF, 1.0 HCl	18	.06	61	10^{13}
F 5500	10 HF, 1.2 HCl	13	.06	61	10^{13}

585402—61——7

hibiting the maximum-type curve are treated according to the theory for random decomposition [16, 29].

The rate at the maximum, $(dc/dt)_{max}$, is related by the expression, $dc/dt=kL/2.7$, to the apparent first-order constant, k, for random cleavage of the bonds of the polymer chains. This random cleavage may be by simple unimolecular dissociation or the net effect of a chain reaction where intermolecular transfer is the chain-carrying process. The parameter, L, is the critical size for decomposition. In the type of open system in which these thermal decompositions are carried out, polymers with fewer than L units evaporate without decomposition [29]. Normally it is assumed that hydrocarbon molecules of molecular weight greater than 1,000 and fluorocarbon molecules greater than 2,000 cannot distill without decomposition. For the polymers with maximum-type curves (figs. 6, 7, 8, 9, and 10) it is from k, calculated by the above expression, that the values of A and E shown in tables 7 and 8 are obtained.

The materials for which data are listed in table 8 are in the main copolymers, although strictly speaking the amidine A1 and polyhexafluoropentyleneadipate should not be considered as such. The latter polymer and all the amidine polymers show both rather low activation energies and low pre-exponential factors. This, in conjunction with the effect of methanol in causing degradation, suggests a mechanism of thermal degradation for the amidine polymers at least partly hydrolytic. These polymers must contain many free amidine groups which become hydrolyzed in the presence of the moisture normally present in the atmosphere. At pyrolytic temperatures, entrapped or bound moisture may play an important role in the degradation. The low A and E values for polyhexafluoropentylene adipate are reminiscent of earlier studies of polyamides and polyesters [22, 23], where hydrolysis is a factor in thermal decomposition. The presence of fluorine in a polyester is quite likely to increase the ease of hydrolysis. Even if no other effect were responsible for the ease of presumably hydrolytic decomposition of polyhexafluoropentylene adipate, its structure can lead to hydrofluoric acid formation which would catalyze hydrolysis. Very small amounts of water contamination would then be responsible for the observed results.

FEP 100–X shows a much lower activation energy than polytetrafluorothylene. The stability of a polypropylene chain, as seen from the results of the pyrolysis of the telomers, is apparently rather low. Thus, the incorporation of hexafluoropropylene in the chain leads to considerable loss in stability, as indicated by the lower activation energy (compare polytetrafluoroethylene, table 7, with FEP 100–X, table 8). However, the pre-exponential factor is also a great deal lower, and hence thermal rates are not greatly different.

In the copolymer 100–X, the isolation of hexafluoropropylene units between tetrafluoroethylene units may, of course, minimize the deleterious effect of the hexafluoropropylene. The copolymers of 1,1-difluorothylene, VFHP-A, F3700, and F5500, have roughly the same rate of decomposition at 350 °C as poly-1,1-difluoroethylene. Although the activation energy for the decomposition of polyhexafluoropropylene is unknown, it is likely to be considerably less than the 55 kcal value for FEP 100–X. Assuming this, it is interesting to note that the activation energies of all the 1,1-difluoroethylene containing copolymers are greater than those of the homopolymers of either of their monomers. At lower temperatures the copolymers would be slower to decompose, and there appears to be then a small mutual inhibition effect for thermal decomposition between the different monomer units.

For a practical comparison of the relative thermal stability of the polymers studied here see figure 13, in which the weight loss for 30-min periods is plotted against temperature. It is immediately evident that the polymers divide according to thermal stability into two groups. The most stable group consists of those which are perfluorinated. The least stable group consists of those polymers containing some hydrogen or chlorine atoms. The best of this group is no better than polyethylene. However, though it seems clear that incompletely fluorinated polymers are unlikely to be exceptionally stable, i.e., no better than the better hydrocarbon materials, the results with the hexafluoropropylene telomers suggest that some polymers containing branched perfluorinated structures are likely to be extremely unstable. Hence, perfluorination per se will not necessarily lead to a more stable structure than its hydrocarbon analogue. From the sparse amount of data available, it appears that structural variations in the fluorocarbons lead to a greater span of stabilities than similar variations in the hydrocarbon. In figure 14 the temperatures at which the listed poly-

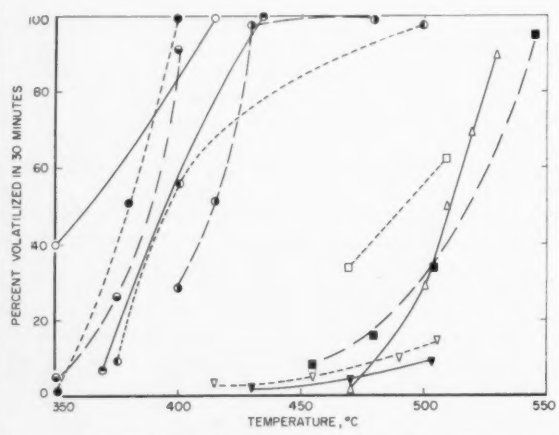

FIGURE 13. *Thermal decomposition of fluoropolymers; amount volatilized in thirty minutes at various temperatures.*

○, Polyhexafluoroethyleneadipate
●, F
◒, F 3700
◓, F 5500
◐, VFHP–A
◑, Polytrifluoroethylene
□, Amidine, A3
■, FEP 100 X
▽, Amidine A2
▼, Amidine A1
△, TFE6 [3]

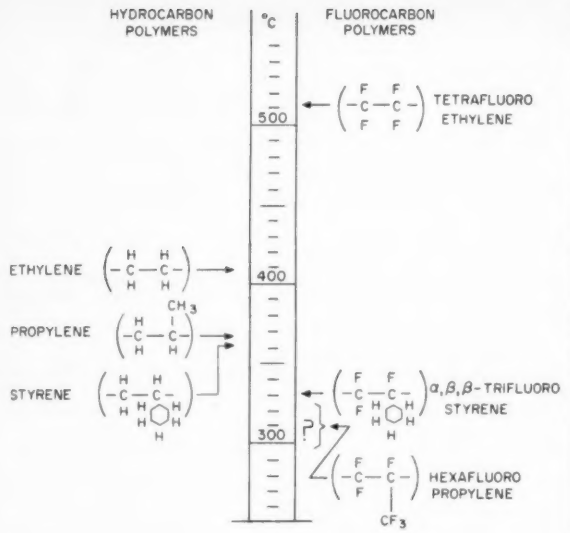

FIGURE 14. *Comparison of the thermal stabilities of hydrocarbon with fluorocarbon polymers temperature at which rate of volatilization is 1 percent/minute.*

mers decompose at a rate of volatilization of 1 percent/min are indicated. Several hydrocarbon polymers are compared to several fluorocarbon polymers. The temperature indicated for polyhexafluoropropylene is an educated guess based on the results with the low molecular-weight telomers.

Unfortunately, thermal decomposition studies on fluorocarbon polymers are limited by the lack of polymers. Since the synthesis of a truly high polymer is often more difficult than smaller molecules, some studies have been made on smaller molecules to ascertain the appropriate approach to a high-temperature polymer. Early work on small fluorocarbon molecule studies is mainly that of Cady [1]. He carried out gas-phase pyrolysis of hexafluoroethane, decafluorocyclopentane, octafluoropropane, decafluoro-*n*-butane, and dodecafluoro-*n*-pentanes. For all these compounds temperatures of 1,000 °C or above were required for decomposition. With hexafluoropropane the activation energy for decomposition was 84 kcal/mole. A low value of 51 kcal/mole found for hexafluoroethane was suspected to be the result of heterogeneous reaction with the platinum filament used for pyrolysis. The compounds studied exhibited the following order of thermal stability:

$$CF_4 > C_2F_6 > \text{cyclo } C_5F_{10} > C_3F_8 > nC_4F_{10} > nC_5F_{12}$$

All of these compounds are much more thermally stable than the telomers of hexafluoropropylene, which decomposed readily at 350 °C.

Recent work [30, 31] on the thermal decomposition of fluoroaromatic compounds has resulted in establishing the following approximate order of stability for certain relative hydro and fluoroaromatics-containing substances:

$$(C_6F_5)_2 > (C_6H_5)_2 > C_6F_5-C_6H_5 > (C_6H_5)_2O > Si(C_6H_5)_4$$
$$> C_6F_4O_2C_6F_4 > Si(C_6F_5)_4 > C_6F_5-O-C_6H_5$$
$$> P(C_6F_5)_3 > P(C_6H_5)_3 > (C_6F_5)_3PO.$$

It is seen that the effect of fluorination depends on the other elements present and on the structure of the molecules. Thus, where the breakdown may be due to the reaction or dissociation of a hydrogen atom, as in diphenyl, fluorine substitution improves the thermal stability. With the tetraphenyl silane the substitution of fluorine decreases the stability, probably by weakening the C—Si bonds. On the other hand, in triphenyl phosphine the effect of fluorine is to make the material more stable, whereas in the oxide form it becomes less stable. The P—C bond is probably stronger in the trispentafluorophenyl phosphine but weaker in the trispentafluorophenyl phosphine oxide compared to triphenyl phosphine. It may be recalled that perfluorotrialkyl amines are not basic and are quite inert and stable materials, as are the perfluorodialkyl ethers. Although detailed thermal decomposition studies have apparently not yet been carried out on these compounds, they are known to be quite stable. In general, from the listing of the compounds shown above and from other fragmentary data, it seems likely that perfluoroaryl ethers are likely to be quite stable, i.e., better than the hydrocarbon analogues. It is interesting to note that, as expected, mixed fluoro-hydro materials are less stable than either the straight fluoro or hydro substances.

Photoinduced Decomposition of Polytrifluorochloroethylene. A preliminary exploration of the photoinduced decomposition of polytrifluorochlorethylene was mentioned earlier, and plots of the reciprocal of rate of depolymerization, V, during the post-irradiation period were shown in figure 12. The linear character of the curves indicates that termination of the radicals is bimolecular. An Arrhenius plot of the slope of the lines in figure 12 yields a curious result (fig. 15). It is suggested that a diffusion effect on the depropagation step may be complicating the mechanism at lower temperatures. A similar result has been seen [32] on the activation energy for the photodecomposition of polymethyl methacrylate. The Arrhenius plot for the photoinduced depolymerization gave a fairly straight line with $E_{ph}=13$ kcal/mole.

The activation energy for the thermal decomposition, E_{th}, is 50 kcal/mole (see table 7). Assuming that transfer reactions are unimportant, E_{th} is given by the relationship:

$$E_{th}=\frac{E_1}{2}+E_2-\frac{E_4}{2}$$

where E_1, E_2, and E_4 are the activation energies, respectively, for the three elementary processes of the thermal depolymerization mechanism,—initiation, depropagation, and termination. In photo-

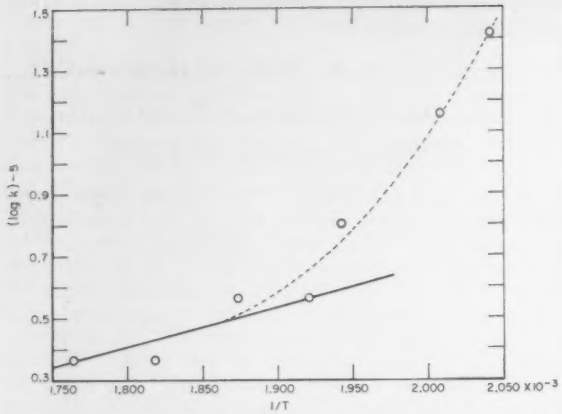

FIGURE 15. *Arrhenius plot of post-irradiation decay of depolymerization rates.*

○, experimental points

induced depolymerization, initiation becomes independent of temperature, and hence $E_{ph}=E_2-(E_4/2)$. The activation energy from the post-irradiation decay, E_{post}, i.e., the value derived from the slope in figure 15, is also related to E_2 and E_4; $E_{post}=E_4-E_2$.

The plot in figure 15 suggests that E_{post} at high temperatures, near those where thermal decomposition occurs, is near zero. However, the curvature suggests that at the lower temperatures E_2 becomes greater, since it is unreasonable to believe that E_4 could become smaller. This suggests that monomer is finding it much more difficult to diffuse away from the radicals. The observed effect correlates nicely with the usual molding temperature or no-strength temperature.

The arbitrary straight full line in figure 15 yields $E_{post}=-3$ kcal, which we shall assume in making subsequent estimates. The dashed line shows the trend as temperature decreases. We can now estimate the values of $E_1=74$, $E_2=23$, and $E_4=20$ kcal/mole for the elementary processes which comprise the mechanism of thermal decomposition for polytrifluorochloroethylene. It is believed likely that initiation occurs at random for both the thermal and the photoinduced decomposition of polytrifluorochloroethylene as the result of a dissociation of a chlorine atom from the chain. The dissociation energy of the polymer into radicals should be given by $D(R-R)=E_1-E_4=54$ kcal/mole [28]. The value obtained is reasonable for a secondary C—Cl bond dissociation.

Much further work is needed on the thermal decomposition of fluoro compounds and polymers. The present investigation has, however, pointed out the general features of their mechanisms of decomposition and certain differences and similarities between the fluorocarbons and the hydrocarbon polymers.

6. References

[1] R. K. Steunenberg and G. H. Cady, J. Am. Chem. Soc. **74,** 4165 (1952).
[2] E. E. Lewis and M. A. Naylor, J. Am. Chem. Soc. **69,** 1968 (1947).
[3] S. L. Madorsky, V. E. Hart, S. Straus, and V. A. Sedlak, J. Research NBS **51,** 327 (1953) RP2461.
[4] R. E. Florin, L. A. Wall, D. W. Brown, L. A. Hymo, and J. D. Michaelsen, J. Research NBS **53,** 121 (1954) RP2480.
[5] L. A. Wall and J. D. Michaelsen, J. Research NBS **56,** 27 (1956) RP2644.
[6] J. C. Siegle and L. T. Muus, Pyrolysis of polytetrafluoroethylene, paper presented at 130th Meeting of the ACS, Sept. 16–21, 1956.
[7] J. D. Michaelsen and L. A. Wall, J. Research NBS **58,** 327 (1957) RP2765.
[8] W. L. Reilly and H. C. Brown, J. Org. Chem. **22,** 698 (1957).
[9] E. V. Gouinlock, Jr., C. J. Verbanic, and G. C. Schweiker, J. Appl. Poly. Sci. **1,** 361 (1959).
[10] S. L. Madorsky and S. Straus, J. Research NBS **55,** 223 (1955) RP2624.
[11] M. Hauptschein, M. Braid, and F. E. Lawlor, J. Am. Chem. Soc. **79,** 2549 (1957).
[12] M. Hauptschein, M. Braid, and A. H. Fainberg, J. Am. Chem. Soc. **80,** 851 (1958).
[13] S. Straus and S. L. Madorsky, Ind. Eng. Chem. **48,** 1, 212 (1956).
[14] S. L. Madorsky, J. Polymer Sci. **9,** 133 (1952).
[15] S. L. Madorsky, J. Polymer Sci. **11,** 491 (1953).
[16] R. Simha and L. A. Wall, J. Phys. Chem. **56,** 707 (1952).
[17] R. Simha, L. A. Wall, and J. Bram, J. Chem. Phys. **29,** 894 (1958).
[18] L. A. Wall and R. E. Florin, J. Research NBS **60,** 451 (1958) RP2860.
[19] L. A. Wall and W. J. Moore, J. of Phys. and Colloid Chem. **55,** 965 (1951).
[20] L. A. Wall and W. J. Moore, J. Am. Chem. Soc. **73,** 2840 (1951).
[21] L. A. Wall, S. Straus, R. E. Florin, F. L. Mohler and Paul Bradt, J. Research NBS **63A,** 63 (1959).
[22] S. Straus and L. A. Wall, J. Research NBS **60,** 39 (1958) RP2818.
[23] S. Straus and L. A. Wall, J. Research NBS **63A,** 269 (1959).
[24] S. L. Madorsky, V. E. Hart, S. Straus and V. A. Sedlak, J. Research NBS **51,** 327 (1953) RP2461.
[25] S. L. Madorsky and S. Straus, J. Research NBS **63A,** 261 (1959).
[26] S. L. Madorsky, J. Research NBS **62,** 219 (1959) RP2957.
[27] D. W. Brown and L. A. Wall, J. Phys. Chem. **62,** 848 (1958).
[28] L. A. Wall, SPE J. **16,** 810 (1960); **16,** 1031 (1960).
[29] R. Simha and L. A. Wall, J. Polym. Sci. **6,** 39 (1951).
[30] L. A. Wall, R. Donadio, and W. J. Pummer, J. Am. Chem. Soc. **82,** 4846 (1960).
[31] L. A. Wall and W. J. Pummer, unpublished.
[32] P. R. E. J. Cowley and H. W. Melville, Proc. of Royal Soc. **210A,** 461 (1951).

(Paper 65A3–106)

JOURNAL OF RESEARCH of the National Bureau of Standards—A. Physics and Chemistry
Vol. 65A, No. 3, May–June 1961

Preparation of Fluoro- and Bromofluoroaryl Compounds by Copyrolysis of Bromofluoroalkanes*

Leo A. Wall, James E. Fearn, Walter J. Pummer, and Robert E. Lowry

(February 14, 1961)

Pyrolysis of tribromofluoromethane yields chiefly hexafluorobenzene. Copyrolysis of this material with several bromine-containing compounds was studied at 540 °C and under several atmospheres' pressure of nitrogen gas. The addition of bromine or dibromodifluoromethane has very little effect on the pyrolysis products of tribromofluoromethane. Copyrolysis with carbon tetrabromide or bromoform yields increased amounts of bromopentafluorobenzene and dibromotetrafluorobenzene at the expense of hexafluorobenzene. The addition of relatively small amounts of 1,1,1-tribromo-2,2,2-trifluoroethane gives a significant yield of octafluorotoluene.

1. Introduction

Synthesis of hexafluorobenzene by the pyrolysis of tribromofluoromethane has been described and investigated by several workers [1–4][1]. The original synthesis [1] was carried out at atmospheric pressure and 640 °C. In a previous study of this reaction in our laboratory [2], we explored the effects of pressure and temperature. On increasing the pressure to 4 atm, optimum yields were obtained near 540 °C, and the maximum yields were somewhat greater than at atmospheric pressure. A secondary product from the pyrolysis of tribromofluoromethane was bromopentafluorobenzene[2,3]. Since this material has great value in synthesis work [5], it was of interest to find means of increasing the relative yield of this product. A conceivable approach to this aim would be to increase the concentration of bromine in the reaction or to introduce carbon tetrabromide or bromoform into the reaction. Introduction of other compounds, it was anticipated, could also lead to the synthesis of various derivatives of hexafluorobenzene or related compounds.

2. Materials

The tribromofluoromethane, obtained from Columbia Organic Chemicals, Inc., was dried over anhydrous calcium sulfate and filtered through glass wool. The carbon tetrabromide, bromoform, and bromine were reagent grades and were used without further purification. The 1,1,1-trifluoroethane was a research sample.[2] The dibromodifluoromethane was obtained as a byproduct in the pyrolytic preparation of hexafluorobenzene.

The tribromotrifluoroethane was prepared by first converting CF_3CH_3 to CF_3CHBr_2 by thermal reaction with Br_2 in a hot-tube apparatus [6]. Then, in a one-liter, three-necked flask equipped with an efficient stirrer and a reflux condenser, a mixture of 242 g (1 mole) of CF_3CHBr_2, 135 g of KOBr (prepared from 112 g of KOH and 160 g of Br_2), and 300 ml of water was cooled for 3 hr in a bath maintained at 15 °C. The mixture was stirred vigorously and irradiated with a 350-watt bulb throughout the reaction. When the exothermic reaction had subsided and the contents of the flask had cooled, the product solidified. The aqueous layer was decanted. The slightly yellow product, 1,1,1-tribromo-2,2,2-trifluoroethane, was briefly dried in air and sublimed. The yield was 257 g (80%).

3. Experimental Procedures

The pyrolysis experiments were carried out as described previously [2]. However, the apparatus used was newly constructed and designed to handle 2 liters of reactants or about 5 kg of tribromofluoromethane. A diagram of the apparatus is shown in figure 1. The pyrolysis tube, platimun 89 percent and ruthenium 11 percent, 76 cm long, 0.95 cm ID, and 1.15 cm OD, was silver-soldered to brass fittings at each end. The reservoir and traps were constructed of welded stainless steel and connected via copper tubing and brass fittings. The only nonmetal component of the apparatus was a thick-walled, hard-glass, solenoid valve which controlled the input of liquid CBr_3F mixtures into the furnace. This glass valve was connected with two glass inner 10/30 standard tapers to two outer 10/30 tapers machined out of brass and silver soldered to copper tubing. The taper joints were waxed together with poly(chlorotrifluoroethylene) wax.

The reservoir was filled with the reactants. Then, after closing the system and bringing the furnace to the desired temperature, set on an indicating, proportioning controller operating from a thermocouple, the pressure of N_2 gas in the system was adjusted, using the reducing valve on the gas cylinder. The flow of N_2, which had been prepurified, was adjusted by bleeding through a brass, blunt-needle valve at the exhaust end of the apparatus. Finally an electric timer was switched on, which periodically allowed pulses of liquid CBr_3F mix-

*Based on Research Supported by Bureau of Naval Weapons, U.S. Navy.
[1] Figures in brackets indicate the literature references at the end of this paper.
[2] The courtesy of the General Chemical Division, Allied Chemical and Dye Corporation, in supplying this material is gratefully acknowledged.

tures to enter the furnace. After the reservoir was emptied the apparatus was shut down and the pressure allowed to drop to atmospheric. The products were drained from the first trap, which was operated at room temperature. Very little material was found in the second trap, which was operated at −78 °C, but its use tended to prevent corrosion of the exhaust valve. The products were worked up as described previously [1–4].

4. Results

Mixtures of CBr_3F with CBr_4, with $CHBr_3$, with Br_2, with CBr_2F_2, and with CF_3CBr_3 were pyrolyzed under conditions listed in table 1. The last three columns in the table give the total amount of recovered material, the weight percent of debromination, and the total weight of products other than bromine. The conditions used were approximately the optimum ones for the production of C_6F_6. The experiments with the first three substances listed were carried out to explore the possibility of synthesizing greater amounts of C_6BrF_5 and $C_6Br_2F_4$. After pyrolysis, the material was first treated to remove Br_2 and then distilled. The fractions collected were analyzed, using a mass spectrometer.

Results from the copyrolysis of CBr_3F with CBr_4 are given in table 2, along with boiling points, weights, and analyses of the fractions. Quantitative results, when given, are expressed in mole percent. A few compounds are merely listed when found in trace amounts. The addition of CBr_4 decreases the yield of C_6F_6 and increases the yields of C_6BrF_5 and $C_6Br_2F_4$. However, the major material was the $C_6Br_2F_4$ and not the more desirable C_6BrF_5.

Table 3 gives the results from copyrolysis of the CBr_3F with $CHBr_3$. Surprising amounts of C_6BrF_5 and $C_6Br_2F_4$ are produced. From $CHBr_3$ it was initially conceivable that C_6HF_5 or even $C_6H_2F_4$ could be a product. However, no products containing hydrogen were detected, excluding the HBr which was qualitatively evident in the exhaust gases.

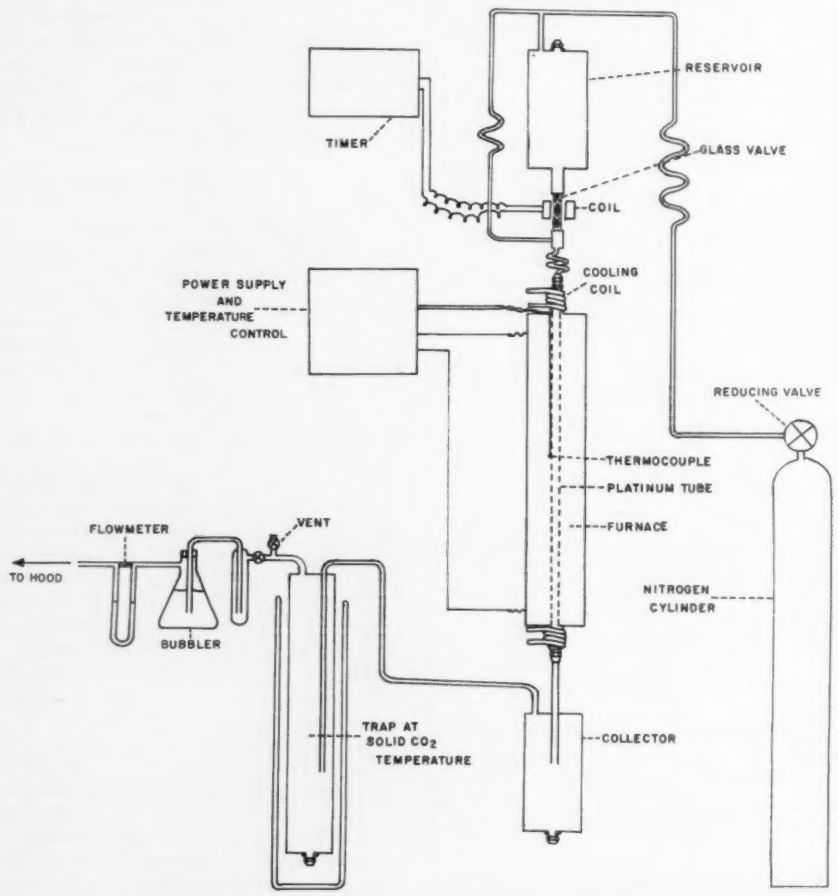

FIGURE 1. *Apparatus for pyrolysis of bromofluorocarbon liquids under pressure.*

TABLE 1. *Pyrolysis of bromofluorocarbon mixtures*

Mixtures	Weight	Moles	Temperature	Pressure	N_2 flow	Time	Recovered material (including Br_2)	Br_2 removal	Products (other than Br_2)
	g		*°C*	*atm*	*cm³/min*	*hr*	%	%	*g*
CBr_3F	2981	11	540	18	25	5	98	87	652
CBr_4	756	2. 2							
CBr_3F	7859	29	540	18	25	7	67	87	1721
CBr_4	1307	3. 8							
CBr_3F	4490	16. 5	545	3. 5	25	5. 2	98. 5	69. 8	740
CBr_4	1100	3. 3							
CBr_3F	4065	15	560	10	25	11. 3	95	96	769
$CHBr_3$	759	3. 1							
CBr_3F	3400	12. 5	540	10	50	11	70	49[a]	416
Br_2	1360	8. 5							$9C_6F_6$
									$197CBr_3F$
									210Residue
CBr_3F	2710	10	540	10	25	5	77	68	420
CBr_2F_2	420	2							$84C_6F_6$
									$210CBr_3F$
									126Residue
CBr_3F	1900	10. 7	560	10	25	4	98	74	793
CF_3CBr_3	210	1							

[a] Does not include the added bromine.

TABLE 2. *Fractional distillation of products from the pyrolysis of* CBr_3F/CBr_4 *mixtures*

Boiling range	Pressure	Weight of fraction	Analysis of fraction
°C	mm	g	*Mole %*
25 to 90	at 760	139	C_6F_6 (80%), CBrFCBrF (10%), CBr_2F_2
90 to 120	at 760	848	CBr_2F (90%), $C_2Br_4F_2$, C_6BrF_5
120 to 145	at 760	160	C_6BrF_5 (79%), $C_2Br_4F_2$ (20%), C_7BrF_7
85 to 95	at 25	218	$C_6Br_2F_4$ (90%), $C_2Br_4F_2$, C_6BrF_5
88 to 98	at 10	61. 5	$C_6Br_2F_4$ (50%), C_2Br_4 (10%)
>100	at 10	268	Not analyzed.

Br_2 seemed to lower the extent of reaction; CBr_2F_2 appeared to have no significant effect. These materials are products from the pyrolysis of CBr_3F itself.

Copyrolysis with CF_3CBr_3 gave a significant yield of $C_6F_5CF_3$, as anticipated (see table 4). This material was also found in the pyrolysis products along with C_6F_6 [3] at 800 °C. However, under the conditions used here it is evident that it is produced as a result of the copyrolysis. This material is difficult to separate from the mixture in which it is produced.

TABLE 3. *Fractional distillation of products from the pyrolysis of* $CBr_3F/CHBr_3$ *mixtures*

Boiling range at 760 mm	Weight of fraction	Analysis of fraction
°C	*g*	*Mole %*
45 to 100	69. 4	C_6F_6 (70%), $CHFBr_2$ (20%)
100 to 125	510. 4	CBr_2F (90%), C_2Br_3F
125 to 140	69. 1	C_6BrF_5 (60%), $CHBr_3$ (30%), C_7BrF_7, C_6HBrF_4
140 to 175	39. 7	$C_4Br_2F_6$, $C_5Br_2F_5$, C_6BrF_7
175 to 200	94. 8	$C_6Br_2F_4$, $C_2Br_4F_2$

Unfortunately, our supply of CF_3CBr_3 was quite limited, and experiments with greater ratios of this material to $CFBr_3$ were not carried out. It is evident, however, that greater ratios would produce such substances as perfluoroxylenes.

TABLE 4. *Fractional distillation of products from the pyrolysis of* CBr_3F/CF_3CBr_3 *mixtures*

Boiling range at 760 mm	Weight of fraction	Analysis of fraction
°C	*g*	*Mole %*
50 to 95	51. 2	C_6F_6 (66%), $C_6F_5CF_3$ (5%), $C_6F_4Br_2$
95 to 106	51. 7	CBr_2F (85%), C_7F_8 (10%), C_6F_6 (5%)
106 to 110	392. 9	CBr_2F (90%), C_7F_8 (5%), $C_2Br_3F_3$
>110	401	Not analyzed.

5. Discussion

The results obtained here are compatible with the type of mechanism assumed previously for this pyrolysis. The stages of reaction can be visualized thus:

$$2CBr_3F \longrightarrow CBr_2FCBr_2F + Br_2$$

$$CBr_2FCBr_2F \longrightarrow CBrF{=}CBrF + Br_2$$

$$3CBrF{=}CBrF \longrightarrow C_6Br_6F_6 \text{ or } C_6Br_4F_6 + Br_2$$

$$C_6Br_6F_6 \xrightarrow{-3Br_2} C_6F_6 \qquad C_6Br_4F_6 \xrightarrow{-2Br_2} C_6F_6$$

No perhalocyclohexanes have been isolated. The effect of pressure in enhancing the yield can be explained on this type of mechanism [2] without $CF \equiv CF$ as an intermediate. The intermediate, $CBrF=CBrF$, was found in the products in trace amounts, but no evidence was found for $CF \equiv CF$ as an intermediate. The $C_6Br_6F_6$ or the $C_6Br_4F_6$ shown are presumed to be extremely unstable; a Fischer-Hirshfelder model of these compounds indicates large steric effects. No evidence exists for the formation of such compounds from C_6F_6 and Br_2, although the $C_6Cl_6F_6$ has been made [1]. The chlorine derivative thermally decomposes near 250 to 300 °C.

It has been reported that $CF \equiv CF$ forms a dimer, presumably tetrafluorocyclobutadiene [7]. So far, no evidence exists for these compounds from the pyrolysis reaction of CBr_3F. However, $CF \equiv CH$ does trimerize to 1,2,4-trifluorobenzene [8], and hexafluoro-2-butyne trimerizes to hexa(trifluoromethyl)benzene [9].

6. References

[1] Y Desirant, Bull. Acad. Roy. Belg., Classe Sci., [5] **41,** 759 (1955).

[2] M. Hellmann, E. Peters, W. J. Pummer, and L. A. Wall, J. Am. Chem. Soc., **79,** 5654 (1957).

[3] Y. Desirant, Bull. Soc. Chim. Belg. **67,** 676 (1958).

[4] J. M. Birchall and R. N. Hazeldine, J. Chem. Soc. **13,** (1959).

[5] W. J. Pummer and L. A. Wall, J. Research NBS **63A,** 167 (1959).

[6] E. T. McBee, H. B. Hass, W. G. Toland, Jr., and A. Truchan, Ind. Eng. Chem. **39,** 420 (1947).

[7] W. J. Middleton, U.S. Patent No. 2,831,835, April 22, 1958.

[8] W. J. Middleton and W. H. Sharkey, J. Am. Chem. Soc. **81,** 803 (1959).

[9] H. C. Brown, H. L. Gewanter, D. M. White, and W. G. Woods, J. Org. Chem. **25,** 634 (1960).

(Paper 65A3–107)

JOURNAL OF RESEARCH of the National Bureau of Standards—A. Physics and Chemistry
Vol. 65A, No. 3, May–June 1961

Thermal Stability of Polydivinylbenzene and of Copolymers of Styrene With Divinylbenzene and With Trivinylbenzene[1]

Sidney Straus and Samuel L. Madorsky

(January 18, 1961)

Samples of polydivinylbenzene (PDVB) and of copolymers of styrene with divinylbenzene (DVB) and with trivinylbenzene (TVB) were pyrolyzed in a vacuum in the temperature range of 346 to 450 °C. The volatile products were collected in two fractions: A heavy fraction volatile at the temperature of pyrolysis and a light fraction volatile at room temperature. Mass spectrometer analysis of the light fraction showed that for the copolymer containing 2 percent DVB the yield of styrene monomer is somewhat greater than for the pure polystyrene. On pyrolysis, of copolymers containing 25 percent of DVB or of TVB yield reduced amounts of styrene monomer; those containing about 50 percent of DVB do not yield any styrene monomer. Rates of thermal degradation of PDVB and of the copolymers were studied in the temperature range of 330 to 390 °C; the activation energies calculated on the basis of these rates were 53, 54, 58, 58, 61, and 65 kcal/mole for the copolymers containing 2 percent DVB, 25 percent DVB, 48 percent DVB, 56 percent DVB, 25 percent TVB, and for PDVB, respectively.

1. Introduction

Polystyrene was found to decompose thermally in a vacuum [1] [2] or in a neutral atmosphere [2, 3] at temperatures below 500 °C by a mechanism consisting of random scissions of C—C bonds, followed by unzipping at the resulting free-radical chain ends to yield monomers and multiples of structural units of an average molecular weight of about 264. Under these conditions complete volatilization of the sample takes place, for example, at 400 °C in about 30 min. of heating. On the other hand, polytrivinylbenzene (PTVB) [3], when pyrolyzed under similar conditions, does not yield any appreciable amounts of either styrene or of trivinylbenzene monomers. Instead, the volatile degradation products consist of a fraction containing a small amount of hydrogen and saturated and unsaturated hydrocarbon fragments having from 1 to 11 carbons; a less volatile fraction consists of larger fragments having an average molecular weight of 372; and the residue consists of a carbonaceous material.

The mechanism of degradation of this highly cross linked PTVB polymer is assumed to be as follows: When a C—C bond in the short connecting links between the phenyl groups breaks, two reactions are possible: (a) A transfer of hydrogen may take place at the site of break so that one end becomes saturated and the other unsaturated, and (b) the two ends become free radicals. In the latter case the free radicals do not unzip to form monomers because of the cross linkages that hold the phenyl groups at other points. Instead, the free radicals abstract hydrogen from the surrounding medium and become saturated. As the number of such scissions increases, fragments of various sizes, which may or may not contain phenyl groups, split off from the chain, abstract some hydrogen from the residue, and vaporize. The residue in the meantime becomes carbonized in the process through loss of hydrogen.

Intermediate between these two extremes are copolymers of styrene with divinylbenzene (DVB) or with trivinylbenzene (TVB). An investigation of the thermal behavior of such copolymers was carried out by Winslow and Matreyek [4] in nitrogen at atmospheric pressure, at temperatures up to about 550 °C. They were interested primarily in the relative thermal stability of these copolymers and in the nature of the residues, and therefore did not study the volatile productions of degradation.

The present study was undertaken to obtain information on the mechanism of thermal degradation of these copolymers through analysis of the volatile products of degradation. A study was also made of the degradation of polydivinylbenzene (PDVB). The present work, as in the case of most of our other work on thermal degradation of polymers, was carried out in a vacuum. In addition to investigation of the nature of the volatile degradation products, the rates and activation energies of degradation were also determined. Allowing for the differences in the experimental conditions, our results are in fairly good agreement with those of Winslow and Matreyek.

2. Materials

The copolymers[3] consisted of polystyrene containing the following amounts, in weight percent, of

This research was supported by the United States Air Force under delivery order No. (33-616)58-8, monitored by Materials Central Directorate of Advanced Systems Technology, Wright Air Development Division.

[2] Figures in brackets indicate the literature references at the end of this paper.

[3] The authors are indebted to F. H. Winslow of Bell Telephone Laboratories for supplying them with samples of these copolymers.

DVB or TVB: 2 percent DVB, 25 percent DVB, 48 percent DVB, 56 percent DVB, and 25 percent TVB. The PDVB was prepared by heating a pure grade of DVB monomer in an evacuated and sealed 6-mm Pyrex tube in an oven at 80 to 90 °C for 6 weeks. The tube was then opened, and the polymer, which was in the form of a rod, was heated further for 1 hr in an evacuated chamber at 120 °C. A loss of 8 percent, presumably monomer, took place during this heating step, but no additional loss occurred on further heating at this temperature.

3. Experimental Procedures

3.1. Pyrolysis

The experimental procedure used in the pyrolysis of PDVB and of the copolymers was the same as that used earlier in the pyrolysis of PTVB and other polymers [3]. Apparatus No. II described in reference [3] was used. Samples weighing 15 to 30 mg were heated in a vacuum by quickly moving a preheated furnace into position surrounding the sample for pyrolysis. Duration of heating was a 5-min period to heat up the sample from room temperature to the temperature of pyrolysis, followed by a 30-min period at the pyrolysis temperature. Fluctuation of the final temperature was ± 2 °C. The residues were weighed, and the volatile products were collected and fractionated. The following volatilized products were obtained: (a) A waxlike fraction designated as V_{pyr}, volatile at the temperature of pyrolysis, but not at room temperature, which consisted of large molecular fragments deposited in the apparatus just beyond the hot zone; (b) a light fraction, V_{25}, volatile at room temperature, collected in liquid-nitrogen-cooled trap; and (c) a gaseous fraction, V_{-190}, not condensable at the temperature of liquid nitrogen.

Fractions V_{pyr} and V_{25} were weighed, and the amount of V_{-190} was determined from pressure, volume, and chemical composition data. Fractions V_{25} and V_{-190} were analyzed in the mass spectrometer. Fraction V_{-190} was very small, less than about 0.1 percent by weight, and was found to consist primarily of CO. This is similar to the results obtained previously [1] in the case of polystyrene.

The relative thermal stabilities of PDVB and of copolymers of styrene with DVB and with TVB are shown in figure 1. Curves for polystyrene and PTVB, included in this figure for comparison, are based on data obtained previously [3, 5]. As can be seen from this figure, a styrene-DVB copolymer containing only a small percentage of DVB has a thermal stability not much different from that of the styrene homopolymer. The copolymer containing 25 percent of DVB shows an increase in stability over that of polystyrene. Still greater quantities of DVB in the copolymers produce further increases in the thermal stability, but at about 50 percent of DVB, stability reaches a maximum and is about equal to that of PDVB homopolymer. Polytrivinylbenzene has a much higher thermal stability than the PDVB, and it requires only 25 percent of TVB in the styrene-TVB copolymer to equal the thermal stability of PDVB.

The amounts of volatilized products from the pyrolysis experiments on PDVB and the copolymers are given in table 1. The V_{25} fractions from a number of experiments on the copolymers were analyzed in the mass spectrometer, and the results are shown in table 2. The mass spectrograph for fraction V_{25} from PDVB was very complex and could not be interpreted completely. The results are therefore not indicated in the table. However, there was a definite indication of the presence of considerable amounts of toluene, benzene, styrene, and xylene.

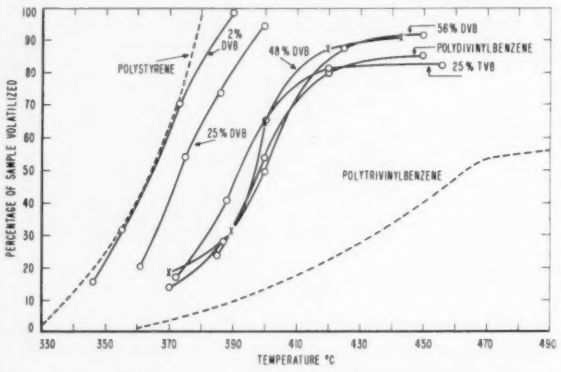

FIGURE 1. *Relative thermal stability of polydivinylbenzene and polytrivinylbenzene, and their copolymers with styrene.*

TABLE 1. *Pyrolysis of polydivinylbenzene and of copolymers of styrene with divinylbenzene and with trivinylbenzene* [a]

Material	Temperature	Volatilization	Fractions, based on volatilization	
			V_{pyr}	V_{25}
	°C	%	%	%
I 2% DVB	346	16.0	42.1	57.9
	355	32.2	42.7	57.3
	373	70.6	47.2	52.8
	390	98.3	48.1	51.9
II 25% DVB	361	20.7	43.0	57.0
	375	54.2	49.7	50.3
	386	73.9	49.1	50.9
	400	94.5	52.1	47.9
III 48% DVB	370	18.6	80.5	19.5
	390	31.1	87.4	12.6
	401	64.6	94.9	5.1
	420	87.5	96.0	4.0
	443	90.7	95.0	5.0
IV 56% DVB	370	14.4	64.0	36.0
	387	28.4	77.4	22.6
	400	50.1	82.9	17.1
	425	87.3	93.2	6.8
	450	91.6	91.8	8.2
V 25% TVB	372	17.3	69.0	31.0
	388	41.1	63.6	36.4
	400	65.6	77.8	22.2
	420	81.4	79.9	20.1
	450	82.0	83.7	16.3
VI Polydivinylbenzene	385	24.0	54.4	45.6
	400	53.8	67.1	32.9
	420	79.8	71.1	28.9
	450	84.7	81.0	19.0

[a] Duration of heating in each experiment was 30 min, preceded by 5 min o preheating.

TABLE 2. *Mass spectrometer analysis of volatile products from pyrolysis of copolymers of styrene with divinylbenzene and trivinylbenzene*

Copolymer	2% DVB		25% DVB		48% DVB			56% DVB		25% TVB	
Temperature, °C	346	390	386	400	370	390	443	400	450	400	420
Component	*wt. %*	*wt. %*	*wt. %*	*wt. %*	*wt. %*	*wt. %*	*wt. %*	*wt. %*	*wt. %*	*wt. %*	*wt. %*
C_3H_6			0.8							0.8	0.4
C_4H_8			0.6								
C_5H_{10}								0.7	0.6		
C_5H_{12}								3.0	2.7		
C_6H_6		0.4	1.5	0.5						0.4	0.4
C_6H_{14}			0.8								
C_7H_8	0.6	1.4	2.8	2.7						2.7	3.0
C_8H_8	51.7	49.8	39.9	34.8						16.2	14.4
C_8H_{10}	2.0		0.9	1.4		0.5	0.6	1.0	1.2	1.3	1.4
C_9H_{10}	0.7		1.7	1.0	0.4	0.4	0.5	0.9		0.4	
C_9H_{12}	2.1		0.7	0.8	0.7	0.8	0.6	0.9	0.9		
$C_{10}H_{12}$				4.8	9.2	7.6	2.0	6.7	0.5		
$C_{10}H_{14}$	0.8		1.0	1.1	8.9	2.9	0.6	1.7	0.5		
Others [a]	0	0.3	0.2	0.8	0.3	0.4	0.7	2.2	1.8	0.4	0.5
Total of V_{25}	57.9	51.9	50.9	47.9	19.5	12.6	5.0	17.1	8.2	22.2	20.1
V_{pyr}	42.1	48.1	49.1	52.1	80.5	87.4	95.0	82.9	91.8	77.8	79.9
Total	100.0	100.0	100.0	100.0	100.0	100.0	100.0	100.0	100.0	100.0	100.0

[a] Components in amounts of 0.3 percent or less are not shown individually in this table.

There was also a group of peaks in the mass-range of 112 to 118, corresponding to a compound C_9H_{10}.

In the 2 percent-DVB copolymer the yield of the styrene monomer, C_8H_8, is slightly greater than in the case of 100 percent polystyrene, which was previously found to be about 40 weight percent of the total volatilized part [1, 5]. The yield of monomer decreases with the increase of DVB content in the copolymer and disappears altogether when the content of DVB is up to about 50 percent. There is, however, considerable monomer content in the volatiles from the 25 percent-TVB copolymer.

3.2. Rates

Rates of thermal degradation of the styrene copolymers and of PDVB were measured in a vacuum by a gravimetric method, which makes use of a very sensitive tungsten spring balance having a sensitivity of about 570 micrograms per millimeter of displacement. The apparatus and experimental procedure have been described in detail in an earlier publication [6]. Samples were limited to about 5 mg and were heated in a platinum crucible.

Cumulative percentages of volatilization for the copolymers and for PDVB are shown plotted in figures 2, 4, 6, 8, 10, and 12. These curves of percentage loss versus time were used in calculating the data for the rate curves, which are shown plotted in terms of percentage loss per minute as a function of cumulative percentage volatilization in figures 3, 5, 7, 9, 11, and 13.[4] In calculating the activation energies of the polymer degradation reactions the maximum rates were used in all cases except for the 25 percent TVB copolymer, where the initial rates, obtained by extrapolation (figure 11) were used. These maximums and initial rates, which are given in table 3, were used to prepare the curves in figure 14 and to calculate the activation energies of the polymers on the basis of the Arrhenius equation.

Numerical values of the activation energies based on the slopes of the straight lines in figure 14 are given in the last column of table 3. Data for PTVB [3] are shown for comparison. The activation energies increase with increase of cross linking agent in the copolymer. An activation energy for polystyrene was previously found to be 55 kcal/mole [7] which is about the same as for the copolymers having small percentages of DVB.

Additional calculations of activation energies for copolymers containing 2, 25, 48, and 56 percent DVB, were made on the basis of rates at 35 and 50 cumulative volatilization losses. The results of these calculations are shown in table 4. These results do not differ much from those based on the corresponding maximums (table 3).

4. Discussion

Allowing for the fact that in the work of Winslow and Matreyek [4] the degradation of the copolymers was carried out in nitrogen at atmospheric pressure, whereas a vacuum was used in the present work, the results are in close agreement, although our rates of degradation are a little higher, as expected.

The mechanism of thermal degradation of the copolymers of styrene with divinylbenzene or with

[4] In figure 13 the separate points are shown. The calculated rates at 390 °C are rather high, and the calculated points show a good deal of scattering.

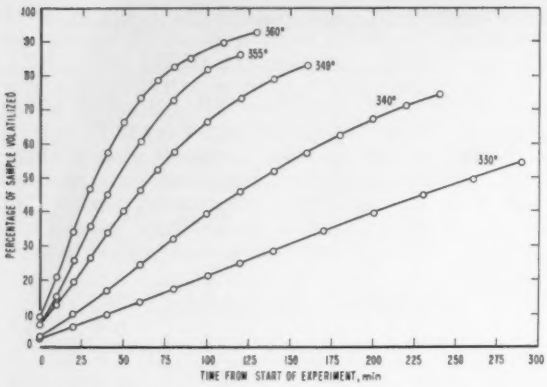

FIGURE 2. *Thermal degradation of copolymer 98 percent styrene—2 percent divinylbenzene.*

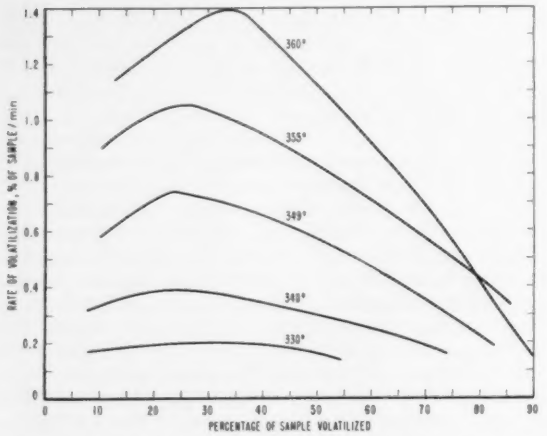

FIGURE 3. *Rates of volatilization of copolymer, 98 percent styrene—2 percent divinylbenzene.*

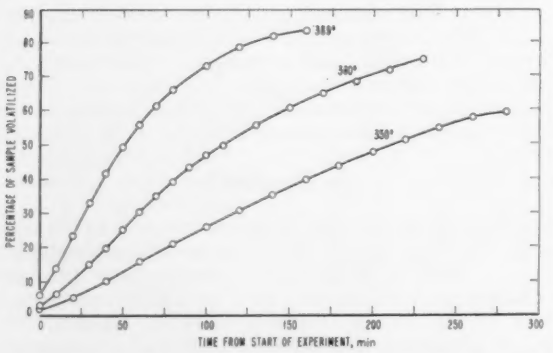

FIGURE 4. *Thermal degradation of copolymer, 75 percent styrene—25 percent divinylbenzene.*

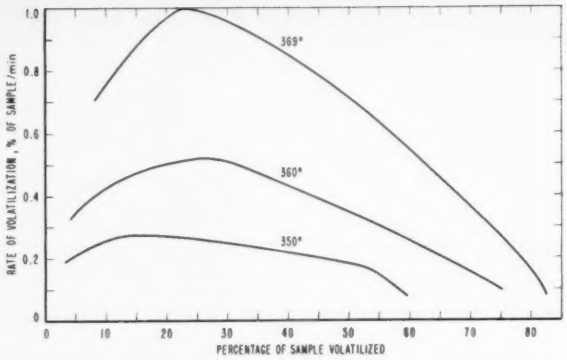

FIGURE 5. *Rates of volatilization of copolymer, 75 percent styrene—25 percent divinylbenzene.*

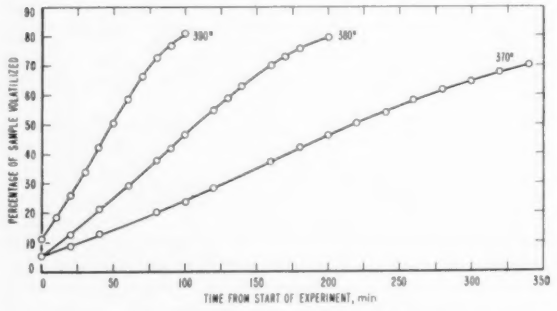

FIGURE 6. *Thermal degradation of copolymer, 52 percent styrene—48 percent divinylbenzene.*

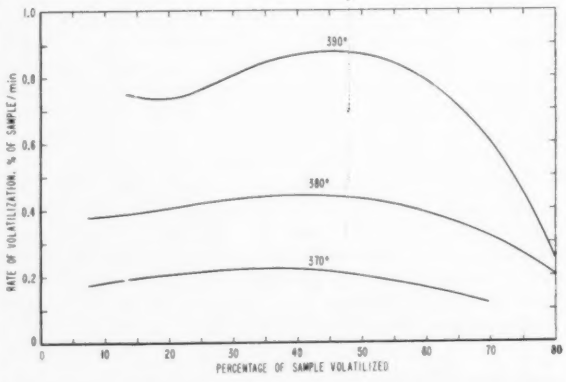

FIGURE 7. *Rates of volatilization of copolymer, 52 percent styrene—48 percent divinylbenzene.*

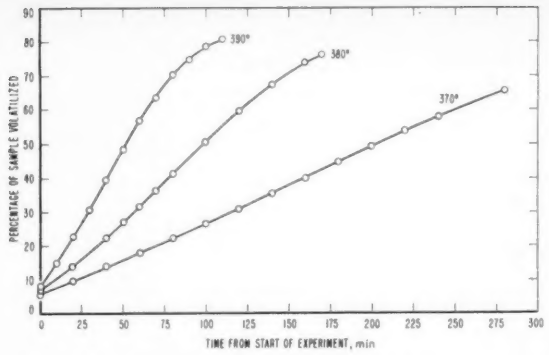

FIGURE 8. *Thermal degradation of copolymer, 44 percent styrene—56 percent divinylbenzene.*

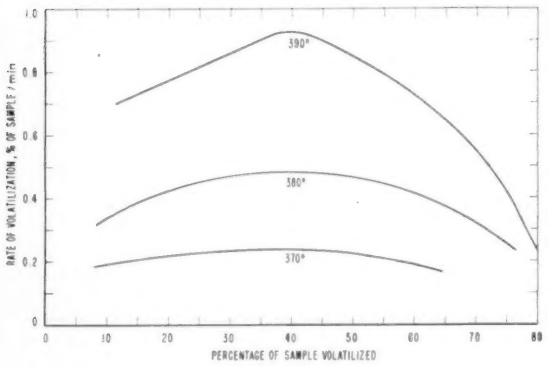

FIGURE 9. *Rates of volatilization of copolymer, 44 percent styrene—56 percent divinylbenzene.*

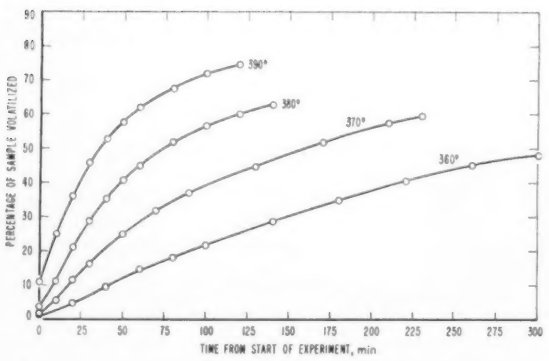

FIGURE 10. *Thermal degradation of copolymer, 75 percent styrene—25 percent trivinylbenzene.*

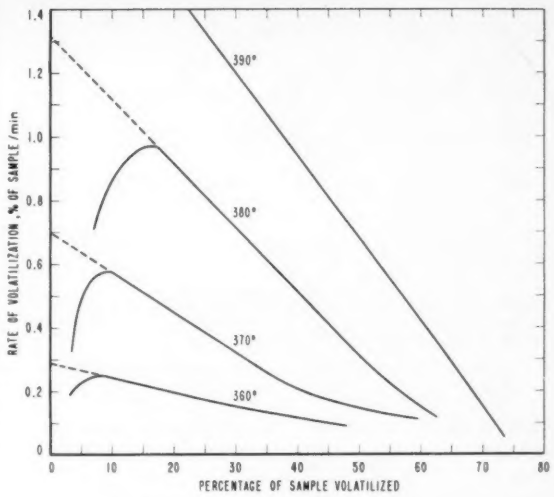

FIGURE 11. *Rates of volatilization of copolymer, 75 percent styrene—25 percent trivinylbenzene.*

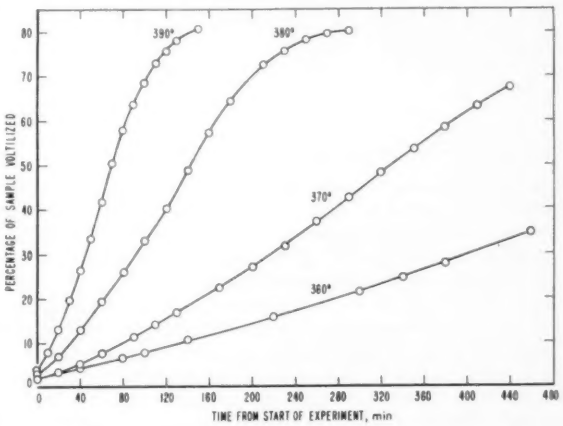

FIGURE 12. *Thermal degradation of polydivinylbenzene.*

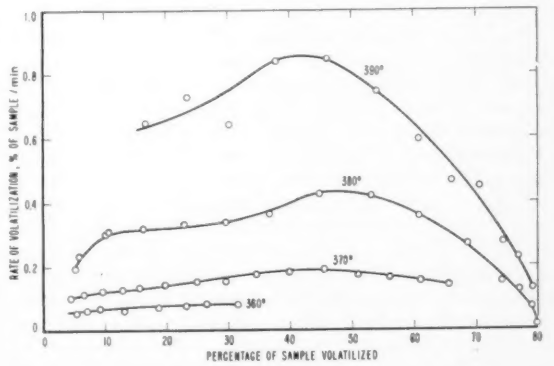

FIGURE 13. *Rates of volatilization of polydivinylbenzene.*

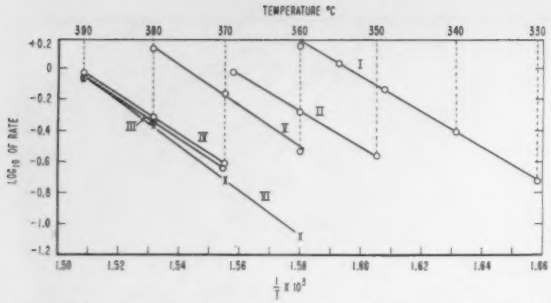

FIGURE 14. *Activation energy curves for the thermal degradation of polydivinylbenzene and of copolymers of styrene with divinylbenzene and with trivinylbenzene:*

I, styrene—2 percent DVB,
II, styrene—25 percent DVB,
III, styrene—48 percent DVB,
IV, styrene—56 percent DVB,
V, styrene—25 percent TVB,
VI, polydivinylbenzene.

trivinylbenzene can be visualized as follows: In polystyrene, cleavage of the chain ordinarily takes place at the weakest bonds, which are the C—C bonds in β-position to the double bonds in the phenyl groups—in this case the ones in the main chain.

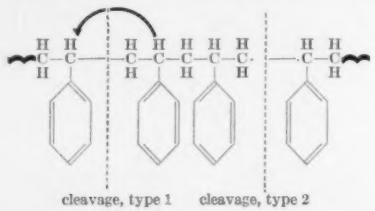

The cleavage can be of two types. Type 1 results in the formation of one saturated and one unsaturated end; and type 2 results in 2 free radicals, which proceed to unzip to give monomer, dimer, and trimer [1]. The monomer appears together with other small fragments in fraction V_{25}, while the dimer, trimer, etc., appear in fraction V_{pyr}. On the addition of a small amount of a crosslinking agent, such as 2 percent divinylbenzene, the unzipping to give dimer and trimer is somewhat blocked by the shortening of the free chain between cross links, and more of the monomer appears at the expense of the multiple units. However, with a further increase of cross links in the chain by the addition of DVB or TVB, the formation of monomer units is blocked.

The yield of monomer falls off for the copolymer containing 25 percent DVB, and even more for the copolymer containing 25 percent TVB. When the amount of the cross linking agent is still further increased, as in the case of copolymers containing 50 percent or more of DVB, no monomer appears among the volatile products.

There were no signs of carbonization of the degradation residues from copolymers with 2 or 25 percent of DVB. However, in the case of the copolymers containing higher percentages of DVB, 25 percent TVB, or of polydivinylbenzene, the volatilization curves begin to level off at about 80 to 90 percent loss (fig. 1), and carbonization of the residue takes place. The polytrivinylbenzened volatilization curve begins to level off at about 53 percent loss, and the residue shows considerable carbonization.

TABLE 3. *Rates of thermal degradation of polymers of divinylbenzene and trivinylbenzene and of their copolymers with styrene*

Material	Temperature	Rate	Activation energy [a]
	°C	%/min	kcal/mole
I 2% DVB	330	0.19	53
	340	.39	
	349	.74	
	355	1.05	
	360	1.39	
II 25% DVB	350	0.27	54
	360	0.52	
	369	1.00	
III 48% DVB	370	0.23	58
	380	.45	
	390	.88	
IV 56% DVB	370	.24	58
	380	.48	
	390	.93	
V 25% TVB	360	.29	61
	370	.70	
	380	1.32	
	390	(b)	
VI Polydivinylbenzene	360	0.08	65
	370	.19	
	380	.44	
	390	.86	
VII Polytrivinylbenzene	394	.03	73
	420	.28	
	430	.59	
	440	1.22	

[a] Activation energies for copolymers I, II, III, IV, and for homopolymer VI were calculated on the basis of maximum rates; those for copolymer V and for homopolymer VII, on the basis of initial rates.
[b] Degradation rate at this temperature was too fast to obtain an accurate extrapolated initial rate.

TABLE 4. *Activation energies based on rates of degradation at 35 percent and 50 percent volatilization*

DVB in copolymer		Percentage degradation	Activation energy
	%	%	kcal/mole
I	2	35	50
		50	50
II	25	35	56
		50	56
III	48 [a]	50	63
IV	56 [a]	50	58

[a] In the case of copolymers containing 48 percent and 56 percent DVB, the maximums in figures 7 and 9, respectively, appear at percentages of volatilization higher than 35; therefore the rates at 35 percent volatilization were not used in calculating activation energies.

5. References

[1] S. L. Madorsky and S. Straus, J. Research NBS **40,** 417 (1948) RP1886.
[2] H. Staudinger and A. Steinhofer, Ann. **517,** 35 (1935).
[3] S. L. Madorsky and S. Straus, J. Research NBS **63A,** 261 (1959).
[4] F. H. Winslow and W. Matreyek, J. Polymer Sci. **23,** 315 (1956).
[5] S. Straus and S. L. Madorsky, J. Research NBS **50,** 165 (1953) RP2405.
[6] S. L. Madorsky, J. Polymer Sci. **9,** 133 (1952).
[7] S. L. Madorsky, J. Research NBS **62,** 219 (1959) RP2957.

(Paper 65A3–108)

JOURNAL OF RESEARCH of the National Bureau of Standards—A. Physics and Chemistry
Vol. 65A, No. 3, May-June 1961

Conformations of the Pyranoid Sugars. IV. Infrared Absorption Spectra of Some Fully Acetylated Pyranoses

R. Stuart Tipson and Horace S. Isbell

(February 1, 1961)

The infrared absorption spectra of twenty pyranose acetates in the range of 5000 to 250 cm^{-1} are reported. The conformation adopted by each of fourteen of the corresponding methyl glycopyranosides (or their acetates) had previously been assigned by us from a study of their infrared spectra. Analysis of the spectra revealed, for the pyranose acetates (as for the methyl glycopyranosides and their acetates), groups of absorption bands which showed a concerted shift on change of anomeric disposition. Assignment of conformation by the methods earlier developed indicated that, for most of the compounds examined, the conformation is the same for the pyranose acetate, methyl glycopyranoside, and acetylated methyl glycopyranoside of one anomer of a monosaccharide.

The following new assignments of conformation were made: the CA conformation for penta-*O*-acetyl-α-L-*xylo*-hexulopyranose and hexa-*O*-acetyl-α-D-*gluco*-heptulopyranose; and, possibly, either a non-chair conformation or a mixture of the CA and CE conformations for hexa-*O*-acetyl-L-*glycero*-β-D-*gluco*-heptopyranose and hexa-*O*-acetyl-D-*glycero*-β-D-*galacto*-heptopyranose.

1. Scope and Purpose of the Project

As the first objective of the present project, the infrared absorption spectra of a variety of fully acetylated pyranoses were recorded for use in identifying supposedly identical samples. The spectra of three of the compounds included in the present study were recorded by Kuhn [1][1] for a limited range (1250 to 667 cm^{-1}). In the following year, the spectra of 17 of the compounds were given (for the range of 5000 to 667 cm^{-1}) by Isbell and coworkers in a privately circulated report [2] which was subsequently published [3]. Fifteen of the spectra obtained by these investigators were later discussed by Whistler and House [4], who noted certain bands in the range of 1170 to 931 cm^{-1}. Next, Barker and coworkers [5] examined the spectra of two of Kuhn's compounds and of the enantiomorph of one, together with those of three others that are included in the present study. These workers [5] discussed some of the bands in the range of 960 to 730 cm^{-1}, but the spectra were published in insufficient detail to permit comparison over a wide spectral range. In the present article, the infrared absorption spectra of 20 fully-acetylated pyranoses, in the range of 5000 to 250 cm^{-1}, are given; all of the bands of all of these esters have been measured and have received consideration.

The second objective was the discovery of correlations that might be of value in structural analysis, both as regards (a) the presence of certain functional groups and (b) the particular conformation assumed by each ester. Isbell and coworkers [3] recorded the infrared spectra of 17 of the esters dissolved in suitable solvents, and were able to reach certain conclusions regarding correlations of the kind mentioned. However, at the low concentrations they employed, minor bands were absent or difficult to detect. The spectrograms have now been recorded for the solid phase, by use of pellets consisting of crystalline ester suspended in an alkali-metal halide.

In parts II and III of this series [6, 7], a method was described for gaining information regarding the conformations of aldopyranosides and their acetates from analysis of their infrared spectra. The analysis revealed groups of absorption bands, characteristic for each group-configuration, which displayed a concerted shift on change of anomeric disposition. This empirical observation was employed, in conjunction with a consideration of instability factors (arrived at on theoretical grounds), in making conformational assignments and in deciding the arrangement of groups (e.g., axial or equatorial) at the anomeric carbon atom of these compounds. The present article describes the results obtained on applying the same kind of analysis to the infrared spectra of (a) 14 fully-acetylated aldopyranoses related to 13 of the methyl aldopyranosides and to 12 of the acetylated methyl aldopyranosides previously studied, and (b) four esters whose corresponding methyl glycopyranoside or its acetate had not been included in parts II and III. Because of a lack of configurationally related esters, the conformations of two of the acetylated pyranoses could not be determined.

2. Compounds Investigated

Table 1 gives a list of the compounds, their code numbers [8], and an index to the spectrograms; the serial number of a compound is the same as the number of its spectrogram. Also included in table 1 are (a) the conformation (where known) of the

[1] Figures in brackets indicate the literature references at the end of this paper. The references for table 1 are given at the end of the table.

TABLE 1. *Compounds measured, stable conformations, and index to spectrograms*

Code [a]	Compound	Reference	Stable conformation [b]				Spectrogram
			Assignment for methyl glycopyranoside [c]	Assignment for acetylated methyl glycoside [d]	Present assignment [e]	Anomeric disposition [e]	
12.11121	Tetra-*O*-acetyl-α-D-xylopyranose	1	CA	CA	CA	α	1
12.11221	Tetra-*O*-acetyl-β-D-xylopyranose	1	CA	CA	CA	ε	2
12.12521	Tetra-*O*-acetyl-α-D-lyxopyranose	2	CA+CE; non-chair.	CA+CE; non-chair.	CA	α	3
12.13421	Tetra-*O*-acetyl-α-L-arabinopyranose	3	CE		CE	ε	4
12.71121	Penta-*O*-acetyl-α-L-*xylo*-hexulopyranose	4			CA	α	5
12.21121	Penta-*O*-acetyl-α-D-glucopyranose	5	CA	CA	CA	α	6
12.21221	Penta-*O*-acetyl-β-D-glucopyranose	6	CA	CA	CA	ε	7
12.81121	Hexa-*O*-acetyl-α-D-*gluco*-heptulopyranose	7			CA	α	8
12.41221	Hexa-*O*-acetyl-L-*glycero*-β-D-*gluco*-heptopyranose	8			CA+CE; non-chair.	α+ε; α, ε, or q	9
12.35?21	Hexa-*O*-acety D-*glycero*-β-D-*ido*-heptopyranose	9					10
12.22121	Penta-*O*-acetyl-α-D-mannopyranose	10	CA	CA	CA	α	11
12.22221	Penta-*O*-acetyl-β-D-mannopyranose	11		CA	CA	ε	12
12.42121	Hexa-*O*-acetyl-D-*glycero*-α-L-*manno*-heptopyranose.	12	CA		CA	α	13
12.26521	Penta-*O*-acetyl-α-D-gulopyranose	9	CA+CE; non-chair.	CA+CE; non-chair.	CA+CE; non-chair.	α+ε; α, ε, or q	14
12.36121	Hexa-*O*-acetyl-D-*glycero*-α-D-*gulo*-heptopyranose	13	CA	CA	CA	α	15
12.36221	Hexa-*O*-acetyl-D-*glycero*-β-D-*gulo*-heptopyranose	13	CA	CA	CA	ε	16
12.23121	Penta-*O*-acetyl-α-D-galactopyranose	14	CA	CA	CA	α	17
12.23221	Penta-*O*-acetyl-β-D-galactopyranose	14	CA	CA	CA	ε	18
12.33521	Hexa-*O*-acetyl-D-*glycero*-β-D-*galacto*-heptopyranose.	15			CA+CE; non-chair.	α+ε; α, ε, or q	19
12.24?21	Penta-*O*-acetyl-α-D-talopyranose	16					20

[a] The third figure after the point was inserted after the present conclusions as to conformation had been reached.
[b] Named by the system of H. S. Isbell and R. S. Tipson, Science **130,** 793 (1959); J. Research NBS **64A,** 171 (1960).
[c] Assignment made by R. S. Tipson and H. S. Isbell, J. Research NBS **64A,** 239 (1960).
[d] Assignment made by R. S. Tipson and H. S. Isbell, J. Research NBS **64A,** 405 (1960).
[e] After accepting several of the assignments for the corresponding unacetylated or acetylated methyl glycopyranosides (see te xt).

References for Table 1

1. C. S. Hudson and J. M. Johnson, J. Am. Chem. Soc. **37,** 2748 (1915).
2. P. A. Levene and M. L. Wolfrom, J. Biol. Chem. **78,** 525 (1928).
3. C. S. Hudson and J. K. Dale, J. Am. Chem. Soc. **40,** 992 (1918).
4. H. H. Schlubach and G. Graefe, Liebigs Ann. Chem. **532,** 211 (1937).
5. A. Georg, Helv. Chim. Acta **12,** 261 (1929).
6. C. S. Hudson and J. K. Dale, J. Am. Chem. Soc. **37,** 1264 (1915).
7. W. C. Austin, J. Am. Chem. Soc. **54,** 1925 (1932).
8. H. L. Frush and H. S. Isbell, unpublished results. The optical rotation of the compound was equal in magnitude, but opposite in sign, to that of its enantiomorph [R. Hann and C. S. Hudson, J. Am. Chem. Soc. **59,** 548 (1937)], and the two compounds had the same melting point.
9. H. L. Frush and H. S. Isbell, J. Research NBS **35,** 111 (1945) RP1663.
10. C. S. Hudson and J. K. Dale, J. Am. Chem. Soc. **37,** 1280 (1915).
11. D. H. Brauns, J. Research NBS **7,** 573 (1931) RP358.
12. H. S. Isbell, F. A. Smith, E. C. Creitz, H. L. Frush, J. D. Moyer, and J. E Stewart, J. Research NBS **59,** 41 (1957) RP2772.
13. C. S. Hudson and E. Yanovsky, J. Am. Chem. Soc. **38,** 1575 (1916).
14. C. S. Hudson and H. O. Parker, J. Am Chem. Soc. **37,** 1589 (1915).
15. E. Montgomery and C. S. Hudson, J. Am. Chem. Soc. **56,** 2463 (1934).
16. W. W. Pigman and H. S. Isbell, J. Research NBS **19,** 189 (1937) RP1021.

corresponding methyl glycoside and acetylated methyl glycoside, as determined in parts II and III of this series [6, 7], and (b) assignments of conformations to the acetylated pyranoses. The conformations are indicated by the system devised by Isbell and Tipson [9].

The spectra were measured in the region of 5000 to 250 cm^{-1}. The spectrograms are given together with a discussion of (a) the structure of the compounds and (b) some of the outstanding features of their spectra.

All of the compounds listed in table 1 are fully acetylated monosaccharides, and all have the pyranoid ring. Compounds 5 and 8 are acetates of ketopyranoses; the rest of the compounds are acetates of aldopyranoses. The pyranose acetates differ in regard to one or more of the following structural features: (a) the α or β anomeric configuration at the reducing carbon atom; (b) the configurations of the other carbon atoms of the pyranoid ring (including C5 in the aldohexose and the heptose acetates); (c) the nature of the substituent, if any, at C5 (including the configuration at C6 of the aldoheptose acetates); and (d) the presence or absence of a *C*-(acetoxymethyl) group at C1 of the pyranoid ring.

3. Reference Aldopyranosides and Their Acetates (of Known Conformation)

In part II of this series, the stable conformations of 13 crystalline aldopyranosides and, in part III, of 12 crystalline acetates thereof, all of which are related to compounds in the present study, were deduced from analysis of their infrared spectra.

In the present study, the crystalline acetates of 14 corresponding pyranoses were available (group A). In addition, six pyranose acetates (group B) whose glycosides or acetylated glycosides had not been available were examined. The spectra of the acetates in group A were analyzed, in order to determine whether they were explicable on the basis that a pyranose acetate has the same conformation as its glycopyranoside and acetylated glycopyranoside relatives. The conclusions drawn from this study were then applied to deducing the stable conformation of members of group B.

4. Classification of the Acetylated Pyranoses into Configurationally Related Groups

The 20 esters were classified into four groups; the members of each group have like configurational features.

4.1. Acetylated Pyranoses of the *xylo* Configuration

The members of this group have general formula I for the CA conformation.

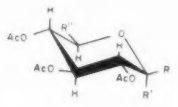

I

The following compounds, in this conformation, have structure I, with the substituents indicated.

1. Tetra-*O*-acetyl-α-D-xylopyranose, R=H; R′=OAc; and R″=H.
2. Tetra-*O*-acetyl-β-D-xylopyranose, R=OAc; R′=H; and R″=H.
5. Penta-*O*-acetyl-α-L-*xylo*-hexulopyranose (penta-*O*-acetyl-α-L-sorbopyranose), R=CH_2OAc; R′=OAc; R″=H; and the molecule is the mirror image of that depicted.
6. Penta-*O*-acetyl-α-D-glucopyranose, R=H; R′=OAc; and R″=CH_2OAc.
7. Penta-*O*-acetyl-β-D-glucopyranose, R=OAc; R′=H; and R″=CH_2OAc.
8. Hexa-*O*-acetyl-α-D-*gluco*-heptulopyranose, R=CH_2OAc; R′=OAc; and R″=CH_2OAc.
9. Hexa-*O*-acetyl-L-*glycero*-β-D-*gluco*-heptopyranose, R=OAc; R′=H; and R=$AcOH_2C—\underset{OAc}{\overset{H}{C}}—$.

Compound 10 has the following formulas (II) for the two chair-conformations.

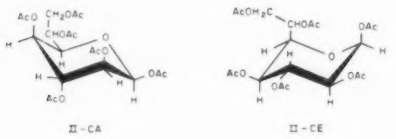

II-CA II-CE

10. Hexa-*O*-acetyl-D-*glycero*-β-D-*ido*-heptopyranose

4.2. Acetylated Pyranoses of the *lyxo* Configuration

Four members of this group have the *lyxo* or *manno* configuration and general formula III for the CA conformation.

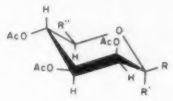

III

The following compounds, in this conformation, have structure III, with the substituents indicated.

3. Tetra-*O*-acetyl-α-D-lyxopyranose, R=H; R′=OAc; and R″=H.
11. Penta-*O*-acetyl-α-D-mannopyranose, R=H; R′=OAc; and R″=CH_2OAc.
12. Penta-*O*-acetyl-β-D-mannopyranose, R=OAc; R′=H; and R″=CH_2OAc.
13. Hexa-*O*-acetyl-D-*glycero*-α-L-*manno*-heptopyranose, R=H; R′=OAc; R″=$AcOH_2C—\underset{OAc}{\overset{H}{C}}—$; and the molecule is the mirror image of that depicted.

Compounds 14 to 16 have the D-*gulo* configuration and the following general formula (IV) for the CA conformation.

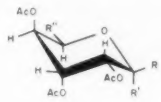

IV

14. Penta-*O*-acetyl-α-D-gulopyranose, R=H; R′=OAc; and R″=CH_2OAc.
15. Hexa-*O*-acetyl-D-*glycero*-α-D-*gulo*-heptopyranose, R=H; R′=OAc; and R″=$AcOH_2C—\underset{OAc}{\overset{H}{C}}—$.
16. Hexa-*O*-acetyl-D-*glycero*-β-D-*gulo*-heptopyranose, R=OAc; R′=H; and R″=$AcOH_2C—\underset{OAc}{\overset{H}{C}}—$.

4.3. Acetylated Pyranoses of the *arabino* Configuration

The CE conformation of compound 4 and the CA conformation of compounds 17 to 19 are depicted in general formula V.

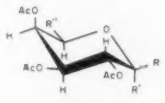

V

4. Tetra-*O*-acetyl-α-L-arabinopyranose, R=OAc; R′=H; and R″=H.

17. Penta-*O*-acetyl-α-D-galactopyranose, R=H; R′=OAc; and R″=CH_2OAc.
18. Penta-*O*-acetyl-β-D-galactopyranose, R=OAc; R′=H; and R″=CH_2OAc.
19. Hexa-*O*-acetyl-D-*glycero*-β-D-*galacto*-heptopyranose, R=OAc; R′=H; and R″=

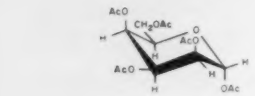

20. Penta-*O*-acetyl-α-D-talopyranose

4.4. Acetylated Aldopyranose of the *ribo* Configuration

The two chair-conformations of compound 20 are depicted in formulas VI.

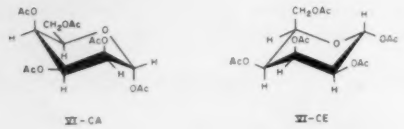

VI-CA VI-CE

5. Discussion of the Spectra

In the present study, the positions of the various absorption bands for each of 20 acetylated pyranoses have been determined; the relative intensities of absorption were not examined in detail. The bands were compiled, and were studied by comparative methods, as previously described [10].

The conformations of 13 of the corresponding glycopyranosides and of 12 of the acetylated glycopyranosides had previously been assigned by us [6,7] from a study of their infrared absorption spectra (see table 1). Assignment was made on the basis of the empirical observation that a change of anomeric disposition was accompanied by a shift of certain absorption bands.

The same kind of examination has now been applied to the spectra of the fully acetylated derivatives of 14 pyranoses related to the glycosides just mentioned, and a similar empirical relationship (between anomeric disposition and the position of certain absorption bands) was observed. On the basis of this finding, conformational assignments were made for these 14 pyranose acetates and were found to be in essential agreement with those for their glycosidic relatives (both acetylated and unacetylated).

The remaining 6 spectra were those of pyranose acetates for whose glycosidic relatives we had made no conformational assignment. The spectra of four of these acetates (compounds 5, 8, 9, and 19 in table 1) were intercompared with those of related acetates, especially in regard to anomer-differentiating absorption bands, and assignments were made (see table 1). For compounds 10 and 20, the spectra of related acetates were not available, and assignments could not be made.

5.1. Absorption Bands Possibly Indicative of the Disposition of Groups at the Anomeric Carbon Atom of the Tetra-*O*-acetyl-pentopyranoses

The spectrum of tetra-*O*-acetyl-β-D-xylopyranose (compound 2) was compared with that of its α anomer (compound 1), in order to determine the effect of changing the anomeric acetoxyl group from equatorial to axial (or vice versa). A comparison was then made with the spectrum of tetra-*O*-acetyl-α-L-arabinopyranose (compound 4).

In table 2 are listed those bands that are essen-

TABLE 2. *Bands (cm^{-1}) shown by both anomers of tetra-O-acetyl-D-xylopyranose (compounds 1 and 2) and by tetra-O-acetyl-α-L-arabinopyranose (4), and positionally corresponding bands of tetra-O-acetyl-α-D-lyxopyranose (3)*

Tetra-*O*-acetyl-D-xylo-pyranoses		Tetra-*O*-acetyl-α-L-arabino-pyranose	Tetra-*O*-acetyl-α-D-lyxo-pyranose
1	2	4	3
Possibly non-configurational bands			
2959	2967	2976	2967
2915	2890	2924	2899
2114	2114	2114	2105
1739	1742	1736	1742
1473	1473	1462	1484
1439	1437	1433	1439
1377	1381	1374	1377
1230	1235	1233	1227
1178	1172	1181	1170
1105	1085	1096	1099
1046	1041	1045	1052
1026	1028(?)	[a] 1024	1021
989	991	995	985
965	962	967	963
947, [a]942	[b] 941	[b] 948	946
899	[b] 899	[b] 900	903, 889
875	[b] 880	[b] 880	885
679	703	679	690
673	671	671	670
643	646	643	647
601	602	600	599
567	568	553	556
545	542	536	534
515	502	506	508
488	491	489	488
398	394	399	395
372	377	379	379
365	364	366	369, 364
358	359	359	358
351	353	351	354
344	342	341	342
288	309	283	297
Bands possibly affected by configuration and conformation			
		2874	
1751	1757	1751	
1330	1326	1332	
1304	1312	1309	
		1295	1295
1261	1258	1263	
1142	1130	1133	
		1116	1111
1066	1071		1073, 1064
[a] 1016	1014		[a] 1009
		956	
930	935		929
		[b] 865	857
		[b] 751	774
520	523		
458	459	457	
448(?)	451(?)		447
443(?)	444(?)	442(?)	
437(?)	436(?)	435(?)	
430(?)	429(?)		
424(?)	423(?)	421	
404	402		
264	268	274, 267	

[a] These bands were mentioned by R. L. Whistler and L. R. House [4].
[b] These bands were mentioned by S. A. Barker and coworkers [5]—for the enantiomorphs of the compounds in tables 2 and 3.

tially the same for these three esters, together with bands (in about the same positions) shown by tetra-*O*-acetyl-α-D-lyxopyranose (compound 3). Bands shown by all four of these acetates are tentatively assumed to be independent of total configuration, whereas those shown by compounds 1 and 2 but not by both compounds 3 and 4, or by compounds 3 or 4 but not by compounds 1 and 2, may possibly be affected by configuration.

The bands shown by only one anomer of tetra-*O*-acetyl-D-xylopyranose are given in table 3, together with corresponding bands of tetra-*O*-acetyl-α-L-arabinopyranose. The resemblance between compounds 2 and 4 may be noted. If these "anomer-differentiating" bands have any relationship to the axial or equatorial disposition of the anomeric acetoxyl group, it may be concluded that compounds 2 and 4 have the same anomeric disposition, whereas that for compound 1 is different. If the assignment previously made [6] for the methyl glycopyranoside corresponding to *any one of these three* esters is extended to the related pyranose acetate, the conformations of the other two are deducible from the results in table 3. Thus, if the anomeric acetoxyl group of compound 2 is equatorial and that of its α anomer is axial, the results indicate that the anomeric acetoxyl group of tetra-*O*-acetyl-α-L-arabinopyranose is equatorial.

On the other hand, the spectrum of compound 3, although showing two bands in common with that of compound 2 (see table 3), bears a much greater resemblance to that of compound 1, suggesting that the crystalline material (3) may have the CA conformation. If this conclusion is correct, it indicates that the stable conformation of a fully acetylated pyranose need not necessarily be the same as the stable conformation of the corresponding fully acetylated methyl glycopyranoside. Presumably, change from the methoxyl group to the acetoxyl group at carbon atom 1 may result in a sufficiently great alteration in nonbonded attractions and repulsions to cause a change in conformation.

5.2. Analysis of the Spectra of Groups of Configurationally Related Pyranose Acetates, Excluding the Pentopyranose Acetates

The spectra of penta-*O*-acetyl-α-L-*xylo*-hexulopyranose (compound 5) and hexa-*O*-acetyl-α-D-*gluco*-heptulopyranose (compound 8) were compared with those of the anomers of penta-*O*-acetyl-D-glucopyranose (compounds 6 and 7). Compounds 5, 6, and 8 show the following bands not shown [2] by compound 7: at 1312 to 1302 cm^{-1}; 1174 to 1168 cm^{-1}; 960 to 949 cm^{-1}; 938 cm^{-1}; 746 to 712 cm^{-1}; 418 to 413 cm^{-1}; and 395 to 394 cm^{-1}. Compounds 5 and 6 show bands (not shown by compounds 7 and 8) at 1115 to 1111 cm^{-1} and 556 to 550 cm^{-1}, and compound 6 does not show a band at 606 to 600 cm^{-1} that is displayed by compounds 5, 7, and 8; with these exceptions, these observations indicate that *compounds 5 and 8 resemble compound 6*. Thus, if compound 6 has an axial anomeric (acetoxyl) group, it seems likely that compounds 5 and 8 also have an axial anomeric acetoxyl group and, consequently, have an equatorial acetoxymethyl group attached to C1 of the xylopyranose ring.

[2] Barker and coworkers [5] originally reported bands at 949 and 938 cm^{-1} for compound 7. In a private communication from S. A. Barker and R. Stephens (August 12, 1960), we learn that they have since recorded the spectrum of a purified sample of compound 7 and find no absorption between 978 and 911 cm^{-1}.

TABLE 3. *Bands (cm^{-1}) shown by only one anomer of the tetra-O-acetyl-D-xylopyranoses (compounds 1 and 2) and by tetra-O-acetyl-α-L-arabinopyranose (4), compared with bands for tetra-O-acetyl-α-D-lyxopyranose (3)*

1	2	4	3
2994	----------	----------	3003
1319	----------	----------	1321
1247	----------	----------	1242
1149	----------	----------	1148
1038	----------	----------	1033
724	----------	----------	----------
469	----------	----------	----------
414	----------	----------	412
386	----------	----------	----------
----------	1222	1225, 1218	1217
----------	[a] 912	[a] 915	----------
----------	656	655	----------
----------	616	615	633
----------	591	582	----------

[a] See footnote b to table 2.

TABLE 4. *Comparison [a] of absorption bands (cm^{-1}) shown by the anomers of penta-O-acetyl-D-glycopyranose (compounds 6 and 7) and by hexa-O-acetyl-L-glycero-β-D-gluco-heptopyranose (9)*

A		B	C		D	E	
6	7	9	6	9	6	7	9
1456	1464	1215(?)	1115	1119	1414	600	597
1383	1381	761	[b] 950	955	1302	442	445
1105	1098		[b,c] 938	941	1238		
1062	1068		[b] [846	[d] 844]	1168		
1038	1044		[b] 746	742	550		
[c] 1022	1010		418	422	399, 395		
[b] 917	[b] 913						
666	654(?)						
474	475						
434, 427	431						
366	368						

[a] Key: A. Bands shown by compounds 6 and 7, but not by 9. B. Bands shown by compound 9, but not by 6 and 7. C. Bands shown by compounds 6 and 9, but not by 7. D. Bands shown by compound 6, but not by 7 and 9. E. Bands shown by compounds 7 and 9, but not by 6.
[b] See footnote b to table 3.
[c] See footnote a to table 2.
[d] Compound 7, in carbon tetrachloride, shows a band at 855 cm^{-1} [3].

The spectrum of hexa-*O*-acetyl-L-*glycero*-β-D-*gluco*-heptopyranose (compound 9) was now compared with those of compounds 6 and 7. The results are given in table 4, from which it may be seen that compounds 6 and 9 have 5 bands in common (column C) that are not shown by compound 7. On the other hand, compounds 7 and 9 show 2 bands (column E) not shown by compound 6, and compound 6 shows 6 bands (column D) not shown by compounds 7 and 9. These results indicate about equal similarity between compounds 7 and 9 as between compounds 6 and 9, and, hence, suggest either (a) that compound 9 adopts a non-chair conformation or a mixture of the CA and CE conformations, or (b) that, in this kind of analysis, the spectrum of a fully acetylated heptopyranose may not necessarily be intercomparable with those of the related hexopyranose acetates.

Penta-*O*-acetyl-β-D-mannopyranose and hexa-*O*-acetyl-D-*glycero*-α-L-*manno*-heptopyranose (compounds 12 and 13) show two bands (at 3003 to 2985 cm^{1-} and at 616 to 615 cm^{-1}) that are not shown by penta-*O*-acetyl-α-D-mannopyranose (compound 11). On the other hand, compounds 11 and 13 show seven bands that are not shown by compound 12: at 1295 to 1294 cm^{1-}, 1081 to 1076 cm^{-1}, 839 to 837 cm^{-1}, 787 to 777 cm^{-1}, 475 to 466 cm^{-1}, 439 to 433 cm^{-1}, and 414 to 413 cm^{-1}; and compound 12 shows 12 bands that are not shown by compounds 11 and 13: at 2882, 1383, 1093, 758 (this band was mentioned by Barker and coworkers [5]), 589, 520, 488, 446, 407, 377, 364, and 345 cm^{-1}. These results indicate a considerable resemblance between compounds 11 and 13. Thus, if the anomeric acetoxyl group of compound 11 is axial, it seems likely that the anomeric acetoxyl group of hexa-*O*-acetyl-D-*glycero*-α-L-*manno*-heptopyranose (13) is also axial.

In parts II and III of this series [6,7], evidence was obtained that indicated that the methyl glycopyranosides and their acetates corresponding to the α and β anomers of hexa-*O*-acetyl-D-*glycero*-D-*gulo*-heptopyranose (15 and 16; see table 1) have the CA conformation, whereas those corresponding to penta-*O*-acetyl-α-D-gulopyranose (compound 14) consist of a mixture of the CA and CE conformations or adopt a non-chair conformation. In table 5,[3] the anomer-differentiating bands of compounds 15 and 16 are compared with bands shown by compound 14. It may be seen that compound 14 shows about equal similarity to either compound 15 or 16; this conclusion suggests that crystalline penta-*O*-acetyl-α-D-gulopyranose (compound 14) exists as a mixture of the CA and CE conformations or as a non-chair conformation.

Finally, an assignment of conformation was sought for hexa-*O*-acetyl-D-*glycero*-β-D-*galacto*-heptopyranose (compound 19). In table 6, the bands differentiating between penta-*O*-acetyl-α-D-galactopyranose (compound 17) and its β anomer (compound 18) are compared with bands for compound 19. It may be seen that compound 19 shows about equal similarity to either compound 17 or 18, suggesting that crystalline hexa-*O*-acetyl-D-*glycero*-β-D-*galacto*-heptopyranose (compound 19) exists as a mixture of the CA and CE conformations or as a non-chair conformation. This conclusion is surprising, as there has hitherto been no indication of such conformations for compounds having a *galacto* configuration. Possibly, as previously mentioned, the spectrum of a fully acetylated heptopyranose may not, in this kind of analysis, necessarily be intercomparable with those of the related hexopyranose acetates.

No assignment could be made for hexa-*O*-acetyl-D-*glycero*-β-D-*ido*-heptopyranose (compound 10), because of the lack of its α anomer. Similarly, no assignment could be made for penta-*O*-acetyl-α-D-talopyranose (compound 20), because of a lack of other pyranose acetates having the *talo* configuration.

[3] To conserve space, bands which do not differentiate between anomers have been omitted from tables 5 and 6.

TABLE 5. *Bands (cm^{-1}) shown [a] by only one anomer of hexa-O-acetyl-D-glycero-D-gulo-heptopyranose (compounds 15 and 16), compared with bands for penta-O-acetyl-α-D-gulopyranose (14)*

A		B	C		D
14	15	16	14	16	15
1462	1453	3003	2941	2941	1366
1304	1304	1280	1443	1443	1064
1114	1114	1205	1318	1319	781
994	983	1105	[b] 1170	1186	718
952	952	1030	1139	1130	
884	887	848	903	899	
816	829	523	769	766	
477	462	444			

[a] Key: A. Bands shown by compounds 14 and 15, but not by 16. B. Bands shown by compound 16, but not by 14 and 15. C. Bands shown by compounds 14 and 16, but not by 15. D. Bands shown by compound 15, but not by 14 and 16.
[b] See footnote a to table 2.

TABLE 6. *Comparison [a] of absorption bands (cm^{-1}) shown by the penta-O-acetyl-D-galactopyranoses (compounds 17 and 18) and by hexa-O-acetyl-D-glycero-β-D-galacto-heptopyranose (19)*

A		B	
17	19	18	19
1779	1770	1156	1155
1250	1252	[b] 1122	1124
1133	[b] 1131	1068	1065
837	832	[c] 916	927
696	700	[c] 869	873
615	610	641	641
		575	573
		366	370

[a] Key: A. Bands shown by compounds 17 and 19, but not by 18. B. Bands shown by compounds 18 and 19, but not by 17.
[b] See footnote a to table 2.
[c] See footnote b to table 2.

From a study of the proton magnetic-resonance spectra of compounds 1 to 4, 6, 7, 11, 12, 14, 17, and 18, Lemieux and coworkers [11] made exactly the same assignments of anomeric disposition as we now find for these compounds (see table 1).

Many of the bands observed for the pyranose acetates cannot yet be assigned to particular vibrational modes; in sections 5.1 and 5.2, we have not been concerned with (a) which bands, arising from vibrations localized in a functional group, are relatively independent of the remainder of the molecule, or (b) which bands involve other parts of the molecule. Bands possibly attributable to specific functional groups are considered in section 5.3.

5.3. Other Absorption Bands

All of the compounds in this study are acetates, and their spectra all show at least one band at 1757 to 1742 cm^{-1} (C=O stretching frequency); at 1269 to 1241 cm^{-1}; at 1236 to 1212 cm^{-1}; at 646 to 626 cm^{-1}; and at 612 to 598 cm^{-1}. All of the spectra show at least one band at 2985 to 2950 cm^{-1} (or 2976 to 2941 cm^{-1}; C—H stretching); and at 1449 to 1420 cm^{-1} and 1333 to 1312 cm^{-1} (C—H bending). All of the spectra show an absorption band at 1381 to 1366 cm^{-1}, presumably caused by deformation of the CH_3 groups. All of the spectra also show a

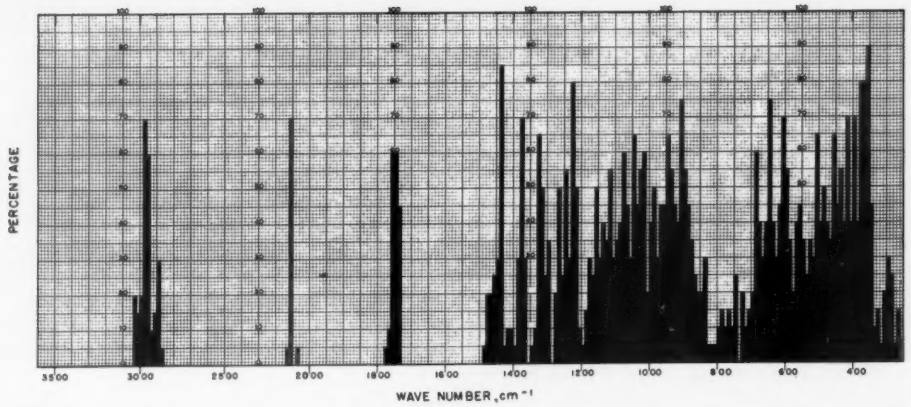

FIGURE 1. *Percentage (of the 20 pyranose acetates) which showed infrared absorption at the various regions of the infrared spectrum (5000 to 250 cm^{-1}).*

band at 1148 to 1114 cm^{-1}; 1105 to 1073 cm^{-1}; 1073 to 1042 cm^{-1}; 1036 to 1011 cm^{-1}; 911 to 899 cm^{-1}; 415 to 399 cm^{-1}; and 377 to 366 cm^{-1} (or 370 to 353 cm^{-1}). All of the spectra seem to show a weak band at 2132 to 2075 cm^{-1}, probably a combination or overtone.

Figure 1 gives the percentage of the 20 acetates in this study that show absorption bands in the various regions of the infrared spectrum. For the range of 5000 to 2000 cm^{-1}, decrements of 20 cm^{-1} were used; and, for the range of 2000 to 250 cm^{-1}, decrements of 10 cm^{-1}.

6. Experimental Procedure

6.1. Preparation and Purification of the Compounds

The compounds listed in table 1 were prepared by the methods given in the references cited. Most of the compounds were prepared in the course of earlier studies on the pyranose acetates. Each acetate was recrystallized from an appropriate solvent until further recrystallization caused no change in its melting point or optical rotation.

6.2. Preparation of the Pellets

Samples used for photometric study consisted of pellets comprising the crystalline acetate suspended in an alkali-metal halide, exactly as previously described [10]. For the range of 5000 to 667 cm^{-1}, a concentration of 0.4 mg of acetate per 100 mg of potassium chloride was used; the spectrum of compound 2 was also recorded for a film prepared on the sodium chloride window by evaporation of a carbon tetrachloride solution of the compound with a heat lamp. For the range of 667 to 250 cm^{-1}, a concentration of 2 mg of acetate per 100 mg of potassium iodide was used, except for compounds 8 and 9 (3 mg per 100 mg).

6.3. Measurement of Infrared Absorption

The spectrograms [4] are shown in figures 2 and 3; they were recorded with a Perkin-Elmer Model 21 (double-beam) spectrophotometer equipped with a prism of sodium chloride (for the range of 5000 to 667 cm^{-1}) and of cesium bromide (for the range of 667 to 250 cm^{-1}), as previously described [10].

Some absorption attributable to water (in the compound, the alkali halide, or both) was observed at 3448 and 1639 cm^{-1} and, attributable to atmospheric water vapor, in the far-infrared curves. These regions are drawn on the spectrograms with dashed lines which are not to be interpreted quantitatively.

6.4. Spectra Measured Under Different Conditions

The spectra of 17 of the pyranose acetates (compounds 1 to 7 and 10 to 19) had previously been measured [3] in carbon tetrachloride or chloroform and in either carbon disulfide or dioxane. Since the infrared absorption spectra of crystalline materials show more bands than the spectra of the same compounds in solution, a larger number of bands were available for correlations than in the previous study [3].

In addition, the spectra of 13 acetylated aldopyranosides had been recorded for the solid phase [7] and for solutions [3]. The spectra for the solid and the liquid phases of these 30 compounds are, in all cases, *in striking agreement* (after making allowance for the sharpening of the bands for the crystalline samples). This observation suggests that, if the geometry of the molecule is reflected in its vibration spectrum, each of these compounds adopts the same conformation(s) in the solid phase as it does in solution.

The authors express their gratitude to H. L. Frush for assistance in preparing the compounds used in this study, and to J. E. Stewart and F. P. Czech for recording the infrared absorption spectra.

[4] A few bands that show clearly in the original spectrograms are difficult to see in the published spectra, because of the reduction in size.

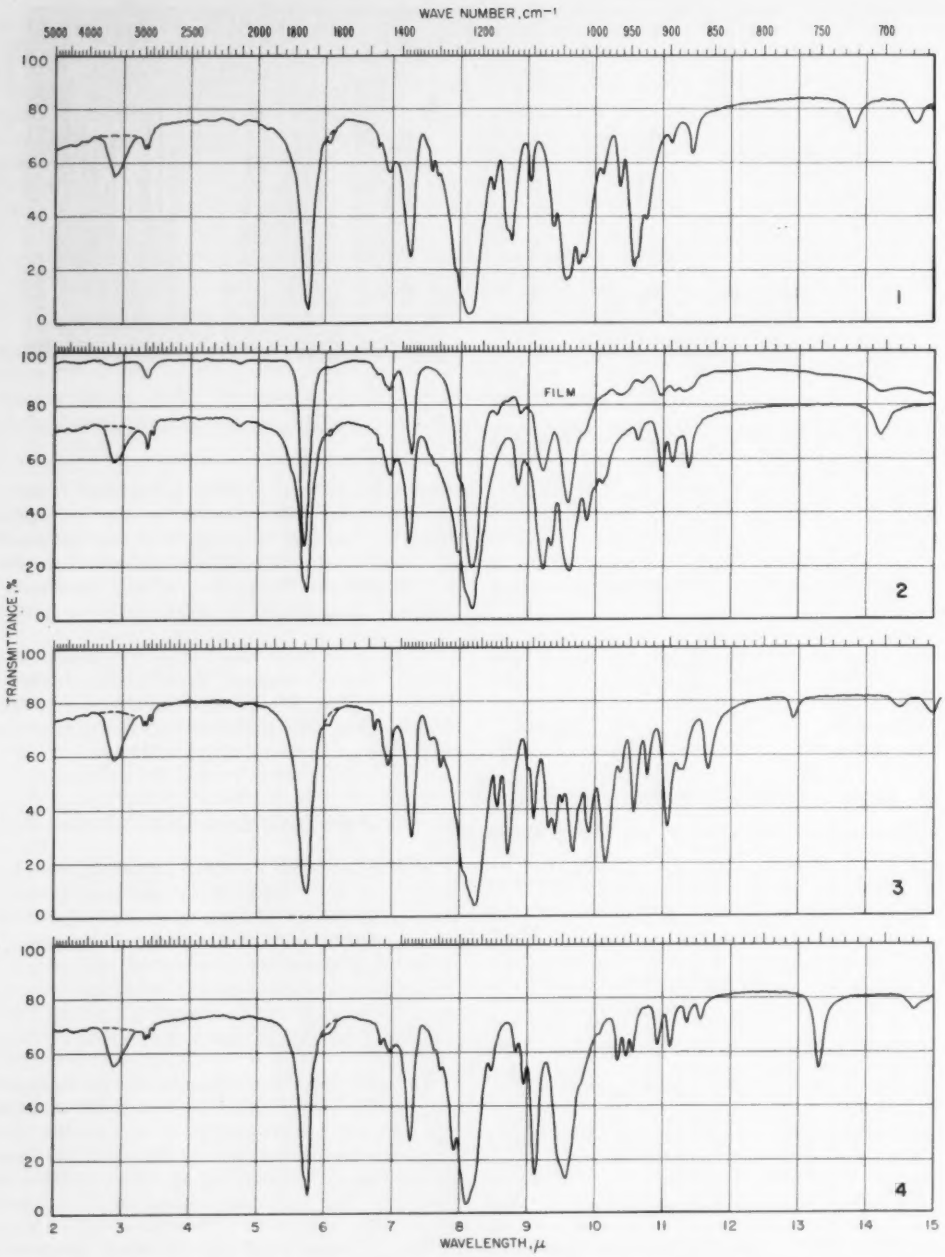

FIGURE 2. *Spectrograms of materials in potassium chloride pellets.*

1, Tetra-*O*-acetyl-α-D-xylopyranose; **2,** tetra-*O*-acetyl-β-D-xylopyranose; **3,** tetra-*O*-acetyl-α-D-lyxopyranose; **4,** tetra-*O*-acetyl-α-L-arabinopyranose.

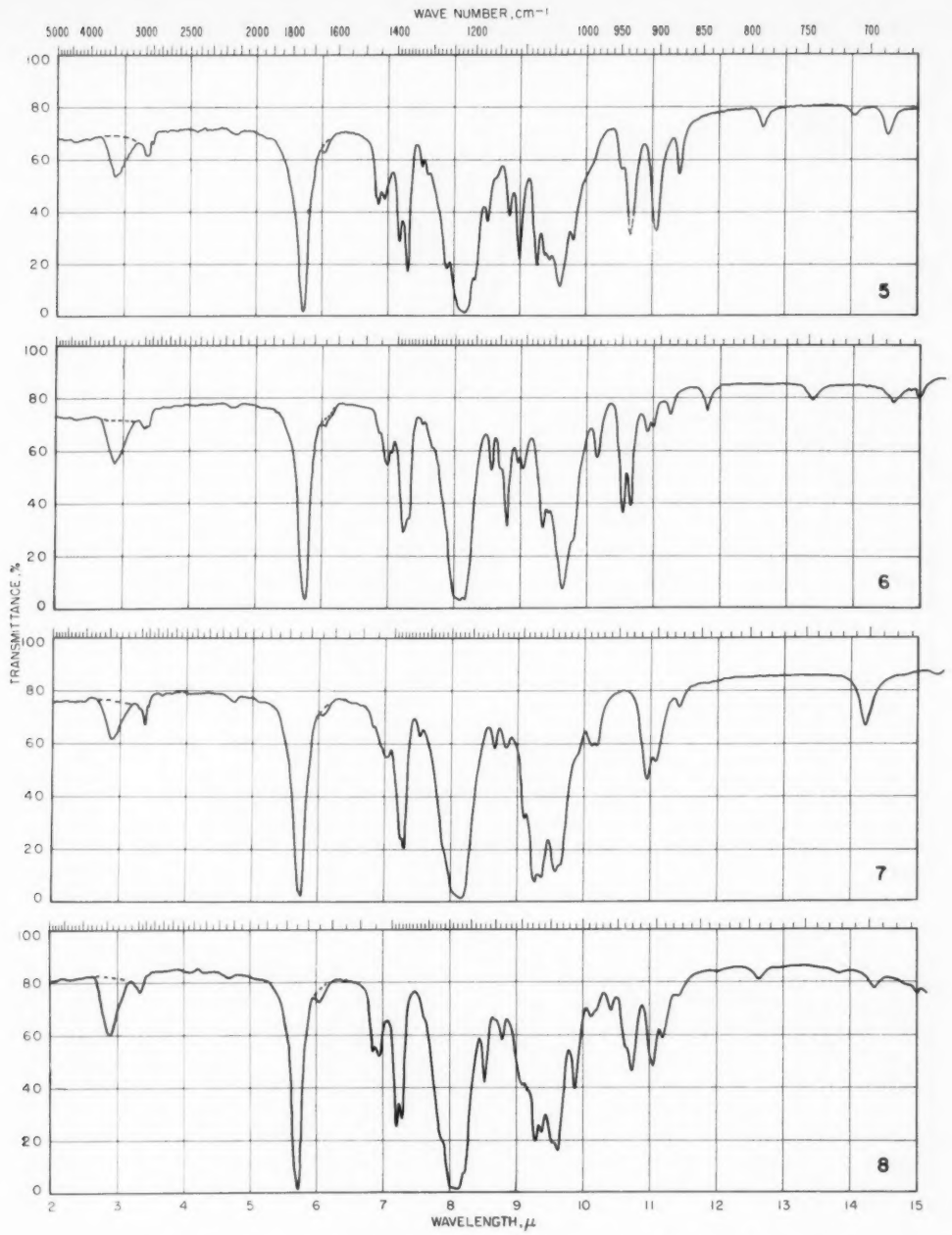

FIGURE 2. *Spectrograms of materials in potassium chloride pellets.*—Continued

5, penta-*O*-acetyl-α-L-*xylo*-hexulopyranose; **6**, penta-*O*-acetyl-α-D-glucopyranose; **7**, penta-*O*-acetyl-β-D-glucopyranose; **8**, hexa-*O*-acetyl-α-D-*gluco*-heptulopyranose.

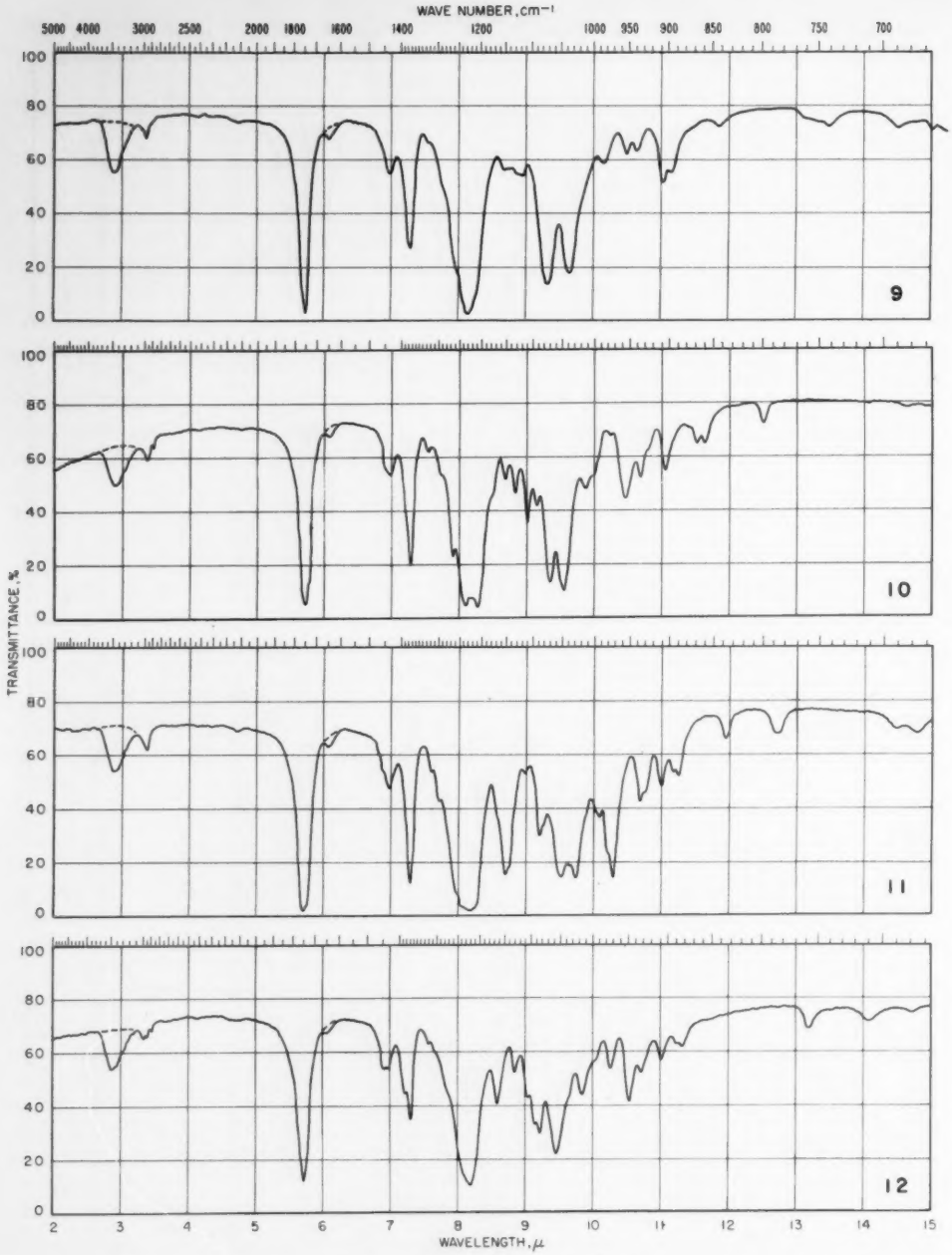

FIGURE 2. *Spectrograms of materials in potassium chloride pellets.*—Continued

9, hexa-*O*-acetyl-L-*glycero*-β-D-*gluco*-heptopyranose; **10,** hexa-*O*-acetyl-D-*glycero*-β-D-*ido*-heptopyranose; **11,** penta-*O*-acetyl-α-D-mannopyranose; **12,** penta-*O*-acetyl-β-D-mannopyranose.

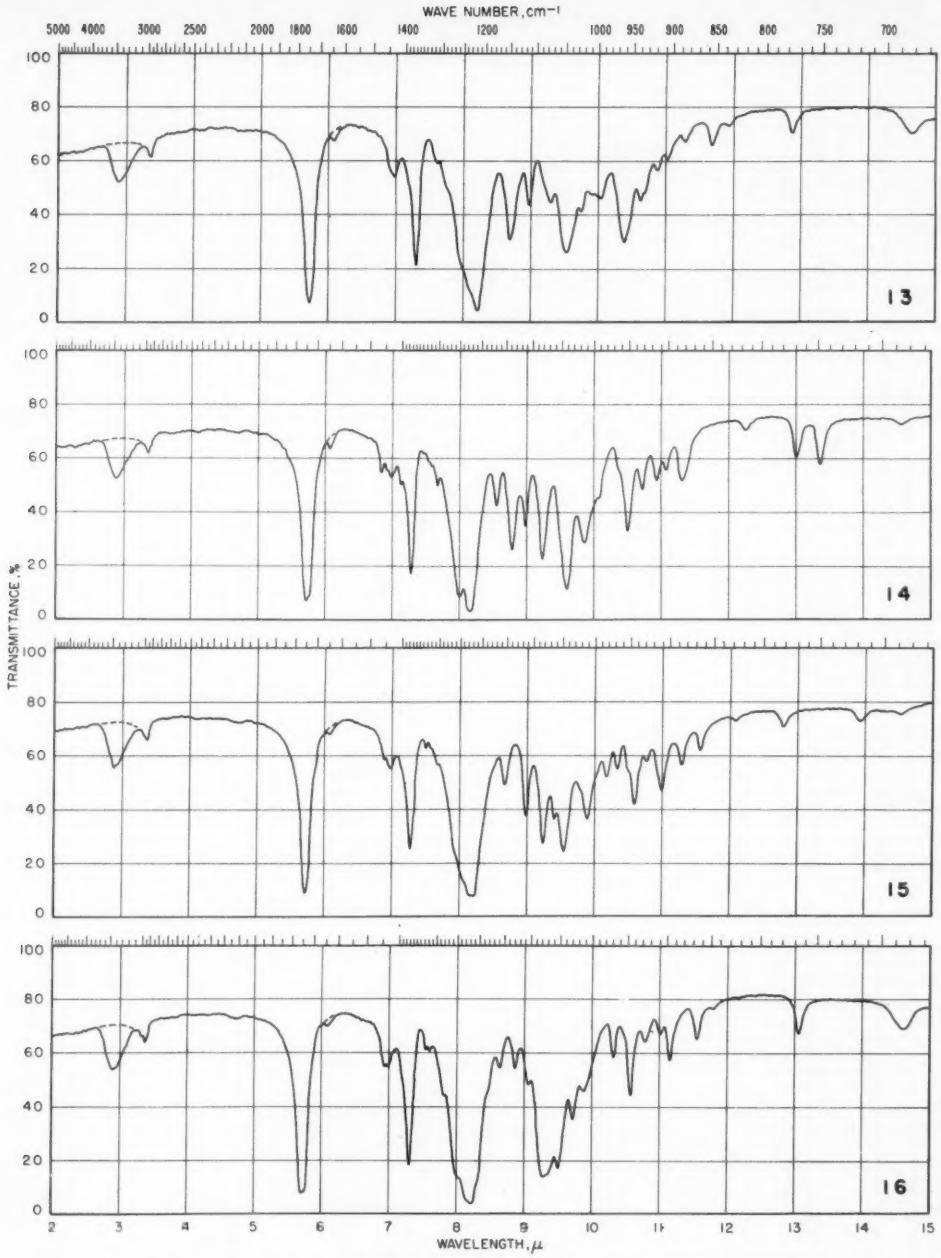

FIGURE 2. *Spectrograms of materials in potassium chloride pellets.*—Continued

13, hexa-*O*-acetyl-D-*glycero*-α-L-*manno*-heptopyranose; **14,** penta-*O*-acetyl-α-D-gulopyranose; **15,** hexa-*O*-acetyl-D-*glycero*-α-D-*gulo*-heptopyranose; **16,** hexa-*O*-acetyl-D-*glycero*-β-D-*gulo*-heptopyranose.

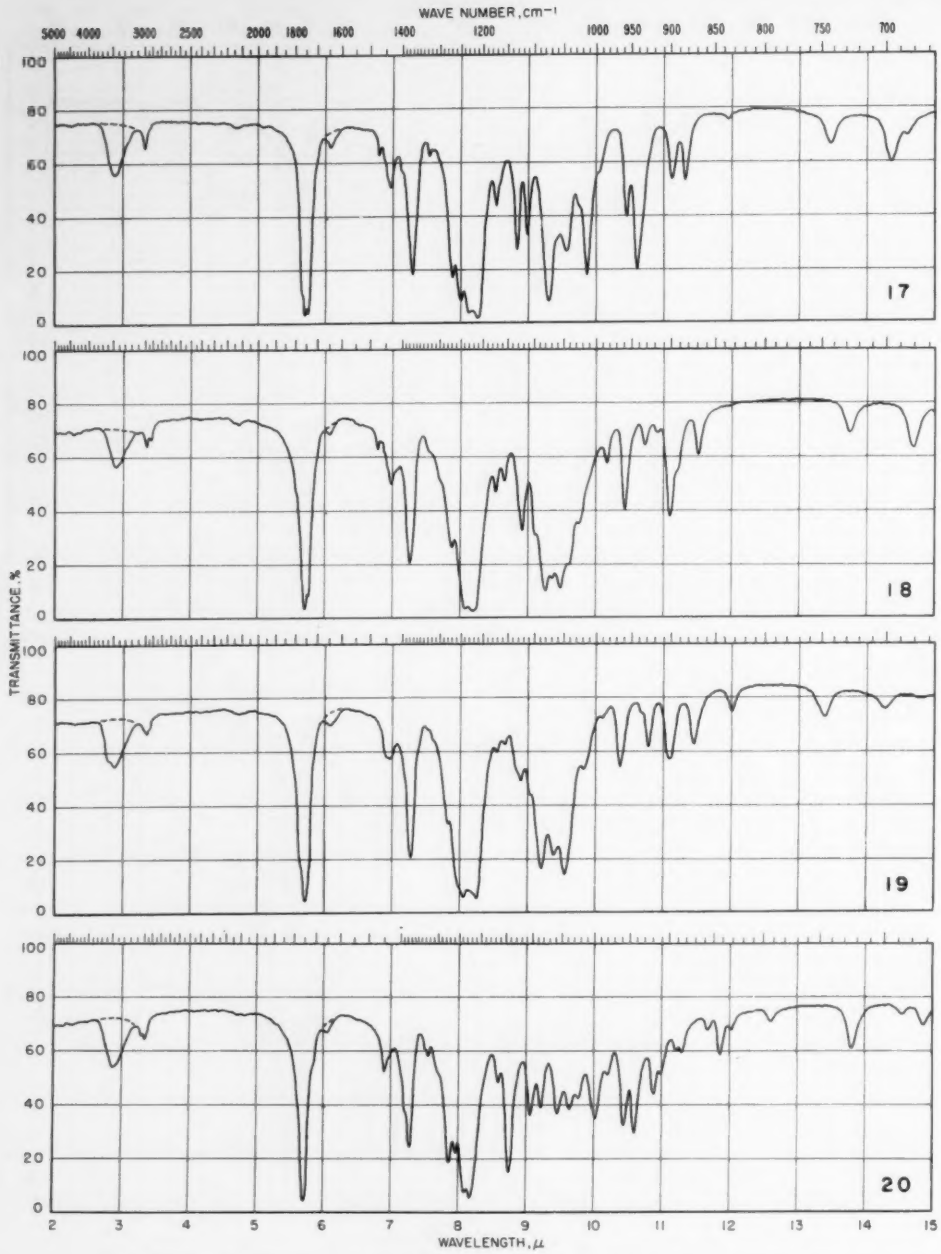

FIGURE 2. *Spectrograms of materials in potassium chloride pellets.*—Continued

17, penta-*O*-acetyl-α-D-galactopyranose; **18,** penta-*O*-acetyl-β-D-galactopyranose; **19,** hexa-*O*-acetyl-D-*glycero*-β-D-*galacto*-heptopyranose; **20,** penta-*O*-acetyl-α-D-talopyranose.

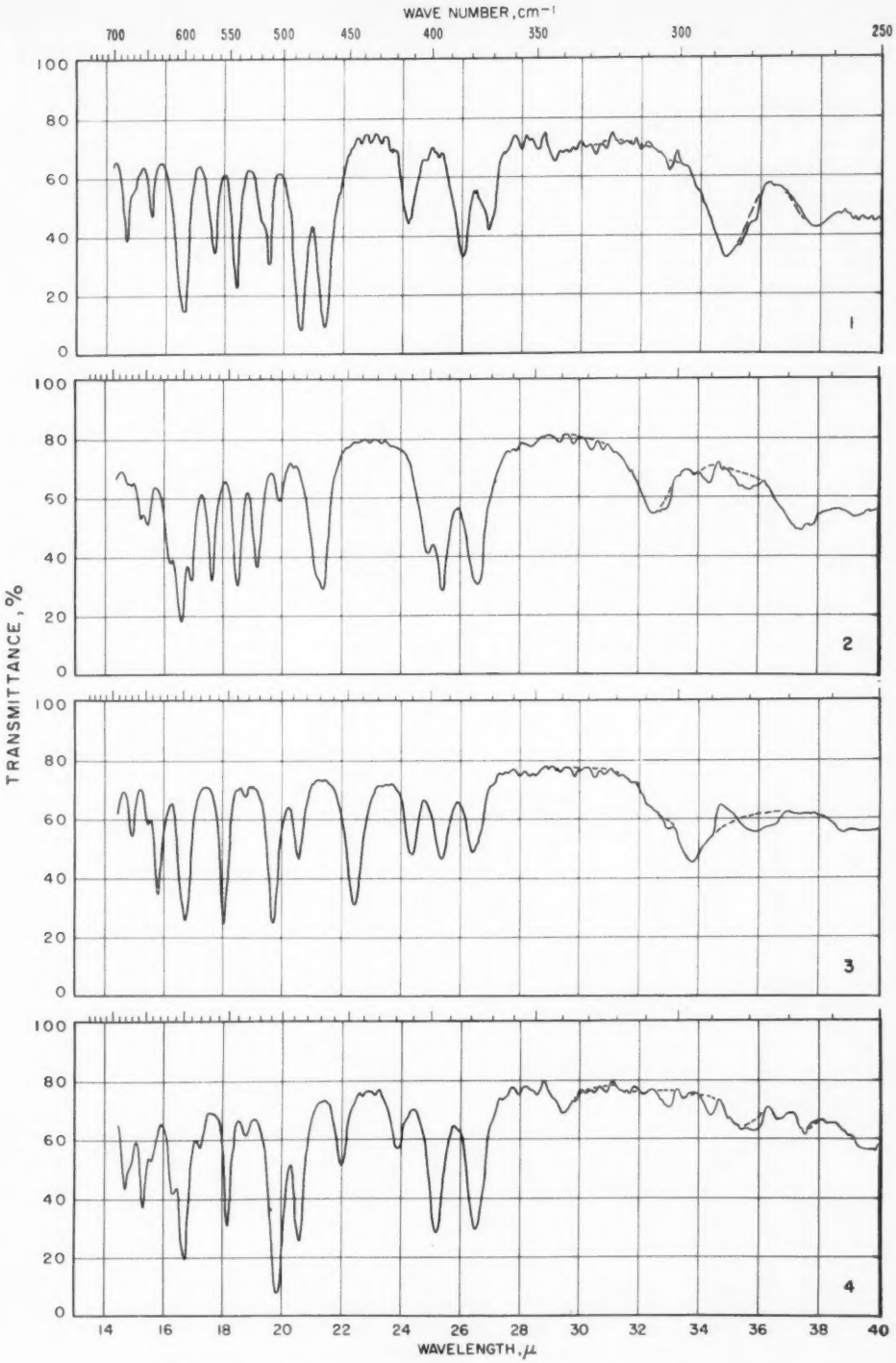

FIGURE 3. *Spectrograms of materials in potassium iodide pellets.*

1, Tetra-*O*-acetyl-α-D-xylopyranose; **2,** tetra-*O*-acetyl-β-D-xylopyranose; **3,** tetra-*O*-acetyl-α-D-lyxopyranose; **4,** tetra-*O*-acetyl-α-L-arabinopyranose.

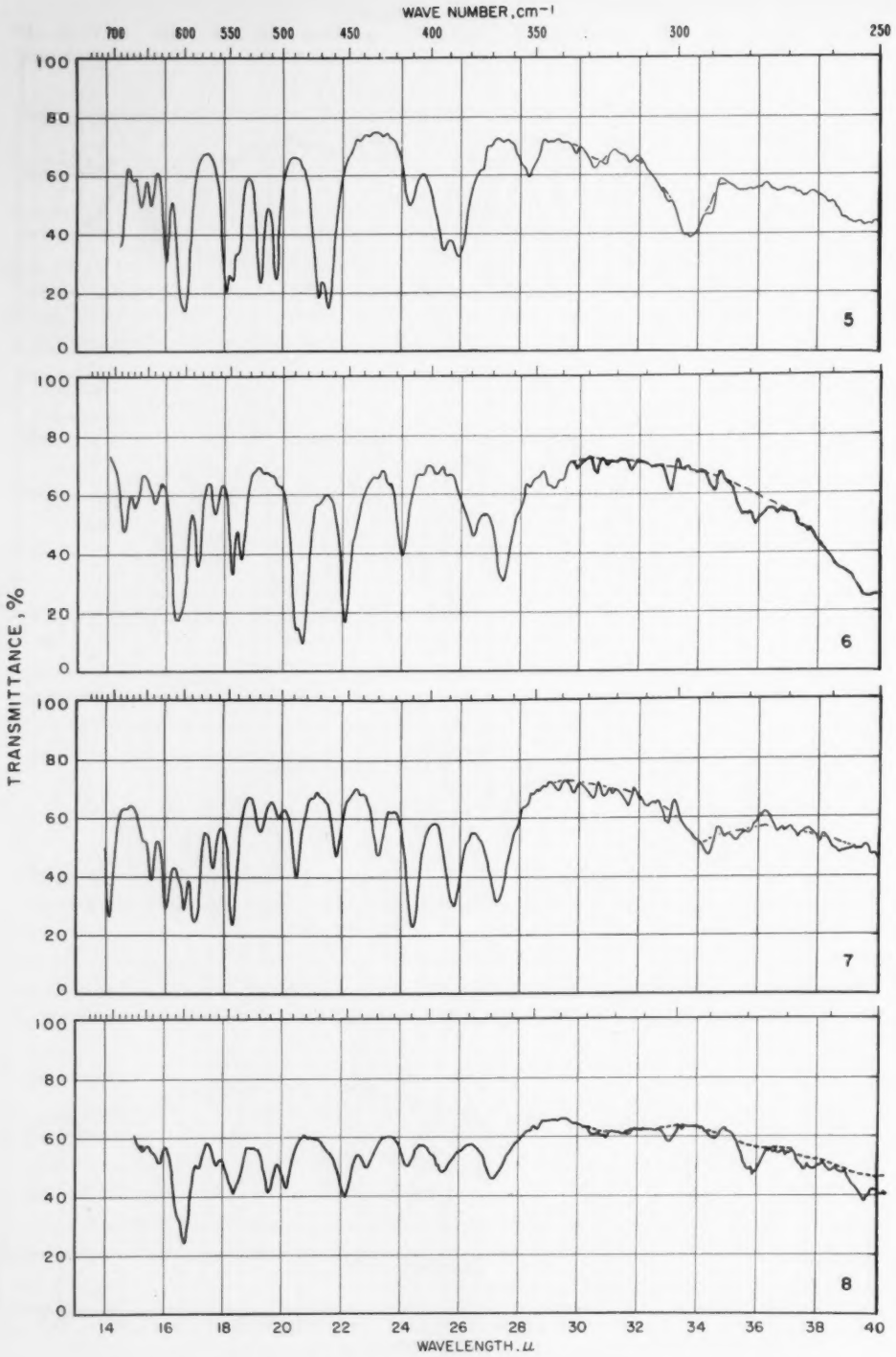

FIGURE 3. *Spectrograms of materials in potassium iodide pellets.*—Continued

5, penta-*O*-acetyl-α-L-*xylo*-hexulopyranose; **6**, penta-*O*-acetyl-α-D-glucopyranose; **7**, penta-*O*-acetyl-β-D-glucopyranose; **8**, hexa-*O*-acetyl-α-D-*gluco*-heptulopyranose.

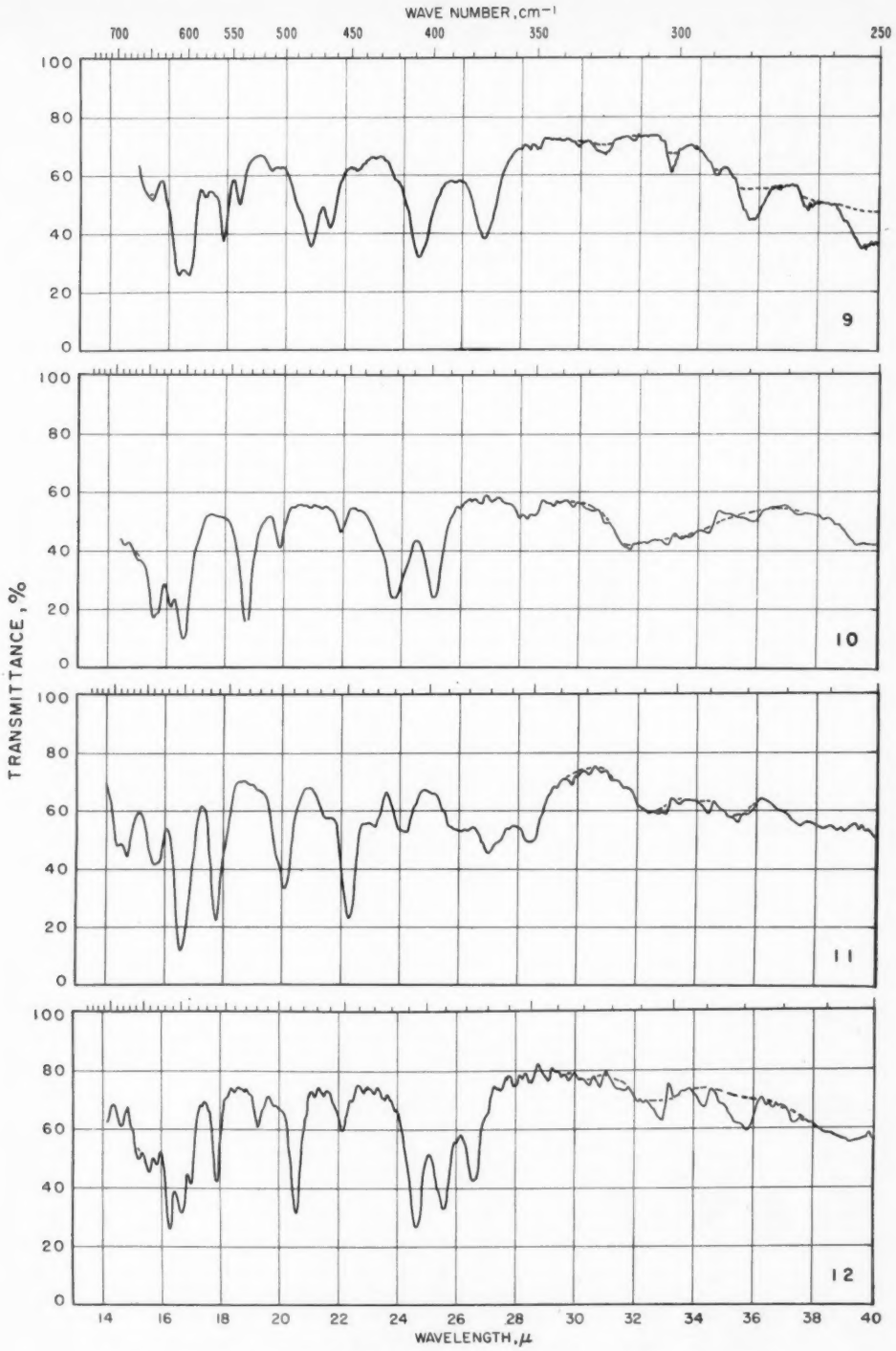

FIGURE 3. *Spectrograms of materials in potassium iodide pellets.*—Continued

9, hexa-*O*-acetyl-L-*glycero*-β-D-*gluco*-heptopyranose; **10,** hexa-*O*-acetyl-D-*glycero*-β-D-*ido*-heptopyranose; **11,** penta-*O*-acetyl-α-D-mannopyranose; **12,** penta-*O*-acetyl-β-D-mannopyranose.

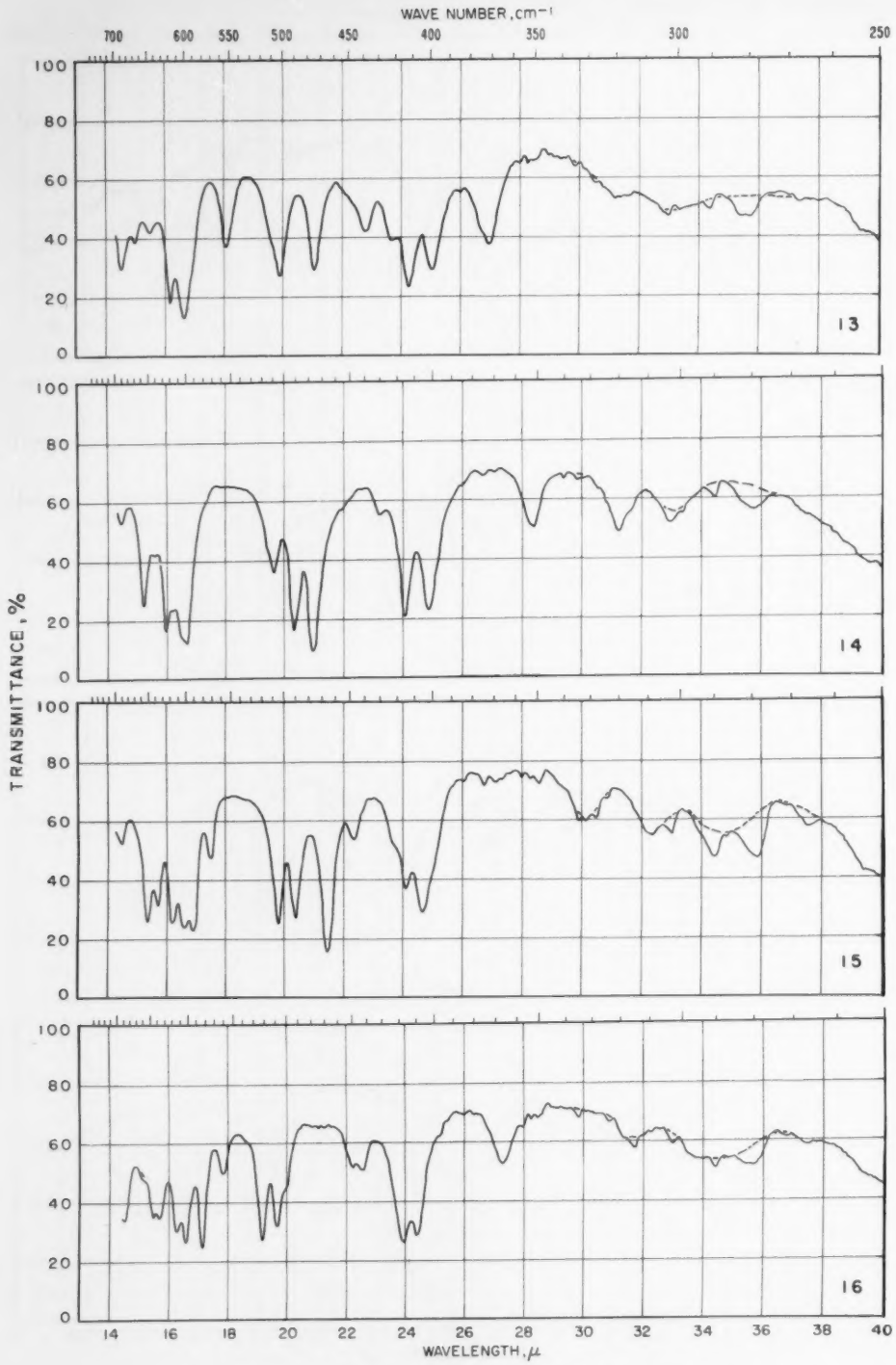

FIGURE 3. *Spectrograms of materials in potassium iodide pellets.*—Continued

13, hexa-*O*-acetyl-D-*glycero*-α-L-*manno*-heptopyranose; **14,** penta-*O*-acetyl-α-D-gulopyranose; **15,** hexa-*O*-acetyl-D-*glycero*-α-D-*gulo*-heptopyranose; **16,** hexa-*O*-acetyl-D-*glycero*-β-D-*gulo*-heptopyranose.

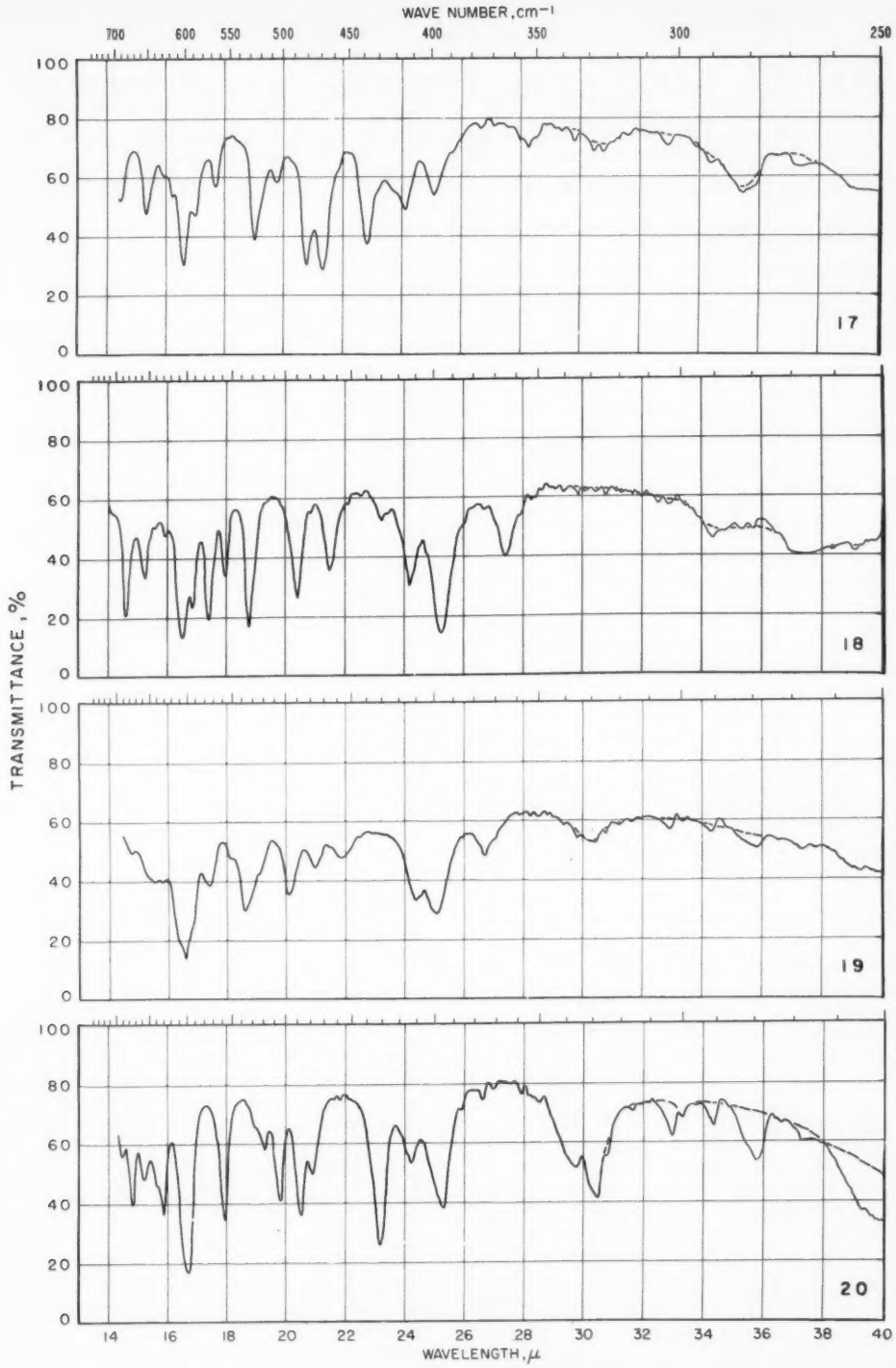

FIGURE 3. *Spectrograms of materials in potassium iodide pellets.*—Continued

17, penta-*O*-acetyl-α-D-galactopyranose; **18,** penta-*O*-acetyl-β-D-galactopyranose; **19,** hexa-*O*-acetyl-D-*glycero*-β-D-*galacto*-heptopyranose; **20,** penta-*O*-acetyl-α-D-talopyranose

7. References

[1] L. P. Kuhn, Anal. Chem. **22,** 276 (1950).
[2] H. S. Isbell, F. A. Smith, C. Creitz, J. D. Moyer, and H. L. Frush, Infrared spectra of sugar acetates and related compounds (informal communication).
[3] H. S. Isbell, F. A. Smith, E. C. Creitz, H. L. Frush, J. D. Moyer, and J. E. Stewart, J. Research NBS **59,** 41 (1957) RP2772.
[4] R. L. Whistler and L. R. House, Anal. Chem. **25,** 1463 (1953).
[5] S. A. Barker, E. J. Bourne, R. Stephens, and D. H. Whiffen, J. Chem. Soc. **1954,** 3468.
[6] R. S. Tipson and H. S. Isbell, J. Research NBS **64A,** 239 (1960).
[7] R. S. Tipson and H. S. Isbell, J. Research NBS **64A,** 405 (1960).
[8] H. S. Isbell, J. Research NBS **57,** 171 (1956) RP2707.
[9] H. S. Isbell and R. S. Tipson, J. Research NBS **64A,** 171 (1960).
[10] R. S. Tipson, H. S. Isbell, and J. E. Stewart, J. Research NBS **62,** 257 (1959) RP2960.
[11] R. U. Lemieux, R. K. Kullnig, H. J. Bernstein, and W. G. Schneider, J. Am. Chem. Soc. **80,** 6098 (1958).

(Paper 65A3–109)

JOURNAL OF RESEARCH of the National Bureau of Standards—A. Physics and Chemistry
Vol. 65A, No. 3, May–June 1961

A Standard for the Measurement of the *p*H of Blood and Other Physiological Media

Vincent E. Bower, Maya Paabo, and Roger G. Bates

(February 14, 1961)

A buffer solution containing potassium dihydrogen phosphate (0.008695 molal) and disodium hydrogen phosphate (0.03043 molal) is proposed as a *p*H standard for the physiologically important range, *p*H 7 to 8. The proposed standard solution is prepared by dissolving 1.179 g (air weight) of potassium dihydrogen phosphate and 4.303 g (air weight) of disodium hydrogen phosphate in ammonia-free water and diluting to 1 liter at 25 °C. The ionic strength is 0.1.

Standard *p*H values (pH_s) were assigned to this reference solution at temperatures from 0 to 50 °C by means of emf measurements of hydrogen-silver chloride cells without liquid junction. The activity coefficient of chloride ion, upon which the assignment of pH_s depends, was evaluated by means of a recently proposed convention. By this means, standard values precise to ± 0.001 unit could be derived from the emf data. At 25 °C pH_s is 7.414, and at 38 °C it is 7.382. The operational consistency of these standard values with those for the 0.025-*m* equimolal phosphate buffer (one of the NBS primary standards) was demonstrated.

1. Introduction

The acid-base behavior of blood and other physiological fluids has been widely studied in recent years in medical and biological laboratories in an attempt to discover the relationships that exist among physiological functions, pathological conditions, and *p*H. Many of these fluids are well buffered, and the detection of any systematic variation of *p*H with physiological condition would therefore be expected to require precise measuring equipment. Such equipment is readily available commercially in the form of the newer highly-sensitive *p*H meters with a glass electrode.

Experience has shown that, with the exercise of care, the investigator or clinician can obtain glass-electrode *p*H values, for reduced blood and other body fluids, that agree within ±0.01 unit with *p*H numbers obtained by means of the hydrogen electrode [1].[1] The high degree of stability in these biological systems and in the measuring apparatus suggests that blood *p*H measurements with a precision of 0.005 unit (or even 0.001 unit) could profitably be made. Meaningful comparisons of highly precise results of different laboratories could then be made, provided that a suitable reference standard were available.

Unfortunately, useful comparisons of *p*H data, quoted to 0.001 unit, from different sources have in general been impossible. The difficulty can be attributed to the fact that in all of the major conventions defining *p*H [2], a nonthermodynamic convention concerning single-ion activity coefficients is by necessity adopted. At the present time no single convention for defining an ionic activity is widely accepted. Although the conventions used heretofore to estimate single-ion activity coefficients are "reasonable" and yield *p*H numbers consistent with each other to within 0.01 unit, they all lack the exactness required for assignment of values to 0.001 unit.

Bates and Guggenheim [3], in a recent report to the International Union of Pure and Applied Chemistry, have proposed a very simple and precise way of defining the single-ion activity for the establishment of *p*H standards. By means of the convention they have set forth, *p*H values precise to within 0.001 unit may be assigned to selected standards in a restricted sector of the *p*H range.

Errors due to the faulty response of the glass electrode are minimized if the *p*H of the standard is close to that of the unknown. The availability of a precise *p*H standard in the physiological range would assist materially in the exact comparison of *p*H measurements made on biological systems in different laboratories.

It is the purpose of this paper to propose, as a physiological *p*H standard, a phosphate buffer mixture with a *p*H of about 7.4 and to assign *p*H values to this standard. The proposed standard has the following composition: KH_2PO_4(0.008695 molal), Na_2HPO_4(0.03043 molal).

2. Method of Defining pH_s

In order to avoid the theoretical and practical difficulties inherent in the estimation of liquid junction potentials, standard *p*H values have been based upon measurements of cells without liquid junction. In this work, hydrogen and silver-silver chloride electrodes were used, measurements being made of the electromotive force of the cell:

$$Pt;H_2(g,1\ atm),\ KH_2PO_4(0.008695\ molal),\ Na_2HPO_4(0.03043\ molal),\ Cl^-,AgCl;Ag. \qquad (A)$$

The electromotive force, E, of cell (A) is related to the standard electrode potential (E°) of the silver-

[1] Figures in brackets indicate the literature references at the end of this paper

585402—61——9

silver-chloride electrode [4] and to the activities of the hydrogen and chloride ions in the solution by the relation

$$E=E^\circ-\frac{RT}{F}\ln(a_H a_{Cl}), \quad (1)$$

where a is the activity (molal basis) of the ionic species designated by the subscript. Rearrangement, conversion to decadic logarithms, and substitution of $m_{Cl}\gamma_{Cl}$ for a_{Cl} yields a thermodynamic acidity function, $-\log(\gamma_H\gamma_{Cl}m_H)$:

$$-\log(\gamma_H\gamma_{Cl}m_H)=(E-E^\circ)F/(2.3026RT)+\log m_{Cl}. \quad (2)$$

In eq (2), m is the molality and γ is the activity coefficient, on the molal scale, of the ions designated by the subscripts.

For satisfactory reproducibility and constancy of the electromotive force, a finite amount of chloride must be present in the buffer solution. Nevertheless, it is the acidity function of the chloride-free buffer solution that is desired. The value of $-\log(\gamma_H\gamma_{Cl}m_H)$ was therefore measured at each of three low chloride concentrations, namely 0.005 m, 0.010 m, and 0.015 m and $-\log(\gamma_H\gamma_{Cl}m_H)^\circ$, the limit of $-\log(\gamma_H\gamma_{Cl}m_H)$ as m_{Cl} approaches zero, was obtained by extrapolation.

If the standard pH (denoted pH$_s$) is defined formally as $-\log a_H$ or $-\log m_H\gamma_H$, then

$$p\mathrm{H}_s=-\log(\gamma_H\gamma_{Cl}m_H)^\circ+\log\gamma^\circ_{Cl}. \quad (3)$$

It will be observed that, according to eq (2), $-\log(\gamma_H\gamma_{Cl}m_H)$ is a measurable quantity. On the contrary, γ_{Cl} in eq (3) is the activity coefficient of a single ion, a quantity that is not measurable. To obtain pH$_s$, therefore, some assumption must be made, or convention adopted, to evaluate γ_{Cl}.

For the purposes of assigning standard pH values to the standard buffers already proposed by the National Bureau of Standards, various assumptions have been used to estimate γ_{Cl} [5,6,7]. If the ionic strength does not exceed 0.1, the numerical values of γ°_{Cl} (obtained from the above assumptions) can all be closely represented by the following form of the Debye-Hückel equation:

$$-\log\gamma^\circ_{Cl}=\frac{A\sqrt{\mu}}{1+Ba_i\sqrt{\mu}}, \quad (4)$$

where μ is the ionic strength, a_i is an adjustable "ion-size parameter", and A and B are constants dependent upon temperature and solvent.[2] In the last analysis, therefore, the differences among the conventions themselves can be expressed as differences in a_i. Fortunately, all "reasonable" conventions for the definition of γ°_{Cl} lead to substantially equivalent values for the pH_s of the standard phosphate buffer (μ=0.1) [10]. All of these values fall within $\pm$0.01 unit of the assigned NBS standard values for this buffer solution. The agreement at lower ionic strengths is even more satisfactory.

[2] Tabulations of A and B are to be found in references [8] and [9].

Since there is really no apparent basis for choice among these assumptions, any one of them may be selected to represent γ°_{Cl}. Bates and Guggenheim have proposed, in their report to the Analytical Chemistry and Physical Chemistry Sections of the International Union of Pure and Applied Chemistry, a value of Ba_i=1.5 mole$^{-1/2}$ kg$^{1/2}$ [3]. The pH values given in the present work are based upon eqs (3) and (4) and this convention of Bates and Guggenheim.

3. Experimental Procedures and Results

The cells used for the measurements have been described in detail in a previous article [6]. Briefly, each cell consists of two electrode compartments and a chamber in which incoming hydrogen is saturated with the vapor over the buffer solution. The chamber terminates in a tube which leads to the jet in the hydrogen electrode compartment of the cell. Hydrogen gas escapes from the top of the hydrogen electrode compartment. The silver-silver chloride electrode compartment is connected to the hydrogen electrode compartment by a broad tube filled with the cell solution.

The standard buffer solution selected was 0.008695 molal in potassium dihydrogen phosphate (molecular weight, 136.092) and 0.03043 molal in disodium hydrogen phosphate (molecular weight, 141.982).[3] These proportions were chosen with the intention of producing a solution of pH about 7.4 at 25 °C and with an ionic strength of 0.1.

The solvent used in this study was ammonia-free distilled water of conductivity no greater than 0.8×10^{-6} ohm^{-1} cm^{-1}. The phosphate salts were specimens of NBS Standard Sample 186Ib (KH_2PO_4) and 186IIb (Na_2HPO_4), dried for an hour in a oven at 110 °C and used without further treatment. The potassium chloride was taken from a highly purified sample whose manner of preparation and purification has been described elsewhere [11].

Twenty cells containing the phosphate buffer with low concentrations of chloride (0.005 m, 0.010 m, or 0.015 m) were made up. The emf of 13 of these cells was measured over the temperature range 0 to 50 °C; five cells were studied over the range, 25 to 50°, one cell over the range 0 to 40°, and one cell at only three temperatures.

After the emf had been corrected to the standard partial pressure of hydrogen (760 mm), the acidity function $-\log(\gamma_H\gamma_{Cl}m_H)$ for each cell was calculated by means of eq (2). Values of $-\log(\gamma_H\gamma_{Cl}m_H)$ are listed in table 1. For these calculations, R was taken as 8.3147 j mole^{-1} deg^{-1} and F as 96,495.4 coul equiv^{-1} [12].

4. Assignment of pH_s Values

The $-\log(\gamma_H\gamma_{Cl}m_H)$ was found to be a linear function of m_{Cl}, and the limiting value, $-\log(\gamma_H\gamma_{Cl}m_H)^\circ$ (at m_{Cl}=0), was evaluated by the method of least

[3] The density at 25 °C of this solution is 1.0020 g/ml. A solution of this composition may be made by dissolving 1.179 g (air weight) KH_2PO_4 and 4.303 g (air weight) Na_2HPO_4 in water and diluting to 1 liter at 25 °C.

TABLE 1. *Electromotive force of cell (A) containing the phosphate buffer solution: 0.008695* m KH_2PO_4, *0.03043* m Na_2HPO_4 *with three molalities of added KCl*

KCl, molality	Temperature °C											
	0	5	10	15	20	25	30	35	38	40	45	50
0.005	0.77510	0.78078	0.78631	0.79187	0.79754	0.80324	0.80897	0.81457	0.81800	0.82018	0.82577	0.83149
.005	.77481	.78037				.80308						
.005	.77502	.78045	.78607	.79168	.79745	.80322	.80888	.81451	.81796	.82018	.82586	.83145
.005	.77484	.78042	.78612	.79177	.79756	.80296	.80893	.81434	.81791	.82021	.82606	.83180
.005	.77537	.78080	.78650	.79198	.79771	.80336	.80902	.81469	.81810	.82048		
.005	.77531	.78063	.78612	.79149	.79722	.80326	.80884	.81450	.81794	.82025	.82578	.83142
.005						.80330	.80884	.81435	.81798	.82025	.82566	.83122
.005						.80322	.80886	.81450	.81798	.82036	.82612	.83151
.010	.75857	.76392	.76912	.77442	.77970	.78512	.79047	.79584	.79916	.80124	.80672	.81222
.010	.75835	.76380	.76899	.77424	.77958	.78508	.79070	.79588	.79909	.80115	.80663	.81200
.010	.75862	.76374	.76903	.77421	.77946	.78506	.79044	.79568	.79903	.80136	.80667	.81188
.010	.75869	.76384	.76915	.77445	.77989	.78506	.79056	.79588	.79911	.80133	.80678	.81224
.010	.75869	.76379	.76920	.77438	.77979	.78500	.79048	.79587	.79906	.80129	.80662	.81222
.010	.75868	.76381	.76922	.77435	.77970	.78517	.79054	.79596	.79921	.80143	.80641	.81235
.010						.78497	.79026	.79563	.79887	.80107	.80659	.81195
.010						.78527	.79048	.79585	.79920	.80135	.80673	.81195
.015	.74873	.75392	.75900	.76406	.76923	.77427	.77966	.78478	.78800	.78993	.79513	.80036
.015	.74859	.75360	.75875	.76383	.76895	.77421	.77949	.78443	.78768	.78966	.79501	.80042
.015	.74895	.75373	.75895	.76394	.76918	.77449	.77947	.78476	.78779	.78999	.79521	.80067
.015						.77446	.77978	.78498	.78803	.79017	.79546	.80049

squares. Figure 1 shows the array of $-\log(a_H\gamma_{Cl})$ or $-\log(\gamma_H\gamma_{Cl}m_H)$ values at two temperatures. Values of $-\log(\gamma_H\gamma_{Cl}m_H)^\circ$ and the standard deviation (σ_i) of the intercept are given in table 2. The quantities $-\log\gamma^\circ_{Cl}$ computed from eq (4) are also listed. The standard pH_s values were derived from $-\log(\gamma_H\gamma_{Cl}m_H)^\circ$ by eq (3). They are listed in the last column of table 2 and are represented graphically as a function of temperature in figure 2.

The standard solution proposed here has an ionic strength of 0.1 and a buffer ratio of 3.5. The difference in pH resulting from small variations in the concentration of one or both phosphates is given with sufficient accuracy by the following expression, based on the mass law:

$$pH_s - pH_x = 0.544 - \log\frac{m_{HPO_4^{--}}}{m_{H_2PO_4^-}} + 3\{\log\gamma^\circ_{Cl}(s) - \log\gamma^\circ_{Cl}(x)\}, \quad (5)$$

where x designates the solution of buffer ratio slightly different from 3.5, and/or ionic strength slightly different from 0.1, and where s designates the standard solution proposed here. Also assumed in the derivation of eq 5 was the approximation

$$\gamma_{HPO_4^{--}} = (\gamma^\circ_{Cl^-})^4 = (\gamma_{H_2PO_4^-})^4.$$

It should be noted that neither of these phosphate salts is a strong enough acid or base to react appreciably with water. Hydrolysis corrections are therefore unnecessary, and the ratio of the concentrations of the phosphate ions is the same as the stoichiometric ratio of the molalities of the two salts. The first term within the braces in eq (5) is given in table 2. The second quantity inside the braces may be calculated from eq (4) with $Ba_i = 1.5$ mole$^{-1/2}$kg$^{1/2}$. For buffer solutions composed of potassium hydrogen phosphate (m_1) and disodium hydrogen phosphate (m_2), $\mu = m_1 + 3m_2$.

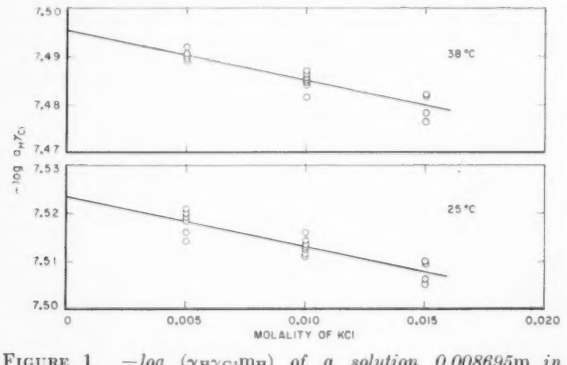

FIGURE 1. *$-\log(\gamma_H\gamma_{Cl}m_H)$ of a solution 0.008695*m *in* KH_2PO_4 *and 0.03043* m *in* Na_2HPO_4 *as a function of molality of added chloride.*

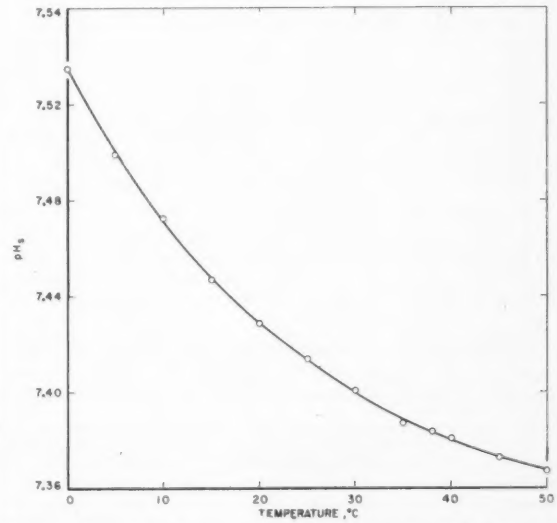

FIGURE 2. *pH_s of a solution 0.008695*m *in* KH_2PO_4 *and 0.03043* m *in* Na_2HPO_4 *as a function of temperature.*

TABLE 2. *pH_s and $-\log(\gamma_H\gamma_{Cl}m_H)^\circ$ for the solution 0.008695 m in KH_2PO_4 and 0.03043 m in Na_2HPO_4*

t°C	$-\log(\gamma_H\gamma_{Cl}m_H)^\circ$	σ_t	$-\log\gamma^\circ_{Cl}$	pH_s (experimental)
0	7.6400	0.0023	0.1055	7.534
5	7.6052	.0018	.1062	7.499
10	7.5793	.0018	.1070	7.472
15	7.5547	.0017	.1078	7.447
20	7.5374	.0019	.1087	7.429
25	7.5234	.0011	.1095	7.414
30	7.5109	.0011	.1104	7.400
35	7.4985	.0014	.1114	7.387
38	7.4955	.0011	.1121	7.383
40	7.4934	.0013	.1125	7.381
45	7.4863	.0016	.1135	7.373
50	7.4816	.0018	.1146	7.367

The "experimental" values of pH_s listed in table 2 were smoothed with respect to the temperature (T) in °K by the method of least squares, with the following result:

$$pH_s=\frac{1592.07}{T}-2.3392+0.014798T. \qquad (6)$$

Recommended values of pH_s, calculated at specified temperatures from eq (6), are given in table 3.

5. Internal Consistency of the Standard *p*H Scale

It was considered desirable to test the operational consistency of the pH_s values defined in this paper with those defined some years ago by Bates and Acree for the equimolal 0.025 m phosphate buffer (0.025 m KH_2PO_4, 0.025 m Na_2HPO_4) [6]. To this end, emf measurements were made with a symmetric cell [13] consisting of two hydrogen electrode compartments connected by a bridge of saturated potassium chloride.

The standard equimolal phosphate buffer solution was placed in one of the hydrogen electrode compartments and the solution of buffer ratio 3.5 in the other. The emf between the two hydrogen electrodes yields the operational pH difference (ΔpH), which can then be compared with the difference of assigned pH_s (ΔpH_s). The assignment of pH_s is made by eq (3), where $\log\gamma^\circ_{Cl}$ is defined by the Bates-Guggenheim convention (and therefore constant for a given value of the ionic strength).[4] The difference in pH_s is therefore equal to the difference between the values of $-\log(\gamma_H\gamma_{Cl}m_H)^\circ$ for the two solutions, namely 7.523−6.972 or 0.551 at 25 °C and 7.496−6.952 or 0.544 at 38 °C.

Measurements of the symmetrical cell with liquid junction were made at 25 and 38 °C. The experimental values of ΔpH at the two temperatures were, respectively, 0.550 and 0.546 pH unit. These values are in good agreement with the values of ΔpH_s given above, which were, of course, derived from the emf of cells without liquid junction.

[4] The earlier assignment of pH_s to the phosphate buffer solution was based on a more complex formula for estimating γ°_{Cl} [6]. The two procedures lead to values of pH_s for the equimolal phosphate standard that differ by only 0.003 unit at 25 °C.

TABLE 3. *Recommended values of pH_s at specified temperatures*

(values calculated from eq (6))

t	pH_s	t	pH_s
0	7.531	30	7.399
5	7.501	35	7.387
10	7.474	38	7.382
15	7.450	40	7.379
20	7.430	45	7.373
25	7.413	50	7.369

The internal consistency of the practical scale to a few thousandths of a unit in the physiological range therefore seems to have been demonstrated. By a similar series of measurements at 25 °C, it has already been shown that the standard phthalate (pH 4.006), phosphate (pH 6.863), and borax (pH 9.183) buffer solutions are consistent among themselves to about ±0.003 unit [14]. In the authors' opinion, these intercomparisons constitute an experimental justification for the assignment of a third decimal to the pH_s for the primary standards of intermediate pH.

6. References

[1] J. Sendroy, Jr., page 55 in Symposium on pH measurement, ASTM Special Technical Publication No. 190, (American Society for Testing Materials, Philadelphia, Pa., 1957).

[2] British Standard 1647; 1950 (British Standards Institution, London, 1950). Japanese Industrial Standard Z 8802–1958 (Japanese Standards Association, Tokyo, 1958). R. G. Bates, J. Research NBS, **47,** 433 (1951) RP2268.

[3] R. G. Bates and E. A. Guggenheim, Pure and Applied Chemistry **1,** 163 (1960).

[4] R. G. Bates and V. E. Bower, J. Research NBS **53,** 283 (1954) RP2546.

[5] W. J. Hamer, G. D. Pinching, and S. F. Acree, J. Research NBS **36,** 47 (1946) RP1690.

[6] R. G. Bates and S. F. Acree, J. Research NBS **30,** 129 (1943) RP1524; **34,** 373 (1945) RP1648.

[7] G. G. Manov, N. J. DeLollis, P. W. Lindvall, and S. F. Acree, J. Research NBS **36,** 543 (1946) RP1721.

[8] G. G. Manov, R. G. Bates, W. J. Hamer and S. F. Acree, J. Am. Chem. Soc. **65,** 1765 (1943).

[9] R. A. Robinson and R. H. Stokes, Electrolyte solutions, second ed. (Academic Press Inc., New York 1959).

[10] R. G. Bates, Chem. Revs. **42,** 1 (1948).

[11] G. D. Pinching and R. G. Bates, J. Research NBS **37,** 311 (1946) RP1749.

[12] E. R. Cohen, K. M. Crowe, and J. W. M. DuMond, Fundamental constants of physics (Interscience Publishers Inc., New York, 1957).

[13] R. G. Bates, G. D. Pinching, and E. R. Smith, J. Research NBS **45,** 418 (1950) RP2153.

[14] R. G. Bates, Chimia **14,** 111 (1960).

(Paper 65A3—110)

JOURNAL OF RESEARCH of the National Bureau of Standards—A. Physics and Chemistry
Vol. 65A, No. 3, May–June 1961

Publications of the National Bureau of Standards

(Including papers in outside journals)

Selected Abstracts

Irrational power series, M. Newman, *Proc. Am. Math. Soc.* **11,** *699–702 (Oct. 1960).*
It is shown that if α is a real number, g a non-constant polynomial, then

$$\sum_{n=0}^{\infty} g([n\alpha])x^n$$

is a rational function of x if and only if α is a rational number. The same statement is proved for the function

$$\sum_{n=0}^{\infty} x^{[n\alpha]}.$$

Ensemble method in the theory of irreversibility, R. Zwanzig, *J. Chem. Phys.* **33,** *No. 5, 1338–1341 (Nov. 1960).*
We describe a new formulation of methods introduced in the theory of irreversibility by Van Hove and Prigogine, with the purpose of making their ideas easier to understand and to apply. The main tool in this reformulation is the use of projection operators in the Hilbert space of Gibbsian ensemble densities. Projection operators are used to separate an ensemble density into a "relevant" part, needed for the calculation of mean values of specified observables, and the remaining "irrelevant" part. The relevant part is shown to satisfy a kinetic equation which is a generalization of Van Hove's "master equation to general order." Diagram summation methods are not used. The formalism is illustrated by a new derivation of the Prigogine-Brout master equation for a classical weakly interacting system.

On the theory of the critical point of a simple fluid, M. S. Green, *J. Chem. Phys.* **33,** *No. 5, 1403–1409 (Nov. 1960).*
The consequences of a new system of integral equations for the theory of the critical point are discussed. Reasons are given for believing that the fundamental assumption of the Ornstein-Zernicke theory about the direct correlation function is incorrect.

Topological derivation of the Mayer density series for the pressure of an imperfect gas, M. S. Green, *J. Math. Phys.* **1,** *No. 5, 391–394 (Sept.–Oct. 1960).*
A new derivation of Mayer's classical density expansion for the pressure of an imperfect gas based on a classification of cluster graphs according topological criteria is presented. The classification is a generalization of the classification of simple trees into trees with centers and trees with bicenters.

Collection of ions produced by alpha particles in air, Z. Bay and H. H. Seliger, *Phys. Rev.* **120,** *No. 1, 141–143 (Oct. 1, 1960).*
In the measurement of the ionization caused by alpha particles in air recombination effects between slowly moving positive and negative ions (the latter formed by electron attachment to oxygen) have to be considered. The usual procedure in such measurements is to determine the saturation current (by extrapolation of reciprocal current versus reciprocal voltage curves to infinite field strength) according to the Jaffé theory. A paper by Wingate, Gross and Failla has cast doubt on the validity of this extrapolation technique, in that the authors propose a field-independent part of the recombination amounting to 3.3 percent at atmospheric pressure in air. This proposal implied that all previous measurements of W_a for air were in error by this amount and that this error is a possible cause for the reported difference (3 to 4 percent) between W values for alpha and beta particles in air. In view of our own W measurements we felt compelled to reexamine this supposedly field-independent part of the recombination. Approximating the experimental conditions of Wingate, Gross and Failla we have not been able to reproduce their effect and our experiments demonstrate the validity of the usual extrapolation techniques.

Megaroentgen dosimetry employing photographic film without processing, W. L. McLaughlin, *Radiation Research* **13,** *No. 4, 594–609 (Oct. 1960).*
The new photographic method of high-level dosimetry of X- and gamma radiation involves two steps: (1) Large radiation exposures are given, resulting in the formation of print-out image in the silver halide emulsion layers of ordinary commercial X-ray films, without requiring photographic processing for the evaluation; (2) The unknown exposure is measured by means of a special densitometric procedure, the exposure being related to the net density of the print-out darkening on a characteristic curve obtained with known exposures. The density readings are made with a narrow band of red light, obtained by placing a suitable band-pass filter between the densitometer light source and the film.

Gamma radiation exposures from 2×10^4 to 10^8 roentgens can be read with a precision limit of ±5 percent, under appropriate conditions of densitometry. The response is rate independent and the print-out image is stable. The chief limitations in the method are a considerable dependence of response upon radiation energy below 0.3 Mev, and the requirement of controlling the temperature during exposure to within ±10 degrees Celsius for accurate readings.

Vibration-rotation bands of N_2O, E. D. Tidwell and E. K. Plyler, *J. Opt. Soc. Am.* **50,** *No. 12, 717–720 (Dec. 1960).*
About 40 bands of nitrous oxide have been measured with a high resolution grating spectrometer in the region from 2395 to 3510 cm^{-1}. Many first and second hot bands were observed and it was possible to obtain accurate-type doubling constants. By the use of bands observed in this work in conjunction with previous work a fairly complete set of vibrational levels for N_2O has been determined. A number of interactions have been observed and the interaction constants calculated. The observed spectra are shown in nine figures. The ground state rotational constants and the vibrational constants have been calculated. Several bands have been identified as arising from isotopic molecules.

Microwave spectrum structure, and dipole moment of propane, D. R. Lide, Jr., *J. Chem. Phys.* **33,** *No. 5, 1514–1518 (Nov. 1960).*
The microwave spectrum of ordinary propane and five isotopic species has been measured and analysed. The rotational constants of C_3H_8 are 29207.36, 8446.07, and 7458.98 Mc, and the dipole moment is 0.083 ± 0.001 D. In its equilibrium configuration the molecule has C_{2v} symmetry with both CH_3 groups staggered with respect to the CH_2 group. The complete structure has been determined by the substitution method. Important parameters are: r(CC) $=1.526\pm0.002$ A,) CCC$=112.4°\pm0.2°$; in the CH_2 group, r(CH)$=1.096\pm0.002$ A,) HCH$=106.1°\pm0.2°$; in the CH_3 groups, r(CH)$=1.091\pm0.010$ A,) HCH$=107.7°\pm1.0°$. The influence of zero-point effects on the structure determination is discussed: these are found to be particularly bad for the CH_3 group, probably because of its large vibrational amplitude.

Structure of the isobutane molecule; change of dipole moment on isotopic substitution, D. R. Lide, Jr., *J. Chem. Phys.* **33,** *No. 5, 1519–1522 (Nov. 1960).*

The microwave spectra of 5 isotopic species of isobutane have been measured and analyzed. The isobutane molecule is shown to belong to point group C_{3v}. The structural parameters determined by the substitution method are: r(CC) = 1.525 A,) CCC = 111.15°, r(CH) = 1.108 A (tertiary), r(CH) = 1.09 − 1.10 A (methyl),) HCH = 107.5°. The structure is compared with that of other hydrocarbons, and it is suggested that a small systematic difference exists between CC distances determined by microwave and electron diffraction methods. Accurate Stark measurements show that the dipole moment of $(CH_3)_2CD$ is 6.5% ±0.9% higher than that of $(CH_3)_3CH$.

Spatial distribution of energy dissipated by fallout-rays, A. E. Boyd and E. E. Morris, *Health Phys.* **2,** *321–325 (1959).*

Calculations are described of the spatial distribution of energy dissipated in air by the delayed beta rays from products of slow neutron U^{235} fission. Results are given for both plane isotropic and point isotropic sources for times after fission of 1.12 and 23.8 hr.

Mismatch errors in microwave phase shift measurements, G. E. Schafer, *IRE Trans. Microwave Theory and Tech.* **MTT-8,** *No. 6, 617–622 (Nov. 1960).*

Mismatch errors in microwave phase shift measurements are analyzed. The results are applied to two measurement techniques. Graphs are presented to estimate the limits of mismatch error when measuring or producing changes in phase of the emergent wave amplitude with a microwave phase shifter or attenuator. The limits of mismatch error for a typical microwave phase shifter in a system with equivalent generator and detector voltage standing wave ratios of 1.05, or less, are estimated to be ±0.90°.

The rotational constants of hydrogen chloride, E. K. Plyler and E. D. Tidwell, *Z. Elektrochem.* **64,** *No. 5, 717–720 (Feb. 1960).*

The fundamental absorption band of hydrogen chloride has been measured on a high resolution spectrometer. Twenty-nine lines of HCl^{35} and twenty-eight lines of HCl^{37} have been measured to a high precision by the use of the fringe system of a Fabry-Perot interferometer.

The average deviation of the observed from the calculated values is ±0.003 cm^{-1}. The rotational constants for each isotopic species have been calculated. The rotational constants have been used to predict the positions of the pure rotational spectra of HCl^{35} and HCl^{37}. The equilibrium separation of the atoms has been calculated to be 1.2746A.

Dipole moments of hydrocarbons, D. R. Lide, Jr., *J. Chem. Phys.* **33,** *No. 6, 1879 (Dec. 1960).*

The dipole moments of several hydrocarbons are considered in terms of hyperconjugation and a bond-moment model. It is shown that hyperconjugation affords a better explanation of both the orientation and magnitude of the observed moments.

Nonresonant microwave absorption and relaxation frequency at elevated pressures, A. A. Maryott and G. Birnbaum, *J. Phys. Chem.* **64,** *No. 11, 1778–1780 (Nov. 1960).*

The microwave absorption in $CClF_3$ has been measured at pressures up to 30 atmospheres at 1190 Mc. Below 10 atm, the absorption due to the pure rotational transitions appears to be negligible compared to the nonresonant contribution. The nonresonant relaxation frequency is found to increase essentially in proportion to the density over the entire range, and, at the highest density, is of the same order as in the liquid state.

Spectrum of ReF_6, J. C. Eisenstein, *J. Chem. Phys.* **33,** *No. 5, 1530–1531 (Nov. 1960).*

The theoretical interpretation of the optical absorption spectrum of ReF_6 is discussed. It is pointed out that the value of the spin-orbit coupling constant required to fit the experimental data is appreciably reduced if a small field of axial symmetry about a threefold axis of the molecule is present.

Nuclear magnetic resonance in tantalum metal, J. I. Budnick and L. H. Bennett, *J. Phys. Chem. Solids* **16,** *No. 1/2, 37–38 (Jan. 12, 1960).*

The nuclear magnetic resonance of Ta^{181} has been observed in tantalum metal. The sample was a stack of high purity foil which was degassed and annealed. No resonance was observed in tantalum metal powder.

Magnetic resonance determination of the nuclear moment of tantalum-181 in $KTaO_3$, L. H. Bennett and J. I. Budnick, *Phys. Rev.* **120,** *No. 5, 1812–1815 (Dec. 1960).*

The nuclear magnetic moment of Ta^{181} is found from the nuclear magnetic resonance of Ta^{181} in $KTaO_3$. The uncorrected value of the moment is 2.340 ± 0.001 nm. Consideration of diamagnetic shielding effects and a possible second order paramagnetic correction leads to the estimated value of $\mu = 2.35 \pm 0.01$ nm.

Green and purple sulfur: Electron-spin resonance studies, H. E. Radford and F. O. Rice, *J. Chem. Phys.* **33,** *No. 3, 774–776 (Sept. 1960).*

Electron spin resonance absorption has been found in the colored deposits formed by condensing heated sulphur vapor on cold surfaces. Complexities in the resonance spectrum give evidence for the existence in the cold deposits of at least two types of trapped sulphur radicals with differing degrees of internal magnetic anisotropy. Measurements of the intensity and stability of the resonance absorption yield information on the radical trapping process.

Effect of structure on the spectra emitted by solid nitrogen during electron bombardment, L. J. Schoen and H. P. Broida, *J. Mol. Spectroscopy* **5,** *No. 5, 416–419 (Nov. 1960).*

Spectra emitted from solids subjected to electron bombardment at low temperature have been found to exhibit a dependence on deposition flow rate. It is shown that the observed changes may be ascribed to the effect of deposition temperature on the structure of the solid.

Chemical reactions to free radicals at low temperatures, R. A. Ruehrwein, J. S. Hashman and J. W. Edwards, *J. Phys. Chem.* **64,** *1317–1322 (1960).*

Free radicals generated by subjecting gases to an electrodeless discharge were condensed in a trap cooled to liquid helium temperature. The nature of the radical reactions which had taken place upon condensation and upon warming the solid deposits was indicated by the analyses of the products obtained. The gases discharged (and the principal products) were $O_2(O_3)$, $HO_2(H_2O_2,H_2)$, N_2, $NO_2(N_2,O_3)$, H_2, $NH_3(N_2,H_2)$, $CO(C,CO_2)$, $CO_2(CO,O_2)$, $SO_2(O_2,S)$, and some mixtures thereof. Also the reactions of O, OH, H, N and HO_2 radicals with O_2, H_2O, NO, NO_2, CO_2, SO_2, CH_4, C_2H_4, i-C_4H_8, CO and CH_3COCH_3 were investigated by blending in the latter downstream from the discharge and ahead of the liquid helium trap. In some of the systems it was apparent that considerable radical reaction occurred before condensation. However most of the experimental results can be interpreted on the basis that at very low temperature the free radicals react by random recombination, by addition to molecules with unpaired electrons, and by addition to carbon–carbon double bonds. It was found that molecular oxygen is loosely bound in several solids such as hydrogen peroxide, water, nitrogen dioxide and probably others. The bound or trapped oxygen is evolved from the solid at temperatures well above the boiling point of oxygen.

The reaction of hydrogen atoms with solid propene at low temperatures, R. Klein, M. D. Scheer and J. G. Waller, *J. Phys. Chem.* **64,** *1247–1250 (1960).*

The reaction of hydrogen atoms with solid films of propene has been studied below 100 °K. The hydrogen atoms diffuse through and react with the propene films to form propane and 2,3-dimethylbutane. A one dimensional diffusion equation containing a chemical reaction term is used to describe the kinetics of this process. A value of 5×10^7 cc/mole sec is obtained for the specific rate constant at 77 °K for the reaction $H + CH_3-CH=CH_2 \rightarrow CH_3-CH-CH_2$. The ratio of propane to 2,3-dimethylbutane is about 9 and does not change as the concentration of propene is varied over two

orders of magnitude. The propane as well as the 2,3-dimethylbutane must therefore be formed by a process which is second order with respect to the isopropyl radical concentration.

Preparation and thermal stability of tetrakis-(pentafluorophenyl)-silane and tris-(pentafluorophenyl)-phosphine, L. A. Wall, R. E. Donadio, and W. J. Pummer, *J. Am. Chem. Soc.* **82,** *No. 18, 4846–4852 (Sept. 1960).*
The completely fluorinated organo-metalloid compounds, tetrakis(pentafluorophenyl) silane, tris(pentafluorophenyl)-phosphine, and tris(pentafluorophenyl)phosphine oxide have been prepared from pentafluorophenyl magnesium bromide and the appropriate metalloid chloride. The thermal stabilities of these compounds have been compared with those of other aromatic substances. It was found in the case of the phosphine, where coordinating electrons exist on the metalloid atoms, that complete fluorine substitution increases its thermal stability and resistance to oxidation. On the other hand, complete fluorination decreases the thermal stability of the silane.

Rate of reaction of nitrogen atoms with ethylene, J. T. Herron, *J. Chem. Phys.* **33,** *No. 4, 1273–1274 (Oct. 1960).*
A mass spectrometric study has been made of the rate of the reaction of nitrogen atoms with ethylene. The average value of the second order rate constant over the temperature interval 200 °C to 330 °C was 5.8×10^{10} cm.^{3}mole^{-1}sec^{-1}.

Surface area determination of kaolinite using glycerol adsorption, K. H. Woodside and W. C. Ormsby, *J. Am. Ceram. Soc.* **43,** *No. 12, 671–672 (Dec. 1960).*
Some work has already been done on the application of the so-called glycerol retention method in the determination of surface areas of clays, including kaolinites, as well as well as other solid adsorbents. The present investigation compares the surface areas of a series of controlled particle-size fractions of a domestic kaolinite using this rapid method with the more conventional but more laborious nitrogen adsorption method. Results showing good agreement confirm the work of earlier investigators and demonstrate the utility of the method when applied to kaolin-type clays.

The heat of combustion of dicyanoacetylene, G. T. Armstrong and S. Marantz, *J. Phys. Chem.* **64,** *1776–1777 (1960).*
The heat of combustion of liquid dicyanoacetylene (C_4N_2) in oxygen to form carbon dioxide and nitrogen has been measured to be 2078.5 ± 0.7 kj mole^{-1} (496.8 ± 0.2 kcal mole^{-1}), the indicated uncertainty being the standard error of the preceding mean. The standard heat of formation, $\Delta H°_{f298}$ [C_4N_2(l)], is calculated to be 120.6 kcal mole^{-1}. The binding energy at 298 °K of the C_4N_2 molecule is calculated to be 783.6 kcal mole^{-1}.

Electrodeless passage of direct current through an electrolyte, A. Brenner, *J. Electrochem. Soc.* **107,** *No. 12, 968–973 (Dec. 1960).*
An experimental setup is described for directly observing the electrical migration of a dye in a conducting system without electrodes. Direct current was produced in a continuous circuit of electrolyte, which included the dye solution, by means of a transformer and a mechanical commutator.

Condensation coefficient of arsenic trioxide glass, A. B. Bestul and D. H. Blackburn, *J. Chem. Phys.* **33,** *No. 4, 1274–1275 (Oct. 1960).*
The maximum rate of vaporization from arsenic trioxide glass at 194 °C has been determined by measurement of weight loss in vacuum. The results lead to a condensation coefficient of 2.2×10^{-6}. It has been shown that undetected surface cooling due to the absorption of latent heat of vaporization cannot account for the major part of the deviation of this value from unity.

The compound $BaTiGe_3O_9$, C. R. Robbins, *J. Am. Ceram. Soc.* **43,** *No. 11, 610 (Nov. 1960).*
$BaTiGe_3O_9$ is stable from 1132° ±10 °C to 1235° ±10 °C. The room temperature X-ray powder diffractometer pattern was indexed on the basis of a hexagonal unit cell with $a=11.73$A, $c=10.02$Å and $c/a=0.8542$. The theoretical density is 4.54 and $Z=6$. The description of $BaTiGe_3O_9$ in the literature apparently describes a solid solution of titania in barium tetragermanate. At room temperature, $BaTiGe_3O_9$ is structurally similar to, but not isostructural with $BaTiSi_3O_9$. Within its temperature stability range, $BaTiGe_3O_9$ is apparently isostructural with $BaTiSi_3O_9$, with $a\cong6.8$Å and $c\cong10.04$Å.

Other NBS Publications

Journal of Research, Section 65C, No. 2, April–June 1961. 75 cents.

An experimental study concerning the pressurization and stratification of liquid hydrogen, A. F. Schmidt, J. R. Purcell, W. A. Wilson, and R. V. Smith.
Temperature dependence of elastic constants of some cermet specimens, S. Spinner.
Analog simulation of zone melting, H. L. Mason.
Residual losses in a guard-ring micrometer-electrode holder for solid-disk dielectric specimens, A. H. Scott and William P. Harris.
A bolometer mount efficiency measurement technique, G. F. Engen.
Telescope for measurement of optic angle of mica, S. Ruthberg.
An automatic fringe counting interferometer for use in the calibration of line scales, H. D. Cook and L. A. Marzetta.

Journal of Research, Section 65D, No. 3, May–June 1961. 70 cents.

Propagation studies using direction-finding techniques, E. C. Hayden.
Diversity effects in long distance high frequency radio pulse propagation, S. A. Bowhill.
Influence of ionospheric conditions on the accuracy of high frequency direction finding, P. J. D. Gething.
Phase difference observations at spaced aerials and their application to direction finding, W. C. Bain.
Research at the National Bureau of Standards applicable to long-distance location and direction-finding problems, R. Silberstein.
Design for spinning goniometer automatic direction finding, W. J. Lindsay and D. S. Heim.
Resolution characteristics of correlation arrays, I. W. Linder.
Instrumentation for propagation and direction-finding measurements, E. C. Hayden.
Brooke variance classification system for DF bearings, E. M. L. Beale.
Estimation of variances of position lines from fixes with unknown target positions, E. M. L. Beale.
Statistics of a radio wave diffracted by a random ionosphere, S. A. Bowhill.
Space analysis of radio signals, J. B. Smyth.
Effect of receiver bandwidth on the amplitude distribution of VLF atmospheric noise, F. F. Fulton, Jr.
Excitation of VLF and ELF radio waves by a horizontal magnetic dipole, J. Galejs.

Climatic charts and data of the radio refractive index for the United States and world, B. R. Bean, J. D. Horn, and A. M. Ozanich, Jr., NBS Mono. **22** (1960) $2.
Units of weight and measure (United States customary and metric) definitions and tables of equivalents, NBS Misc. Publ. **233** (1960) 40 cents.
Report of the 45th national conference on weights and measures 1960, NBS Misc. Publ. **235** (1960) 75 cents.
Standard frequencies and time signals from NBS stations WWV and WWVH, NBS Misc. Publ. **236** (1960) 10 cents.
Research highlights of the National Bureau of Standards, Annual Report, fiscal year 1960, NBS Misc. Publ. **237** (1960) 65 cents.
Report of the International Commission on radiological units and measurements (ICRU) 1959, NBS Handb. H78 (1961) 65 cents.
Supplementary world maps of F2 critical frequencies and maximum usable frequency factors, D. H. Zacharisen, NBS TN2–2 (PB151361–2) (1960) $3.50.

Vapor pressures of organic compounds in the range below one millimeter of mercury, E. E. Hughes and S. G. Lias, NBS TN70 (PB161571) (1960) 75 cents.

Quarterly radio noise data—June, July, August 1960, W. Q. Crichlow, R. D. Disney, and M. A. Jenkins, NBS TN18–7 (PB151377–7) (1960) $1.75.

VHF radio propagation data for Cedar Rapids-Sterling, Anchorage-Barrow, and Fargo-Churchill test paths April 1951 through June 1958, G. R. Sugar and K. W. Sullivan, NBS TN79 (PB161580) (1960) $4.00.

Bibliography of tropospheric radio wave scattering, R. L. Abbott, NBS TN80 (PB161581) (1960) $2.25.

A survey of spread-f, F. N. Glover, NBS TN82 (PB161583) (1960) $1.75.

The NBS meteor-burst propagation project—a progress report, C. E. Hornback, L. D. Breyfogle, and G. R. Sugar, NBS TN86 (PB161587) (1960) $1.25.

A theoretical study of sporadic-*E* structure in the light of radio measurements, K. Tao, NBS TN87 (PB161588) (1961) $1.25.

Flexural strength of specimens prepared from several uranium dioxide powders; its dependency on porosity and grain size and the influence of additions of titania, F. P. Knudsen, N. S. Parker, and M. D. Burdick, J. Am. Ceram. Soc. **43,** No. 12, 641–647 (Dec. 1960).

Correlation of an auroral arc with a subvisible monochromatic 6300 A arc with outer-zone radiation on November 28, 1959, B. J. O'Brien, J. A. Van Allen, F. E. Roach, and C. W. Gartlein, J. Geophys. Research **65,** No. 9, 2759–2766 (Sept. 1960).

Report on the standardization of *p*H and related terminology, R. G. Bates and E. A. Guggenheim, Intern. Union Pure and Appl. Chem. **1,** No. 1, 163–168 (1960).

Regulated power supply for instruments, W. V. Loebenstein, Electronics **33,** No. 48, 132 (Nov. 1960).

Some ceramic dielectrics with a very low temperature coefficient of capacitance, S. Marzullo and E. N. Bunting, J. Am. Ceram. Soc. **43,** No. 11, 609, (Nov. 1960).

The sample, the procedure, and the laboratory, W. J. Youden, Anal. Chem. **32,** No. 13, 23A–37A (Dec. 1960).

Residual arc spectra of seventy elements diluted in copper, C. H. Corliss, W. F. Meggers, and B. F. Scribner, Book, Colloquium spectroscopicum internationale **VIII,** 119–121 (1959).

The relation of h_{max} F2 to M(3000)F2 and H_pF2, J. W. Wright and R. E. McDuffie, J. Radio Research Lab. **7,** No. 32, 409–420 (July 1960).

8-quinolinol precipitation of the elements, J. I. Hoffman, Chem. Anal. **49,** No. 4, 126 (Dec. 1960).

A test of a procedure for easy estimation of representative monthly electron density profiles for the ionosphere, J. W. Wright, J. Geophys. Research **65,** No. 10, 3215–3217 (Oct. 1960).

A method for efficiently providing low temperature liquids on a large scale to an accelerated experimental program, A. K. Stober, Proc. 10th Intern. Congress of Refrigeration, Copenhagen, Denmark **1,** No. 1, 17–18 (Pergamon Press Ltd., London, England, 1959).

Seasonal variations in the twilight enhancement of [OI] 5577, L. R. Megill, P. M. Jamnick and J. E. Cruz, J. Atmospheric and Terrest. Phys. **18,** 309–314 (Aug. 1960).

Synthetic mica, A. V. Valkenburg, Book, Encyclopedia of Chemical Technology, p. 480–487 (Interscience Encyclopedia, Inc., New York, N. Y., 1960).

Precipitation of the elements on addition of aqueous ammonia to their clear solution, J. I. Hoffman, Chem. Anal. **49,** No. 3, 94 (Sept. 1960).

Low scatter high current gas target for D-D neutrons, A. C. B. Richardson, Rev. Sci. Inst. **31,** No. 11, 1202–1203 (Nov. 1960).

Evaluation of resistance strain gages at elevated temperatures, R. L. Bloss, Am. Soc. Testing Materials Proc. **1,** No. 1, 9–15 (Jan. 1961).

Errors in dielectric measurements due to a sample insertion hole in a cavity, A. J. Estine, and H. E. Bussey, IRE-Trans. Microwave Theory and Tech. **MTT–8,** No. 6, 650-653 (Nov. 1960).

Determination of pentosans. Interlaboratory comparison of the aniline acetate, orcinol, and bromination methods, W. K. Wilson and J. Mandel, Tappi **43,** No. 12, 998–1004 (Dec. 1960).

A research for geomagnetic singular days, C. Warwick, T. Pohrte, and N. MacDonald, J. Geophys. Research **65,** No. 9, 3013–3015 (Sept. 1960).

Letter to editor of Revue Des Matériaux (first), E. S. Newman and H. A. Berman, Revue Des Matériaux C, No. 540, 231 Dec. 1, 1960).

Geomagnetic storms and the space around the earth, S. Chapman, Nature **187,** No. 4740, 824–827 (Sept. 3, 1960).

Some implications of slant-E_s, E. K. Smith and R. W. Knecht, Polar Atmosphere Symp., Part 2, Ionospheric Section, Oslo, Norway, July 2–8, 1956, p. 195–204 (Pergamon Press, Inc., New York, N.Y., 1957).

Experimental investigation of creep deflection of extruded and riveted I–beams, L. Mordfin and N. Halsey, NASA Tech. Note D–662 (December 1960).

The measurement of thermal conductivity, D. C. Ginnings, Book, Thermoelectric materials and devices, edited by I. B. Cadoff and E. Miller. Chapter 8 113–132 (Rheinhold Publishing Corporation, New York, N. Y., 1960).

Programming for a closed-loop, manned-machine combined system, D. C. Friedman, Proc. Combined Analog-Digital Computer Systems Symp., December 16 and 17, 1960, Philadelphia, Pa., 12th Article (Dec. 1960).

Analytical study of creep deflection of structural beams, L. Mordfin, NASA Tech. Note D–661 (Dec. 1960).

Evaluation of ball bearing separator materials operating submerged in liquid nitrogen, W. A. Wilson, K. B. Martin, J. A. Brennan, and B. W. Birmingham, ASLE. ASME Lubrication Conf., October 17–19, 1960 (Boston, Mass.), Am. Soc. Lubrication Engrs. preprint No. 60 LC–4 (1960).

Aircraft storage batteries, W. J. Hamer, AIEE and Am. Inst. Elec. Engr. Trans. **79,** Pt. II, 1–11 (Sept. 1960).

Stress-strain relationships in yarns subjected to rapid impact loading. Part VI: Velocities of strain waves resulting from impact, J. C. Smith, J. M. Blanford, and H. F. Schiefer, Textile Research J. **30,** No. 10, 752–760 (Oct. 1960).

The centennial of spectrochemistry, W. F. Meggers, J. L Tech, J. Opt. Soc. Am. **50,** No. 11, 1035–1038 (Nov. 1960).

Publications for which a price is indicated (except for NBS Technical Notes) are available only from the Superintendent of Documents, U.S. Government Printing Office, Washington 25, D.C. (foreign postage, one-fourth additional). Technical Notes are available only from the Office of Technical Services, U.S. Department of Commerce, Washington 25, D.C. (order by PB number). Reprints from outside journals and the NBS Journal of Research may often be obtained directly from the authors.

UNIVERSITY OF MICHIGAN
ORD # 56-160074
PHYSICS LIBRARY, 2035 RANDALL LAB.
ANN ARBOR MICH
SJR-A DEC D-18220 BA

UNITED
GOVERNMENT PRINTING OFFICE
DIVISION OF PUBLIC DOCUMENTS
WASHINGTON 25, D.C.

OFFICIAL BUSINESS

PENALTY FOR PRIVATE USE TO AVOID PAYMENT OF POSTAGE, $300 (GPO)

JOURNAL OF RESEARCH of the National Bureau of Standards — Vol. 65A, No. 3 — May–June 1961

A. Physics and Chemistry

Contents

	Page
International practical temperature scale of 1948. Text revision of 1960. H. F. Stimson.	139
Evaluation of the NBS unit of resistance based on a computable capacitor. Robert D. Cutkosky.	147
Wavelengths and intensities in the first spectrum of bromine, 2000 to 13000 A. Jack L. Tech and Charles H. Corliss.	159
Torsional resonance vibrations of uniform bars of square cross section. Wayne E. Tefft and Sam Spinner.	167
Infrared studies of aragonite, calcite, and vaterite type structures in the borates, carbonates, and nitrates. C. E. Weir and Ellis R. Lippincott.	173
Dielectric properties of polyamides: polyhexamethylene adipamide and polyhexamethylene sebacamide. Alexander J. Curtis.	185
Heat of formation of calcium aluminate monocarbonate at 25 °C. H. A. Berman and E. S. Newman.	197
Thermodynamic constants for association of isomeric chlorobenzoic and toluic acids with 1,3-diphenylguanidine in benzene. Marion Maclean Davis and Hannah B. Hetzer.	209
Heats of combustion and formation of trimethylborane, triethylborane, and tri-*n*-butylborane. Walter H. Johnson, Marthada V. Kilday, and Edward J. Prosen.	215
Pyrolysis of linear copolymers of ethylene and propylene. Sidney Straus and Leo A. Wall.	221
Pyrolysis of fluorocarbon polymers. Leo A. Wall and Sidney Straus.	227
Preparation of fluoro- and bromofluoroaryl compounds by copyrolysis of bromofluoroalkanes. Leo A. Wall, James E. Fearn, Walter J. Pummer, and Robert E. Lowry.	239
Thermal stability of polydivinylbenzene and of copolymers of styrene with divinylbenzene and with tribinylbenzene. Sidney Straus and Samuel L. Madorsky.	243
Conformations of the pyranoid sugars. IV. Infrared absorption spectra of some fully acetylated pyranoses. R. Stuart Tipson and Horace S. Isbell.	249
A standard for the measurement of the *p*H of blood and other physiological media. Vincent E. Bower, Maya Paabo, and Roger G. Bates.	267
Publication of the National Bureau of Standards.	271

For sale by the Superintendent of Documents, U.S. Government Printing Office, Washington 25, D.C. Price 70 cents (single copy)
Subscription price: $4.00 a year; 75 cents additional for foreign mailing.

UNITED STATES GOVERNMENT PRINTING OFFICE, WASHINGTON : 1961